UNIVERSITÉ DU QUÉBEC

THÉSE PRÉSENTÉE À

L'UNIVERSITÉ DU QUÉBEC À CHICOUTIMI

COMME EXIGENCE PARTIELLE

DU DOCTORAT EN RESSOURCES MINÉRALES

PAR

BÉLINDA GODEL

Ph. D.

RÔLE DES LIQUIDES SULFURÉS DANS LA FORMATION DES MINERALISATIONS RICHES EN ELEMENTS DU GROUPE DU PLATINE: APPLICATIONS AU COMPLEXE DU BUSHVELD (AFRIQUE DU SUD) ET AU COMPLEXE DE STILLWATER (ÉTATS-UNIS)

Septembre 2007

Bibliothèque
Paul-Émile-Boulet

UQAC
Université du Québec
à Chicoutimi

Mise en garde/Advice

Afin de rendre accessible au plus grand nombre le résultat des travaux de recherche menés par ses étudiants gradués et dans l'esprit des règles qui régissent le dépôt et la diffusion des mémoires et thèses produits dans cette Institution, **l'Université du Québec à Chicoutimi (UQAC)** est fière de rendre accessible une version complète et gratuite de cette œuvre.

Motivated by a desire to make the results of its graduate students' research accessible to all, and in accordance with the rules governing the acceptation and diffusion of dissertations and theses in this Institution, the **Université du Québec à Chicoutimi (UQAC)** is proud to make a complete version of this work available at no cost to the reader.

L'auteur conserve néanmoins la propriété du droit d'auteur qui protège ce mémoire ou cette thèse. Ni le mémoire ou la thèse ni des extraits substantiels de ceux-ci ne peuvent être imprimés ou autrement reproduits sans son autorisation.

The author retains ownership of the copyright of this dissertation or thesis. Neither the dissertation or thesis, nor substantial extracts from it, may be printed or otherwise reproduced without the author's permission.

RESUMÉ

Les grandes intrusions litées mafiques et ultramafiques comme le Complexe du Bushveld (Afrique du Sud) et le Complexe de Stillwater (Montana, Etats-Unis) peuvent contenir des niveaux minéralisés riches en EGP appelé « reef ». Le Merensky Reef (Complexe du Busveld) et le J-M Reef (Stillwater complex) sont deux exemples de niveaux minéralisés enrichis en EGP associés avec des sulfures disséminés (pyrrhotite, pentlandite et chalcopyrite) et localisés dans la partie inférieure (~ 1/3 de la base) d'intrusions litées.

Plusieurs processus ont été envisagés pour tenter d'expliquer la présence de ces zones minéralisées enrichies en EGP et métaux communs. Deux modèles de formation pour ces types de minéralisation sont principalement proposés, mais restent sujet à de nombreux débats. Certains auteurs ont suggéré que les EGP sont colléctés par un liquide sulfuré enrichis en métaux de base. Ce liquide sulfuré ségrége à partir du magma et percole vers le bas dans la pile de cumulat (silicates et/ou oxydes). D'autres auteurs ont proposés que les EGP sont plutôt captés par des fluides aqueux d'origine magmatique enrichis en chlore qui percolent vers le haut dans la pile de cumulat lors de la compaction et précipitent les EGP, S, Ni, Cu lorsque le fluide se dissout dans le liquide silicaté intercumulus.

Le but premier de cette thèse est de tester par une approche multidisciplinaire (microtomographique, microstructurale, et géochimique) le modèle d'accumulation des EGP par un liquide sulfuré d'origine magmatique et d'évaluer le rôle de la compaction sur la distribution des minéraux sulfurés. Dans un deuxième temps, la redistribution des EGP par des fluides sera considérée. Ces deux études devront permettre de mieux contraindre le

mode de formation des minéralisations enrichies en EGP dans les intrusions litées. Cette étude sera réalisée sur des échantillons du Merensky Reef et du J-M Reef.

Cette étude impliquera :

- la détermination de la distribution en 3-D (par microtomographie) et en 2-D (en lame mince) des minéraux sulfurés
- la détermination du rôle de la compaction et/ou de la lithologie sur la distribution des sulfures (i.e. sur la migration des liquides sulfurés)
- la détermination des phases contenant les EGP (sulfures, minéraux du groupe du platine ou autres phases)
- la détermination du rôle des liquides sulfurés et de l'altération sur l'enrichissement en EGP
- la synthèse des différents résultats pour proposer un modèle de formation pour ce type de minéralisation riche en EGP

L'étude microtomographique a permis de mettre en évidence que :

- les sulfures dans les roches silicatées du Merensky Reef et du J-M Reef sont localisés dans des réseaux verticaux d'échelle millimétrique à centimétrique. Dans le Merensky Reef, ces réseaux de sulfures s'arrêtent au niveau de chromite sous-jacente où les sulfures sont sous forme de gouttelettes
- dans le Merensky Reef, le contenu en sulfure diminue vers le haut de la section et est maximal juste au-dessus des niveaux de chromite

Les études microstructurales des échantillons du Merensky Reef et du J-M Reef montrent que :

- toutes les lithologies contiennent des indices de déformation des cristaux à hautes températures (contacts indentés, macles de déformations, extinction ondulantes, bandes de déformation, etc.)
- les sulfures sont distribués en réseaux verticaux et localisés le long de la bordure entre les grains de pyroxène, olivine et/ou plagioclase

Toutes les observations sont en accord avec une direction de compression maximale ($\sigma 1$) orientée selon la paléo-verticale et due à la compaction de la pile de minéraux cumulats. Pendant cette compaction, des zones de moindres contraintes (dilatences) se formeraient et faciliteraient la percolation vers le bas des liquides sulfurés.

Les analyses géochimiques et minéralogiques ainsi que les résultats des modélisations indiquent que :

- dans les deux complexes, Pt et Au ne se concentrent pas dans les sulfures mais se trouvent sous forme de minéraux du groupe du platine (principalement des sulfures de Pt+/-Pd, des tellures de Pt+/-Pd, et des alliages de Pt-Fe) et de l'electrum
- dans les deux cas, la plupart des autres EGP se retrouve dans la pentlandite et la pyrrhotite et le restant des EGP se retrouve sous forme de minéraux du groupe du platine (principalement laurite et alliage de Pd-Cu pour le J-M Reef)

- tous les EGP présents dans les roches silicatées du Merensky Reef et du J-M Reef peuvent être modélisés par le processus de capture des EGP par un liquide sulfuré d'origine magmatique
- les EGP observés dans les niveaux de chromite ont deux origines et deux processus se superposent : la cristallisation primaire à partir du magma silicaté de minéraux du groupe du platine (avant la saturation en sulfure du magma) ; et par la suite la percolation d'un liquide sulfuré immiscible et enrichis en EGP
- les alliages de platine (isoferroplatinum) observés dans les deux zones minéralisées seraient produits par la désulfurisation partielle des sulfures
- les autres minéraux de groupe du platine (tellures et sulfures) s'exsolveraient à partir des sulfures lors du refroidissement
- dans le J-M Reef, un événement tardif (*i.e.* après la capture des EGP par un liquide sulfuré et après la désulfurisation partielle des sulfures) aurait provoqué un enrichissement de certains échantillons en Pd et Pt et aurait lessivé partiellement les cumulats situés sous la zone minéralisée. Cela se serait produit à une température située entre 250 et 465°C (basée sur la composition des alliages de Pd-Cu)

ABSTRACT

Major platinum-group element (PGE) deposits are found associated with large layered intrusions such as the Bushveld Complex (South Africa) and the Stillwater Complex (Montana, U.S.A.). These PGE deposits are referred to as "reef". The Merensky Reef (Bushveld Complex) and the J-M Reef (Stillwater Complex) are two examples of PGE reefs associated with base-metal sulphides that are located about one third from the base of the layered intrusions.

Several processes have been proposed to explain these PGE and base metal enrichments in the layered intrusions. Two models are commonly cited and represent two different schools of thought. Some authors have suggested that the PGE are collected by a magmatic base-metal sulphide liquid. The dense sulphide liquid segregated from the magma and percolated downwards in the cumulate pile. Other authors propose that the PGE are collected by a magmatic aqueous fluids enriched in Cl that percolated upwards through the cumulate. The PGE, S, and base metals precipitated when this fluid dissolved into the intercumulate silicate liquid.

The goal of this thesis is to test the models for collection of the PGE by a magmatic base-metal sulphide liquid and the role of compaction on the sulphide liquid migration, using different approaches based on microstructural, geochemical and mineral analyses. Possible constraints on PGE remobilization by fluids will also be evaluated.

This study was carried out using samples of the Merensky and J-M Reefs.

The major aims were:

- to determine the distribution of the base-metal sulphides (BMS) in 3-D (using X-ray Computed Tomography) and in 2-D (from thin sections) in the samples.
- to determine the role of compaction and/or lithologies on BMS distribution (or sulphide liquid migration)
- to determine the hosts of the PGE (BMS minerals, platinum-group minerals or others phases)
- to consider the role of a BMS liquid and of fluid migration on PGE enrichment
- to synthesize all the results in order to propose a model for the formation of this type of PGE mineralization

Microtomographical (X-ray computed tomography) analyses indicate that:

- the BMS in the silicate rocks of both the Merensky and the J-M Reefs are located along millimetre- to centimetre-scale vertical network. In the Merensky Reef, the network terminates in the underlying chromitite where the sulphides occur as small droplets
- in the Merensky Reef, the BMS content decreased up-section and the BMS are more abundant just above each chromitite layer

Microstructural analyses of the samples from both Merensky and J-M Reefs show that:

- all lithologies exibit high temperature crystal deformation features such as indented contacts between orthopyroxene, deformation twins in plagioclase, undulose extinction, and the development of sub-grains;
- the BMS are located along pyroxene, olivine and/or plagioclase grain boundaries and form a vertical network along faces of these crystals.

All the observed features are consistent with a paleovertical maximum principal compressive stress ($\sigma 1$) that is responsible for compaction as the cumulate pile formed. During the compaction vertical dilatancies formed and may have been filled by the base metal sulphide liquid.

Geochemical and mineralogical analyses and modelling calculations indicate that:

- in both reefs, most of the PGE are found in pentlandite and pyrrhotite or in platinum-group mineral (PGM) associated with them;
- exceptions to this are Os-Ir-Ru in the chromitites of the Merensky Reef which are found in laurite grains with chromites and silicate minerals and Pd-Cu alloy found in secondary magnetite in one J-M Reef sample;
- in both the Merensky Reef and the J-M Reef, Pt and Au are not hosted by BMS, but are found as platinum-group minerals (mainly Pt +/- Pd sulphides and tellurides, and Pt-Fe alloys) and electrum within the BMS;

- in the J-M Reef the footwall cumulates have Pd/Pt ratios of 0.3 to 0.7 that are lower than the reef samples averaging Pd/Pt ratio of 3.3.

These observations suggest that:

- all the PGEs found in the silicate rocks of the Merensky Reef and the J-M Reef were initially collected by a sulphide liquid;
- the PGE observed in the chromitite layers of the Merensky Reef are the result of the combination of two processes: primary crystallisation of laurite from the silicate magma (before sulphide liquid segregated); and the later percolation of PGE-rich immiscible sulphide liquid;
- the Pt-Fe alloys observed in both mineralized zones are produced by the partial desulfurization of MSS;
- the others PGMs (telluride and sulphide essentially) are exsolved from the BMS upon cooling;
- in the J-M Reef, a later event, post dating the collection of the PGE by a BMS liquid has increased Pd and, to a lesser extent, Pt contents in some of the samples and removed these elements from the footwall cumulats rocks. This alteration may have occurred at a temperature between 250 and 465 °C (based on the composition of the Pd-Cu alloy).

REMERCIEMENTS

« Il est possible de tout faire dans la vie, absolument n'importe quoi, mais jamais avec n'importe qui. »

Olivier de Kersauson
Trophée Jules Verne, Mai 2004

Je tiens particulièrement à remercier:

- ma directrice de thèse Dr. Sarah-Jane Barnes pour m'avoir fait confiance au départ, pour m'avoir permis de réaliser ce projet et de découvrir le monde fascinant des EGP qui, je dois le reconnaître, était plus qu'obscure il y a 3 ans, pour sa grande disponibilité et ses conseils ainsi que pour sa patience lors de la correction des articles.
- Dr. Wolfgang Maier pour ses conseils et suggestions, pour sa disponibilité et le temps passé à la relecture des différents papiers, pour m'avoir fait partager ses connaissances sur le Bushveld en Afrique du Sud et pour m'avoir permis après mon accident de profiter (physiquement et moralement) du spectacle jusqu'au bout.
- Dr. Edward Sawyer pour ses conseils, pour ses réponses à mes questions « microstructurales et métamorphiques » et, pour le temps passé à la relecture du manuscript.
- Dr. Ambre Luguet et Dr. Marc Constantin pour leurs corrections du manuscript.
- Dr. Richard Cox, Dr. Paul Bédard et Dany Savard pour leurs conseils et leur grande disponibilité lors des analyses géochimiques à l'UQAC.
- Dr. Michael Zientek (USGS) pour ses conseils sur le complexe de Stillwater et pour m'avoir transmis certaines de ses données non-publiées à titre de comparaison.
- l'équipe de « Maudits Français » et l'« Ambassade de France à Chicoutimi » (ils se reconnaîtront !) qui, au cours de ces années, ont été formidables à tous points de vue.

Finalement, ma famille et amis restés en France pour leur soutient à distance et pour toujours avoir respecté mes choix…

TABLE DES MATIERES

CHAPITRE 1

CHAPITRE 2

3-D DISTRIBUTION OF SULPHIDE MINERALS IN THE MERENSKY REEF (BUSHVELD COMPLEX, SOUTH AFRICA) AND THE J-M REEF (STILLWATER COMPLEX, USA) AND THEIR RELATIONSHIP TO MICROSTRUCTURES USING X-RAY COMPUTED TOMOGRAPHY.54

CHAPITRE 3

PLATINUM-GROUP ELEMENTS IN SULPHIDE MINERALS, PLATINUM-GROUP MINERALS, AND THE WHOLE ROCK OF THE MERENSKY REEF (BUSHVELD COMPLEX, SOUTH AFRICA): IMPLICATION FOR THE FORMATION OF THE REEF 106

CHAPITRE 4

PLATINUM-GROUP ELEMENTS IN SULFIDE MINERALS AND THE WHOLE ROCKS OF THE J-M REEF (STILLWATER COMPLEX): IMPLICATIONS FOR THE FORMATION OF THE REEF 196

CHAPITRE 5

IMAGES ANALYSIS AND COMPOSITION OF PLATINUM-GROUP MINERALS IN THE J-M REEF OF THE STILLWATER COMPLEX (U.S.A.) 266

CHAPITRE 6

SYNTHESE ET CONCLUSIONS: MERENSKY REEF VS J-M REEF SIMILITUDES ET DIFFERENCES 324

LISTE DES FIGURES

CHAPITRE 1

CHAPITRE 2

CHAPITRE 3

CHAPITRE 4

CHAPITRE 5

CHAPITRE 6

APPENDIX 4

APPENDIX 5

APPENDIX 6

LISTE DES TABLEAUX

CHAPITRE 1

CHAPITRE 2

CHAPITRE 3

CHAPITRE 4

CHAPITRE 5

APPENDIX 4

APPENDIX 5

APPENDIX 6

LISTE DES ANNEXES

CHAPITRE 1

INTRODUCTION,

PROBLEMATIQUE ET MÉTHODOLOGIE

1.1- INTRODUCTION

Les éléments du groupe du platine (EGP : Pt, Pd, Ir, Os, Ru, Rh) et les métaux communs (principalement Ni et Cu) ont à l'heure actuelle une importance économique considérable. Les EGP sont utilisés dans différents domaines : dans l'industrie automobile (pot catalytique essentiellement); en médecine (traitement contre le cancer, la dentisterie etc.); en joaillerie; ainsi que dans de nombreux domaines de hautes technologies (élèctronique, pile à combustible etc.). La forte demande en EGP a provoqué depuis quelques années une recrudescence de l'exploration minérale pour ces éléments. Par conséquent, un des problèmes majeurs à l'heure actuelle en géologie économique est de mieux comprendre les phénomènes pouvant engendrer la formation de ces minéralisations.

Les minéralisations riches en Ni, Cu et éléments du groupe du platine (EGP) sont souvent associées avec des roches mafiques à ultramafiques. Ces minéralisations peuvent être divisées en deux catégories (Naldrett, 1989):

- (i) celles comprenant des minéralisations riches en Ni et Cu et dans lesquelles les EGP sont des sous-produits (exemples : Nkomati en Afrique du Sud, Noril'sk en Russie, Voisey's Bay au Labrador, Kabanga en Tanzanie)
- (ii) celle où les EGP sont les ressources principales et le Ni et Cu sont des sous-produits (exemples : UG-2 et Merensky Reef dans le Complexe du Bushveld en Afrique du Sud, John Manville (J-M) Reef et Picket Pin Reef dans le Complexe de Stillwater dans le Montana aux Etats-Unis).

Seul la deuxième catégorie de minéralisation (EGP comme ressources principales) va faire l'objet de ce travail de doctorat.

Il existe une très grande variété de styles de minéralisations riches en EGP peuvant se retrouver dans différentes parties des intrusions et être soit (Maier, 2005):

- (i) situées à la base de l'intrusion au contact ou dans la roche encaissante (par exemples: le Platreef dans la partie nord du Complexe du Bushveld (Manyeruke *et al.*, 2005; Holwell and McDonald, 2006) ; le Complexe de Portimo en Finlande (Alapieti and Lahtinen, 2002))
- (ii) situées dans la partie inférieure des intrusions (<1000 m de la base) constituées essentiellement de péridotites et de pyroxénites (par exemple : Main Sulphide Zone du Great Dyke au Zimbabwe (Oberthür, 2002) ; Keivitsa en Finlande (Alapieti and Lahtinen, 2002) ; Lower Zone (Volspruit farm) située dans la partie nord du Complexe du Bushveld (Harmer, 2004)
- (iii) associées à des niveaux de chromites (par exemple : UG-2 et les niveaux de chromites du Merensky Reef, Complexe du Bushveld (Barnes and Maier, 2002a).
- (iv) situées dans la partie centrale des intrusions et associées généralement à des unités cycliques (par exemple : Merensky Reef (Complexe du Bushveld) et J-M Reef (Complexe de Stillwater).
- (v) situées dans la partie supérieure des intrusions (par exemple : instrusion de Stella en Afrique du Sud (Maier *et al.*, 2003))
- (vi) dues à une activité hydrothermale (exemple du Lac des Iles en Ontario (Brügmann *et al.*, 1989)).

Dans ce travail de doctorat, nous nous concentrerons plus particulièrement sur les minéralisations qui sont situées dans la partie centrale des intrusions litées en prenant le Merensky Reef dans le Complexe du Bushveld et le J-M Reef dans le Complexe de Stillwater (Montana, Etats-Unis) comme exemples.

1.2.- PROBLEMATIQUE

Les minéralisations riches en EGP telles que le Merensky Reef ou le J-M Reef sont en générale associées à des sulfures disséminés (1 à 5 % en volume) dans diverses lithologies (Table 1.1). En général, ces minéralisations enrichies en EGP forment des horizons de faible épaisseur (quelques dizaines de centimètres à quelques mètres maximum) et riches (un à plusieurs dizaines de ppm) en EGP. Ces horizons minéralisés sont appelés « reefs ».

Les EGP sont en général étroitement associés à des minéraux sulfurés : pentlandite ((Fe, $Ni)_9S_8$)) ; pyrrhotite ((Fe(1-x)S) (x=0-0.17)) et chalcopyrite ($CuFeS_2$) essentiellement. Les EGP se retrouvent en solution solide dans les sulfures et/ou sous forme de minéraux du groupe du platine (MGP) (Kingston and El-Dosuky, 1982 ; Kinloch, 1982 ; Zientek and Oscarson, 1986 ; Ballhaus and Ryan, 1995 ; Ballhaus and Sylvester, 2000 ; Zientek *et al.*, 2002 ; Prichard *et al.*, 2004).

Bien que de nombreux travaux aient été réalisés depuis quelques décennies, la genèse de ces dépôts reste mal comprise et source à de nombreux débats. Deux « écoles de pensées » sont communément utilisées pour tenter d'expliquer l'origine des minéralisations enrichies en EGP.

De nombreux chercheurs pensent que les EGP et les métaux de bases seraient collectés par des liquides sulfurés enrichis en métaux de base qui percoleraient dans la pile de cristaux. Les EGP seraient ainsi principalement concentrés par des sulfures d'origine magmatique (Campbell and Naldrett, 1979; Campbell *et al.*, 1983 ; Naldrett *et al.*, 1986 ; Barnes and Maier, 2002a).

Table 1.1: *Exemples de lithologies associées à des minéralisations enrichies en EGP localisées dans certains complexes intrusifs.*

Nom du complexe ou de l'intrusion*	**Nom de la zone minéralisée enrichie en EGP**	**Lithologie**	**Références**
Bushveld	Merensky Reef	chromite, mélanorite	Barnes and Maier (2000a)
	UG-2	chromite	Cawthorn (2002)
Stillwater	JM Reef	troctolite, anorthosite, gabbronorite	Zientek *et al.* (2002)
Great Dyke	Main Sulphide Zone	websterite	Oberthür (2002)
Munni Munni	Porphyritic Websterite Zone	websterite	Barnes and Hoatson (1994)
Penikat	Paasivaara Reef (PV reef)	gabbro	Alapieti and Lahtinen (2002)
	Ala–Penikat Reef (AP reef)	anorthosite et gabbronorite	
	Sompujarvi Reef (SJ reef)	gabbronorite, chromite	
Portimo	SK reef	orthopyroxenite, gabbro	Alapieti and Lahtinen (2002)
	RK reef	anorthosite, norite	Alapieti and Lahtinen (2002)
Skaergaard	Platinova Reefs	gabbro	Andersen *et al.* (2002)

* La localisation des complexes intrusifs est donnée sur la Fig. 1.1.

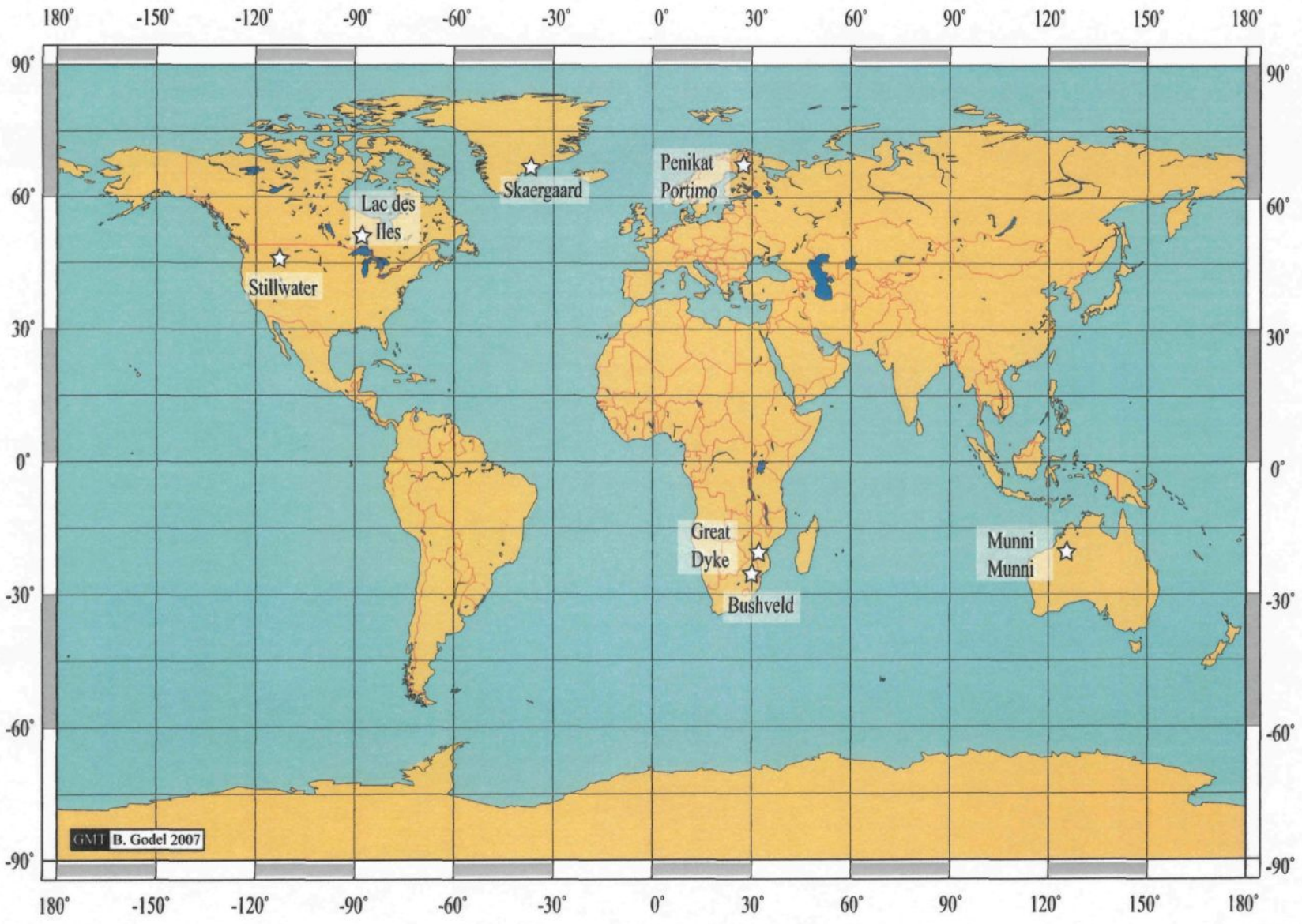

Figure 1.1: Carte de localisation des complexes intrusifs contenant des minéralisations enrichies en EGP.

Au contraire, d'autres auteurs pensent que les EGP seraient plutôt concentrés par des fluides aqueux tardi-magmatiques (Boudreau and McCallum, 1992a ; Boudreau and McCallum, 1992b ; Boudreau and Meurer, 1999 ; Willmore *et al.*, 2000) qui percoleraient vers le haut lors de la compaction. D'autres modèles ont également été proposés et seront plus amplement discutés au Chapitre 3, 5 et 5.

Le but premier de ce doctorat est de tester en 2-D et 3-D le modèle de collection des EGP par un liquide sulfuré initialement proposé par Campbell et Naldrett (1979) et Naldrett *et al.* (1996) et modifié par Barnes et Maier (2002a). Cette étude multidisciplinaire sera principalement réalisée sur le Merensky Reef du Complexe du Bushveld. Dans un deuxième temps, l'influence possible des fluides (magmatiques, hydrothermaux et/ou magmatiques) sur la répartition des minéralisations enrichies en EGP pourra également être évaluée à partir d'échantillons du J-M Reef dans le Complexe de Stillwater.

1.2.1. – Collecte des EGP par des sulfures magmatiques primaires

1.2.1.1. – Principes de base

Le modèle de collecte des EGP par un liquide sulfuré (Campbell and Naldrett, 1979) est basé sur le fait que : (i) les EGP et les métaux de bases ont des coéfficients de partage très élevés dans les liquides sulfurés (Table 1.2) ; (ii) la concentration en EGP et métaux de base dans les sulfures est dépendante du volume de magma silicaté qui interagit avec le liquide sulfuré. Pour un système fermé, la concentration d'un élément dans un liquide sulfuré (C_{Sul}) est donnée par l'équation suivante (Campbell and Naldrett, 1979):

$$C_{Sul} = C_{Sil}\, D^{sul/sil}(R+1)/(R+D^{sul/sil})$$

où C_{Sil} est la concentration de l'élément dans le liquide (magma) silicaté, $D^{sul/sil}$ est le coéfficient de partage de l'élément entre le liquide sulfuré et le magma silicaté et R (appelé « R-factor ») est le rapport de volume entre le magma silicaté et le liquide sulfuré. Plus R est grand plus le liquide sulfuré interagit avec une grande quantité de magma et plus les métaux sont concentrés dans le liquide sulfuré.

Plus récemment, Brügmann *et al.* (1993) ont proposé une nouvelle équation basée sur l'équation de « *zone refining* ». Dans ce cas, la composition des goutellettes de sulfures (C_{Sul}) qui percolent dans une colonne de magma est donnée par la formule suivante :

$$C_{Sul} = C_{Sil}\, [D^{Sul/Sil} - (D^{Sul/Sil} - 1)\, .\, e^{-(1/\, DSul/Sil\, x\, N)}]$$

où N est le rapport de masse entre le magma silicaté et le liquide sulfuré.

Lors de la compaction de la pile de minéraux cumulus, le liquide sulfuré enrichi en métaux de base et EGP percolerait vers le bas et se concentrerait dans des zones où la perméabilité ne serait plus suffisante pour qu'il migre plus bas (Barnes et Maier, 2000b).

Table 1.2: *Coéfficients de partage pour les EGP et métaux de base entre différentes phases.*

d'après Barnes et Maier (1999)

Os	Ir	Ru	Rh	Pt	Pd	Au	Ni	Cu
Sulphide liquid – Silicate liquid								
> 31 000	> 50 000	> 12 000	> 140 000	> 18 000	> 92 000		810-1 300	
	130 000			9 100	88 000	1 200		
230	310 000	2 500	27 000	> 1 000 000	55 000	16 000		
	35 000				43 000			
	450 000				33 000			
				36 000	25 000			
10 000	51 000	35 000		13 000	25 000	1 200		
	14 000				23 000	15 000 – 18 000	575 - 836	1383
30 000	26 000	6 400		10 000	17 000			
700 – 5 300	1 500 – 4 700	1 200 – 4 100		1 100 – 6 900	1 200 – 6 300	30 – 3 000		
48 000								
							315 - 424	913 - 1006
						110 – 1 300	350 - 1070	
Monosulphide Solid Solution – Sulphur Saturated Sulphide Liquid								
4.3	3.6	4.2	3.03	0.2	0.2	0.09	0.84	0.27
3.4 - 11		1.17 – 3.0	0.05 – 0.13	0.09 – 0.2		0.36 – 0.8	0.2 – 0.25	
Monosulphide Solid Solution – Sulphur Undersaturated Sulphide Liquid								
0.77 - 1	0.14	0.19	0.02		0.23			
	0.08 – 1.4		0.4 – 0.8	0.01 – 0.05	0.01 – 0.07		0.18 – 0.36	0.17 – 0.2
Monosulphide Solid Solution – Sulphur Oversaturated Sulphide Liquid								
	5 - 17		3.9 - 11	0.14 – 0.24	0.13 – 0.24		0.7 – 1.2	0.22 – 0.27

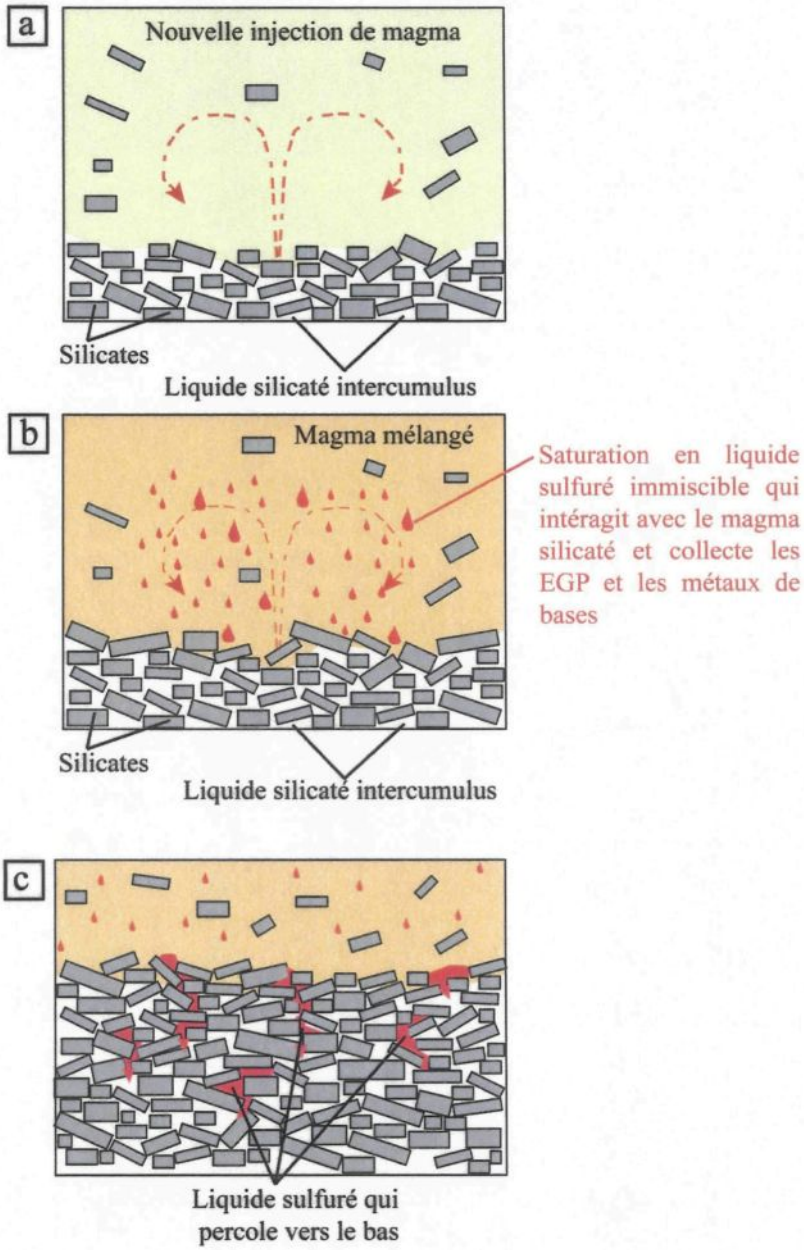

Figure 1.2: Modèle de collecte des EGP par un liquide sulfuré (modifié d'après Barnes et Maier, 2002b).

1.2.1.2. – Facteurs « critiques » pour la formation des minéralisations

L'application de ce modèle nécessite plusieurs choses :

- le magma silicaté d'origine mantellique doit être riche en EGP et métaux de bases,
- ce magma doit atteindre la croûte supérieure sans atteindre la saturation en soufre (celle-ci engendrerait une perte en EGP et aurait donc un effet négatif sur la formation de minéralisation)
- lors de l'emplacement dans la croûte supérieure, le magma doit devenir saturé en soufre pour qu'un liquide sulfuré immiscible ségrége et collecte les EGP.

➢ *Formation d'un magma riche en EGP*

La formation d'un magma riche en EGP (exemple des magmas parentaux pour le complexe du Bushveld, Table 3.14) nécessite que les EGP présent dans le manteau supérieur fractionnent dans le magma lors de la fusion partielle. La solubilité des EGP dans les magmas et le mode de transfert des EGP entre le manteau et le magma issu de la fusion partielle restent à l'heure actuelle mal défini. Les phases présentes dans le manteau sont Barnes: des silicates (~98%) ; des spinelles (~2%) ; des sulfures (~0.07 %, Lorand (1990)) et des alliages métalliques (~0.05 %). Les EGP dans le manteau sont concentrés par des sulfures et/ou aux alliages. Des travaux expérimentaux et empiriques (Capobianco et Drake, 1990 ; Capobianco *et al.*, 1994 ; Sattari *et al.*, 2002 ; Righter *et al.*, 2004) ont montré que Ru, Rh, Ir, et Os pourraient également être contenu dans les spinelles. Afin d'obtenir un magma enrichi en EGP, les sulfures (et possiblement les alliages) doivent fondre et se dissoudre (avec les EGP) dans le magma. La solubilité du soufre dans un magma silicaté dans les conditions du manteau supérieur est de 0.1-0.2 % (Mavrogenes et O'Neill, 1999). Cela implique un degré de fusion partielle important (~25-

30 %) pour que tous les sulfures présents dans le manteau soient fondus. Ces taux de fusions sont caractéristiques des komatiites et des basaltes riches en Mg. Il est à noter que la majorité des minéralisations riches en EGP est associée avec des magmas magnésiens (exemple du complexe du Bushveld, Table 3.14).

➢ *Processus pouvant provoquer la saturation en S*

La solubilité du soufre (S) dans un magma mafique dépend de plusieurs paramètres (Naldrett, 1969 ; Haughton *et al.,* 1974 ; Poulson et Ohmoto, 1990 ; Mavrogenes et O'Neill, 1999): la composition du magma, la température, la fS_2, la fO_2 et la pression.

La solubilité du soufre dans un magma basaltique augmente avec la diminution de la pression et décroît avec la température lors du refroidissement du magma (Wendlandt, 1982; Mavrogenes et O'Neill, 1999). Les magmas mantelliques basiques ou ultrabasiques doivent être sous-saturés en soufre lors de leur emplacement (même si à l'origine ils étaient saturés en soufre). Par conséquent, la saturation en soufre du magma doit être atteinte après l'emplacement du magma dans la croûte supérieure, en engendrant ainsi la ségrégation d'un liquide sulfuré immiscible et la collection des EGP.

Li et Ripley (2005) ont montré empiriquement que la concentration en S au moment de la saturation en sulfure du magma peut être définie par :

$$\text{Ln } X_S = 1.229 - 0.74\,(10^4/T) - 0.021(P) - \ln X_{FeO} - 6.166\,X_{SiO2} - 9.153\,X_{Na2O}$$
$$+ K_2O - 1.914\,X_{MgO} + 6.594\,X_{FeO}$$

avec T la température en Kelvin, X_y la fraction molaire de y, et P la pression en kbar.

Plus récemment, les travaux expérimentaux de Liu *et al.* (2007) ont permis de proposer une autre formule plus complexe pour déterminer la teneur en S lors de la saturation d'un magma

au moment de la saturation en sulfure du magma. Dans ce cas, la concentration de S au moment de la saturation en sulfure du magma est définie par :

$$\ln (S \text{ in ppm}) = 11.35251 - (4454.6 / T) - 0.03190 (P / T) + 0.71006 \ln(MFM)$$

$$- 1.98063 [(MFM) (X_{H2O}^{melt})] + 0.21867 \ln (X_{H2O}^{melt}) + 0.36192 \ln X_{FeO}^{melt}$$

avec

$$MFM \text{ (fraction molaire des cations)} = [(Na+K+ 2(Ca+Mg+Fe^{2+})] / [Si \times (Al + Fe^{3+})]$$

où T est la température en Kelvin, P est la pression en Bar, X_y^{melt} est la fraction molaire de y.

Plusieurs processus peuvent engendrer la saturation en soufre d'un magma et la formation d'un liquide sulfuré immiscible :

- La différenciation
- La cristallisation fractionnée de minéraux riches en Fe (olivine, pyroxène, magnétite, chromite) qui réduit la solubilité de S (Haughton *et al.*, 1974 ; Li *et al.*, 2001a)
- Le mélange de magmas de compositions différentes (Naldrett and VonGruenewaldt, 1989 ; Li *et al.*, 2001a ; Li et Ripley, 2005).
- La contamination du magma avec plus ou moins d'addition de soufre par : (i) dévolatilisation, assimilation ou fusion partielle de roches encaissantes riches en soufre (Ripley, 1999); (ii) par addition de silice par assimilation crustale (Li et Naldrett, 1993).

1.2.2.. - Collecte des EGP par des fluides magmatiques et/ou hydrothermaux

Des études expérimentales ont montré que certains EGP (Pd et Pt) peuvent être, sous certaines conditions, dissout dans des fluides (Hsu *et al.*, 1991 ; Fleet et Wu, 1993 ; Baker *et al.*, 2001 ; Wood, 2002 ; Hanley *et al.*, 2005a ; Hanley *et al.*, 2005b, Peregoedova *et al.*, 2006) et

ainsi être transportés. De plus, plusieurs évidences de transport et de précipitation des EGP par des fluides hydrothermaux dans divers environnements géologiques existent (*e.g.* McCallum *et al.*, 1976 ; Olivo *et al.*, 2001 ; Cabral *et al.*, 2002).

Vermaak (1976) et VonGrunewaldt (1979) ont proposé que l'enrichissement en EGP dans le Complexe du Bushveld pouvait être dû à la migration de fluides (tardi-magmatiques ou hydrothermaux). Plus récemment, des études principalement basées sur l'étude de la teneur en Cl des apatites et sur l'observation de texture pegmatoïdale dans certaines lithologies minéralisées (Boudreau *et al.*, 1986 ; Boudreau et McCallum, 1992a; Boudreau et McCallum, 1992b; Boudreau et Meurer, 1999 ; Willmore *et al.*, 2000) ont montré que les apatites associées au zones enrichies en EGP sont riches en Cl. L'enrichissement en EGP pourrait ainsi être provoqué par la migration de fluide aqueux riche en Cl (et enrichis en métaux de base, S et EGP).

Dans ce modèle (Fig. 1.3), lors de la solidification des cumulats, le liquide fractionné intercumulus devient saturé en un fluide aqueux riche en Cl. Les EGP, S et métaux de base partitionnent dans ce fluide qui migre vers le haut dans la pile de cumulats lors de la compaction. Ce fluide contenant S, Ni, Cu et certains EGP percole jusqu'à ce qu'il atteigne un niveau où le liquide silicaté intercumulus est sous-saturé en fluide. A ce niveau, le fluide se dissout dans le liquide intercumulus et précipite S et les métaux (Ni, Cu et EGP) sous forme de sulfures enrichis en EGP.

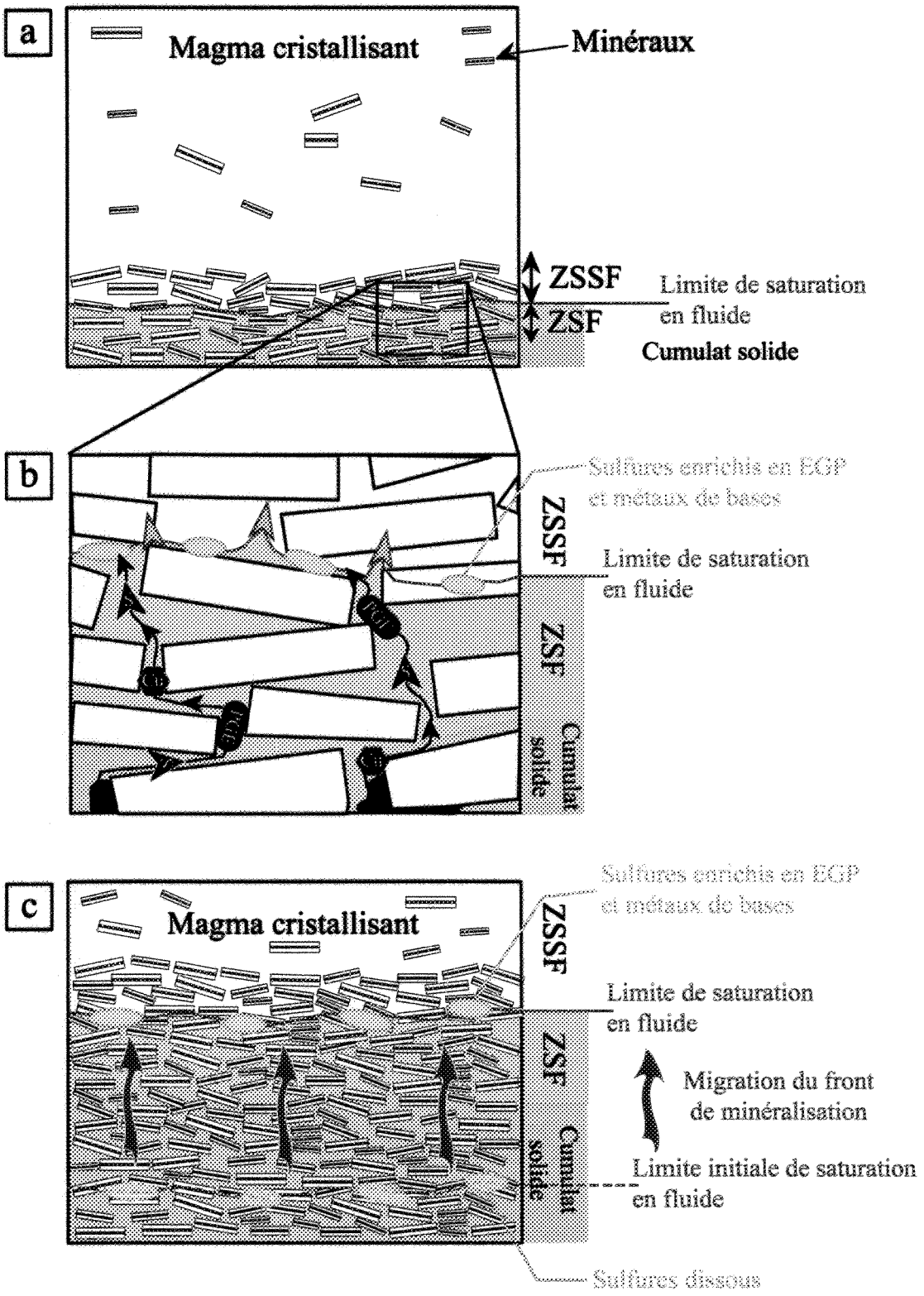
a
Magma cristallisant
Minéraux
ZSSF
ZSF
Limite de saturation en fluide
Cumulat solide
b
Sulfures enrichis en EGP et métaux de bases
ZSSF
Limite de saturation en fluide
ZSF
Cumulat solide
c
Magma cristallisant
Sulfures enrichis en EGP et métaux de bases
ZSSF
Limite de saturation en fluide
ZSF
Migration du front de minéralisation
Cumulat solide
Limite initiale de saturation en fluide
Sulfures dissous

Figure 1.3: Modèle de dépôts des EGP par un fluide enrichi en chlore.

A- Lors de la solidification de la pile de cumulat, le liquide silicaté interstitiel devient saturé en fluide aqueux (riche en Cl).
B- Lors de la compaction, ce fluide migre vers le haut en apportant avec lui le soufre, les métaux de base et les EGP. La migration du liquide s'arrête à l'interface entre la zone saturée en fluide (Z.S.F) et la zone sous-saturée en fluide (Z.S.S.F). Au niveau de la limite de saturation en fluide, le fluide se redissout dans le liquide silicaté interstitiel (sous-saturé en fluide). Lorsque le soufre, les métaux et les EGP sont saturés dans le liquide silicaté interstitiel, ils précipitent sous forme de sulfures enrichis en EGP.
C- Au fur et à mesure que la pile de cumulat se solidifie, le front de minéralisation se déplace vers le haut de la pile de cumulats

1.3. – OBJECTIFS

L'objectif principal de ce doctorat est de tester (en 2-D et 3-D) par une approche multi-disciplinaire le modèle de collecte des EGP par un liquide sulfuré enrichi en métaux de bases qui percolerait dans la pile de cumulats durant sa compaction. Dans un deuxième temps, l'étude de l'altération pourra permettre d'évaluer l'implication possible de fluides dans l'enrichissement en EGP.

Afin de répondre aux questions posées ci-dessus, plusieurs objectifs secondaires sont envisagés et peuvent être résumés selon les points suivants :

- **Déterminer les processus physiques pouvant expliquer ou contrôler la répartition des sulfures**
  - Déterminer et quantifier la répartition en 3-D et 2-D des minéraux sulfurés dans les échantillons considérés.
  - Déterminer le rôle de la compaction dans la répartition des minéralisations sulfurées sur les échantillons considérés.
  - Déterminer la topologie des sulfures afin d'évaluer si il existe une différence de comportement entre les différentes lithologies.

- **Déterminer les phases contenant des EGP**
  - Déterminer les concentrations en EGP, autres métaux (Ni, Cu, Co, Au, Ag etc.) et S des roches totales (pour les différentes lithologies du Merensky Reef et du J-M Reef)

- Déterminer la concentration en EGP et métaux de base dans les sulfures (analyse *in-situ*) et voir si il existe des variations en fonction de la lithologie et/ou de la stratigraphie
- A partir des analyses de roches totales et des analyses des sulfures, déterminer si les sulfures sont les principaux minéraux hotes des EGP.
- Déterminer quelles sont les autres phases pouvant contenir des EGP (minéraux du groupe du platine, chromite etc.)

➢ **Déterminer le rôle des liquides sulfurés enrichis en métaux de base sur l'enrichissement en EGP**

- Modéliser la composition des liquides sulfurés à l'aide des équations de Campbell et Naldrett (1979) et de Brügmann *et al.* (1993)
- Déterminer si les EGP contenus dans les roches totales peuvent être expliqués par ségrégation de liquides sulfurés à partir d'un magma silicaté (basalte)

➢ **Dans le cas où l'enrichissement en EGP ne s'explique pas seulement par ségrégation de liquide sulfuré**

- Evaluer le rôle des autres phases (minéraux du groupe du platine, chromite…)
- Evaluer le rôle des processus (désulfurisation, altération et/ou métamorphisme) pouvant avoir engendré une remobilisation et/ou un enrichissement en EGP au niveau des zones minéralisées

➢ **Synthétiser les différents résultats pour proposer un/des modèle(s) de formation pour le Merensky Reef (Complexe du Bushveld) et le J-M Reef (Complexe de Stillwater).**

1.4. – ZONES D'ETUDES ET ECHANTILLONS

Cette partie a pour but de faire une présentation plus générale des deux complexes et des zones minéralisées étudiées (*i.e.* Merensky Reef dans le complexe du Bushveld et le J-M Reef dans le complexe de Stillwater).

1.4.1. - Complexe du Bushveld (Afrique du Sud) et Merensky Reef

1.4.1.1. – Géologie et stratigraphie générale

Le Complexe du Bushveld (2054 +/- 2.8 Ma, Harmer et Armstrong, 2000) est le plus gros complexe intrusif au monde (Fig. 1.4). Ce complexe contient les principales ressources mondiales en EGP, en Cr et en V ainsi que d'importantes ressources en Ni, Cu, Sn, et de fluor (Maier, 2006).

Il est constitué d'une suite litée mafique-ultramafique appelée « Rustenburg Layered Suite » d'une épaisseur de ~6-8 km, d'intrusions de granites « Lebowa Granite Suite » et de granophyres « Rashoop Granophyre Suite ».

La suite litée mafique-ultramafique forme trois parties : Est (« Eastern Limb »), Ouest (« Western Limb ») et Nord (« Northern Limb »). Elle est composée de la base au sommet (Fig. 1.4) des zones suivantes (Hall, 1932 ; Cawthorn, 2006 ; Maier, 2006):

- ***la « Marginal Zone »*** formée de norites et de gabbronorites ayant une épaisseur variant de 0 à 400 mètres environ.

- ***la « Lower Zone »*** dont la composition est variable. Dans la partie ouest, elle est formée de la base au sommet : de cumulats à olivine, de pyroxénites, de harzburgites et de dunites. Dans la partie est, elle est formée d'orthopyroxénites et de roches riches en olivine (Cameron, 1978). Dans la partie nord, elle est formée de roches riches en chrome et en olivine.

- ***la « Critical Zone »*** est subdivisée en deux « sous-zones » :

- *la « Lower Critical zone »* d'une épaisseur d'environ 800 m est composée de pyroxénites, d'une zone riche en olivine et de niveaux de chromite (9 niveaux).
- *la « Upper Critical zone »* d'une épaisseur d'environ 500 mètres est composée à sa base d'un niveau d'anorthosite. Cette zone est caractérisée par la présence d'unités cycliques (plus ou moins complètes) composées successivement de chromitite (Fig. 1.5), harzburgite, pyroxénite, norite et anorthosite. Dans la partie supérieure de cette zone se retrouvent deux des principales ressources mondiales en EGP : le niveau de chromite de l'UG 2 et le Merensky Reef (voir ci-dessous).

- ***la « Main Zone »*** est formée d'une séquence d'environ 3 000 mètres d'épaisseur constituée de la base au sommet de norites, gabbronorites, et de norites.

- ***la « Upper Zone »*** d'une épaisseur d'environ 2 500 mètres est formée de gabbronorites, de niveaux de magnétite, de diorites, d'anorthosite, de gabbros, et à certains endroits de niveaux de nelsonites.

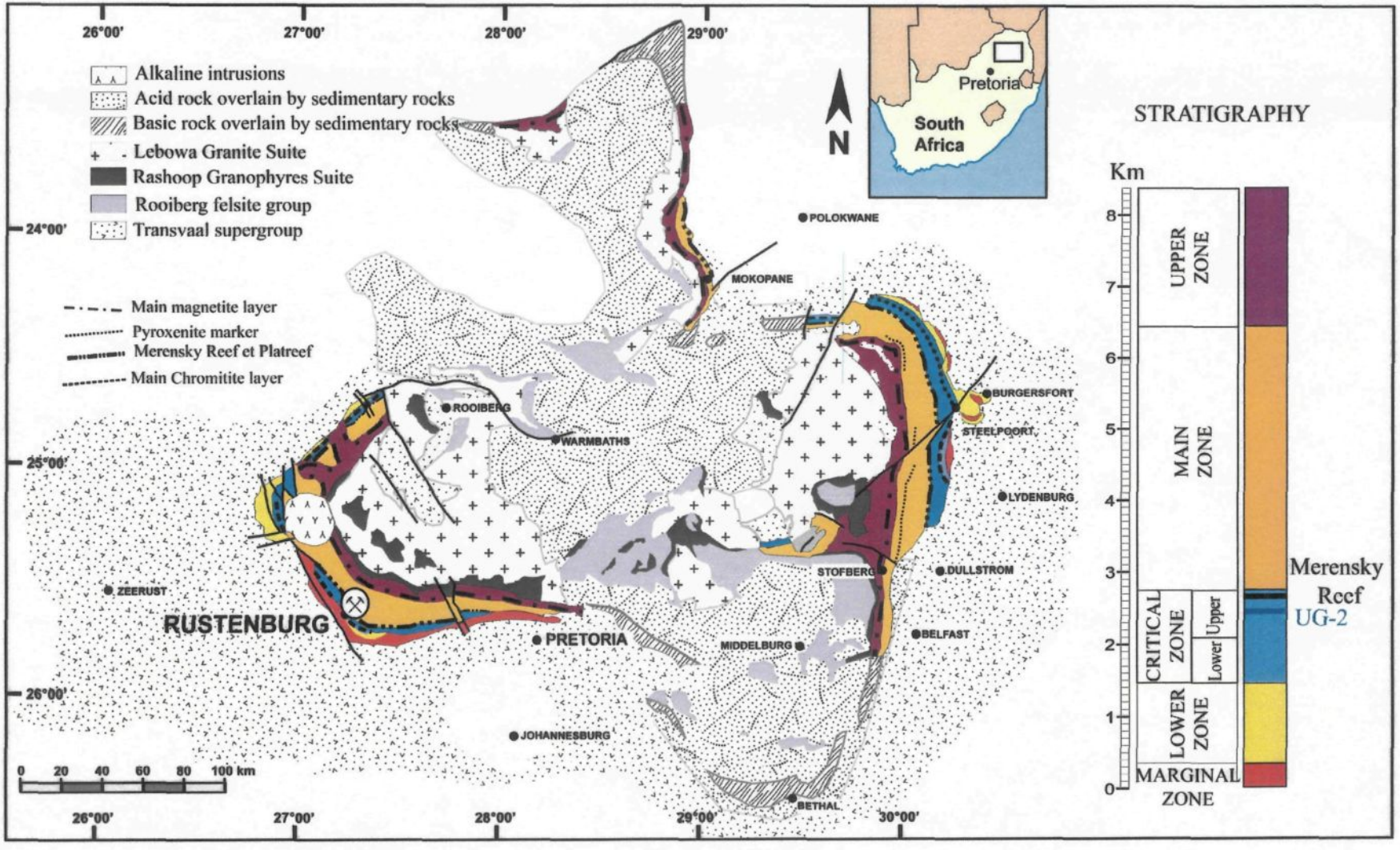

Figure 1.4: Carte géologique simplifiée du Complexe du Bushveld (modifié d'après VonGruenewaldt, 1979).

1.4.1.2. – Le Merensky Reef

Le Merensky Reef est une zone minéralisée enrichie en EGP localisé dans la partie supérieure de l'«Upper Critical zone » (Fig. 1.5 et 1.6). Cette zone minéralisée se retrouve sur plus de 280 km dans le Complexe du Bushveld (Cawthorn, 2002). Cette zone d'épaisseur ne dépassant rarement 1 mètre d'épaisseur contient environ 3 % volume de sulfures (pentlandite, pyrrhotite, et chalcopyrite) disséminés dans différentes lithologies (anorthosite, niveaux de chromite et pyroxénite, voir description aux Chapitres 2 et 3 et Fig. 1.6) et contient en moyenne entre 6 et 8 ppm de Pt et Pd (Lee, 1983 ; Barnes and Maier, 2002a).

Plusieurs types de Merensky Reef existent (Fig. 1.7):

- *Merensky Reef de type « Normal »* (Fig. 1.6, type étudié et décrit au cours de ce doctorat, voir Chapitre 2 et Chapitre 3)
- *Merensky Reef de type « Pothole »* (*e.g.* Leeb-Du Toit, 1986 ; Viljoen and Hieber, 1986 ; Kinloch and Peyerl, 1990) est caractérisé par l'absence de concordance entre le "reef" et le mur, et par l'absence d'une certaine partie de la stratigraphie entre le Merensky Reef et l'UG-2. La formation des « potholes » pourrait être due à de nombreux mécanismes : l'érosion thermique provoquée par l'influx d'un nouveau magma (Campbell *et al.*, 1983) ; par l'amincissement, dû aux mouvements le long de failles listriques, de la partie partiellement consolidée de la chambre magmatique (Carr *et al.*, 1994), ou à la percolation de fluide (Kinloch and Peyerl, 1990).

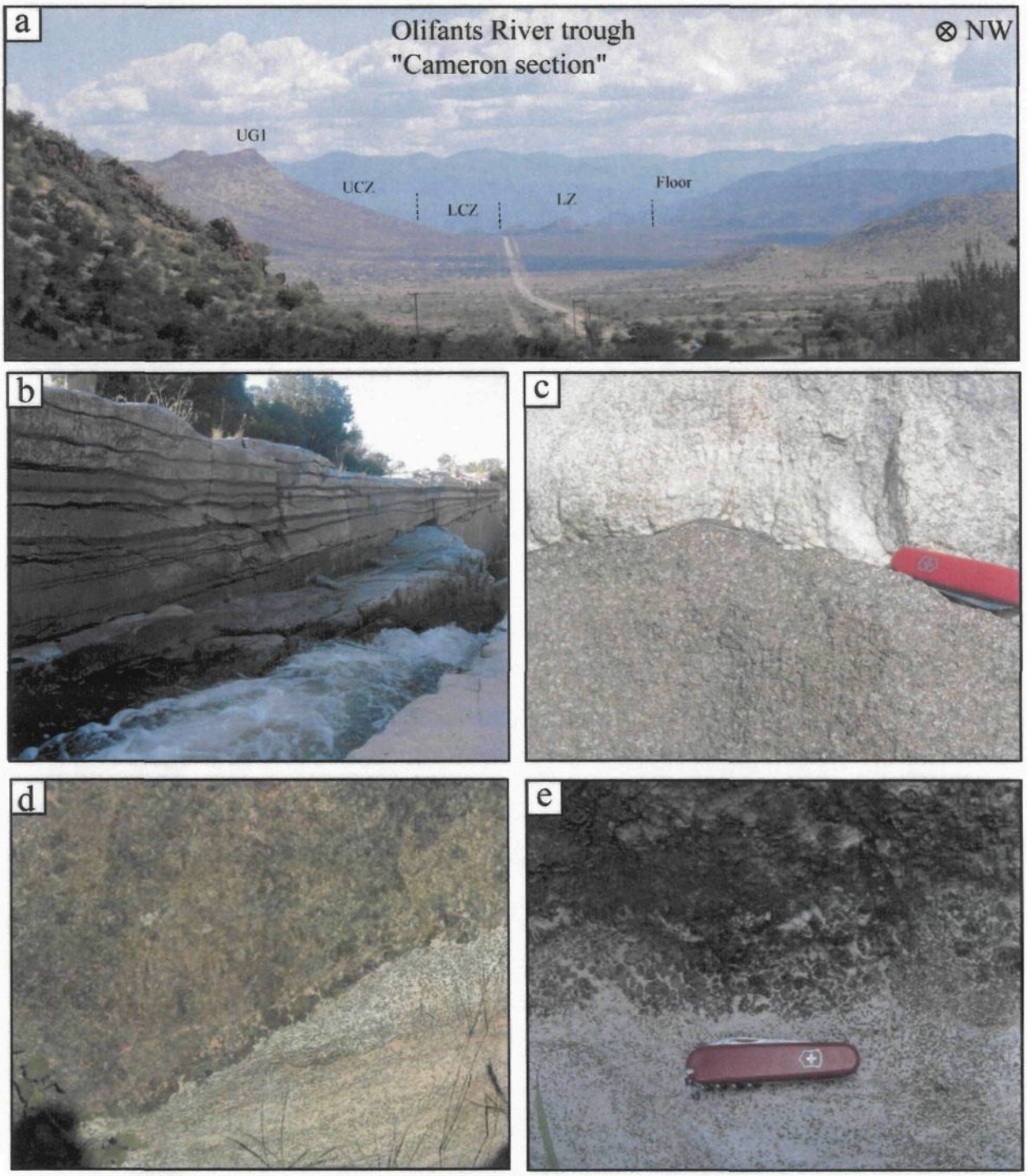

Figure 1.5: Photographies du Complexe du Bushveld.
(a) "Cameron Section", coupe à travers le Bushveld (partie Est) ; (b) niveaux de chromites de l'UG1 (site Dwars River) ; (c) Zone de contact entre la Lower et l'Upper Critical zone (Cameron section) ; (d) et (e) Exemple de Merensky Reef localisé dans la partie est du Complexe du Bushveld

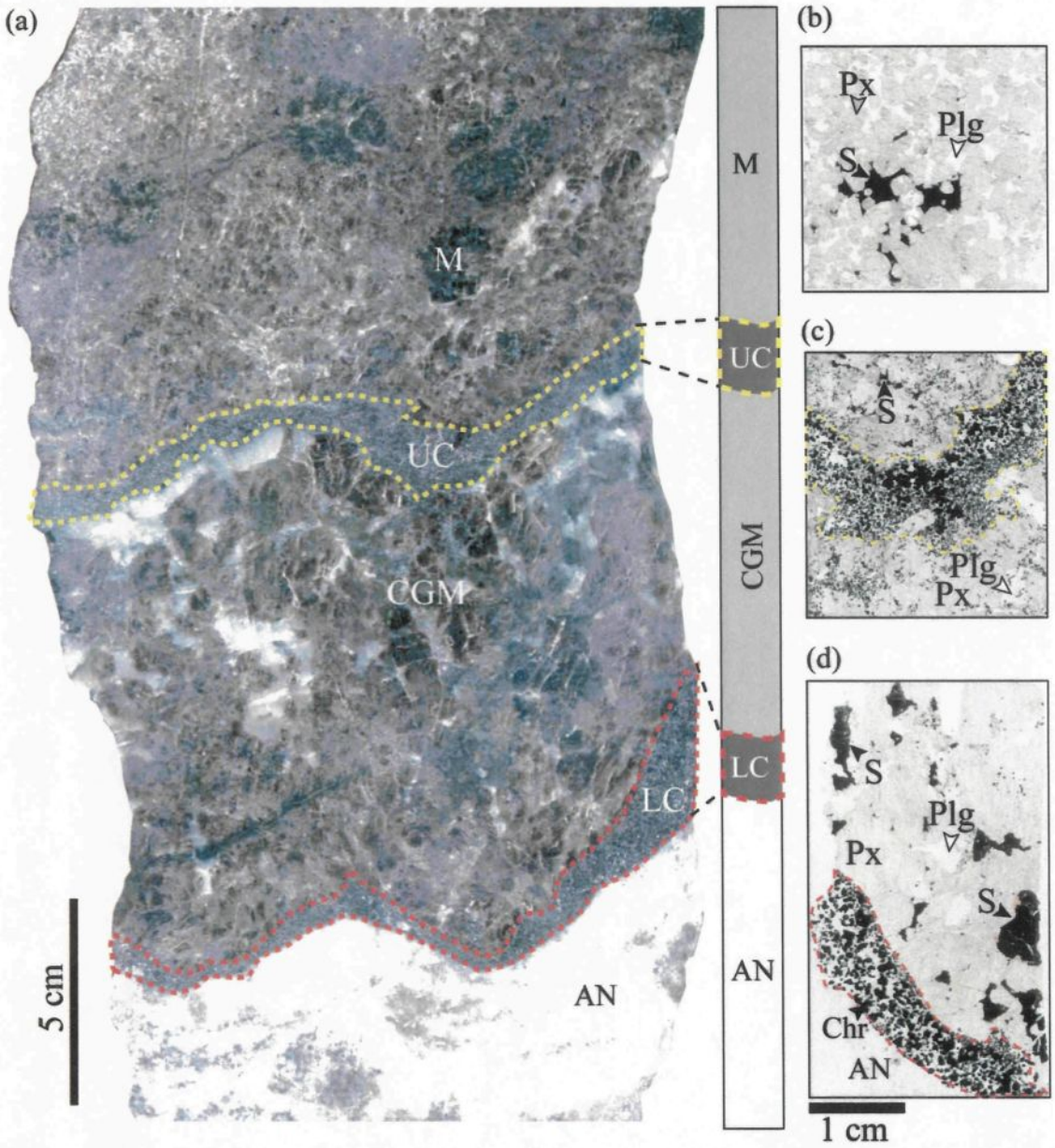

Figure 1.6: Echantillon macroscopique (a) et lames minces (b, c, et d) du Merensky Reef à la Rustenburg Pt Mine.

AN: anorthosite ; LC : niveau inférieur de chromitite ; CGM : mélanorite pégmatoïdale ; UC : niveau supérieur de chromitite ; M : mélanorite ; Chr: chromite ; Px : pyroxène ; Plg : plagioclase ; S : sulfures

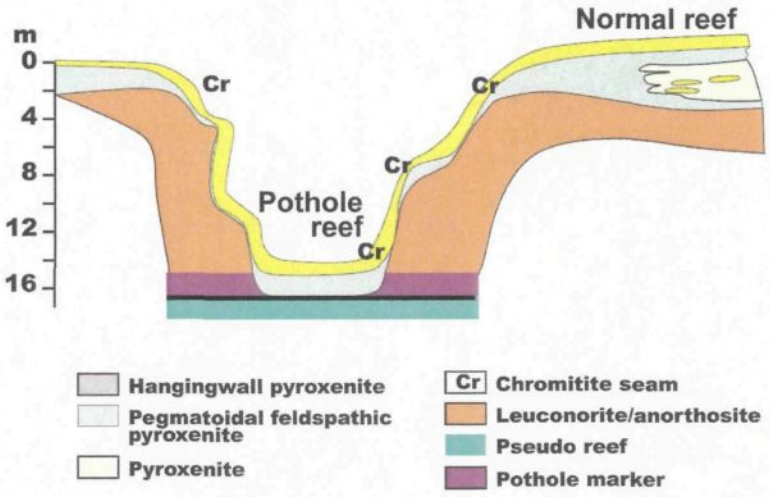

Figure 1.7: Coupe à travers différentes lithologies du Complexe du Bushveld.

Modifié d'après Viljoen (1999)

1.4.2. - Complexe de Stillwater (Montana, Etats-Unis) et J-M Reef

1.4.2.1. – Géologie et stratigraphie générale

Le Complexe de Stillwater, localisé dans le sud-ouest du Montana (Etats-Unis), et est composé principalement de roches mafiques et ultra-mafiques (Fig. 1.8). Le Complexe de Stillwater s'est mis en place et a cristallisé durant le tardi-archéen (2705 $^{+}/_{-}$ 4Ma, âge U-Pb sur zircon, Premo *et al.* (1990). Ce complexe d'orientation NW-SE s'étend sur environ 42 km et a une épaisseur d'environ 5 500 mètres (Zientek *et al.*, 2002). Plusieurs épisodes d'intrusion et/ou de déformation ont affecté le complexe après sa solidification. Les différents épisodes sont résumés dans la Table 1.3.

La plupart des roches observées dans le Complexe de Stillwater sont des cumulats. Ces roches litées ont été classées en unités stratigraphiques appelées « series » définies en fonction de la proportions des minéraux présents et des séquences de types de roches (Zientek *et al.*, 2002). Cinq séries ont été définies (Czamanske et Zientek, 1985) et sont de la base au sommet:

- ***la « Basal Series » :*** Cette série d'une épaisseur d'environ 150 m est subdivisée en deux zones appelées « Upper Basal bronzite cumulate zone » et « Lower Basal norite zone » (Zientek *et al.*, 1985). Ces deux zones sont formées pratiquement entièrement de cumulats à bronzite. Les orthopyroxènes sont les principaux minéraux cumulus avec localement d'autres minéraux cumulus tels que le plagioclase, l'olivine, l'augite ou des grains de chromite. Les sulfures enrichis en métaux de bases sont présents près de la base du complexe (Zientek *et al.*, 2002). Cette zone est également recoupée par de nombreux sills et dykes (Helz, 1985).

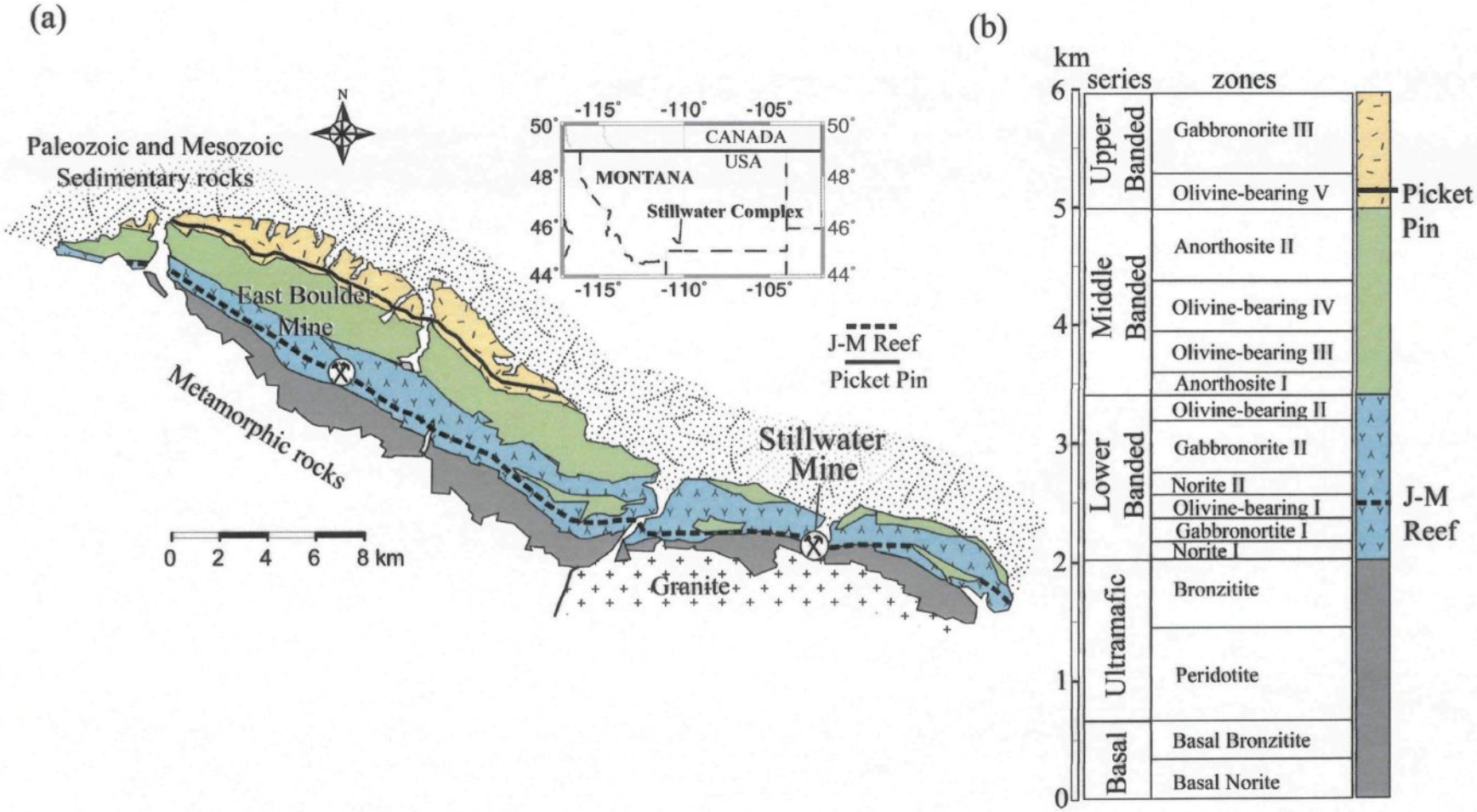

Figure 1.8: Carte géologique simplifiée du Complexe de Stillwater, Montana, U.S.A. (modifiée d'après Zientek *et al.*, 2002).

- ***« l'Ultramafic series» :*** Cette série d'une épaisseur d'environ 1000 mètres est composée de cumulats à olivine, orthopyroxène et chromite (Zientek *et al.*, 1985). La série est subdivisée en deux zones appelées « Peridotite zone » et « Bronzitite zone ». Des niveaux de chromite sont associés avec les cumulats à olivine. Quelques minéraux sulfurés sont présents et associés à la « Peridotite Zone » (Zientek *et al.*, 2002).

- ***la « Lower Banded series » :*** Cette série est située entre le sommet de l'« Ultramafic series » et l'« Anorthosite I zone». Elle est subdivisée en 6 zones (Fig. 1.8) avec de la base au sommet (McCallum *et al.*, 1980 ; Zientek *et al.*, 1985):

- *la « Norite I zone, NI »* formée de cumulat à plagioclase et bronzite
- *la « Gabbronorite I zone, GNI)* formée de roche litée composée de cumulats à plagioclase, orthopyroxène et augite.
- *la «Olivine-bearing I zone, OBI »* formée de cumulats à olivine, de cumulats riches en olivine et/ou plagioclase et/ou bronzite. Cette zone contient la zone minéralisée en EGP appelée John-Manville Reef (J-M Reef, voir ci-dessous).
- *la « Norite II zone, N II »* composée de cumulat à plagioclase et bronzite
- *la « Gabbronorite II zone, GN II »* composée essentiellement de cumulats à plagioclase-bronzite-augite
- *la « Olivine-bearing II zone, OB II »* composée de cumulats riches en olivine.

- ***la « Middle Banded Series » :*** Cette série est composée de 4 zones, de la base au sommet :

- *l' «Anorthosite I»* composées de cumulats de plagioclase pegmatoidale avec ~20 % de pyroxènes interstitiels.

- *l'«Olivine-bearing III zone, OB III»* formée d'une séquence litée de cumulats à plagioclase, augite et olivine.
- *l'«Olivine-bearing IV zone, OB IV»* constituée essentiellement de cumulats à plagioclase, de cumulats à plagioclase et olivine, et de cumulats à plagioclase-olivine-augite.
- *l'« Anorthosite II »* est similaire à l'Anorthosite I et contient au sommet une zone à sulfures riches en palladium et platine appelée la « Picket Pin zone » (McCallum *et al.*, 1980; Boudreau et McCallum, 1986 ; Zientek *et al.*, 2002).

➢ ***la « Upper Banded Series » :*** Cette série est composée de deux zones, de la base au sommet :

- *l'« Olivine-bearing zone V, OB V »* est composée de cumulats à plagioclase et olivine surmonté de cumulats à plagioclase, orthopyroxène et augite.
- *la «Gabbronorite III zone, GN III»* est composée essentiellement de cumulats à plagioclase-bronzite-augite.

1.4.2.2. – John Manville (J-M) Reef

Le John Manville (J-M) Reef du Complexe de Stillwater est une zone riche en sulfures disséminés riches en EGP (en moyenne ~18.8 ppm de Pt+Pd, Zientek *et al.*, 2002). Cette zone minéralisée est située à la base de l'« Olivine-bearing I, OB I » (Bow *et al.*, 1982 ; Barnes et Naldrett, 1985). Cette zone d'une épaisseur variant entre 1 et 3 mètres contient de 0.5 à ~3 %vol de minéraux sulfurés (Barnes et Naldrett, 1985; Zientek *et al.*, 2002).

Table 1.3: *Résumé des épisodes d'intrusion, de déformation et de métamorphisme ayant affecté le Complexe de Stillwater.*

Age	Système	Evénement	Références
2705+/- 4 Ma	U-Pb zircon	Emplacement et cristallisation du magma à l'origine du complexe de Stillwater Métamorphisme de contact des roches plus anciennes	Premo *et al.* (1990)
~ 2 700 Ma	U-Pb sur zircon	Emplacement de quartz monzonite Métamorphisme de contact des roches plus anciennes	Nunes et Tilton (1971)
2650 Ma à 2441 Ma	Sm-Nd et K-Ar	Emplacement de dikes mafiques	Baadsgaard et Mueller (1973)
1640 Ma	K-Ar	Emplacement de dikes mafiques	Baadsgaard et Mueller (1973)
à		Episode de déformation	Page et Page et Zientek (1985)
Cambrien moyen		Métamorphisme de bas degré (schiste vert)	
Crétacé supérieur		Orogénie Laramidienne Intrusions de sills et de dykes de composition intermédiaire	Zientek *et al.* (2002)

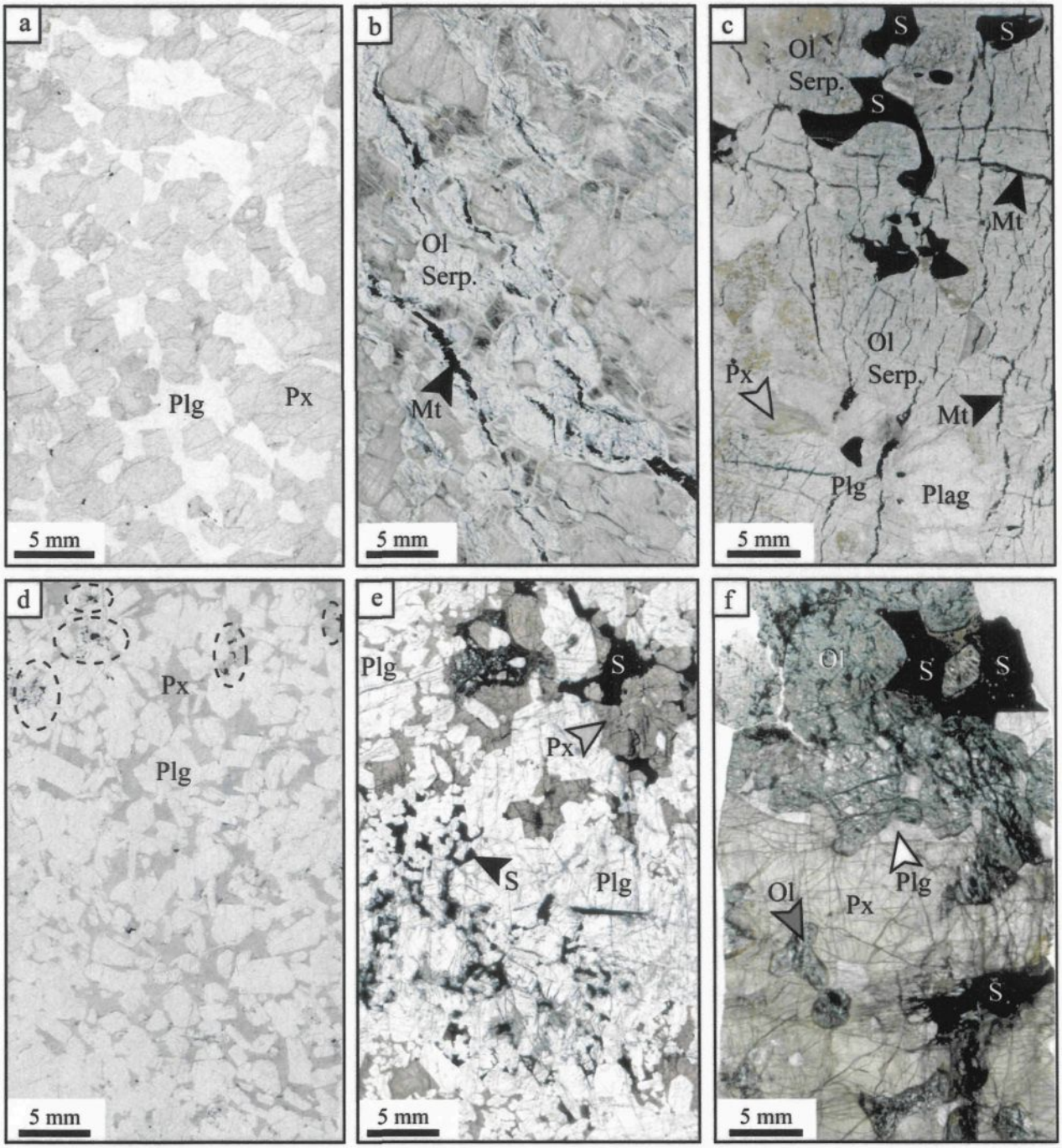

Figure 1.9: Lames minces digitalisées de différents échantillons du J-M Reef.

(a) Melanorite ; (b) Melagabbronorite à olivine; (c) Troctolite; (d) Norite ; (e) Leucogabbronorite; et (f) Melagabbronorite à olivine.

Cette zone est en général plus riche en Pd qu'en Pt. Le rapport Pd/Pt varie de 0.1 à plus de 15 avec une valeur moyenne de 3.3 (USGS database, M. Zientek, com. pers. 2006).
Les échantillons étudiés au cours de ce doctorat sont décrits au Chapitre 4 et quelques exemples de lames minces sont donnés en Fig. 1.9.

1.5. – METHODOLOGIE

Cette partie a pour but de faire une synthèse rapide de la majorité des méthodes utilisées pour tenter de répondre aux questions posées dans la problématique et les objectifs. Pour plus de détails sur les méthodes analytiques ou numériques, le lecteur est invité à se référer aux chapîtres cités.

1.5.1. – Détermination de la distribution en 3-D des sulfures

La structure interne d'un objet solide (roche par exemple) peut être définie en 3-D en utilisant plusieurs techniques destructives par polisages progressifs de surface (Marschallinger, 1998) ou non destructive par microtomographie « X-ray Computed Tomography » (Carlson et Denison, 1992 ; Denison et Carlson, 1997 ; Denison *et al.*, 1997 ; Ketcham et Carlson, 2001 ; Kyle et Ketcham, 2003 ; Kyle et Iturrino, 2005 ; Ketcham *et al.*, 2005).

Dans notre cas, la distribution des sulfures en 3-D a été déterminée en utilisant la microtomographie. Les échantillons ont été scannés à l'aide du scanner de l'INRS (Institutut National de la Recherche Scientifiques) à Québec afin d'obtenir les images séquentielles nécessaires à la reconstruction de la distribution en 3-D.

Le traitement et l'analyse des images ont été effectués à l'UQAC. La première partie de ce doctorat a été dédiée au traitement des images et à l'analyse quantitative de la distribution des

minéraux sulfurés. Le logiciel commercial 3-D Doctor *(Able Software Corp.)* qui est habituellement utilisé dans les hôpitaux pour les diagnostiques médicaux a été choisi (après en avoir testés d'autres) pour effectuer le traitement des images, l'«extraction » des minéraux d'intérêts et la représentation graphique en 3-D. L'analyse quantitative de la distribution en 3-D des minéraux sulfurés a été réalisée (par moi-même) à l'aide de code IDL ou GMT créés spécifiquement pour l'étude. Les principes et méthodes développés pour cette étude sont plus amplement décrits dans le Chapitre 2.

1.5.2. – Analyses microstructurales

1.5.2.1. – Détermination de la contrainte principale pendant la formation des cumulats

Une analyse microstructurale détaillée en lames minces a été réalisée pour définir la direction de contrainte principale ($\sigma 1$) lors de la formation des cumulats et ainsi caractériser le rôle de compaction. Le but de cette analyse est de retrouver des indicateurs de déformation des cristaux à hautes températures. Ces indicateurs sont décrits au Chapitre 2.

1.5.2.2. – Topologie des liquides sulfurés dans les différentes lithologies

La méthode est décrite en détail au Chapitre 2, paragraphe 2.8.3.

1.5.3. – Analyses géochimiques et minéralogiques

Après avoir évalué le rôle des processus « physiques » sur la migration possible des liquides sulfurés, et afin de mieux contraindre le/les modèle(s) de formation des minéralisations enrichies en EGP, il est nécessaire de voir si il existe des variations géochimiques à l'échelle de

la roche totale et des minéraux (sulfures et minéraux du groupe du platine). Pour cela plusieurs types d'analyses ont été réalisés.

1.5.3.1. – Analyses des roches totales

➢ *Analyse du soufre*

L'analyse du S a été réalisée à l'UQAC par combustion dans un flux d'oxygène par fournaise EMIA-220V de HORIBA. La poudre d'échantillon (1 gr) est placé dans un creuset en porcelaine avec ~1 gr de Fe, ~2 gr de W et ~0.3 gr de Cu (Fe, W et Cu servent de fondant). Lors du chauffage S réagit avec O pour former SO_2 . Durant ce processus, l'eau est dégagée sous forme d'H_2O et d'H_2. L'eau est éliminée par déshydratation à l'aide de $Mg(ClO_4)_2$. La teneur en SO_2 est analysée par un détecteur infrarouge et la teneur en S de l'échantillon est déterminée.

➢ *Analyse des EGP*

Le contenu en EGP des échantillons (roches totales) a été déterminé par activation neutronique (INAA) après pré-concentration par des sulfures de nickel. Les analyses ont été réalisées sur 10 et 15 gr d'échantillon en suivant la méthode de Bédard et Barnes (2002) pour les roches silicatées et la méthode de Bédard et Barnes (2004) pour les chromites. Le protocole de concentration des EGP dans les « boutons » de sulfures de Ni est résumé en Table 1.4.

➢ *Analyse des éléments traces*

L'analyse des éléments traces a été réalisée par activation neutronique. Pour les roches silicatées, les capsules d'activation sont entièrement remplies (soit entre ~2 g et ~3g d'échantillon selon la lithologie). Pour les chromites, 0.5 g d'échantillon est introduit dans la capsule et le reste est rempli avec un matériel inerte (sucre). Les capsules sont irradiées dans le réacteur Slowpoke

II à l'École Polytechnique de Montréal. Les spectres sont ensuite analysés et les concentrations déterminées à l'aide du logiciel EPAA.

- *Analyse du Ni et du Cu*

L'analyse du Ni et du Cu a été réalisée par absorption atomique (AA) à l'UQAC. Le protocole de préparation est le suivant. L'échantillon (1 g) est pesé dans un bêcher de 400 mL et 20 mL de HCl concentré est ajouté. L'ensemble est couvert et placé sur une plaque chauffante à ~ 75 °C pendant 15 mn. Ensuite, 15 mL de HNO_3, 20 mL de HCl concentré et 20 mL d'eau distillée sont ajoutées. L'ensemble est couvert et mis à ébullition pour chasser les gaz de digestion. La solution est ensuite filtrée et mise en fiole de 100 mL (avec ajout d'eau distillée pour arriver à 100 mL). Cette solution est ensuite analysée par spectrométrie à absorption atomique. Pour Ni et Cu aucune interférence est reconnue. Pour Ni, les concentrations obtenues par AA ont été comparées avec les concentrations obtenues par INAA sur les poudres. Cette comparaison permet de voir si la digestion à l'eau régale extrait également Ni des silicates. Dans le cas des échantillons du Merensky Reef, les valeurs obtenues par AA sont plus basses que celles obtenues par INAA et cela implique que les pyroxènes contiennent entre 560 et 800 ppm de Ni (comparable aux valeurs obtenue par Arndt *et al.*, 2005 et N. Lafrance, thèse en cours). Pour les échantillons du J-M Reef riche en olivine, les valeurs obtenues entre les deux méthodes (INAA et AA) sont très peu différentes, cela implique que le Ni contenu dans les olivines a été partiellement (ou totalement) mis en solution par l'eau régale. Par conséquent, pour ces échantillons la concentration en Ni utilisée est celle obtenue à partir des poudre par INAA. Pour les calculs, les valeurs ont été corrigées pour prendre en compte le Ni présent dans les olivines (voir Chapitre 4, paragraphe 4.9.1).

Table 1.4: *Composition des « boutons » de sulfures.*

Composant	Roche silicatée	Chromite
Echantillon	10 g	10 g
Silice	-	9 g
$NaPO_3$	-	10 g
$NaCO_3$	6 g	15 g
$Li_2B_4O_7$	-	30 g
$Na_2B_4O_7$	12 g	-
Ni*	2.2 g	7.5 g
S*	1.65 g	4.5 g

* Quantité totale prenant en compte la concentration présente dans l'échantillon

1.5.3.2. – Analyses in-situ des sulfures

L'analyse *in-situ* des sulfures (pyrrhotite, pentlandite et chalcopyrite) a été réalisée par ablation laser et spectrométrie de masse inductivement couplée à un plasma (LA-ICP-MS). La description détaillée de la méthode d'analyse est donnée aux chapîtres 3 et 4.

1.5.3.3. – Analyse des minéraux du groupe du platine

La localisation des minéraux du groupe du platine (MGP) présents dans les échantillons a été réalisée à partir de certaines lames minces et/ou sections polies par images en électrons rétrodiffusés et la détermination des MGP a été réalisée par analyse à la microsonde. Cette analyse a été réalisée au Laboratoire de Microanalyse de l'Université Laval à Québec.

1.5.4. – Calculs et modélisations géochimiques

1.5.4.1. – Calculs de la composition de l'assemblage de minéraux sulfurés

La proportion de chaque sulfure (pyrrhotite, pentlandite et chalcopyrite) présent dans un échantillon donné peut être calculée à partir des analyses de roches totales (Ni, Cu, S) et des analyses minérales à la microsonde (Naldrett et Duke, 1980 ; Li *et al.*, 2001).

Le principe de base de ce calcul repose sur les faits suivants:

- le soufre ne se concentrent pas dans les silicates ou les oxydes. Par conséquent, le soufre présent dans les échantillons est attribué aux sulfures.
- la chalcopyrite est le seul sulfure de Cu présent dans nos échantillons et le Cu ne se partage pas dans les silicates ou les oxydes. Par conséquent, Cu peut être entièrement attribué à la chalcopyrite.

- la pentlandite est le seul sulfures de Ni présent dans les échantillons. Pour les échantillons du J-M Reef un facteur de correction a été appliqué pour prendre en compte le Ni dans les olivines.

Les équations utilisées sont décrites dans le Chapitre 3, pour les échantillons du Merensky Reef et dans le Chapitre 4, pour les échantillons du J-M reef.

1.5.4.2. – Calculs du contenu en EGP recalculé à 100% de sulfures

Les métaux (EGP ou métaux de base) sont contenus dans les sulfures. Afin de comparer différentes roches entre elles, il est nécessaire de recalculer la concentration en métaux dans 100% de sulfures. Dans les roches contenant essentiellement de la pyrrhotite, de la pentlandite et de la chalcopyrite, la concentration d'un élément dans les sulfures peut être calculé en utilisant la formule suivante (Barnes et Lightfoot, 2005):

$$C_{(100\%\ sul)} = C_{WR} \times 100 / (2.527 \times C_S + 0.3408 \times C_{Cu} + 0.4715 \times C_{Ni})$$

où $C_{(100\%\ sul)}$ est la concentration d'un élément recalculé à 100% de sulfures ; C_{WR} est la concentration d'un élément dans la roche totale et C_S, C_{Cu} et C_{Ni} sont les concentrations en S, Cu et Ni (en % poids) dans la roche totale.

1.5.4.3. – Calculs de balance de masse des métaux entre sulfures et roches totales

Les analyses *in-situ* des sulfures et les analyses de roches totales permettent de déterminer les proportions de chaque métal présent dans chaque type de sulfures et ainsi d'évaluer qu'elle est la proportion de métaux contenus dans d'autres phases (minéraux du groupe du platine, chromite etc.). Les équations sont détaillées au Chapitre 3 pour les échantillons du Merensky Reef et au Chapitre 4 pour les échantillons du J-M reef.

1.5.4.4. – Modélisation des liquides sulfurés

Les équations de Campbell et Naldrett (1979) et de Brügmann *et al.* (1993) ont été utilisées de deux manières différentes :

- directement pour modéliser les liquides sulfurés ayant ségrégé à partir d'un magma silicaté. Cela implique que la composition (en métaux) du ou des magma(s) silicaté(s) soit relativement bien définie. Cette application directe est utilisée pour modéliser les sulfures du Merensky Reef du complexe du Bushveld (Chapitre 3)
- indirectement en utilisant la composition en S, EGP et métaux de bases des roches totales pour essayer d'évaluer la composition du magma silicaté ayant engendré la concentration des métaux dans les sulfures. Cette inversion est utilisée pour modéliser la composition « théorique » du magma silicaté ayant engendré le J-M reef dans le complexe de Stillwater (Chapitre 4).

1.6 – FORMAT DE LA THESE

Cette thèse est de type « recueil d'articles scientifiques » qui sont au moment du dépôt final soit publiés, soit acceptés, soit soumis pour fin d'évaluation par les journaux.

Le premier article a été publié dans le périodique « Journal of Petrology » en Mai 2006 sous le titre : « 3-D distribution of the sulphide minerals in the Merensky Reef (Bushveld Complex, South Africa) and the J-M Reef (Stillwater Complex, U.S.A) and their relationships to microstructures using X-ray computed tomography» et constitue le Chapitre 2 de cette thèse. Le manuscrit présente les processus physiques (étude de la distribution 3-D des sulfures par microtomographie et l'analyse microstructurale) dans les échantillons du Merensky Reef et de J-

M Reef. Cette étude permet de proposer les premiers fondements d'un modèle de formation des niveaux enrichis en éléments du groupe du platine dans les intrusions litées. Ce modèle de base sera par la suite modifié pour chacun des complexes en prenant en compte les différentes données géochimiques (analyses des EGP et autres métaux dans les roches totales et les sulfures, et analyses des minéraux du groupe du platine réalisées sur les mêmes échantillons).

Le deuxième article a été publié en Aout 2007 dans la revue « Journal of Petrology » sous le titre « Platinum-Group Elements in Sulphide Minerals, Platinum-Group Minerals, and the Whole Rock of the Merensky Reef (Bushveld Complex, South Africa) : Implication for the Formation of the Reef» et constitue le Chapitre 3 de la thèse. Ce manuscrit présente une étude géochimique détaillée de chaque lithologie du Merensky Reef. L'analyse des roches totales, l'analyse *in-situ* des minéraux sulfurés (pentlandite, pyrrhotite, et chalcopyrite) et l'analyse détaillée des minéraux du groupe du platine (analyse d'images et analyses géochimiques qualitatives et/ou quantitatives) permettent de calculer un bilan de masse entre les différentes phases pouvant contenir les EGP. Cette étude permet de préciser le modèle de formation du Merensky Reef en mettant en évidence, deux étapes pour la formation et l'enrichissement, dans les niveaux de chromites en EGP (soit la cristallisation de PGM avant la saturation en soufre, suivie de la percolation après saturation d'un liquide sulfuré enrichi en EGP) et une étape pour la formation les mélanorites enrichies en EGP (soit la percolation d'un liquide sulfuré immiscible enrichis en EGP).

Pour le J-M Reef du Complexe de Stillwater, deux articles ont été rédigés à l'aide des analyses géochimiques et sont insérés dans les Chapitres 4 et 5, respectivement.

Le troisième article a été accepté pour publication en Mai 2007 pour un numéro spécial de la revue « Chemical Geology » intitulé « Chemical Geology Special Volume on Highly Siderophile Elements ». Ce manuscrit fait suite à une présentation réalisée lors d'un cours intensif

intitulé « The 3rd International Workshop on Highly Siderophile Elements » à l'université de Durham (Angleterre) en Juillet 2006. L'article intitulé « Platinum-group elements in sulfide minerals and whole rocks of the J-M Reef (Stillwater complex, U.S.A.): Implication for the formation of the reef» présente les résultats des analyses géochimiques réalisées sur les échantillons d'une section du J-M Reef (mur, zone minéralisée et toit). Ces analyses permettent de mieux contraindre le rôle des sulfures dans la formation du J-M Reef, d'estimer la composition en EGP et métaux de base du magma ayant engendré le J-M Reef, et d'évaluer le rôle des fluides dans la remobilisation et/ou l'enrichissement en Pd et Pt.

Le quatrième article a été accepté pour publication dans la revue « Economic Geology » le en Septembre 2007. L'article s'intitule "Image analysis and composition of platinum-group minerals in the J-M Reef, Stillwater Complex (U.S.A)". Ce manuscrit décrit en détails les minéraux du groupe du platine observés dans les échantillons minéralisés du J-M Reef (Complexe de Stillwater). Cette étude des relations texturales entre les minéraux du groupe du platine et les autres phases telles que les sulfures, les silicates d'altération et/ou la magnétite secondaire permet de préciser le modèle de formation du J-M Reef proposé dans l'article précèdent.

Le Chapitre 6 est une synthèse comparative des différents résultats obtenus lors des différentes analyses réalisées sur les deux complexes. Cela permet de mieux mettre en évidence les similitudes et les différences entre le Merensky Reef et le J-M Reef et d'évaluer lors de la conclusion les processus majeurs qui ont permis l'enrichissement en EGP de ces niveaux.

1.7 – REFERENCES

Alapieti, T. T. et Lahtinen, J. J. 2002. Platinum-group element mineralization in layered intrusions of Northern Finland and the Kola Peninsula, Russia. In: Cabri, L. J. (ed.) Geology, Geochemistry, Mineralogy and Mineral benefication of Platinum Group Element. Special Volume, **54**: 507 - 546.

Arndt, N., Jenner, G., Ohnenstetter, M., Deloule, E. et Wilson, A. 2005. Trace elements in the Merensky Reef and adjacent norites Bushveld Complex South Africa. Mineralium Deposita, **40**(5): 550-575.

Baadsgaard, H. et Mueller, P. A. 1973. K-Ar and Rb-Sr ages of intrusive Precambrien mafic rocks, southern Bearthooth Mountains, Montana and Wyoming. Geological Society of America Bulletin, **84**:3635-3644.

Baker, D. R., Barnes, S.-J., Simon, G. et Bernier, F. 2001. Fluid transport of sulfur and metals between sulfide melt and basaltic melt. Canadian Mineralogist, **39**: 537-546.

Ballhaus, C. et Ryan, C. G. 1995. Platinum-group elements in the Merensky reef. I. PGE in solid solution in base metal sulfides and the down-temperature equilibration history of Merensky ores. Contributions to Mineralogy and Petrology, **122**(3): 241-251.

Ballhaus, C. et Sylvester, P. 2000. Noble Metal Enrichment Processes in the Merensky Reef, Bushveld Complex. Journal of Petrology, **41**(4): 545-561.

Barnes, S.-J. et Maier, W. D. 2002a. Platinum-Group Element Distributions in the Rustenburg Layered Suite of the Bushveld Complex, South Africa. In: Cabri, L. J. (ed.) Geology, Geochemistry, Mineralogy and Mineral benefication of Platinum Group Element. Canadian Institute of Mining, Metallurgy and Petroleum, **Special Volume 54**: 553-580.

Barnes, S.-J. et Maier, W. D. 2002b. Platinum-group elements and microstructures of Normal Merensky Reef from Impala Platinum Mines, Bushveld Complex. Journal of Petrology, **43**: 1, 103-128.

Barnes, S.-J. et Lightfoot, P. C. 2005. Formation of magmatic nickel sulfide deposits and processes affecting their copper and platinum-group element contents. Economic Geology, **100th Anniversary Volume**: 179-213.

Barnes, S. J. et Naldrett, A. J. 1985. Geochemistry of the J-M (Howland) Reef of the Stillwater Complex, Minneapolis Adit Area. I. Sulfide chemistry and sulphide-olivine equilibrium. Economic Geology, **80:** 627-645.

Barnes, S. J. et Hoatson, D. M. 1994. The Munni-Munni Complex, Western-Australia - stratigraphy, structure and petrogenesis. Journal of Petrology, **35**(3): 715-751.

Barnes, S.-J. et Maier, W. D. 1999. The fractionation of Ni, Cu and the noble metals in silicate and sulfide liquid. In: Keays, R. R. L., C.M.; Lightfoot, P.C. and Farrow, C.E.G (ed.) Dynamic Processes in Magmatic Ore Deposits and their application in mineral exploration. Geological Association of Canada, Short Course Notes, **Vol. 13**: 69 - 106.

Bédard, L. P. et Barnes, S.-J. 2002. A comparison of the capacity of FA-ICP-MS and FA-INAA. Journal of Radioanalytical and Nuclear Chemistry, **254**(2): 319-329.

Bédard, L. P. et Barnes, S.-J. 2004. Improved platinum-group element extraction by NiS Fire assay from chromitite ore samples using a flux containing sodium metaphosphate. Geostandards and Geoanalytical Research **28**(2): 311-316.

Boudreau, A. et McCallum, I. S. 1986. Investigations of the Stillwater Complex: III. The Picket Pin Pt/Pd deposit. Economic Geology, **81**: 1953-1975.

Boudreau, A. E. et McCallum, I. S. 1992a. Concentration of platinum-group elements by magmatic fluids in layered intrusions. Economic Geology, **87**(7): 1830-1848.

Boudreau, A. E. et McCallum, I. S. 1992b. Infiltration metasomatism in layered intrusions- an example from the Stillwater Complex, Montana. Journal of Volcanology and Geothermal Research, **52**(1-3): 171-183.

Boudreau, A. E. et Meurer, W. P. 1999. Chromatographic separation of the platinum-group elements, gold, base metals and sulfur during degassing of a compacting and solidifying igneous crystal pile. Contributions to Mineralogy and Petrology, **134**(2-3): 174-185.

Boudreau, A. E., Mathez, E. A. et McCallum, I. S. 1986. Halogen geochemistry of the Stillwater and Bushveld Complexes: Evidence for transport of the platinum-group elements by Cl-rich Fluids. Journal of Petrology, **27**(4): 967-986.

Bow, C., Wolfgram, D., Turner, A. R., Barnes, S. J. et Evans, J. 1982. Investigations of the Howland Reef of the Stillwater Complex, Minneapolis Adit area: stratigraphy, structure, and mineralization. Economic Geology, **77**: 1481-1492.

Brügmann, G. E., Naldrett, A. J. et MacDonald, A. J. 1989. Magma mixing and constitutional zone refinning in the Lac des Iles Complex, Ontario: genesis of platinum-group element mineralization. Economic Geology, **84**: 1557-1573.

Brügmann, G. E., Naldrett, A. J., Asif, M., Lightfoot, P. C., Gorbachev, N. S. and Fedorenko, V. A. 1993. Siderophile and chalcophile metals as tracers of the evolution of the Siberian Trap in the Noril'sk region, Russia. Geochimica et Cosmochimica Acta, **57**(9): 2001-2018.

Cabral, A. R., Lehmann, B., Kwitko, R. et Costa, C. H. C. 2002. The Serra Pelada Au-Pd-Pt Deposit, Carajas Mineral Province, Northern Brazil: Reconnaissance mineralogy and chemistry of very high grade palladian gold mineralization. Economic Geology, **97**(5): 1127-1138.

Cameron, E. M. 1978. The Lower Zone of the eastern Bushveld complex in the Olifants River trough. Journal of Petrology, **19**: 437-462.

Campbell, I. H. et Naldrett, A. J. 1979. The influence of silicate silicate: sulphide ratios on the geochemistry of magmatic sulphides. Economic Geology, **74**: 1503-1505.

Campbell, I. H., Naldrett, A. J. et Barnes, S. J. 1983. A model for the origin of the platinum-rich sulfide horizons in the Bushveld and Stillwater Complexes. Journal of Petrology, **24**(2): 133-165.

Capobianco, C. J. et Drake, M. J. 1990. Partitioning of ruthenium, rhodium, and palladium between spinel and silicate melt and implications for platinum group element fractionation trends. Geochimica et Cosmochimica Acta, **54**(3): 869-874.

Capobianco, C. J., Hervig, R. L. et Drake, M. J. 1994. Experiments on crystal/liquid partitioning of Ru, Rh and Pd for magnetite and hematite solid solutions crystallized from silicate melt. Chemical Geology, **113**(1-2): 23-43.

Carlson, W. D. et Denison, C. 1992. Mechanisms of Porphyroblast Crystallization : Results from High-Resolution Computed X-Ray Tomography. Science, **257**(5074), 1236-1239.

Carr, H. W., Groves, D. I. et Cawthorn, R. G. 1994. Controls on the distribution of Merensky Reef potholes at the Western Platinum Mine, Bushveld Complex, South Africa: Implictions for disruptions of the layering and potholes formation in the complex. South African Journal of Geology, **97**: 431-441.

Cawthorn, R. G. 2002. Platinum-group element deposits in the Bushveld Complex, South Africa. In: Cabri, L. J. (ed.) Geology, Geochemistry, Mineralogy and Mineral benefication of Platinum Group Element. Canadian Institute of Mining, Metallurgy and Petroleum, **Special Volume 54**: 389 - 429.

Czamanske, G. K. et Zientek, G. K. 1985. The Stillwater Complex, Montana : geology and guide. (ed.) Butte, Montana: Montana College of Mineral Science and Technology, Special publication / Montana Bureau of Mines and Geology, **no. 92**: 396.

Denison, C. et Carlson, W. D. 1997. Three-dimensional quantitative textural analysis of metamorphic rocks using high-resolution computed X-ray tomography.2. Application to natural samples. Journal of Metamorphic Geology, **15**(1), 45-57.

Denison, C., Carlson, W. D. et Ketcham, R. A. 1997. Three-dimensional quantitative textural analysis of metamorphic rocks using high-resolution computed X-ray tomography .1. Methods and techniques. Journal of Metamorphic Geology, **15**(1): 29-44.

Fleet, M. E. et Wu, T.-W. 1993. Volatile transport of platinum-group elements in sulfide-chloride assemblages at 1000°C. Geochimica et Cosmochimica Acta, **57**(15): 3519-3531.

Grokhovskaya, T. L., Bakaev, G. F., Shelepina, E. P., Lapina, M. I., Laputina, I. P. et Muravitskaya, G. N. 2000. PGE mineralization in the Vuruchuaivench gabbronorite Massif, Monchegorsk Pluton (Kola Peninsula, Russia). Geology of Ore Deposits, **42**: 133-146.

Hall, A. L. 1932. The Bushveld Igneous Complex in the central Transvaal. Geological society of South Africa, Memoir, **28**: 544 pp.

Hanley, J. J., Mungall, J. E. et Spooner, E. T. C. 2005a. Fluid and melt inclusion evidence for platinum-group element transport by high salinity fluids and halide melts below the J-M Reef, Stillwater Complex, Montana, U.S.A. 10th International Platinum Symposium "Platinum-Group Elements - from Genesis to Beneficiation and Environmental Impact", Törmänen, T. O. & Alapieti, T. T., Oulu, Finland, Geological Survey of Finland, **Extended Abstract**: 94-97.

Hanley, J. J., Pettke, T., Mungall, J. E. et Spooner, E. T. C. 2005b. The solubility of platinum and gold in NaCl brines at 1.5 kbar, 600 to 800°C: A laser ablation ICP-MS pilot study of synthetic fluid inclusions. Geochimica et Cosmochimica Acta, **69**(10): 2593-2611.

Harmer, R. E. 2004. The Volspruit PGE-Ni reef: Platinum mineralization in the Lower Zone south of Mokopane (Potgietersrus), South Africa. Geosciences Africa, Johannesburg, **Abstract**: 256-257.

Harmer, R. E. et Armstrong, R. A. 2000. Duration of Bushveld Complex (seno lato) magmatism: Constraints from new SHRIMP zircon chronology. Workshop on the Bushveld Complex, Gethane Lodge, Burgersfort., abstracts and program.

Haughton, D. R., Roeder, P. L. et Skinner, B. J. 1974. Solubility of sulfur in mafic magmas. Economic Geology, **69**(4): 451-467.

Helz, R. T. 1985. Compositions of fine-graines mafic rocks from sills and dikes associated with the Stillwater Complex. In: Czamanske, G. K. and Zientek, M. L. (ed.) The Stillwater Complex, Montana : geology and guide. Butte, Montana: Montana Bureau of Mines and Geology, Special Publication, **no. 92**: 21-32.

Holwell, D. et McDonald, I. 2006. Petrology, geochemistry and the mechanisms determining the distribution of platinum-group element and base metal sulphide mineralisation in the Platreef at Overysel, northern Bushveld Complex, South Africa. Mineralium Deposita, 41(6):575-598.

Hsu, L. C., Lecherler, P. J. et Nelson, J. H. 1991. Hydrothermal solubility of palladium in chloride solutions from 300 °C to 700°C: Preliminary experimental results. Economic Geology, **86**: 422-427.

Ketcham, R. A. et Carlson, W. D. 2001. Acquisition, optimization and interpretation of X-ray computed tomographic imagery: applications to the geosciences. Computers and Geosciences, **27**(4): 381-400.

Ketcham, R. A. et Iturrino, G. J. 2005. Nondestructive high-resolution visualisation and measurement of anisotropic effective porosity in complex lithologies using high-resolution X-ray computed tomography. Journal of Hydrology, **302**: 92-106.

Ketcham, R. A., Meth, C., Hirsch, D. M. et Carlson, W. D. 2005. Improved methods for quantitative analysis of three-dimensional porphyroblastic textures. Geosphere, **1**: 42-59.

Kingston, G. A. et El-Dosuky, B. T. 1982. A contribution on the Platinum-Group Mineralogy of the Merensky Reef at the Rustenburg Platinum Mine. Economic Geology, **77**(6): 1367-1384.

Kinloch, E. D. 1982. Regional Trends in the Platinum-Group Mineralogy of the Critical Zone the Bushveld Complex, South-Africa. Economic Geology, **77**(6): 1328-1347.

Kinloch, E. D. et Peyerl, W. 1990. Platinum-Group Minerals in Various Rock types of the Merensky Reef: Genetic Implications. Economic Geology, **85**: 537-555.

Kyle, J. R. et Ketcham, R. A. 2003. In Situ Distribution of Gold in Ores using High-Resolution X-Ray Computed Tomography. Economic Geology, **98**(8): 1697-1701.

Kyle, J. R., Ketcham, R. A. et Mote, A. S. 2004. Contributions of high resolution X-ray computed tomography to ores studies. In: Muhling, J. (ed.) Extended Abstracts, Predictive Mineral Discovery Under Cover. University of Western Australia: 387-390.

Lee, C. A. 1983. Trace and Platinum-Group Element Geochemistry and the Development of the Merensky Unit of the Western Bushveld complex. Mineralium Deposita, **18** : 173-190.

Leeb-Du Toit, A. 1986. The Impala Platinum Mines. In: Anhaeusser, C. R. & Maske, S. (ed.) Mineral Deposits of Southern Africa. Johannesburg: Geological Society of South africa, I and II: 1901-1106.

Li, C. et Naldrett, A. J. 1993. Sulfide capacity of the magma: A quantitative model and its implication to the formation of the sulfide ores at Sudbury. Economic Geology, **88**: 1253-1260.

Li, C. et Ripley, E. M. 2005. Empirical equations to predict the sulfur content of mafic magmas at sulfide saturation and applications to magmatic sulfide deposits. Mineralium Deposita,**46** : 218-240.

Li, C., Maier, W. D. et de Waal, S. A. 2001a. The role of magma mixing in the genesis of PGE mineralization in the Bushveld Complex: Thermodynamic calculations and new interpretations. Economic Geology, **96**(6): 1487-1487.

Li, C., Maier, W. D. et de Waal, S. A. 2001b. Magmatic Ni-Cu versus PGE deposits: Contrasting genetic controls and exploration implications. South African Journal of Geology, 104(4): 309.

Liu, Y., Samaha, N.-T. et Baker, D. R. 2007. Sulfur concentration at sulfide saturation (SCSS) in magmatic silicate melts. Geochimica Cosmochimica Acta, 71(7): 1783-1799.

Lorand, J. P. 1990. Are spinel lherzolite xenoliths representative of the abundance of sulfur in the upper mantle? Geochimica Cosmochimica Acta, **54**(5): 1487-1492.

Maier, W. D. 2005. Platinum-group element (PGE) deposits and occurrences: Mineralization styles, genetic concepts, and exploration criteria. Journal of African Earth Sciences, 41: 165-191.

Maier, W. D. 2006. Mineral deposits of the Bushveld Complex. Short Course, University of Western Australia, Perth, 113 pp.

Maier, W. D., Barnes, S. J., Gartz, V. et Andrews, G. 2003. Pt-Pd reefs in magnetites of the Stella layered intrusion, South Africa: A world of new exploration opportunities for platinum group elements. Geology 31(10): 885-888.

Manyeruke, T. D., Maier, W. D. et Barnes, S.-J. 2005. Major and trace element geochemistry of the Platreef on the farm Townlands, northern Bushveld Complex. South African Journal of Geology, 108(3): 381-396.

Marschallinger, R. 1998. A method for three-dimensional reconstruction of macroscopic features in geological materials. Computers and Geosciences, **24**(9): 875-883.

Mavrogenes, J. A. et O'Neill, H. S. C. 1999. The relative effects of pressure, temperature and oxygen fugacity on the solubility of sulfide in mafic magmas. Geochimica Cosmochimica Acta, 63(7-8): 1173-1180.

McCallum, I. S., Raedeke, L. D. et Mathez, E. A. 1980. Investigations of the Stillwater Complex: Part I. Stratigraphy and Structure of the Banded Zone. American Journal of Science, **280-A**: 59-87.

McCallum, M. E., Loucks, R. R., Carlson, R. R., Cooley, E. F. et Doerge, T. A. 1976. Platinum metals associated with hydrothermal copper ores of the New Rambler Mine, Medicine Bow Mountains, Wyoming. Economic Geology, 71(7): 1429-1450.

Naldrett, A. J. 1969. A Portion of System Fe-S-O between 900°C and 1080 °C and Its Application to Sulfide Ore Magmas. Journal of Petrology, 10(2): 171-201.

Naldrett, A. J. 1989. Magmatic Sulfide Deposits. (ed.) Oxford University Press, 189 pp.

Naldrett, A. J. et Duke, J. M. 1980. Platinum metals in magmatic sulfides ores. Science, **208**: 1417-1428.

Naldrett, A. J. et von Gruenewaldt, G. 1989. Association of platinum-group elements with chromitite in layered intrusions and ophiolite complexes. Economic Geology, **84**: 180-187.

Naldrett, A. J., Gasparrini, E. C., Barnes, S. J., Von Gruenewaldt, G. et Sharpe, M. R. 1986. The Upper Critical Zone of the Bushveld Complex and the origin of Merensky-Type ores. Economic Geology, 81(5): 1105-1117.

Nunes, P. D. et Tilton, G. R. 1971. Uranium-lead ages of minerals from the Stillwater Complex and associated rocks, Montana. Geological Society of America Bulletin, **82**: 2231-2250.

Oberthür, T. 2002. Platinum-group element mineralization of the Great Dyke, Zimbabwe. Geology, Geochemistry, Mineralogy and Mineral benefication of Platinum Group Element **Special Volume 54**: 483 - 506.

Olivo, G. R., Gauthier, M., Williams-Jones, A. E. et Levesque, M. 2001. The Au-Pd mineralization at the Conceicao Iron Mine, Itabira District, Southern Sao Francisco Craton, Brazil: An Example of a Jacutinga-Type Deposit. Economic Geology, 96(1): 61-74.

Page, N. J. 1977. Stillwater Complex, Montana: rock succesion, metamorphism and structure of the complex and adjacent rocks. U.S. Geological Survey Professional paper, 999.

Poulson, S. R. et Ohmoto, H. 1990. An evaluation of the solubility of sulfide sulfur in silicate melts from experimental-data and natural samples. Chemical Geology, 85(1-2): 57-75.

Premo, W. R., Helz, R. T., Zientek, M. L. & Langston, R. B. 1990. U-Pb and Sm-Nd ages for the Stillwater Complex and its associated sills and dikes, Beartooth Mountains, Montana: Identification of a parent magma? Geology, **18**: 1065-1068.

Prichard, H. M., Barnes, S.-J., Maier, W. D. et Fisher, P. C. 2004. Variations in the nature of the platinum-group minerals in a cross-section through the Merensky Reef at Impala Platinum: Implications for the mode of formation of the reef. Canadian Mineralogist, 42: 423-437.

Righter, K., Campbell, A. J., Humayun, M. et Hervig, R. L. 2004. Partitioning of Ru, Rh, Pd, Re, Ir, and Au between Cr-bearing spinel, olivine, pyroxene and silicate melts. Geochimica et Cosmochimica Acta, 68(4): 867-880.

Ripley, E. A. 1999. Systematics of sulfur and oxygen isotopes in mafic igneous rocks and related Cu-Ni-PGE mineralization. In: Keays, R. R., Lesher, C. M., Lighfoot, P. C. and Farrow, C. E. G. (ed.) Geological Association of Canada, Short course Notes, **13**: 133-158.

Sattari, P., Brenan, J. M., Horn, I. et McDonough, W. F. 2002. Experimental constraints on the sulfide- and chromite-silicate melt partitioning behavior of rhenium and platinum-group elements. Economic Geology, **97**(2): 385-398.

Vermaak, C. F. 1976. Merensky Reef - Thoughts on its environment and genesis. Economic Geology, **71**(7): 1270-1298.

Viljoen, M. J. 1999. The nature and origin of the Merensky Reef of the western Bushveld Complex based on geological facies and geophysical data. South African Journal of Geology, **102**(3): 221-239.

Viljoen, M. J. et Hieber, R. 1986. The Rustenburg section of the Rustenburg Platinum Mines Limited, with reference to the Merensky Reef. In: Anhaeusser, C. R. & Maske, S. (ed.) Mineral Deposits of Southern Africa. Johannesburg: Geological Society of Southern Africa, II: 1107-1034.

VonGruenewaldt, G. 1979. A review of some recent concepts of the Bushveld Complex, with particular reference to sulfide mineralization. Canadian Mineralogist, **17**: 233-256.

Wendlandt, R. F. (1982). Sulfur saturation of basalt and andesite melts at high pressures and temperatures. American Mineralogist, **67**: 877-885.

Willmore, C. C., Boudreau, A. E. et Kruger, F. J. 2000. The halogen geochemistry of the Bushveld Complex, Republic of South Africa: Implications for chalcophile element distribution in the lower and critical zones. Journal of Petrology, **41**(10): 1517-1539.

Wood, S. A. 2002. The aqueous geochemistry of the platinum-group elements with applications to ore deposits. In: Cabri, L. J. (ed.) Geology, Geochemistry, Mineralogy and Mineral benefication of Platinum Group Element. Canadian Institute of Mining, Metallurgy and Petroleum, **Special Volume 54**: 211-249.

Zientek, M. L. et Oscarson, R. L. 1986. Textural association of platinum-group minerals from the J-M Reef, Stillwater Complex, Montana. U.S. Geological Survey Circ. **995**: 75-76.

Zientek, M. L., Czamanske, G. K. et Irvine, T. N. 1985. Stratigraphy and nomenclature for the Stillwater Complex. In: Czamanske, G. K. & Zientek, M. L. (ed.) The Stillwater Complex, Montana : geology and guide. Butte, Montana: Montana Bureau of Mines and Geology, Special Publication, **no. 92**: 21-32.

Zientek, M. L., Cooper, R. W., Corson, S. R. et Geraghty, E. P. 2002. Platinum-group element mineralization in the Stillwater Complex, Montana. In: Cabri, L. J. (ed.) Geology, Geochemistry, Mineralogy and Mineral benefication of Platinum Group Element. Canadian Institute of Mining, Metallurgy and Petroleum, **Special Volume 54**: 459 - 481.

CHAPITRE 2

3-D DISTRIBUTION OF SULPHIDE MINERALS IN THE MERENSKY REEF (BUSHVELD COMPLEX, SOUTH AFRICA) AND THE J-M REEF (STILLWATER COMPLEX, USA) AND THEIR RELATIONSHIP TO MICROSTRUCTURES USING X-RAY COMPUTED TOMOGRAPHY.

BELINDA GODEL, SARAH-JANE BARNES & WOLFGANG D. MAIER

UNIVERSITE DU QUEBEC A CHICOUTIMI, SCIENCES DE LA TERRE, CHICOUTIMI, G7H 2B1, CANADA

Journal of Petrology, 2006, Vol. 47, pp. 1853- 1872

2.1 – RESUMÉ

Les grandes intrusions mafiques et ultramafiques peuvent dans certains cas contenir des niveaux enrichis en éléments du groupe du platine (EGP). Dans la plupart des cas, les EGP sont associés à des sulfures disséminés dans les roches. Dans ce travail nous avons étudié la distribution en trois dimensions (3-D) des minéraux sulfurés dans deux échantillons orientés, l'un provenant du Merensky Reef (Complexe du Bushveld, Afrique du Sud) et l'autre du J-M Reef (Complexe de Stillwater, Montana, USA). Le but de l'étude est de tester l'hypothèse selon laquelle les sulfures cristallisent à partir d'un liquide sulfuré enrichi en métaux de base qui percole vers le bas lors de la compaction des cumulats.

La distribution en 3-D des sulfures a été quantifiée en utilisant la microtomographie au rayon X (CT Scan) et en effectuant une analyse microstructurale en sections polies orientées par rapport à la paléo-verticale. Pour l'échantillon du Merensky Reef, l'analyse et la mesure des angles dihédraux entres les sulfures et les silicates ou les oxydes (chromite) a également permis de déterminer la topologie du liquide sulfuré dans les différentes lithologies. Comme l'échantillon de J-M Reef est altéré, aucune mesure d'angle n'a pu être réalisée (le contact exact entre silicate primaire/sulfures étant difficilement visible).

L'échantillon de Merensky Reef est composé de cinq lithologies distinctes. De la base au sommet, on retrouve : (i) un niveau d'anorthosite ; (ii) un niveau de chromite d'environ 1 cm d'épaisseur ; (iii) un niveau de mélanorite pegmatoïdale d'une dizaine de centimètres d'épaisseur ; (iv) d'un second niveau de chromite d'environ 1.5 cm et finalement (v) d'un niveau de mélanorite. L'échantillon de J-M Reef est une gabbronorite à olivine.

Dans le Merensky Reef et le J-M Reef, les sulfures forment des réseaux connectés en 3-D et remplissent des dilatances formées lors de la compaction des cumulats. Ces dilatances facilitent la percolation vers le bas du liquide sulfuré.

Une étude plus détaillée du Merensky Reef montre que dans la mélanorite, le contenu en sulfures augmente de haut en bas et atteint une valeur maximale juste au dessus des niveaux de chromite (inférieur et supérieur). Dans les niveaux de chromite, la connectivité des liquides sulfurés est négligeable. Par conséquent, les niveaux de chromite agiraient comme des barrières limitant la percolation vers le bas des liquides sulfurés dans la pile de cumulats. Ces résultats permettent de partiellement expliquer l'enrichissement en EGP des niveaux de chromitite et la faible quantité de sulfure présente sous les niveaux de chromites dans l'anorthosite.

2.2 – ABSTRACT

Large mafic-ultramafic layered intrusions may contain layers enriched in platinum-group elements (PGE). In many cases, the PGE are hosted by disseminated sulphides. We have investigated the distribution of the sulphides in 3-D in two oriented samples of the Merensky Reef and the J-M Reef. The aim of the study was to test the hypothesis that the sulphides crystallized from a base metal sulphide liquid that percolated through the cumulate pile during compaction. Distribution of sulphides was quantified using: (i) X-Ray Computed Tomography; (ii) microstructural analysis of polished thin sections oriented parallel to the paleovertical; (iii) measurement of dihedral angles between sulphides and silicates or oxides. In the Merensky Reef and the J-M Reef, sulphides are connected in 3-D and fill paleovertical dilatancies formed during compaction, which facilitated the downward migration of sulphide liquid in the cumulate. In the melanorite of the Merensky Reef, the sulphide content increases from top to bottom, reaching a maximum value above the underlying chromitite layer. In the chromitite layers sulphide melt connectivity is negligible. Thus, the chromitite may have acted as a filter, preventing extensive migration of sulphide melt downwards into the footwall. This could partially explain the enrichment in PGE of the chromitite layer and the observed paucity of sulphides in the footwall.

2.3 – INTRODUCTION

Large mafic and ultramafic layered intrusions, such as the Bushveld Complex (South Africa) or the Stillwater Complex (Montana, U.S.A), contain layers enriched in platinum-group elements (PGE) that are called "reefs" (a mining term, which refers to a layer of rock containing mineable grades of metal). Exactly how these layers formed is still much debated with various authors emphasizing different processes. One school of thought suggests that the PGE crystallize directly from magma in the form of platinum-group minerals (PGM) which accumulate on the crystal pile (Hiemstra, 1979) ; another suggests that the PGE were collected by a sulphide liquid that segregated from the magma and accumulated on the cumulate pile (Campbell *et al.*, 1983; Naldrett *et al.*, 1986); some authors suggest that the PGE were collected by a fluid migrating upwards through the cumulate pile during compaction and that this fluid precipitated the sulphides and the PGE at the level of the reefs (Boudreau and McCallum, 1992; Willmore *et al.*, 2000); finally, some authors have noted that the silicates and sulphides of some reefs have undergone low temperature alteration, which may have modified the base metal and possibly the PGE concentrations in the reef (Li *et al.*, 2004) . These processes are not necessarily mutually exclusive. For example, Brenan and Rose (2002) suggested a modification of the PGM collection model, with PGM crystallizing first, followed by base metal sulphides infiltrating the crystal pile and absorbing the PGM. Barnes and Maier (2002) modified the sulphide collection model by suggesting that the PGE-rich sulphide liquid percolated through the crystal pile along dilatancies formed during compaction. In order to explain the extreme enrichment in IPGE (the iridium subgroup of PGE: Os, Ir and Ru) and Pt found in the Merensky Reef chromitite layers, Prichard *et al.* (2004) added a step to this model which requires the upward migration of S-undersaturated fluid or magma. This fluid partially dissolved the accumulated base metal sulphides in the chromitite layer creating a PGE-enriched residual sulphide. Although the exact mechanism of

how PGE collection occurs remains unclear, it is clear that the PGE are found in base metal sulphides and in PGM that are associated with the sulphides (Kinloch, 1982; Ballhaus and Sylvester, 2000; Zientek *et al.*, 2002).

In order to better understand how the base metal sulphides and, hence, the reefs form we have investigated the distribution of sulphides in two oriented reef samples: one of the Merensky Reef at Rustenburg Platinum Mine (Bushveld Complex, South Africa); and one of the J-M Reef at Stillwater Mine (Stillwater Complex, Montana, U.S.A). The distribution and quantity of the sulphide minerals was determined in three dimensions (3-D) using X-ray computed tomography (X-ray CT). The relationship between the sulphide distribution and microstructures was investigated by examining oriented polished thin sections from these samples. In the following text, "vertical" corresponds to the paleo-vertical direction.

2.4 - GEOLOGICAL SETTINGS

2.4.1 - Bushveld Complex

The Bushveld Complex (Fig. 2.1a) is by far the largest layered intrusion in the world. The complex is 2054 +/- 2.8 Ma old (Harmer and Armstrong, 2000) and has undergone very little deformation, or metamorphism, after solidification of its crystal pile. The ultramafic and mafic rocks of the Bushveld Complex are referred to as the Rustenburg Layered Suite (South African Committee for Stratigraphy, 1980). The Suite is composed of five units (Fig. 2.1b), from bottom to top: the Marginal Zone; the Lower Zone; the Critical Zone; the Main Zone and the Upper Zone. Although there are a number of layers enriched in PGE within the intrusion only three are sufficiently enriched in PGE, and continuous enough, to be called reefs: the Merensky Reef, the Upper Group Chromitite 2 (UG-2) and the Platreef. The Platreef is situated at the base of the

intrusion, whereas the Merensky Reef and UG-2 chromitite are located in the upper part of the Critical Zone (Fig. 2.1b), some 2 km above the base. The sample of Merensky Reef (MR) investigated here represents normal Merensky Reef and was collected underground at Rustenburg Platinum Mines (Fig. 2.1a), in the south-western portion of the Bushveld Complex. A detailed description of the Rustenburg Layered Suite at Rustenburg Platinum Mines is given by Viljoen & Hieber (1986).

2.4.2 - Stillwater Complex

The 2705 +/- 4 Ma (Premo *et al.*, 1990) Stillwater Complex (Fig. 2.2a) is a layered ultramafic to mafic intrusion. Its original size is unknown as only a part of the complex is exposed along the northern margin of the Bearthtooth uplift of south-western Montana (Page and Zientek, 1985). The layered rocks are divided into five series (Fig. 2.2b), from bottom to top: the Basal series is composed of orthopyroxene cumulates; the Ultramafic series contains various proportions of cumulus olivine, orthopyroxene and chromite; the Lower-, Middle- and Upper-Banded series contain mainly cumulus plagioclase with minor amounts of olivine in places (McCallum *et al.*, 1980; Zientek *et al.*, 1985; Zientek *et al.*, 2002). As is the case in the Bushveld Complex, the Stillwater Complex contains several layers enriched in PGE, amongst them the John Manville Reef (J-M Reef) and the Picket Pin deposit. The sample studied in this work is from the J-M Reef at Stillwater Mine (Fig. 2.2a). The J-M Reef is associated with an olivine-bearing cumulate (OB-1) of the Lower Banded series (Barnes and Naldrett, 1985; Turner *et al.*, 1985; Zientek *et al.*, 1985; Zientek *et al.*, 2002). Unlike the Bushveld Complex, the Stillwater Complex has undergone regional deformation and metamorphism (Zientek *et al.*, 2002).

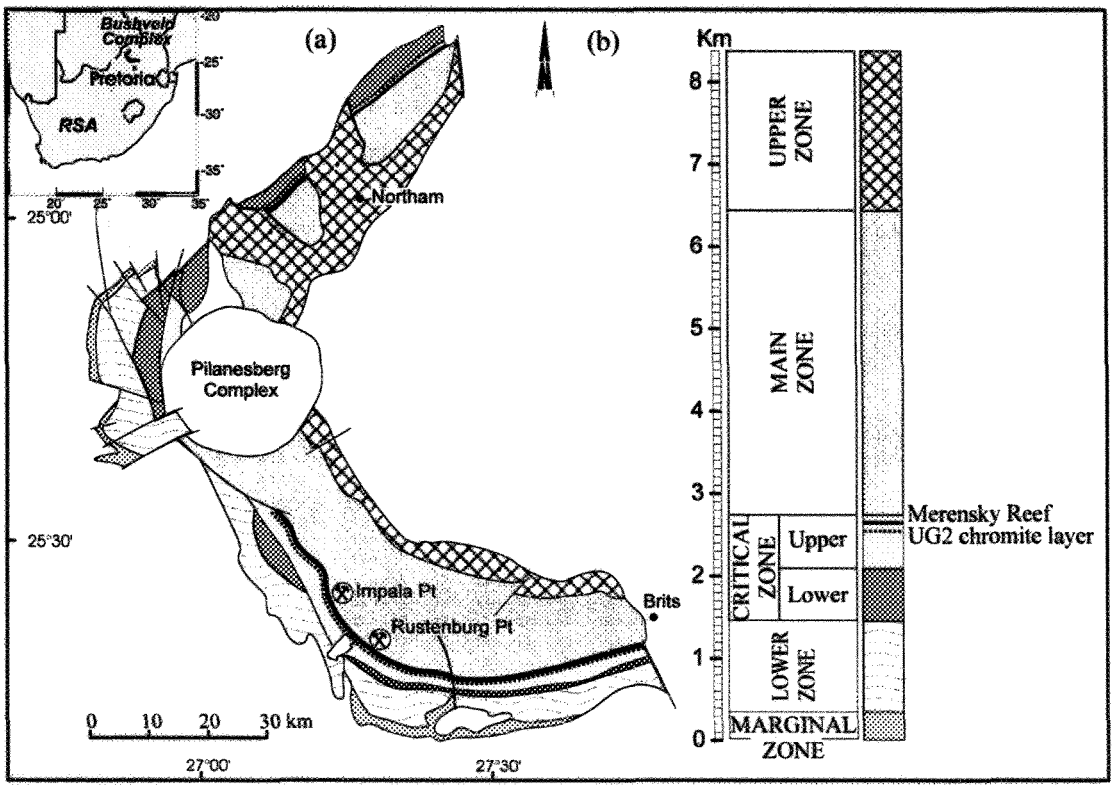

Figure 2.1: Details of the geology of the western lobe of the Bushveld Complex, Republic of South Africa (RSA).

(a) Simplified geological map of the western lobe of the Bushveld Complex (modified after Von Gruenewaldt *et al.*, 1986 and 1989).
(b) Generalized stratigraphy of the Bushveld Complex (modified after Eales & Cawthorn, 1996).

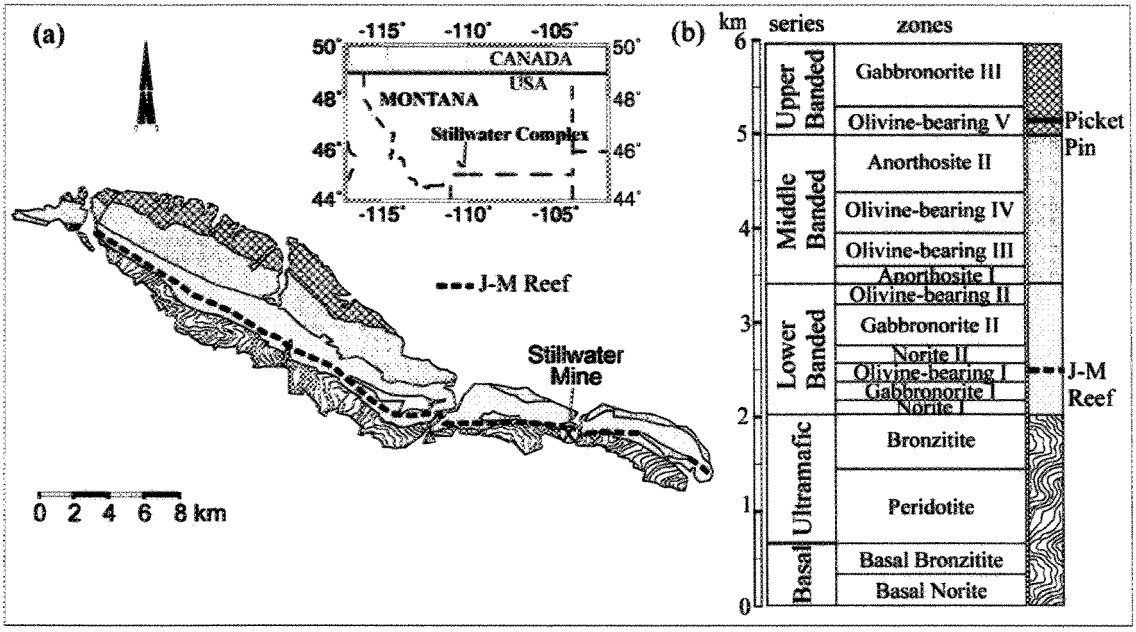

Figure 2.2: Details of the geology of the Stillwater Complex, Montana, U.S.A.

(a) Simplified geological map of the Stillwater Complex (modified after McCallum *et al.*, 1980 and Zientek *et al.*, 2002).
(b) Generalized stratigraphy of the Stillwater Complex (modified after Zientek *et al.*, 2002).

2.5 – METHODS

2.5.1 - X-Ray Computed Tomography

2.5.1.1 – Principle and methods

X-ray Computed Tomography (X-ray CT) is an entirely non-destructive technique which allows visualization and reconstruction of the internal structure of solid objects in 3-D. Initially, X-ray CT was developed and used as a medical imaging technique (Hounsfield, 1973). However, this technique can also be used for qualitative and quantitative analysis of geological materials (Ketcham and Carlson, 2001) such as metamorphic rocks (Carlson and Denison, 1992; Denison and Carlson, 1997; Denison *et al.*, 1997), sedimentary rocks (Flisch and Becker, 2003; Michaud *et al.*, 2003), soils (Delerue *et al.*, 2003), rare meteorites (Kondo *et al.*, 1997), fossils (Brochu, 2000) or ores (Kyle and Ketcham, 2003; Kyle *et al.*, 2004). The details of the principle and the functioning of the X-ray CT have been developed in many papers (Denison and Carlson, 1997; Denison *et al.*, 1997; Ketcham and Carlson, 2001; Mees *et al.*, 2003; Ketcham and Iturrino, 2005) and only a brief description is given in the following. In the present study, the samples were scanned at the INRS (Institut Nationale de la Recherche Scientifique, Quebec, Canada) using an X-ray CT scanner "Siemens Somatom Volume Access". The CT system is described in Fig. 2.3. An important aspect of this scanner is that samples with a length of several 10s of centimetres can be scanned. The scanning unit (more precisely, the tubes) can be operated at maximum power for a limited time only. This reduces its capacity to scan a large sample at high resolution. Consequently, due to the size of the Merensky Reef sample and in order to obtain a better resolution, data for this sample were collected in two continuous steps (the second scan starting at the position of the last slice of the first scan incremented by one slice thickness). The X-ray tubes were operated at 140 kv accelerating potential and 112 mA current for the J-M Reef and at 140 kv accelerating potential and 245 mA current for the Merensky Reef. The images were

reconstructed using a filtered back-projection and corrections to reduce the effect of beam-hardening or ring artefact (see further description) at INRS. The output images were then digitized as DICOM (Digital Imaging and Communication in Medicine) formatted 16-bit files with 512 x 512 pixels. Merensky Reef voxels (*i.e.* pixels in 3-D) are 0.25 mm x 0.25 mm x 1 mm, and J-M Reef voxels are 0.125 mm x 0.125 mm x 0.5 mm, where the larger dimension is the vertical one. In this study, 305 slices were obtained for the Merensky Reef, and 219 slices were obtained for the J-M Reef. Each slice is a map of the variation of X-ray attenuation across the sample. X-rays are attenuated through the sample of rock following the Beer-Lambert Law (Boespflug *et al.*, 1995)

$$I = I^{\circ} e^{-\mu h}$$

where I° is the initial intensity of the incident X-ray beam, I is the intensity measured by the detector, h is the sample thickness and μ is a linear attenuation coefficient which depends on the average atomic number and the density of the material. The attenuation coefficient of the sample (μs) is expressed in Tomographic Intensity (TI), or in CT number (CT) (Hounsfield, 1973)

$$TI = (\mu s / \mu w - 1) \times 1000$$

where μw is water coefficient attenuation. Using the CT scanner settings, the variation of X-ray attenuation shows the distribution of specific minerals across the sample. All further image processing, analysis and stacking for the determination and quantification of sulphide mineral distribution was performed using 3D-Doctor (Able Software Corp.), IDL (Interactive Data Language, Research Systems Inc.) and GMT (Wessel and Smith, 1998) software.

2.5.1.2 - Definition of sulphide mineral boundaries

For each slices, the sulphide mineral boundaries were defined using a segmentation (threshold) value. In our case, the sulphide minerals are an intergrowth of pyrrhotite, pentlandite

and chalcopyrite (the proportions of each phase vary as a function of the lithology, but on average it contain ~40% pyrrhotite, ~40% pentlandite and 20% chalcopyrite). These sulphides contain also significant amount (up to 800 ppm) of PGE in solid solution (Ballhaus and Ryan, 1995; Ballhaus and Sylvester, 2000). In order to correctly access the sulphide distribution in both samples, CT scan results were compared with the corresponding thin sections (*i.e.* the same minerals). Profiles of CT number were determined across known (*i.e.* observed both on slices and corresponding thin sections) sulphides and others minerals of various sizes. Examples of profiles obtained for the minerals are given in Fig. 2.4. All results for sulphides were then compared and an optimal segmentation value for our sulphides was defined using the minimum CT number obtained for the sulphides as lower boundary. This threshold value is 1540, all minerals with a CT number higher than 1540 are sulphides. Consequently, the volume of sulphides in our sample was calculated by summing all voxels with a CT number above 1540 (see further description).

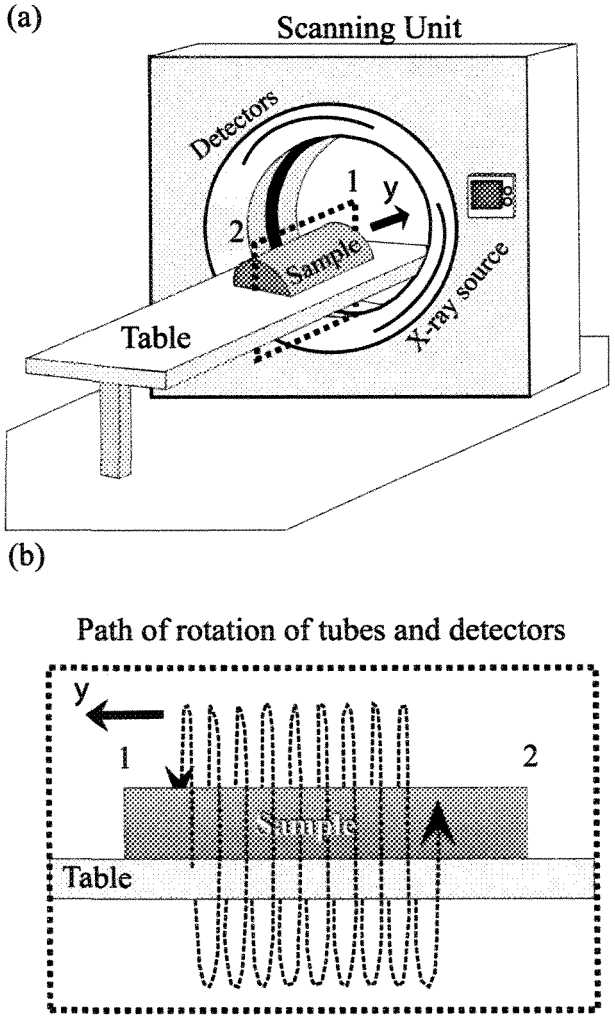

Figure 2.3: Schematic diagram of the X-ray Computed Tomography (CT) scanner.

(a) The CT system comprises principally: a scanning unit composed of detectors and X-ray sources (tubes); a table where samples were positioned to undergo scanning.
(b) The sample on the table is moved through the scanner in the y direction while the gantry performs multiple 360° rotation around the sample. Consequently, X-rays trace a spiral around the sample and produce a data volume created by a multitude of 3-D pixels called "voxels". Images ("slices") are generated using special reconstruction principles and filtering techniques. The 3-D view is obtained by stacking all the slices.

2.5.1.3 - Artefacts and uncertainty on measurements

X-ray computed tomography produce sometimes images in which some peculiar features are artefacts (beam-hardening, ring artefacts or partial-volume effects for examples). The characteristics of these artefacts have been reviewed in detail in the literature (Denison *et al.*, 1997; Ketcham and Carlson, 2001; Mees *et al.*, 2003) and no further description is presented here. Beam-hardening and ring artefacts were minimized by using a correction and filter during the reconstruction and the post-processing at INRS. Sulphide minerals and silicates (essentially pyroxenes and plagioclases) considered in this work have very different attenuation values and the sulphides are randomly oriented. Following Johns et al. (1993) and Wellington & Vinegar (1987), the errors due to partial-volume effects can be neglected without major consequence on the measurements. In order to estimate the uncertainties on the measurements of the sulphide volume, final results obtained by CT scan were compared with the macroscopic and microscopic observations (Fig. 2.5). The CT image of sulphides (the inset on Fig. 2.5b) was compared with their corresponding images in the thin section (Fig. 2.5c). First, the number of pixels with CT number > 1540 (*i.e.* corresponding to the sulphide) was calculated, and then this result was compared to the area enclosed by the sulphide in the thin section. The uncertainty on measurement was calculated by comparing the number of the pixels obtained in both cases. This uncertainty on the measurement of sulphide volume by the CT scan is ~5 %. Another uncertainty on the sulphide volume calculation arise from small sulphides (*i.e.* having a size lower than the voxel size, see below) which were not include in the calculation. The sulphides observed in the thin sections of all lithologies (except the anorthosite) are bigger than the voxel size (in ~90% of the cases). In the anorthosite, a few sulphides (~0.1 %) were observed in thin section but were usually not identified and measured by the CT scan analysis. As these sulphides in the anorthosite are very small and rare, they have no real effect on sulphide volume calculation. However, in

order to take into account the small (lower than voxel size) sulphides, the uncertainty on measurement was overestimated to 10% (Table 2.1 and 2.2).

2.5.2 - Analysis of microstructures

In order to determine whether there is a relationship between sulphide distribution and microstructures in the two samples, oriented polished thin sections were examined with an optical microscope. For the MR sample, thin sections were oriented so that the long axis corresponds to the paleovertical. For the J-M Reef sample, the paleovertical was represented by the short axis (the long axis corresponding to the width of the drill-core). The presence and orientation of the optical microstructures were then compared with the 3-D distribution of the sulphides obtained by X-Ray CT. Finally, in order to characterize sulphide melt connectivity in the MR sample, measurements from the thin sections were used for the calculation of dihedral angles.

2.6 – PETROGRAPHY

2.6.1 - Merensky Reef Sample

The MR sample is an oriented polished slab of 30 cm height, 11 cm width and on average 3.5 cm thickness. Our sample resembles other MR samples described by a number of authors. It consists of, from the bottom to the top, a layer of anorthosite overlain by a chromitite of variable thickness (between 2 to 7 mm), ca. 11 cm of coarse-grained melanorite (which some workers refer to as a "pegmatoidal pyroxenite"), a second chromitite of variable thickness (between 3 to 10 mm), and finally melanorite. The sample contains between 0.5 vol% to 6 vol% sulphide minerals, disseminated throughout the various layers in the sample, with the exception of the

basal anorthosite that contains very little sulphides. In all rock types the sulphide phases are made up of intergrowths of pyrrhotite, pentlandite, and chalcopyrite.

The layer of anorthosite is composed of ~95 modal % cumulus plagioclase and ~5 % oikocrysts of orthopyroxene with minor (<0.5 %) randomly distributed sulphide minerals. The plagioclase grains are subhedral with a grain size ranging from ~1 to ~5 mm. The long axes of the larger plagioclase grains are oriented parallel to the horizontal direction and parallel to the contact with the overlying chromitite. These plagioclase crystals have rectilinear twins (*i.e.* igneous twins) and few of them are zoned. The anorthosite is not deformed and the preferred orientation of the plagioclase is interpreted as an igneous lamination.

The contact between the anorthosite and the overlying chromitite undulates on a centimetre scale (Fig. 2.5a). The chromitite is made up of ~50 % amoeboïdal to euhedral chromite, ~40 % poikilitic plagioclase, ~9 % orthopyroxene, and ~1 % sulphide minerals. The silicate minerals show signs of high temperature deformation. Oikocrysts of plagioclase show deformation twins (Fig. 2.6). Furthermore, plagioclase and orthopyroxene exhibit undulose extinction. Three different forms of sulphides are present as: (i) inclusions in chromite grains; (ii) disseminated grains at the contacts between chromite and plagioclase, or pyroxene grains and, (iii) inclusions in unstrained poikilitic plagioclase or pyroxene.

The contact between the lower chromitite and the overlying melanorite also undulates on a centimetre scale (Fig. 2.5). The melanorite is made up of ~70 % coarse-grained orthopyroxene crystals (ranging from 2 to 10 mm in width), ~20 % interstitial plagioclase, ~7 % euhedral chromite grains, ~1 % biotite, and ~2 % interstitial sulphide minerals.

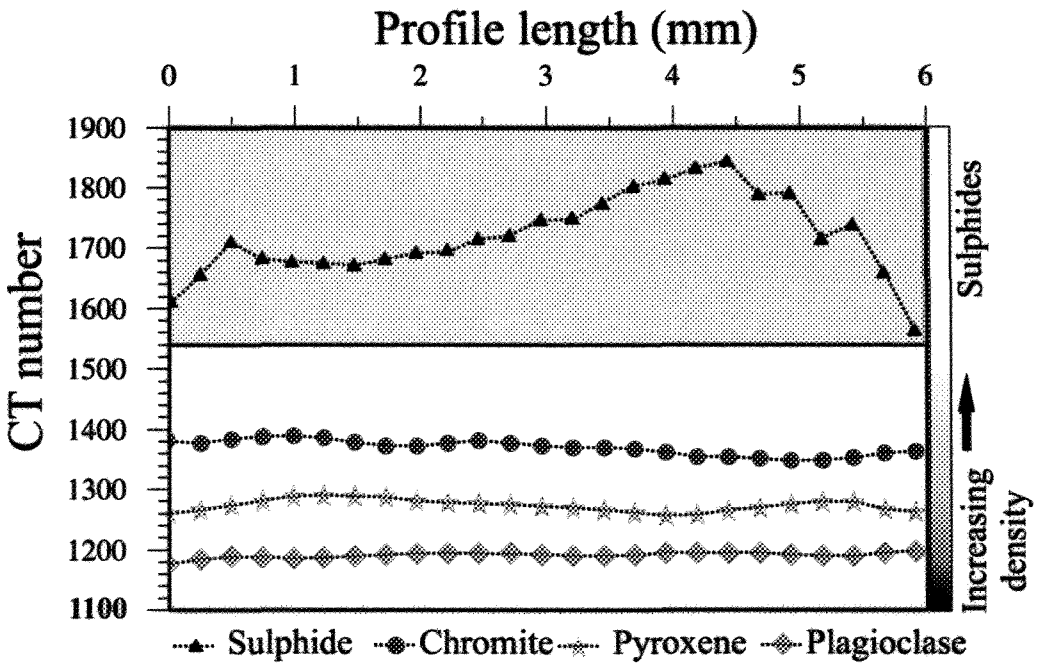

Figure 2.4: Profiles of CT number across minerals.

The profiles of CT number are calculated using the slices obtained by the CTscan. Minerals observed in thin sections are compared with their corresponding minerals observed on the slices. The profile length corresponds to the length or width of a specific mineral. Sulphide minerals are characterized by a CT number greater than 1540 (see text for explanation).

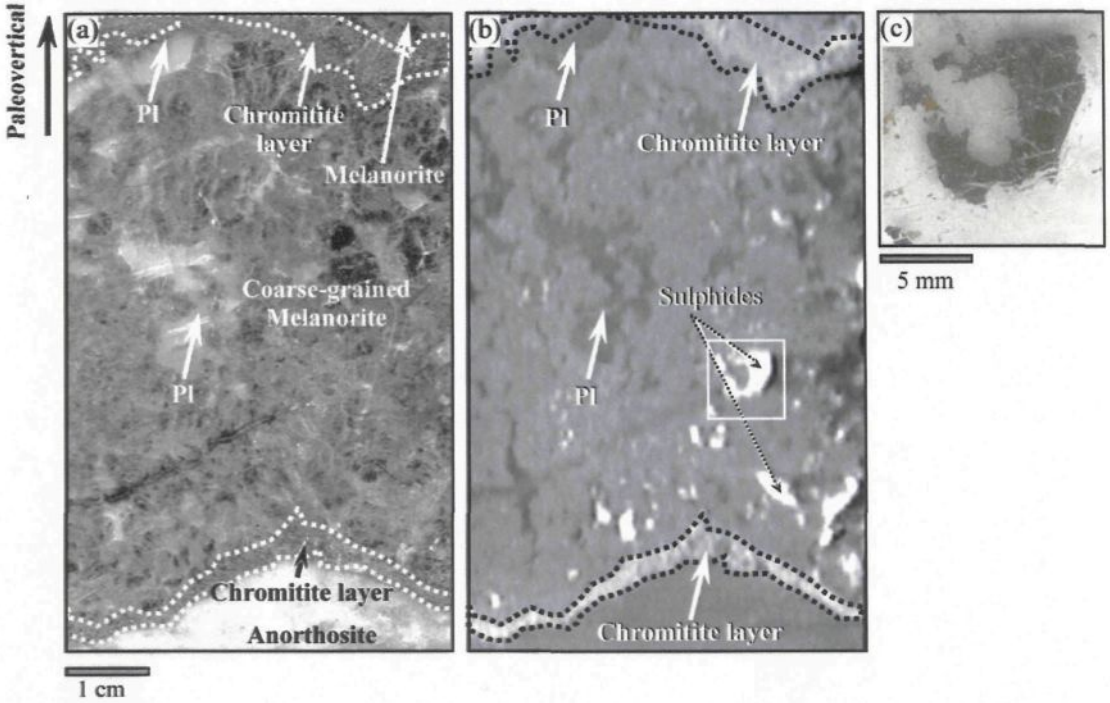

Figure 2.5: Comparison between results obtained by CT scan, macroscopic and microscopic observations for the Merensky Reef sample.

(a) Photograph of a part of the polished slab of the Merensky Reef sample.
(b) Slice obtained by CT scan corresponding to photograph (a). The images are displayed on a greyscale where dark grey and white correspond to materials of lower and higher density, respectively.
(c) Part of a thin section showing sulphides which corresponds to the inset in (b). From bottom to top, the sample shown is made up of: a layer of anorthosite; a layer of chromitite (lower chromitite) containing sulphides (white); a coarse-grained melanorite (grey on b) with interstitial plagioclase (dark grey on b) and containing sulphides which are only visible on the slice analysed by CT scan (b); a second layer of chromitite (upper chromitite). Sulphides observed in (b) show a good shape correlation with the same sulphides observed in thin section.

As described by Barnes and Maier (2002), large orthopyroxenes seem to be the product of suturing of several smaller orthopyroxene grains, and the contacts between original small orthopyroxene grains are marked by trains of small euhedral chromite grains. Furthermore, in one thin section, interstitial sulphide minerals are present along the sutures between the original, smaller orthopyroxene grains. Orthopyroxene grains are indented and exhibit undulose extinctions. Some crystals of orthopyroxene have clinopyroxene exsolution blebs (Fig. 2.6c) oriented parallel to cleavage planes. Plagioclase exhibits both deformation twins and rectilinear twins (Fig. 2.6a, b and f).

The contact between the melanorite and the upper chromitite is irregular. The chromitite layer is made up of ~50 % cubic chromite grains, ~25 % poikilitic unstrained plagioclase crystals, ~24 % orthopyroxene oikocrysts, and ~1 % sulphide minerals. Some of the chromite grains occur along orthopyroxene sutures (Fig. 2.6a). Oikocrysts of plagioclase and orthopyroxene both exhibit undulose extinction. Furthermore, plagioclase shows extensive development of deformation twins (see further description in caption to Fig. 2.6).

The melanorite at the top of the sequence (Fig. 2.6f) is made up of ~60 % subhedral orthopyroxene, ~20% interstitial and poikilitic plagioclase, ~10 % clinopyroxene, ~6 % chromite, ~2 % biotite and ~2 % sulphide minerals. In some cases, plagioclase exhibits kink bands and deformation twins (Fig. 2.6e). Many of the orthopyroxene crystals are indented and show undulose extinction and kinking (Fig 2.6b and f). In a few cases, cleavage planes in orthopyroxene are curved around the indentations suggesting that bending of the lattice has occurred. Sulphide minerals are located along orthopyroxene grain boundaries, which in some cases impinge on each other, or are kinked.

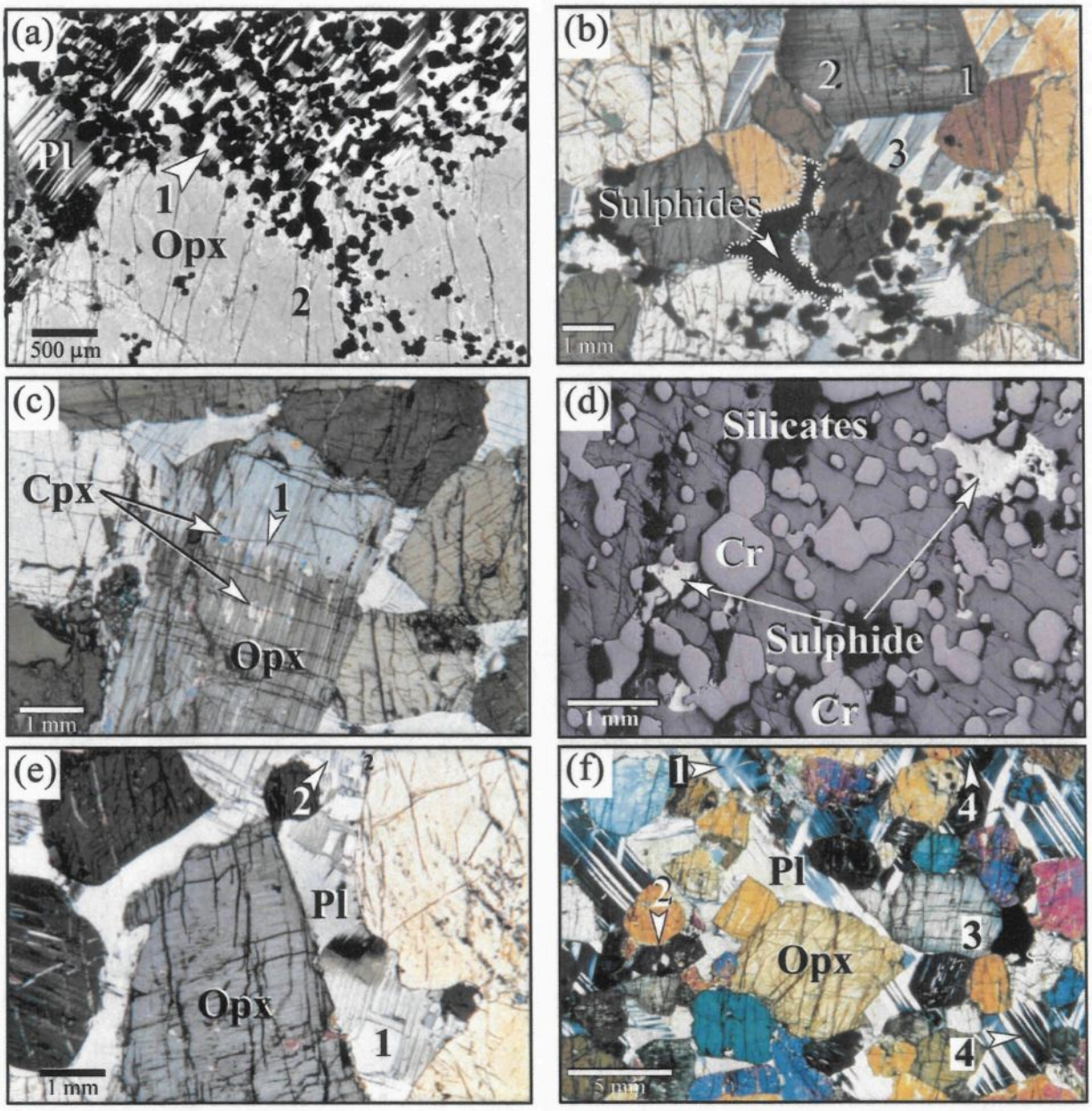
(a)
Pl
1
Opx
2
500 µm
(b)
2
1
3
Sulphides
1 mm
(c)
Cpx
1
Opx
1 mm
(d)
Silicates
Cr
Sulphide
Cr
1 mm
(e)
2
2
Pl
Opx
1
1 mm
(f)
1
4
Pl
2
3
Opx
4
5 mm

Figure 2.6: Photomicrographs of microstructures observed in the Merensky Reef sample.

All photomicrographs are oriented with the paleovertical upwards.
Abbreviations: Opx: orthopyroxene; Pl: plagioclase; Cpx: clinopyroxene; Cr: chromite; S: sulphide minerals; Px: pyroxene.
(a) Contact between upper chromitite and the underlying melanorite. Pl enclosing Cr grains exhibit extensive deformation twins (1) oriented close to the paleovertical. Note Cr grains along contact between Opx grains (2).
(b) Melanorite with interstitial sulphides located along Opx crystal faces. Some Opx have indented contacts (1) and subgrains (2) developed between Opx contacts. Furthermore, Pl have bent twins (3) and undulose extinction.
(c) Kink band (1) in Opx crystal and exsolution of Cpx along Opx cleavages due to strain on Opx lattice.
(d) Sulphides in chromitite layer (in reflected light).
(e) Deformation band (1) and deformed twins (2) in interstitial Pl in melanorite.
(f) Melanorite with interstitial sulphide and several deformation features in Px and Pl: (1) undulose extinctions in Pl; (2) indented contacts in Px; (3) undulose extinctions in Px; (4) spindle-shaped twins in Pl.

2.6.2 - J-M Reef sample

The J-M Reef sample was collected from a drill-core at the Stillwater Mine oriented along the paleo-vertical. The sample consists of olivine melagabbronorite and is 11 cm height, an average of 5 cm wide and an average of 1.5 cm thick. It contains ~62 % pyroxene, ~15 % olivine, ~15 % plagioclase, ~3 % biotite and an average of ~5 % disseminated sulphides composed, of pyrrhotite, pentlandite and chalcopyrite. Some of the orthopyroxene crystals contain inclusions of clinopyroxene along cleavage planes. Sulphides generally define a vertical network between deformed pyroxenes and rounded olivine crystals (Fig. 2.7). Secondary chalcopyrite is recrystallized in tremolite + actinolite + calcite alteration zones around silicate minerals such as olivine or pyroxene (Fig. 2.7). The chalcopyrite is oriented perpendicular to the crystal faces of the silicate phases. This alteration occurs only at contacts between silicate minerals and sulphides. As previously described for the UG-2 and the Merensky Reef by Li *et al.* (2004), the alteration could be due to the interaction between the base metal sulphides and a low temperature aqueous fluid. Furthermore, in some parts of the thin sections, myrmekitic textures were observed. These structures have previously been described by McCallum *et al.* (1980) and according to the mine geologists are found in many samples (E. Geraghty, pers. com.).

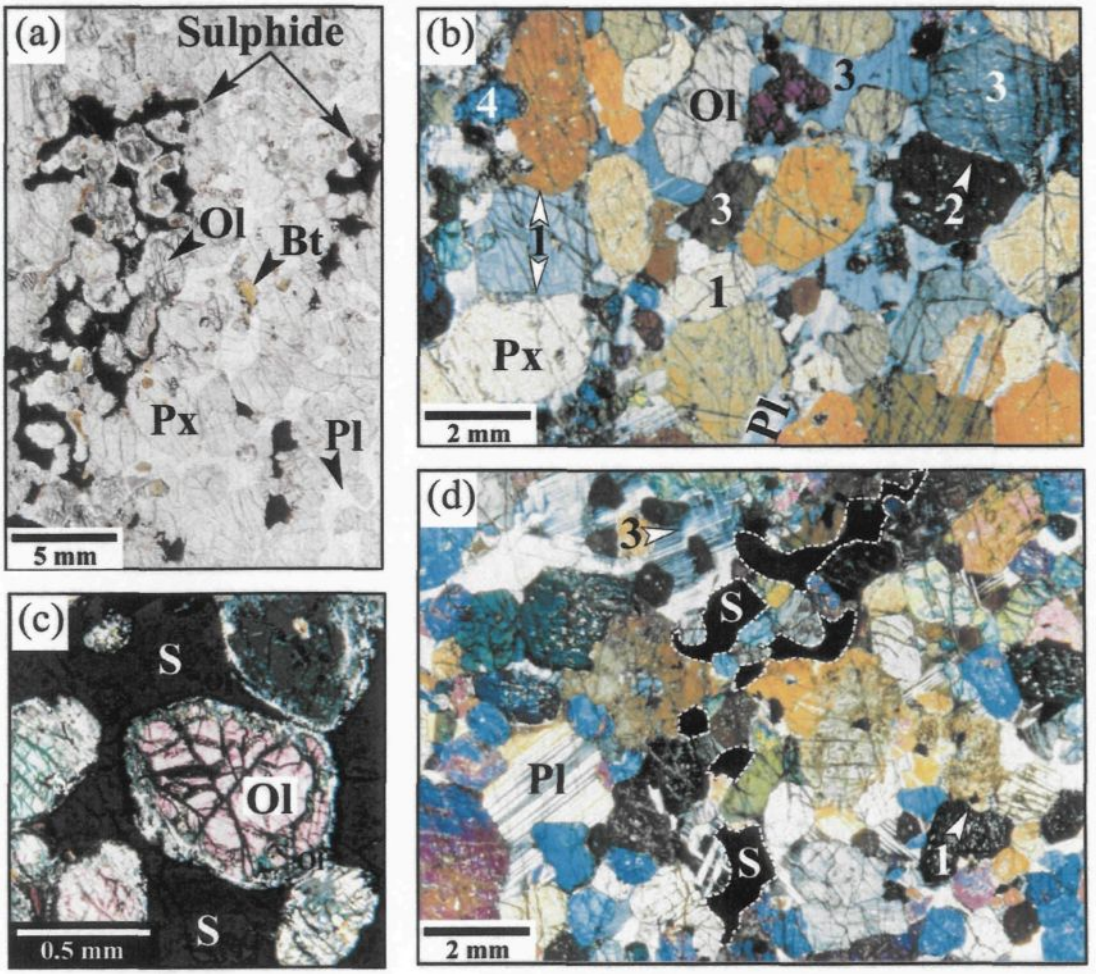

Figure 2.7: Photomicrographs of microstructures observed in the J-M Reef sample.

Note: All photomicrographs are oriented with paleovertical upwards. S: sulphide minerals, Px: pyroxene, Pl: plagioclase, Ol: olivine, Bt: biotite.
(a) Olivine-melagabbronorite with interstitial sulphides (black) located in vertical networks along silicate grain boundaries.
(b) Olivine-melagabbronorite with deformation features and sulphides located along vertical network. Deformation is marked by: (1) intended contacts to Px; (2) subgrains development at Px contacts; (3) undulose extinction in both Px and Pl.
(c) Rounded olivines surrounded by sulphide minerals. Note the corona formed by a mixture of alteration mineral and chalcopyrite around olivine grains.
(d) Deformed olivine-melagabbronite with interstitial sulphide minerals located along a vertical network. Note: numbers are same as (b) and, (4) indicates deformation twins in Pl.

2.7 - RESULTS

2.7.1 - 3-D distribution of sulphide minerals

Stacking the slices (obtained by CT scan) shows the 3-D distribution of sulphide minerals[1] within the sample (Figs. 8b and 9a) or a sub-volume. In order to quantitatively measure the distribution of sulphide minerals across each sample, the position and volume of the sulphide minerals were calculated (Figs. 2.8c and 2.9b).

2.7.1.1 - Calculation methods for quantitative analysis of the distribution of sulphide mineral

In order to quantify the distribution of sulphide, a sub-volume entirely enclosed by the Merensky Reef sample was defined. The new, virtual, parallelepiped sample volume is 282 mm high, 67 mm wide and 12.75 mm thick (Fig. 2.8b). The J-M sample is a part of a drill core, and thus its shape is relatively constant. Consequently, contrary to the MR sample, the entire sample was taken into account. Sulphide grain boundaries were defined in each lithology using the minimum threshold CT value of 1540 (previously described). Sulphide volume was then calculated by summing the voxels with a CT number greater than 1540. Results were smoothed by averaging results of 5 slices (for MR) and 10 slices (J-M Reef), representing 5 mm in height according to paleo-vertical (Fig. 2.8c and Fig. 2.9b, Table 2.1 and 2.2).

2.7.1.2 - 3-D distribution of sulphides in the Merensky Reef sample

Variation of the sulphide mineral content as a function of paleo-vertical position (0 being arbitrarily defined as the base of the lower chromitite and height increases up-section) shows that the sulphides are present in chromitite layers and melanorites, but are rare in the anorthosite (Figs. 2.8b & 2.8c and Table 2.1 and Table 2.2). The presence of ~0.1 to 5.9 +/- 0.6 % sulphides

[1] 3-D animation of both samples are available online at http://petrology.oxfordjournals.org/

in the chromitite and melanorite is confirmed by petrographic observation, except for the anorthosite (see below).

The amount of sulphides present in the lower chromitite layer is 0.9 +/- 0.1 % (Table 2.1 and Fig. 2.8c). This increases up-section into the coarse-grained melanorite to reach a maximum of 5.5 +/- 0.5 % at a height of 15 mm above the lower chromitite (Fig. 2.8c). Thereafter the amount of sulphide decreases up-section to be <0.1 % at a height of 90 mm. In the upper chromitite layer the sulphide content increases from 1.0 +/- 0.1 % (at 95 mm) to 2.2 +/- 0.2 % (at 115 mm) and continues to increase in the overlying melanorite to reach a maximum of 5.9 + 0.6 % at 140 mm above the lower chromitite seam. In the remainder of the melanorite, the sulphide content is generally low (~0.2 %), but there are three peaks at 185 mm, 220 mm and 240 mm where the sulphide content rises above 1.0 +/- 0.1 %.

In the melanorites, sulphide minerals are distributed along networks, which are oriented sub-parallel to the paleo-vertical (Fig. 2.8b) and which are 10 to 40 mm in height. These networks terminate in the underlying chromitite, and the sulphides are generally more abundant above troughs in the chromitite layers (Fig. 2.8b).

By considering qualitative and quantitative 3-D distribution of sulphide minerals, several features can be highlighted: (i) there is a peak in sulphide content a few centimetres above the chromite layers, after which the sulphide content in both melanorites decreases up-section, (ii) the distribution of sulphide minerals correlates with variations in the shape of the chromitite layer in that sulphides are more abundant above troughs in the chromitite; (iii) there are very few sulphide minerals in the anorthosite.

2.7.1.3 - J-M Reef sample

In thin sections, sulphide minerals form connected vertical networks along the grain boundaries of silicate grains (Fig. 2.7). This feature was also observed in the 3-D (Fig. 2.9a) scans. The areas of sulphide minerals have various sizes from one millimetre up to two centimetres, but they have a relatively constant elongate shape. The quantitative analysis (Fig. 2.9b and Table 2.2), indicates that, overall, sulphide minerals represent about 7.6 +/- 0.76 vol% of the rock. The sulphide content ranges from 2.3 +/- 0.2 to 13.1 +/- 1.3 vol% and does not appear to show any correlation with height in the core sample. At the bottom right of the sample, massive sulphides are present and occupy a volume of about 2 cm width, 0.5 cm height and 0.5 cm of thickness. The thin section information (Fig. 2.7d) is interpreted as evidence that sulphide liquids have percolated downward through the pyroxene and olivine framework and have been collected, or trapped, in this small volume.

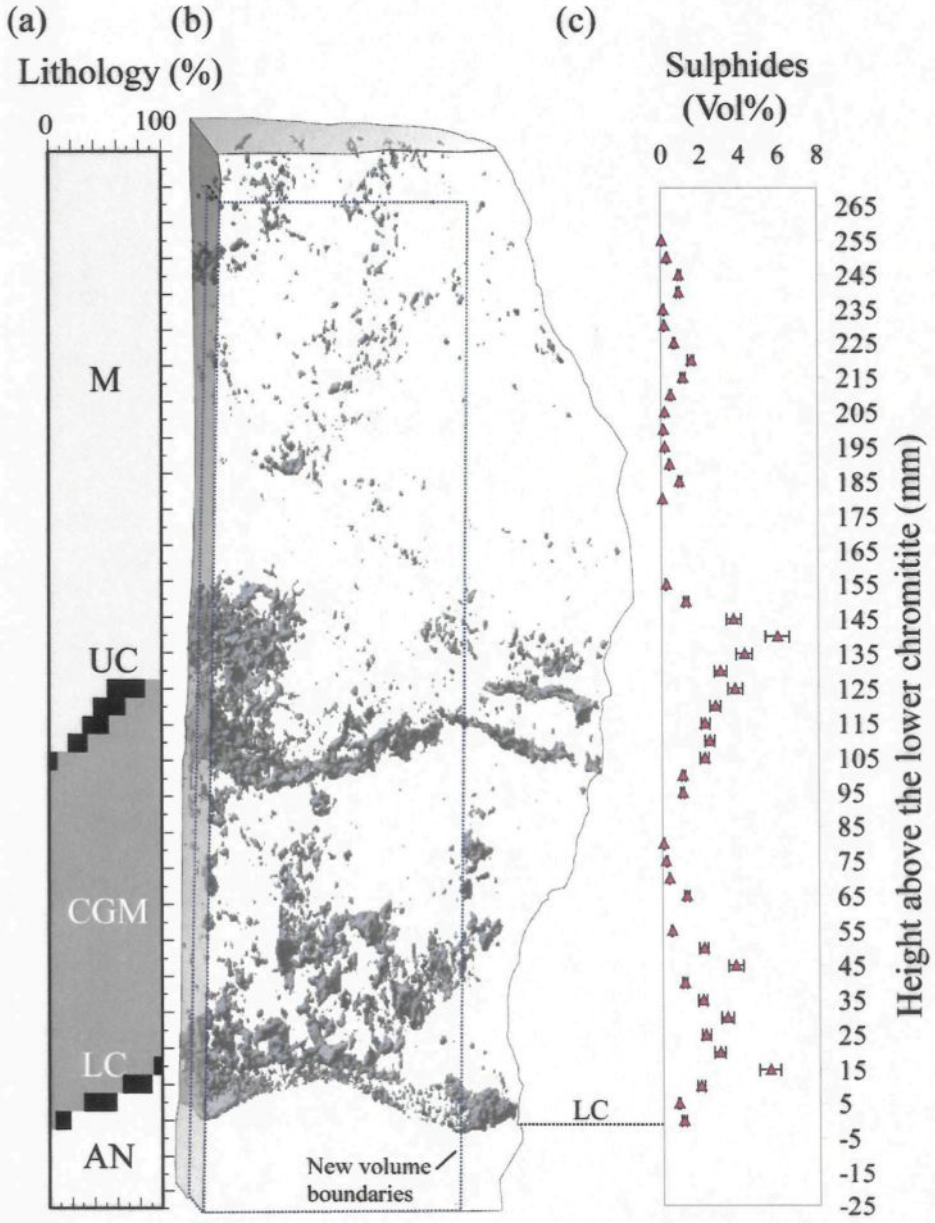

Figure 2.8: Distribution of sulphide minerals in the Merensky Reef sample based on results from CT scans.

All calculations have been made using a new defined volume (dotted line in b) entirely enclosed by the sample.
(a) Lithology calculated from CT scan slices.
(b) 3-D visualization with sulphides represented by black and grey shading.
(c) Quantification of sulphide mineral content (see text for calculation method). Note: 0 is arbitrarily defined as the base of the lower chromitite and height increases up-section.
Abbreviations: M: melanorite; UC: upper chromitite; CGM: coarse-grained melanorite; LC: lower chromitite; AN : anorthosite.

Table 2.1: *Calculated sulphide mineral content and lithologies in the Merensky Reef.*

Height* (mm)	Lithology** (%)					Volume % sulphide	Host of sulphide*** (%)				
	M	UC	CGM	LC	An		M	UC	CGM	LC	An
270	100	-	-	-	-	<0.1	0	0	0	0	0
265	100	-	-	-	-	<0.1	0	0	0	0	0
260	100	-	-	-	-	<0.1	0	0	0	0	0
255	100	-	-	-	-	0.1 +/- 0.01	100	0	0	0	0
250	100	-	-	-	-	0.3 +/- 0.03	100	0	0	0	0
245	100	-	-	-	-	1.0 +/- 0.10	100	0	0	0	0
240	100	-	-	-	-	0.9 +/- 0.09	100	0	0	0	0
235	100	-	-	-	-	0.1 +/- 0.01	100	0	0	0	0
230	100	-	-	-	-	0.2 +/- 0.02	100	0	0	0	0
225	100	-	-	-	-	0.7 +/- 0.07	100	0	0	0	0
220	100	-	-	-	-	1.5 +/- 0.15	100	0	0	0	0
215	100	-	-	-	-	1.1 +/- 0.11	100	0	0	0	0
210	100	-	-	-	-	0.5 +/- 0.05	100	0	0	0	0
205	100	-	-	-	-	0.2 +/- 0.02	100	0	0	0	0
200	100	-	-	-	-	0.1 +/- 0.01	100	0	0	0	0
195	100	-	-	-	-	0.2 +/- 0.02	100	0	0	0	0
190	100	-	-	-	-	0.4 +/- 0.04	100	0	0	0	0
185	100	-	-	-	-	1.0 +/- 0.10	100	0	0	0	0
180	100	-	-	-	-	0.1 +/- 0.01	100	0	0	0	0
175	100	-	-	-	-	<0.1	100	0	0	0	0
170	100	-	-	-	-	<0.1	100	0	0	0	0
165	100	-	-	-	-	<0.1	100	0	0	0	0
160	100	-	-	-	-	<0.1	100	0	0	0	0
155	100	-	-	-	-	0.2 +/- 0.02	100	0	0	0	0
150	100	-	-	-	-	1.2 +/- 0.12	100	0	0	0	0
145	100	-	-	-	-	3.7 +/- 0.37	100	0	0	0	0
140	100	-	-	-	-	5.9 +/- 0.59	100	0	0	0	0
135	100	-	-	-	-	4.2 +/- 0.42	100	0	0	0	0
130	100	-	-	-	-	3.0 +/- 0.30	100	0	0	0	0
125	100	-	-	-	-	3.7 +/- 0.37	100	0	0	0	0
120	100	-	-	-	-	2.7 +/- 0.27	100	0	0	0	0
115	53	34	13	-	-	2.2 +/- 0.22	95	5	0	0	0
110	40	27	31	-	-	2.4 +/- 0.24	40	60	0	0	0
105	30	24	46	-	-	2.2 +/- 0.22	54	41	5	0	0
100	16	18	66	-	-	1.1 +/- 0.11	65	26	9	0	0
95	-	6	94	-	-	1.0 +/- 0.10	43	39	18	0	0
90	-	-	100	-	-	<0.1	0	0	100	0	0
85	-	-	100	-	-	<0.1	0	0	100	0	0
80	-	-	100	-	-	0.1 +/- 0.01	0	0	100	0	0
75	-	-	100	-	-	0.2 +/- 0.02	0	0	100	0	0
70	-	-	100	-	-	0.3 +/- 0.03	0	0	100	0	0
65	-	-	100	-	-	1.2 +/- 0.12	0	0	100	0	0
60	-	-	100	-	-	<0.1	0	0	100	0	0
55	-	-	100	-	-	0.5 +/- 0.05	0	0	100	0	0
50	-	-	100	-	-	2.1 +/- 0.21	0	0	100	0	0

Table 2.1 (suite): *Calculated sulphide mineral content and lithologies in the Merensky Reef sample.*

Height*	Lithology** (%)					**Volume %**			Host of sulphide*** (%)				
(mm)	M	UC	CGM	LC	An	**sulphide**			M	UC	CGM	LC	An
45	-	-	100	-	-	3.8	+/-	0.38	0	0	100	0	0
40	-	-	100	-	-	1.1	+/-	0.11	0	0	100	0	0
35	-	-	100	-	-	2.0	+/-	0.20	0	0	100	0	0
30	-	-	100	-	-	3.3	+/-	0.33	0	0	100	0	0
25	-	-	100	-	-	2.2	+/-	0.22	0	0	100	0	0
20	-	-	100	-	-	2.9	+/-	0.29	0	0	100	0	0
15	-	-	95	5	-	5.5	+/-	0.55	0	0	99	1	0
10	-	-	70	27	9	1.9	+/-	0.19	0	0	98	2	0
5	-	-	30	30	40	0.8	+/-	0.08	0	0	57	43	0
0	-	-	4	15	83	1.1	+/-	0.11	0	0	12	88	0
-5	-	-	-	-	100		<0.1		0	0	0	0	100
-10	-	-	-	-	100		<0.1		0	0	0	0	100
-15	-	-	-	-	100		<0.1		0	0	0	0	100
-20	-	-	-	-	100		<0.1		0	0	0	0	100
-25	-	-	-	-	100		<0.1		0	0	0	0	100

* Height above the base of the Lower Chromitite layer.

** Average lithology calculated from CT scan slices.

*** Lithology (calculated from CT scan slices) host of the total sulphides minerals.

M : melanorite; UC : upper chromitite; CGM : coarse-grained melanorite; LC : lower chromitite; An : anorthosite.

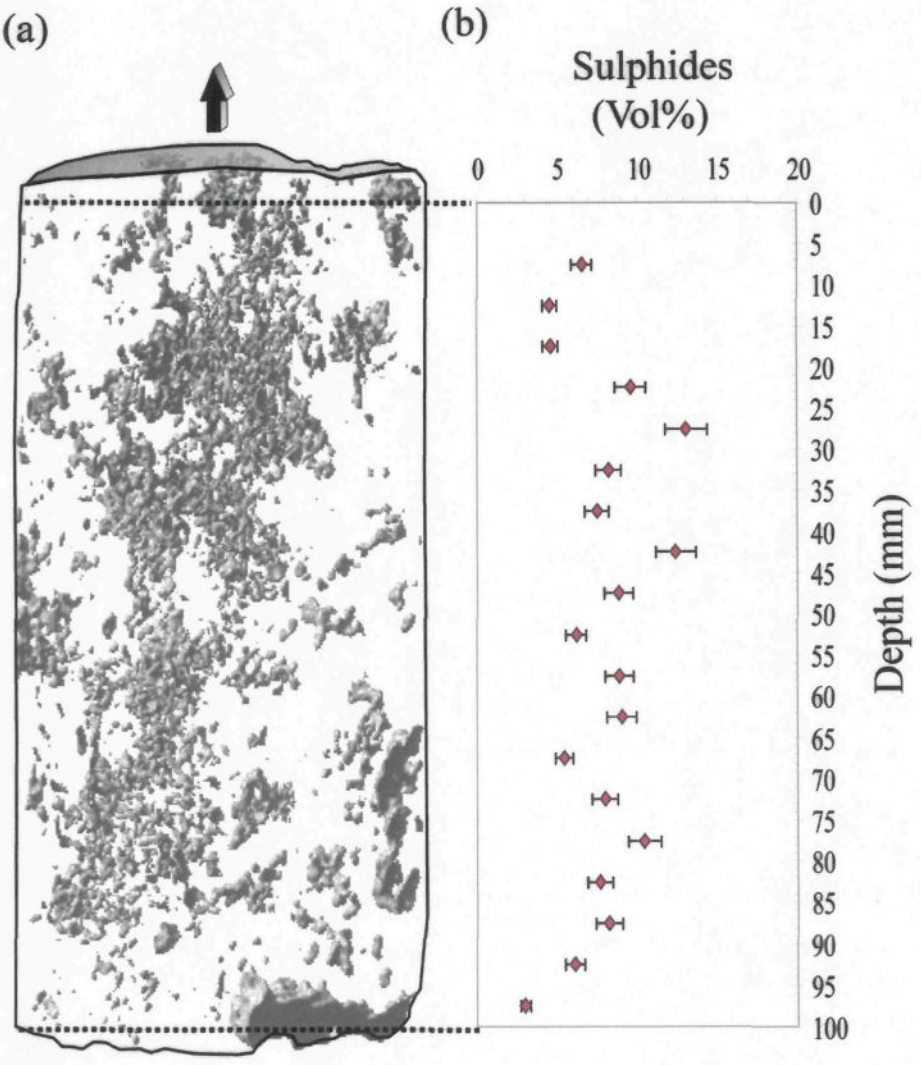

Figure 2.9: Distribution of sulphide minerals in the J-M Reef sample based on results from CT scans.

(a) Sulphide minerals are represented by grey shading. Paleovertical is represented by the black arrow.
(b) Calculated content of sulphide minerals.

Table 2.2: *Sulphide mineral content in the J-M Reef,*

Depth (mm)	Sulphide (vol%)			Depth (mm)	Sulphide (vol%)		
2.5	2.3	+/-	0.23	52.5	6.2	+/-	0.62
7.5	6.6	+/-	0.66	57.5	8.9	+/-	0.89
12.5	4.6	+/-	0.46	62.5	9.1	+/-	0.91
17.5	4.6	+/-	0.46	67.5	5.4	+/-	0.54
22.5	9.6	+/-	0.96	72.5	8.0	+/-	0.80
27.5	13.1	+/-	1.31	77.5	10.5	+/-	1.05
32.5	8.2	+/-	0.82	82.5	7.7	+/-	0.77
37.5	7.5	+/-	0.75	87.5	8.2	+/-	0.82
42.5	12.4	+/-	1.24	92.5	6.1	+/-	0.61
47.5	8.9	+/-	0.89	97.5	3.0	+/-	0.30

2.8 - Microstructural analysis

2.8.1 - Deformation during crystallisation

2.8.1.1 - Merensky Reef sample

Both samples (MR and J-M Reef samples) contain high temperature crystal deformation features. Microstructures observed in this study are very similar to those observed by Barnes and Maier (2002) in samples from the Merensky Reef at Impala Platinum mines. In the chromitite layers and the melanorites, the orthopyroxene, clinopyroxene, and plagioclase all exhibit high-temperature deformation features. In both melanorite layers, several cumulus orthopyroxene crystals impinge on each other and have produced indented contacts (Fig. 2.10a). The indented contacts are close to the horizontal direction, whereas the vertical contacts are not indented. In many cases, cleavage planes and exsolution lamellae are straight near the contacts between minerals, indicating that, in most cases, diffusion creep or dissolution has occurred. However, in one case (Fig. 2.10), the cleavage planes were curved around the indentation indicating that bending of the lattice has also occurred. In both the melanorites and the upper chromitite layer, orthopyroxene shows undulose extinction and contains deformation bands (Fig. 2.10). Furthermore, small subgrains are developed at the horizontal contacts between some of the pyroxene crystals (Fig. 2.10). This indicates that part of the deformation in the pyroxene was by dislocation creep.

The interstitial plagioclase shows undulose extinction, many deformation twins (spindle-shaped perpendicular and bent twins), and deformation bands (Fig. 2.10). The deformation twins have a preferred shape orientation (Fig. 2.10) close to the vertical (+/- 35°) direction. These deformation features are present in both the melanorites and chromitite layers.

Most of the sulphides in the melanorite layers occur in a vertical network (Fig. 2.10), and most sulphide minerals are located at contacts between orthopyroxene crystals. Some of the

orthopyroxene crystals have undergone deformation by dislocation creep, dissolution, or diffusion creep (Fig. 2.10). In the coarse-grained melanorite, sulphides were also found located in a vertical network along the contacts between orthopyroxene and deformed interstitial plagioclase crystals (Fig. 2.10). In contrast to the vertically elongate distribution of sulphides in the melanorites, the distribution of sulphides in the chromitite layer is in the form of isolated droplets, (Fig. 2.4d) and they are not interconnected.

2.8.1.2 - J-M Reef Sample

The olivine-melagabbronorite of the J-M Reef has undergone deformation during crystallisation. This deformation is well displayed in the pyroxene framework and the interstitial plagioclase. Some of the pyroxenes show indented contacts (Fig. 2.11). In all cases, the cleavage planes and exsolution lamellae are straight around contacts between pyroxene crystals. As in the case of the Merensky Reef sample, this indicates that deformation of the pyroxenes probably occured by diffusion creep or dissolution. Some of the pyroxenes also exhibit undulose extinction and kinks (Fig. 2.11). Moreover, small subgrains of clinopyroxene are well developed at the edges of crystals along contacts with other pyroxenes.

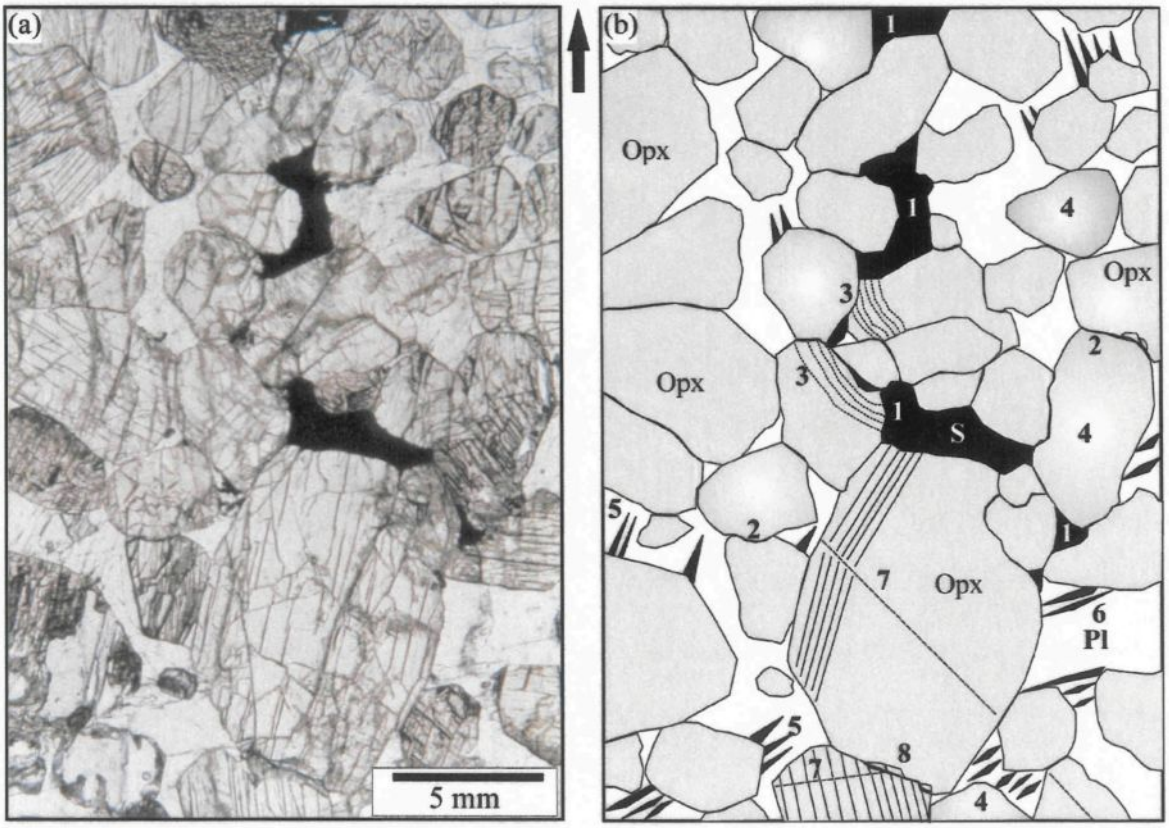

Figure 2.10: Summary of microstructures observed in the Merensky Reef sample.

(a) Photomicrograph of melanorite. Paleovertical is represented by the back arrow.
(b) Sketch showing microstructures present in the photomicrograph (a): 1 - sulphide minerals distributed along vertical segments and located between Opx contacts; 2 - indented contact between Opx crystals; 3 - bent Opx cleavage around indented contacts; 4- undulose extinctions in Px; 5 - deformation twins with tapering edges in Pl nucleated on high stress site; 6 - spindle shaped twins in Pl; 7 - kink planes in Opx ; 8 - subgrains development. Opx: orthopyroxene, Pl: plagioclase.

These features indicate that the crystals have been affected by dislocation creep and recovery. Interstitial plagioclase shows evidence for deformation after the crystal mush was consolidated.

Plagioclase exhibits spindle-shaped twins, bent twins, perpendicular twins and undulose extinctions. Generally, these twins are oriented at angles of about +/- 35 degrees relative to the vertical. Furthermore, sulphide minerals are distributed along the crystal boundaries of deformed pyroxenes and rounded olivine and form vertically linked networks.

2.8.2 - Deduction of the principal compressive stress during the formation of the cumulate

In both the Merensky Reef and J-M Reef samples, the deformation features of the crystals and the distribution of the sulphides are very similar (Fig. 2.10 and 2.11). The principal compressive stress during formation of the cumulate can be inferred by considering the paleo-vertical orientation, orientation of deformation features and the location of the sulphide minerals described previously. The pyroxenes exhibit undulose extinctions, kinks, and subgrain developments. Some cumulus pyroxene crystals have impinged on each other and indented contacts or subgrain developments are generally oriented along sub-horizontal pyroxene contacts, but not along vertical ones. The interstitial plagioclase is characterized by the presence of widespread deformation in the two samples. This intracrystalline deformation is demonstrated by the presence of spindle-shaped twins, bent twins, perpendicular twins, and undulose extinctions. Deformation twins in plagioclase with tapering edges nucleated at high stress sites at the edges of the crystals. In both samples, spindle-shaped twins, or bent twins, have a preferred shape orientation (Fig. 2.10 and Fig. 2.11) close to the vertical (+/- 35 degree) direction.

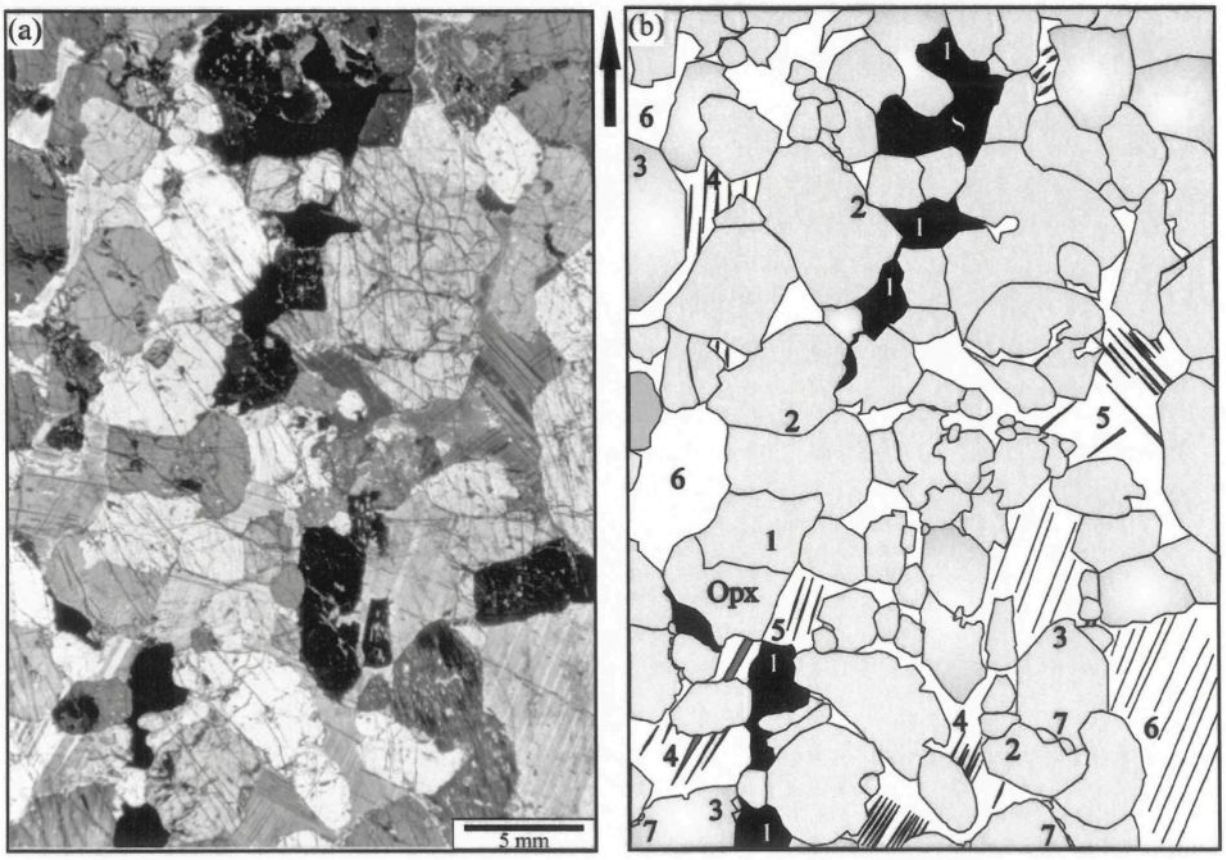

Figure 2.11: Summary of microstructures observed in the J-M Reef Sample.

(a) Photomicrographs of gabbronorite. Paleovertical is represented by the back arrow.
(b) Sketch showing microstructures present in the photomicrograph (a) : 1 - sulphide minerals distributed along vertical network and located between Opx contacts ; 2 - indented contacts between Opx crystals ; 3- undulose extinction in Px ; 4 - deformation twins in Pl with tapering edges nucleated on high stress site ; 5 - spindle-shaped twins in Pl ; 6 - undulose extinction in Pl ; 7 - subgrains development in Opx. Opx: orthopyroxene, Px: pyroxene; Pl: plagioclase.

Late intercumulus minerals, such as biotite, do not show deformation features. Consequently, it seems that deformation occured during the crystallisation of pyroxenes and the interstitial plagioclase, but before late minerals formed. Furthermore, sulphide minerals are, in many cases, located along pyroxene grains boundaries, and they form a vertical network along the faces of silicate crystals, mainly pyroxene or olivine. However, in the melanorite layer of the Merensky Reef, some of the sulphide minerals have crystallized at the contact between deformed plagioclase and pyroxene and these sulphide minerals form a vertical network, or elongate pockets of sulphide trapped and surrounded by plagioclase. In this case, it is possible that sulphide migration has been arrested due to the lack of permeability where extensive interstitial plagioclase crystallisation had taken place.

As described by Barnes and Maier (2002), these high-temperature deformation features are consistent with a paleo-vertical maximum principal compressive stress ($\sigma 1$), and this is responsible for compaction during the formation of the cumulates. Thus, the distribution of the sulphide minerals is interpreted to indicate that they filled vertical dilatancies that formed between silicate mineral grain boundaries during compaction.

2.8.3 - Connectivity of the sulphide melt

The distribution of melt in a solid matrix is controlled by the relative energies of crystal-crystal and crystal-melt interfaces. By considering that in a solid matrix (*i.e.* crystals), the surface energy is isotropic, the 3-D melt topology could be predicted by considering the cross-sectional geometry of the solid-liquid interface (Watson and Brenan, 1987; Laporte and Provost, 2000; Rose and Brenan, 2001; Brenan and Rose, 2002; Holness *et al.*, 2005), in other words, by

considering dihedral angles. At equilibrium, the dihedral angle (Θ) at the contact between melt and two crystals is defined as:

$$\Theta = 2 \arccos (\gamma cc / 2\ \gamma cm)$$

where (cc and (cm are the crystal-crystal and crystal-melt surface energies, respectively. Where $0 < \Theta < 60°$, the melt is considered to wet crystal faces and is interconnected in 3-D, even for a low melt fraction (Von Bargen and Waff, 1986). Where $\Theta > 60°$, the melt is considered not to wet crystal faces and melt interconnectivity is not achieved at a low melt fraction (Von Bargen and Waff, 1986). Consequently, melt is confined to isolated pockets at grain corners and the migration of melt is negligible. Thus measurements of the dihedral angles between sulphides and others minerals (silicates and/or oxides) in our samples can be used to characterize the sulphide melt topology and interconnectivity in these natural rocks. As the sulphides contained in the J-M Reef are partially altered, dihedral angles between sulphides and silicates are obscured by the products of alteration. Consequently, no measurements were made in the J-M Reef sample.

2.8.3.1 - Dihedral angle measurements in the MR sample

In order to decide whether the sulphide liquid is interconnected or not in the melanorites and chromitite layers, the dihedral angles between sulphides and silicates and/or oxides were measured from polished thin sections using an optical microscope . For each sample, a population of angles (>100 angles) were measured on the two-dimensional thin sections, with an error on each measurement of a few degrees. Angles differ due to the anisotropy of interfacial energies, and can assume a range of values depending on the orientation of the crystal lattices. However, according to previous workers (Harker and Parker, 1945; Riegger and Van Vlack, 1960; Holness et al., 2005; Holness, pers. com.), the median angle of this 2-D angle population can be correlated

(with a minor error ~1°) with the true 3-D angle. Results obtained for the MR sample are summarized in Table 2.3.

In the melanorite, dihedral angles were measured at pyroxene-sulphide and plagioclase-sulphide junctions. Dihedral angles vary from 18 to 139°, but the median value of 103 measurements is 53°. In the chromitite layers, dihedral angles were measured at chromite-sulphide interfaces. In this case, dihedral angles vary from 25 to 144°, and the median value of 141 measurements is 95°. Thus, the sulphide liquid behaves differently in melanorite compared with chromitite layers. Dihedral angles between silicate and sulphide melt in the melanorite are lower than 60°, which implies that sulphide melt could be interconnected and could have infiltrated into it. In contrast, the dihedral angles in chromitite layers where sulphides occur as small droplets are largely greater than 60° implying that sulphide melt connectivity is negligible. Consequently, sulphide melt percolation in chromitites was very limited.

Table 2.3: *Results of dihedral angle measurements in the Merensky Reef sample.*

Lithology	Minerals			Number of mesurements	Median angle (°)	Angle (°)	
						Min	Max
Melanorite	Px	Px	S	89	51.5	18	123
Melanorite	Px	Pl	S	14	71.5	22	139
Melanorite		Total		103	53	18	139
Upper chromitite (UC)	Cr	Cr	S	86	95	37	144
Lower chromitite (LC)	Cr	Cr	S	55	103.5	35	139
Chromitite (UC & LC)	Cr	Cr	S	141	96.5	25	144

Px: pyroxene; Pl: plagioclase; Cr: chromite; S: sulphide minerals.

2.9 – DISCUSSION

The two samples examined in this study show considerable variation in lithology. The MR sample contains several distinct rock types (anorthosite, chromitite and melanorite) whereas the J-M Reef sample consists of a relatively homogenous olivine-melagabbronorite. Despite the difference in lithology between the MR and J-M Reef samples, the 3-D distribution of sulphide minerals and microstructures show that both the reefs have several features in common.

2.9.1 - Connectivity of the sulphide melt and the role of compaction

The dihedral angles measured in the MR sample, the distribution of the sulphides observed in thin section, and the X-ray CT analysis showed that the sulphide minerals occur as an interconnected vertical network in the melanorite which spreads out and is arrested in the chromitite layers. In the J-M Reef sample the distribution of sulphides observed in thin section and X-ray CT analysis shows that the sulphide minerals form a network interconnected vertically. Microstructural analysis indicates that both samples have undergone crystal deformation at high temperature (*i.e.* during crystallisation of the cumulate minerals). The deformation was only observed in pyroxenes and interstitial plagioclase; late minerals such as biotite, were not deformed. All deformation features are consistent with a principal compressive stress ($\Phi 1$) oriented sub-parallel to the paleo-vertical, and could have been induced by compaction of the crystal pile during formation of the cumulate.

In the Merensky Reef sample, the highest concentration of sulphide mineral contents was observed just above the two chromitite layers. We suggest that in the melanorites, sulphide melt accumulated at the top of the cumulate pile. During compaction of the pile, dilatancies formed

between pyroxene and plagioclase crystals, as a result of extension in the plane of the layer and the sulphide liquid migrated into these dilatant sites and downwards into the crystal pile.

2.9.2 - Role of chromitite layers in migration of sulphide melt

The most striking difference between the two samples is that the J-M Reef sample consists of one rock type, whereas the Merensky Reef sample consists of five layers and three different rock types. In the Merensky Reef, the sulphides are concentrated in the troughs above the chromitite layers and then appear to form a cast of the chromitite layers. This observation could be explained by the difference in dihedral angles between sulphides and silicates and between sulphides and chromites. Because the sulphide melt could wet the silicates, it was able to percolate through the silicate pile. In contrast, the sulphide melt could not wet the chromites, thus the sulphide melt formed droplets against the chromite, ceased to be interconnected and could, therefore, no longer percolate through the cumulate pile.

Experimental studies by Rose and Brenan (2001) and Brenan and Rose (2002), at conditions close to FMQ and 1300 C°, showed that wetting angles between olivine and sulphide liquid are higher than those between chromite and sulphide liquid. Thus, these authors suggest that sulphide melt will show a stronger interconnectivity in chromitite layers than in silicate (olivine) layers, contrary to our observations. We do not have an explanation as to why the experiments and the natural sample yield contradictory results.

2.9.3 - Implications for the formation of the Merensky Reef

A number of authors (Campbell *et al.*, 1983; Naldrett *et al.*, 1986) suggested that the Merensky Reef formed from a new batch of magma injected into the magma chamber. At the base of the Merensky cycle, a layer of chromitite formed followed by melanorite (Fig. 2.12a). An immiscible sulphide liquid collected the PGE and then settled onto the crystal pile (Fig. 2.12b). On the basis of microstructural work at Impala Platinum Mines, Barnes and Maier (2002) modified this model and concluded that in 2-D space, sulphides appear to have percolated downwards, and to have filled interstitial spaces in the crystal framework, thereby forming a sub-vertical network during compaction. Our results using different imaging techniques on the Merensky Reef at Rustenburg Platinum Mine and on the J-M Reef at Stillwater Mine suggest that this conclusion holds in 3-D too (Fig. 2.12c). The sulphide networks in both melanorites of the MR sample terminate at their respective underlying chromitite (Fig. 2.12d). By considering a single chromitite layer and its overlying melanorite (supposed to have formed by one magmatic event), the sulphide mineral content increases from the top to the bottom in the melanorite (with a maximum value just above the chromitite) and that the content of sulphides decreases from the top to the bottom in the chromitite layer. According to the dihedral angle measurements in this natural sample, sulphide migration in the chromitite was inhibited and extensive downward infiltration of a sulphide melt is unlikely (Fig. 2.12d). These interpretations are supported by the fact that in our sample the underlying anorthosite contains only minor sulphide mineralization. This point was made for the Merensky Reef in general by Viljoen *et al.* (1986) and Cawthorn (1999) who noted the high abundance of sulphide at the level of the Merensky Reef strongly decreases in the footwall anorthosite.

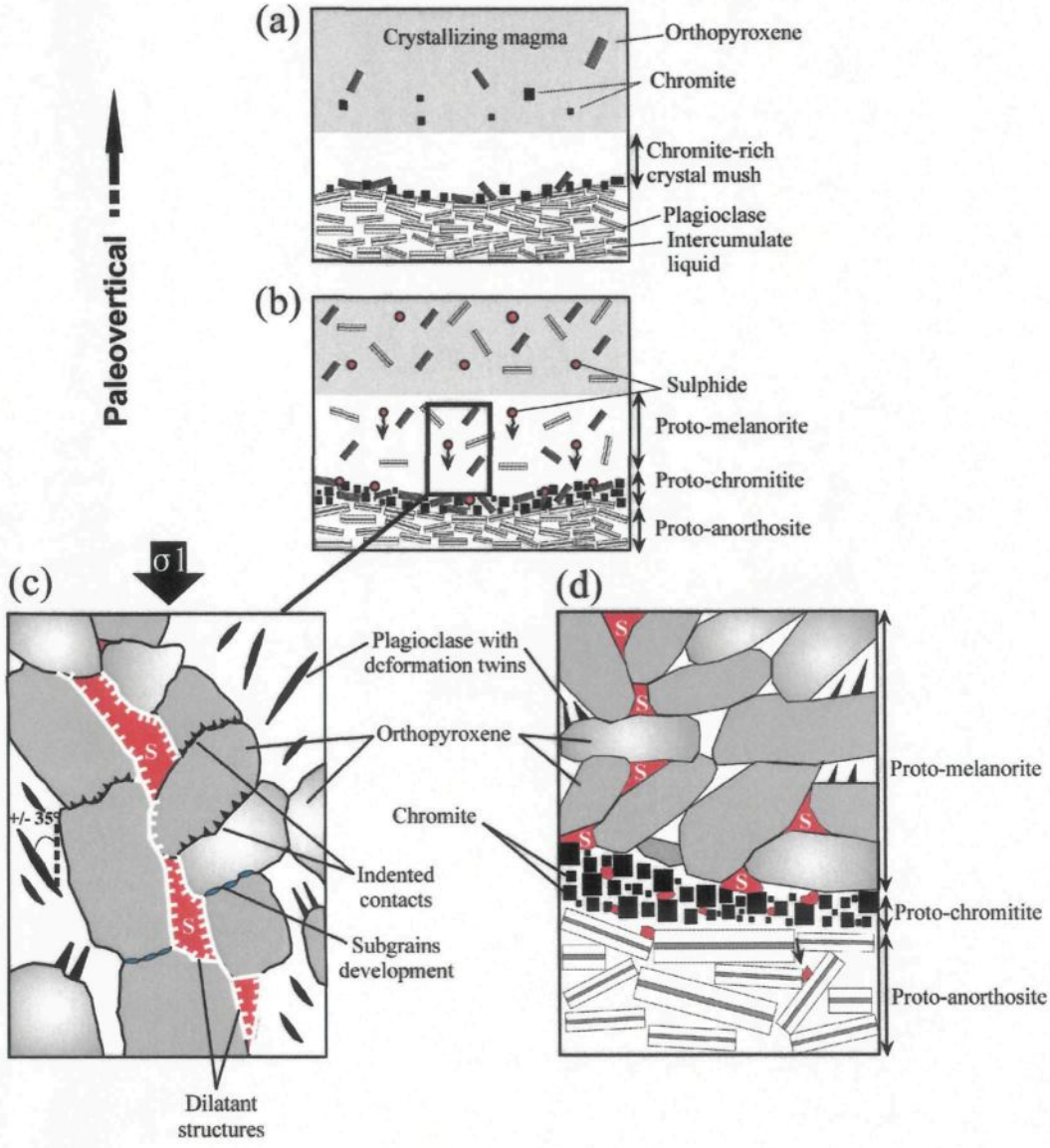

Figure 2.12: Model of formation of the Merensky Reef.

(a) Crystallization of chromite and orthopyroxene on cumulate pile to form chromite layer.
(b) Immiscible sulphides percolate into the cumulate pile.
(c) High-temperature deformation (indented contact, deformation twins, undulose extinctions, sub-grain development) in melanorite under a vertical principal compressive stress ($\sigma 1$) triggered by compaction of the cumulate pile. The downward percolation of sulphide (S) through dilatant structures is improved by the compaction of the cumulate.
(d) The vertical sulphide network stops at the underlying chromitite layer due to the lack of interconnectivity of the sulphide liquid in this layer. Sulphides in the chromitite appear as small droplets. The chromitite seems to act as a filter, preventing extensive downward percolation of the sulphide liquid in the underlying anorthosite.

Cawthorn (1999), interpretated the decrease in the sulphide mineral content into the footwall of the Merensky Reef to be the result of the low permeability in the footwall. We suggest that another factor is the lack of interconnectivity of the sulphide melt in the chromitite layers. The sulphide liquid beaded in the chromitite layers thus impeding further downward migration. This resulted in high PGE contents of the chromitite layers.

2.10 – CONCLUSIONS

X-ray computed tomography is a powerful technique allowing 3-D analysis and quantification of minerals in 10 centimetre-sized samples. The analysis has highlighted the distribution of sulphide minerals in two samples from the Bushveld and Stillwater Complexes. In the light of the results obtained for the MR and J-M Reef samples, it appears that downward migration of sulphide melt in a cumulate pile can be facilitated by compaction. Furthermore, connectivity of dense sulphide melt is high in melanorite and is negligible in chromitite layers of the MR sample. Thus, chromitite layers may play an important role in preventing further downward migration of sulphide melt. This could partially explain the enrichment of PGE in chromitite layers, and the decrease in the modal abundance of sulphide minerals in the footwall of the Merensky Reef.

2.11 – ACKNOWLEDGEMENTS

Rustenburg Platinum Mine is thanked for allowing access to their properties and allowing sampling of the Merensky Reef. Stillwater Mining Company is thanked for hosting the "9th International Platinum Symposium" field trip and allowing sampling of the J-M Reef core. Paul Bedard (UQAC) is thanked for the suggestion that we use the CT imaging to study the sulphide distribution. Edward Sawyer (UQAC) is thanked for proof reading early drafts of the manuscript.

Jacques Labrie is thanked for assistance in using the INRS CT scanner facility. David Hirsch, Richard Kyle and Michael Zientek are thanked for their constructive reviews. This work was funded by a Discovery Grant from Natural Science and Engineering Research Council of Canada and the Canadian Research Chair in Magmatic Metallogeny

2.12 – REFERENCES

Ballhaus, C. & Ryan, C. G. (1995). Platinum-group elements in the Merensky reef. I. PGE in solid solution in base metal sulfides and the down-temperature equilibration history of Merensky ores. *Contributions to Mineralogy and Petrology* **122**, 241-251.

Ballhaus, C. & Sylvester, P. (2000). Noble metal enrichment processes in the Merensky Reef, Bushveld Complex. *Journal of Petrology* **41**, 545-561.

Barnes, S.-J. & Maier, W. D. (2002). Platinum-group elements and microstructures of Normal Merensky Reef from Impala Platinum Mines, Bushveld Complex. *Journal of Petrology* **43**, 103-128.

Barnes, S. J. & Naldrett, A. J. (1985). Geochemistry of the J-M (Howland) Reef of the Stillwater Complex, Minneapolis Adit Area. I. Sulfide Chemistry and Sulphide-Olivine Equilibrium. *Economic Geology* **80**, 627-645.

Boespflug, X., Long, B. F. N. & Occhietti, S. (1995). CAT-scan in marine stratigraphy: a quantitative approach. *Marine Geology* **122**, 281-301.

Boudreau, A. E. & McCallum, I. S. (1992). Infiltration metasomatism in layered intrusions - an example from the Stillwater Complex, Montana. *Journal of Volcanology and Geothermal Research* **52**, 171-183.

Brenan, J. M. & Rose, L. A. (2002). Experimental constraints on the wetting of chromite by sulfide liquid. *Canadian Mineralogist* **40**, 1113-1126.

Brochu, C. A. (2000). A digitally rendered endocast for Tyrannosaurus Rex. *Journal of Vertebrate Paleontology* **20**, 1-6.

Campbell, I. H., Naldrett, A. J. & Barnes, S. J. (1983). A model for the origin of the platinum-rich sulfide horizons in the Bushveld and Stillwater Complexes. *Journal of Petrology* **24**, 133-165.

Carlson, W. D. & Denison, C. (1992). Mechanisms of porphyroblast crystallization : results from high-resolution computed X-Ray Tomography. *Science* **257**, 1236-1239.

Cawthorn, R. G. (1999). Permeability of the footwall cumulates to the Merensky Reef, Bushveld Complex. South African *Journal of Geology* **102**, 293-302.

Delerue, J. F., Perrier, E., Timmermann, A. & Swennen, R. (2003). 3D soil image characterization applied to hydraulic properties computation. In: Mees, F., Swennen, R., Van Geet, M. & Jacobs, P. (ed.) *Application of X-ray Computed Tomography in the Geosciences.* London: Geological Society, Special Publication, 1-6.

Denison, C. & Carlson, W. D. (1997a). Three-dimensional quantitative textural analysis of metamorphic rocks using high-resolution computed X-ray tomography.2. Application to natural samples. *Journal of Metamorphic Geology* **15**, 45-57.

Denison, C., Carlson, W. D. & Ketcham, R. A. (1997b). Three-dimensional quantitative textural analysis of metamorphic rocks using high-resolution computed X-ray tomography .1. Methods and techniques. *Journal of Metamorphic Geology* **15**, 29-44.

Eales, H. V. & Cawthorn, R. G. (1996). The Bushveld Complex. In: Cawthorn, R. G. (ed.) *Layered Intrusions.* Amsterdam, The Nederlands: Elsevier, 181-230.

Flisch, A. & Becker, A. (2003). Industrial X-ray computed tomography studies of lake sediments drill cores. In: Mees, F., Swennen, R., Van Geet, M. & Jacobs, P. (ed.) *Application of X-ray Computed Tomography in the Geosciences.* London: Geological Society, Special Publication, 205-212.

Harker, D. & Parker, E. R. (1945). Grain shape and grain growth. *Transactions of the American Society of Metals* **34**, 156-195.

Harmer, R. E. & Armstrong, R. A. (2000). Duration of Bushveld Complex (seno lato) magmatism: Constraints from new SHRIMP zircon chronology. Workshop on the Bushveld Complex, Gethane Lodge, Burgersfort., abstracts and program.

Hiemstra, S. A. (1979). The role of collectors in the formation of the platinum deposits in the Bushveld Complex. *Canadian Mineralogist* **17**, 469-482.

Holness, M. B., Cheadle, M. J. & McKenzie, D. (2005). On the use of Cchanges in dihedral angle to decode late-stage textural evolution in cumulates. *Journal of Petrology* **46**, 1565-1583.

Hounsfield, G. N. (1973). Computerized transverse axial scanning tomography .1. Description of system. British **Journal of Radiology 46**, 1016-1022.

Johns, R. A., Steude, J. S., Castanier, L. M. & Roberts, P. V. (1993). Nondestructive measurements of fracture aperture in crystalline rock cores using X-ray computed tomography. *Journal of Geophysical Research* **98** (B2), 1889-1900.

Ketcham, R. A. & Carlson, W. D. (2001). Acquisition, optimization and interpretation of X-ray computed tomographic imagery: applications to the geosciences. *Computers and Geosciences* **27**, 381-400.

Ketcham, R. A. & Iturrino, G. J. (2005). Nondestructive high-resolution visualisation and measurement of anisotropic effective porosity in complex lithologies using high-resolution X-ray computed tomography. *Journal of Hydrology* **302**, 92-106.

Kinloch, E. D. (1982). Regional trends in the Platinum-Group Mineralogy of the Critical Zone of the Bushveld Complex, South-Africa. *Economic Geology* **77**, 1328-1347.

Kondo, M., Tsuchiyama, A., Hirai, H. & Koishikawa, A. (1997). High resolution X-ray computed tomographic (CT) images of chondrites and a chondrule. *Twenty-first symposium on Antarctic meteorites*, Tokyo, Japan, **10**, 437-447.

Kyle, J. R. & Ketcham, R. A. (2003). In Situ distribution of gold in ores using high-resolution X-ray computed tomography. *Economic Geology* **98**, 1697-1701.

Kyle, J. R., Ketcham, R. A. & Mote, A. S. (2004). Contributions of high resolution X-ray computed tomography to ores studies. In: Muhling, J. (ed.) *Extended Abstracts, Predictive Mineral Discovery Under Cover.* University of Western Australia, 387-390.

Laporte, D. & Provost, A. (2000). The grain-scale distribution of silicate, carbonate and metallosulfide partial melts: a review of theory and experiments. In: Bagdassarov, N., Laporte, D. & Thompson, A. B. (ed.) Physics *and Chemistry of Partially Molten Rocks*. Dordrecht, The Netherlands: Kluwer Academic Publishers, 93-140.

Li, C., Ripley, E. M., Merino, E. & Maier, W. D. (2004). Replacement of base metal sulfides by actinolite, epidote, calcite, and magnetite in the UG2 and Merensky Reef of the Bushveld Complex, South Africa. *Economic Geology* **99**, 173-184.

McCallum, I. S., Raedeke, L. D. & Mathez, E. A. (1980). Investigations of the Stillwater Complex: Part I. Stratigraphy and Structure of the Banded Zone. *American Journal Of Science* **280-A**, 59-87.

Mees, F., Swennen, R., Van Geet, M. & Jacobs, P. (2003). Applications of X-ray computed tomography in the geosciences. (ed.) London: Geological Society, 215 pp.

Michaud, E., Desrosiers, G., Long, B., de Montety, L., Cremer, J.-F., Pelletier, E., Locat, J., Gilbert, F. & Stora, G. (2003). Use of axial tomography to follow temporal changes of benthic

communities in an unstable sedimentary environment (Baie des Ha! Ha!, Saguenay Fjord). *Journal of Experimental Marine Biology and Ecology* **285-286**, 265-282.

Naldrett, A. J., Gasparrini, E. C., Barnes, S. J., Von Gruenewaldt, G. & Sharpe, M. R. (1986). The Upper Critical Zone of the Bushveld Complex and the origin of Merensky-type ores. *Economic Geology* **81**, 1105-1117.

Page, N. J. & Zientek, M. L. (1985). Geologic and structural setting of the Stillwater Complex. In: Czamanske, G. K. & Zientek, M. L. (ed.) *The Stillwater Complex, Montana : geology and guide*. Butte, Montana: Montana Bureau of Mines and Geology, Special Publication, *no. 92*, 1-8.

Premo, W. R., Helz, R. T., Zientek, M. L. & Langston, R. B. (1990). U-Pb and Sm-Nd ages for the Stillwater Complex and its associated sills and dikes, Bearthooth Mountains, Montana: Identification of a parent magma? *Geology* **18**, 1065-1068.

Prichard, H. M., Barnes, S.-J., Maier, W. D. & Fisher, P. C. (2004). Variations in the nature of the platinum-group minerals in a cross-section through the Merensky Reef at Impala Platinum: Implications for the mode of formation of the reef. *Canadian Mineralogist* **42**, 423-437.

Riegger, O. K. & Van Vlack, L. H. W. (1960). Dihedral angle measurement. *Transactions of the Mettalurgical Society of the AIME* **218**, 933-935.

Rose, L. A. & Brenan, J. M. (2001). Wetting properties of Fe-Ni-Co-Cu-O-S melts against olivine: Implications for sulfide melt mobility. *Economic Geology* **96**, 145-157.

South African Committee For Stratigraphy. (1980). Stratigraphy of Southern Africa. Part 1. Lithostratigraphy of South Africa, South West / Namibia, and the Republics of the Boputhatswana, Trankei, and Venda. In: (ed.) Geological Survey of South Africa Handbook. 8, 690.

Turner, A. R., Wolfgram, D. & Barnes, S. J. (1985). Geology of the Stillwater County sector of the J-M Reef, including the Minneapolis Adit. In: Czamanske, G. K. & Zientek, M. L. (ed.) *The Stillwater Complex, Montana : geology and guide*. Butte, Montana: Montana Bureau of Mines and Geology, Special Publication, **no. 92**, 210-230.

Viljoen, M. J. & Hieber, R. (1986a). The Rustenburg section of the Rustenburg Platinum Mines Limited, with reference to the Merensky Reef. In: Anhaeusser, C. R. & Maske, S. (ed.) *Mineral Deposits of Southern Africa*. Johannesburg: Geological Society of Southern Africa, II, 1107-1034.

Viljoen, M. J., Theron, J., Underwood, B. M., Walters, J. & Peyerl, W. (1986b). The Amandelbult section of Rustenburg Platinum Mines Limited, with reference to the Merensky Reef. In: Anhaeusser, C. R. & Maske, S. (ed.) Mineral *Deposits of Southern Africa.* Johannesburg: Geological Society of Southern Africa, II, 1041-1060.

Von Bargen, N. & Waff, H. S. (1986). Permeabilities, interfacial areas and curvatures of partially molten systems. Results of numerical computations of equilibrium microstructures. *Journal of Geophysical Research* **91**, 9261-9276.

VonGruenewaldt, G. (1986). Platinum-group element-chromitite associations in the Bushveld Complex. *Economic Geology* **81**, 1067-1079.

VonGruenewaldt, G. (1989). Contrasting platinum-group element concentration patterns in cumulates of the Bushveld Complex. *Mineralium Deposita* **24**, 219-229.

Watson, E. B. & Brenan, J. M. (1987). Fluids in the lithosphere, 1. Experimentally-determined wetting characteristics of CO_2-H_2O fluids and their implications for fluid transport, host-rock physical properties, and fluid inclusion formation. *Earth and Planetary Science Letters* **85**, 497-515.

Wellington, S. L. & Vinegar, H. J. (1987). X-ray computerized tomography. *Journal of Petroleum Technology* **39**, 885-898.

Wessel, P. & Smith, W. H. F. (1998). New, improved version of Generic Mapping Tools released. *EOS Trans. Amer. Geophys.* **U. 79**, 579

Willmore, C. C., Boudreau, A. E. & Kruger, F. J. (2000). The halogen geochemistry of the Bushveld Complex, Republic of South Africa: Implications for chalcophile element distribution in the lower and critical zones. *Journal of Petrology* **41**, 1517-1539.

Zientek, M. L., Czamanske, G. K. & Irvine, T. N. (1985). Stratigraphy and nomenclature for the Stillwater Complex. In: Czamanske, G. K. & Zientek, M. L. (ed.) The *Stillwater Complex, Montana : geology and guide.* Butte, Montana: Montana Bureau of Mines and Geology, Special Publication, **no. 92**, 21-32.

Zientek, M. L., Cooper, R. W., Corson, S. R. & Geraghty, E. P. (2002). Platinum-Group Element Mineralization in the Stillwater Complex, Montana. In: Cabri, L. J. (ed.) *Geology, Geochemistry, Mineralogy and Mineral beneficiation of Platinum Group Element.* Canadian Institute of Mining, Metallurgy and Petroleum, **Special Volume 54**, 459 - 481.

CHAPITRE 3

PLATINUM-GROUP ELEMENTS IN SULPHIDE MINERALS, PLATINUM-GROUP MINERALS, AND THE WHOLE ROCK OF THE MERENSKY REEF (BUSHVELD COMPLEX, SOUTH AFRICA): IMPLICATION FOR THE FORMATION OF THE REEF

BELINDA GODEL[1]*, SARAH-JANE BARNES[1] & WOLFGANG D. MAIER[2]

[1] UNIVERSITE DU QUEBEC A CHICOUTIMI, SCIENCES DE LA TERRE, CHICOUTIMI, G7H 2B1, CANADA

[2] CENTRE FOR EXPLORATION TARGETING, UNIVERSITY OF WESTERN AUSTRALIA, CRAWLEY, 6009, AUSTRALIA

Journal of Petrology, 2007, Vol. 48, pp. 1569- 1604.

3.1. – RESUMÉ

Dans un premier temps, la concentration des éléments du groupe du platine (PGE) ainsi que Ni, Cu, Co, Re, Au et Ag a été déterminée dans les sulfures enrichis en métaux de base (pyrrhotite, pentlandite, chalcopyrite) et les échantillons d'une section du Merensky Reef (Complexe du Busveld). Dans un deuxième temps, l'ensemble des minéraux du groupe du platine (PGM) a été répertorié et analysé (analyses géochimiques et analyses d'images).

Le but de l'étude était d'établir :

- (i) si les sulfures sont les hôtes principaux de ces éléments
- (ii) si la concentration de ces éléments varie d'un sulfure (pyrrhotite, pentlandite, chalcopyrite) à l'autre
- (iii) si la concentration de ces éléments varie en fonction de la position stratigraphique de l'échantillon considéré et/ou de la lithologie
- (iv) la proportion de PGE contenue dans les PGM
- (iv) si les sulfures et les PGM sont les seules phases présentes qui peuvent contenir des PGE

Dans l'ensemble des lithologies, la plupart des PGE (~65 à 85%) sont contenus dans les PGM (alliage de Pt-Fe, sulfure de Pt-Pd, bismuthotellurure de Pt-Pd essentiellement). Une quantité mineure de PGE est contenu en solution solide dans les sulfures enrichis en métaux de base (BMS). La pentlandite est le BMS qui contiennent le plus de PGE (à l'exception de Pt) avec des concentrations pouvant atteindre 600 ppm (essentiellement Pd et Rh). La pyrrhotite contient Rh, Os, Ir, Ru mais exclu le Pt et le Pd. La chalcopyrite contient très peu de PGE mais concentre l'Ag et le Cd. Le platine et l'or ne se concentrent dans aucun des BMS. Ces métaux se retrouvent seulement sous la forme de minéraux du groupe du platine et d'electrum.

Les niveaux de chromite sont enrichis en PGE (à l'exception de Pd) d'un facteur 5 par rapport aux S, Ni, Cu et Au. Cet enrichissement pourrait être attribué à une plus forte concentration en EGP dans les sulfures contenus dans les chromites. Cette hypothèse est peu vraisemblable car le contenu en EGP des sulfures varie peu en fonction de la lithologie et de la position stratigraphique. Les sulfures contenus dans les chromites contiennent seulement deux fois plus de PGE que les sulfures contenus dans les roches silicatées du Merensky Reef. Cela n'explique donc pas le fort enrichissement observé dans les chromites.

L'ensemble des résultats permet de proposer que l'enrichissement particulier en EGP des niveaux de chromites et des roches silicatés du Merensky Reef est du à deux processus successifs et complémentaires.

Dans les roches silicatées, les PGE sont seulement collectés par un liquide sulfuré qui percole dans la pile de cristaux. Dans les niveaux de chromite : (i) des PGM cristallisent avant la saturation en soufre du magma et se déposent avec les grains de chromite formant un niveau enrichi en chromite et PGE ; (ii) dés que le magma est saturé en soufre, un liquide sulfuré immiscible se forme et collecte le reste des PGE présents. Ce liquide percole vers le bas dans la pile de cristaux lors de la compaction. La migration des liquides sulfurés s'arrête au niveau de chromite sous-jacent.

3.2. – ABSTRACT

The concentrations of platinum-group elements (PGE), Co, Re, Au and Ag have been determined in the base-metal sulphide (BMS) of a section of the Merensky Reef. In addition we performed detailed image analysis of the platinum-group minerals (PGM). The aims of the study were to establish: (i) whether the BMS are the principal host of these elements; (ii) whether individual elements preferentially partition into a specific BMS; (iii) whether the concentration of the elements varies with stratigraphy or lithology; (iv) what is the proportion of PGE hosted by PGM; and (v) whether the PGM and the PGE found in BMS could account for the complete PGE budget of the whole rocks.

In all lithologies, most of the PGE (~65 up to ~85 %) are hosted by PGM (essentially Pt-Fe alloy, Pt-Pd sulphide, Pt-Pd bismuthotelluride). Lesser amounts of PGE occur in solid solution within the BMS. In most cases, the PGM occur at the contact between the BMS and silicates or oxides, or are included within the base metal sulphides. Pentlandite is the principal BMS host of all of the PGE, except Pt, and contains up to 600 ppm combined PGE. It is preferentially enriched in Pd, Rh and Co. Pyrrhotite contains, Rh, Os, Ir, Ru, but excludes both Pt and Pd. Chalcopyrite contains very little of the PGE, but does concentrate Ag and Cd. Platinum and Au do not partition into any of the BMS. Instead, they occur in the form of PGM and electrum.

In the chromitite layers, the whole rock concentrations of all the PGE except Pd are enriched by a factor of 5 relative to S, Ni, Cu and Au. This enrichment could be attributed to BMS in these layers being richer in PGE as the BMS in the silicate layers. However, the PGE content in the BMS varies only slightly as a function of the stratigraphy. The BMS in the chromitites contain twice as much PGE than the BMS in the silicate rocks, but this is not sufficient to explain the strong enrichment of PGE in the chromitites. In the light of our results, we propose that the collection of the PGE occurred in two steps in the chromitites: some PGM

formed before sulphide saturation during chromitite layer formation. The remaining PGE were collected by an immiscible sulphide liquid which percolated downward until it encountered the chromitite layers. In the silicate rocks, PGE were only collected by the sulphide liquid.

Keywords: Merensky Reef, Rustenburg Platinum Mine, sulphide, platinum-group elements, image analysis, laser ablation ICP-MS

3.3. – INTRODUCTION

Many large mafic and ultramafic layered intrusions, such as the Bushveld Complex (South Africa), contain thin layers enriched in platinum-group elements (PGE) and Au. These are commonly referred to as reefs. The Merensky Reef is one of the PGE-rich layers of the Bushveld Complex and, after the UG2 chromitite, the second largest PGE resource in the world (Cawthorn, 1999b). Several processes have been proposed to explain the enrichment of the PGE and the other noble metals in cumulates of layered intrusions. Some authors suggested that the PGE could crystallise from the magma as platinum-group minerals (PGM) which accumulate on the top of the crystal pile (*e.g.* Hiemstra, 1979). Others suggest that PGE are collected by a sulphide liquid that segregated from the magma and this sulphide liquid accumulated on the crystal pile (*e.g.* Campbell *et al.*, 1983; Naldrett *et al.*, 1986). Another process proposed is the collection of PGE by magmatic fluids enriched in Cl (Boudreau and McCallum, 1992; Willmore *et al.*, 2000) which percolated upwards through the cumulate pile and precipitated sulphides and PGE. The cumulate could also have undergone a low temperature alteration which modified the PGE distribution (Li *et al.*, 2004; Polovina *et al.*, 2004). Although the processes through which PGE collection occurs remain unclear, it is clear that the PGE in the reefs are in many cases found associated with base-metal sulphides (BMS) and/or occur in PGM that are associated with these BMS (Kinloch, 1982; Ballhaus and Sylvester, 2000; Zientek *et al.*, 2002; Prichard *et al.*, 2004). The reef associated with chromitites and magnetites usually contain few visible BMS. However, this is interpreted to be the result of magmatic or post-magmatic BMS resorption (Naldrett and Lehmann, 1988; Maier *et al.*, 2003). Ballhaus and Sylvester (2000) reported the PGE concentrations in pyrrhotite and pentlandite and the presence of PGM inclusions in olivine, chromite and BMS from four samples of the Merensky Reef at Rustenburg Platinum Mine. They concluded that apart from Pt, the PGE are largely present in pyrrhotite and pentlandite. However, the presence of PGE-rich inclusions

in olivine and chromite, and the presence of PGE-rich zones in the BMS suggested to Ballhaus and Sylvester (2000) that the magma was initially saturated in platinum-group minerals (PGM) as minute grains and that these grains were incorporated by the sulphide liquid and other minerals at the stratigraphic layer that is now the Merensky Reef.

Barnes and Maier (2002a) examined the PGE, S, Ni and Cu concentrations of each rock type in the reef at Impala Platinum Mines (Fig. 3.1). They concluded that the PGE concentrations in the silicate rocks could be modelled by collection of the PGE by a base metal sulphide liquid from the magma followed by percolation of the dense sulphide liquid down through the compacting cumulate pile. They also concluded that this model would not suffice to explain PGE distribution in the chromitite layers and suggested that in addition to the collection of the PGE by sulphide liquid either: (i) some PGM crystallized and settled onto the chromitite layer before the base metal sulphide liquid percolated down through the cumulate pile; or (ii) the BMS that were originally in the chromitite layer had interacted with the chromite (Naldrett and Lehmann, 1988) resulting in loss of S, Cu and Pd from the chromitite layer. Prichard *et al.* (2004) investigated the PGM present in the Impala Platinum Mines samples to test whether any primary PGM are present in the chromitite layers which would support the model requiring crystallization of PGM directly from the magma. They found that both in the chromitite layers and the silicate rocks most (~84%) PGM are within the BMS or at the contact between BMS and silicates and appear to have formed by exsolution from the BMS. Thus, the PGM mineralogy does not provide any evidence that primary PGM have crystallized directly from the magma. The close association of the PGE with BMS suggests that they were initially collected by base metal sulphide liquid. However the BMS in the chromitite layers has been depleted in S, Fe, and Pd either by dissolution of the original BMS by rising hydrous fluid, or by reequilibration of the BMS with chromite.

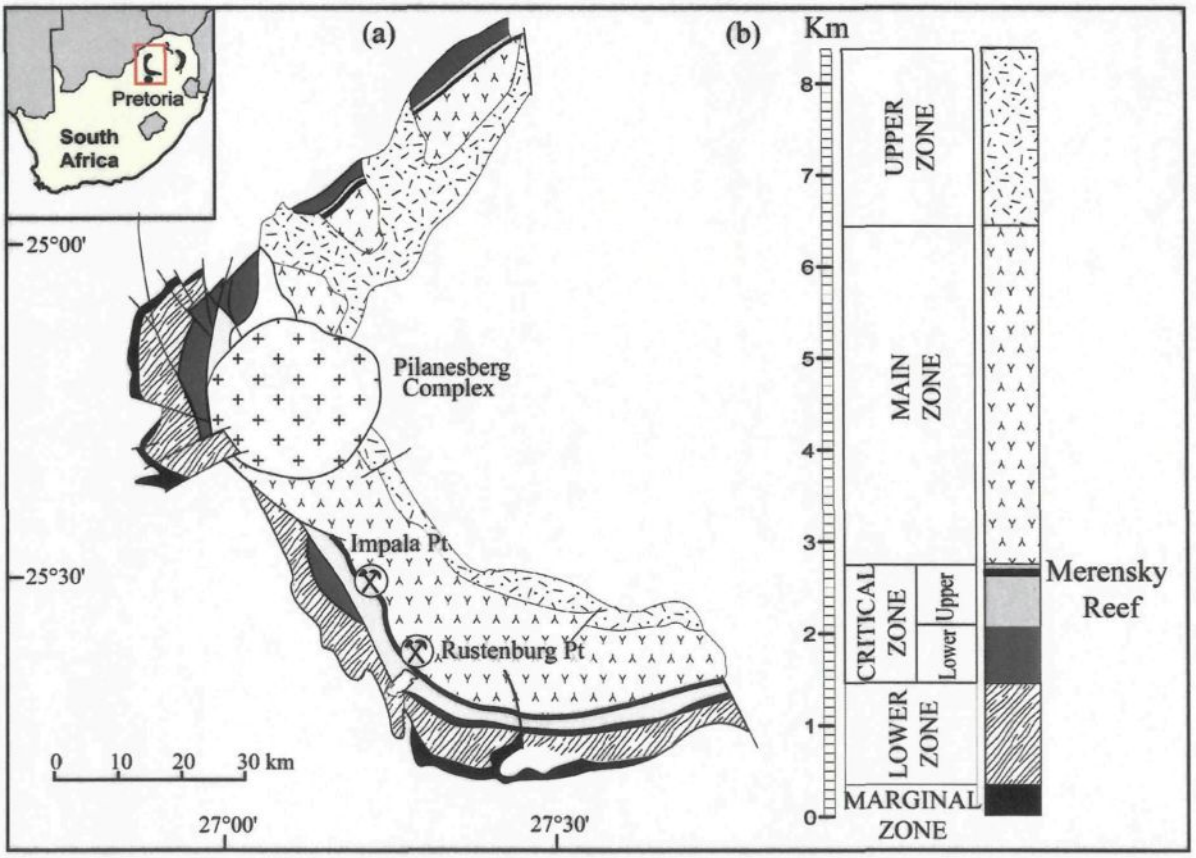

Figure 3.1: Details of the geology of the western lobe of the Bushveld Complex, South Africa.

(a) Simplified geological map (modified after Von Gruenewaldt *et al.,* 1986 and 1989).
(b) Generalized stratigraphy of the Bushveld Complex (modified after Eales & Cawthorn, 1996).
The study locality is Rustenburg Platinum Mines, Frank Shaft.

Godel *et al.* (2006), in a 3-D textural study on samples from Rustenburg Mine (Fig. 3.1), showed that the BMS form networks following vertical dilatancies interpreted to be formed during compaction and that dihedral angles between silicates and BMS are much lower than those between BMS and chromite. These observations suggest that the sulphide liquid wet the silicate minerals more efficiently than chromite. Thus the sulphide liquid could have percolated downwards through the cumulate pile until it encountered the chromitite layer. Because the sulphide liquid could not easily wet the chromite surface it would tend to accumulate at the top of the chromitite layer (Godel *et al.*, 2006).

In the current work we have attempted to establish which minerals host the PGE in order to better constrain these models. The first aim of this study is to determine the concentration of PGE, Re, Ag, Au, Cd and Co in the BMS (pentlandite, pyrrhotite and chalcopyrite) and the whole rocks, within different lithologies (anorthosite, chromitites, melanorites) of the Merensky Reef at Rustenburg Platinum Mine. This was done to establish; (i) whether the BMS are the principal hosts of these elements; (ii) whether these elements preferentially partition into specific BMS; (iii) whether PGE and other metal contents of the BMS vary with stratigraphic position and/or lithologies. In addition, detailed image analysis of the platinum-group mineral distribution has been conducted. Together with the BMS compositional data, this allowed the calculation of a PGE mass balance.

3.4. - GEOLOGY AND PETROGRAPHY

The Merensky Reef is one of several layers enriched in platinum-group element (PGE) in the Upper Critical Zone of the Bushveld Complex, South Africa (Fig. 3.1). It contains 5-10 ppm PGE (Barnes and Maier, 2002a; Cawthorn, 2002). In most cases, the PGE are associated with disseminated BMS (Viljoen and Hieber, 1986). The sample studied in detail in this work is a slab

of normal "narrow" Merensky Reef from Frank Shaft, Rustenburg Platinum Mine (Fig. 3.1). The sample was previously used for microtomographical and microstructural analyses (Godel *et al.*, 2006). More details on the reef type and its extension are notably described in Viljoen and Hieber (1986), Viljoen *et al.* (1986) and Loeb-du-Toit (1986).

The petrography of the sample has been described in detail in the previous paper (Godel *et al.*, 2006), and only a summary is presented here. The Merensky Reef sample is composed, from bottom to top, of five layers (Fig. 3.2): a basal anorthosite overlain by a 0.7 to 1 cm chromitite which undulates on a centimetre scale; a coarse-grained melanorite of ~10 cm thickness; a second layer of chromitite of ~1cm thickness and finally a melanorite. All lithologies contain disseminated BMS (Fig. 3.3). The BMS content varies (from 0.5 to 8 vol%) as a function of the stratigraphy of the Merensky Reef (Godel *et al.*, 2006). The BMS are composed of intergrowths of pyrrhotite, pentlandite and chalcopyrite and are in the silicate rocks located in 3-D vertical networks interpreted to have formed during the compaction of the cumulate pile (Godel *et al.*, 2006). In contrast, in the chromitite layers the BMS occur as small droplets.

3.5. - ANALYTICAL METHODS

Oriented polished thin sections with a thickness of 100 microns were cut along a vertical section across the slab (Fig. 3.2). Base-metal sulphides (pyrrhotite, pentlandite and chalcopyrite, Fig. 3.3) in the thin sections were examined with an optical microscope and sites were then selected for further analysis. In order to assess the exact position of the analysed BMS in the Reef, thin sections and selected BMS were referenced to the paleovertical.

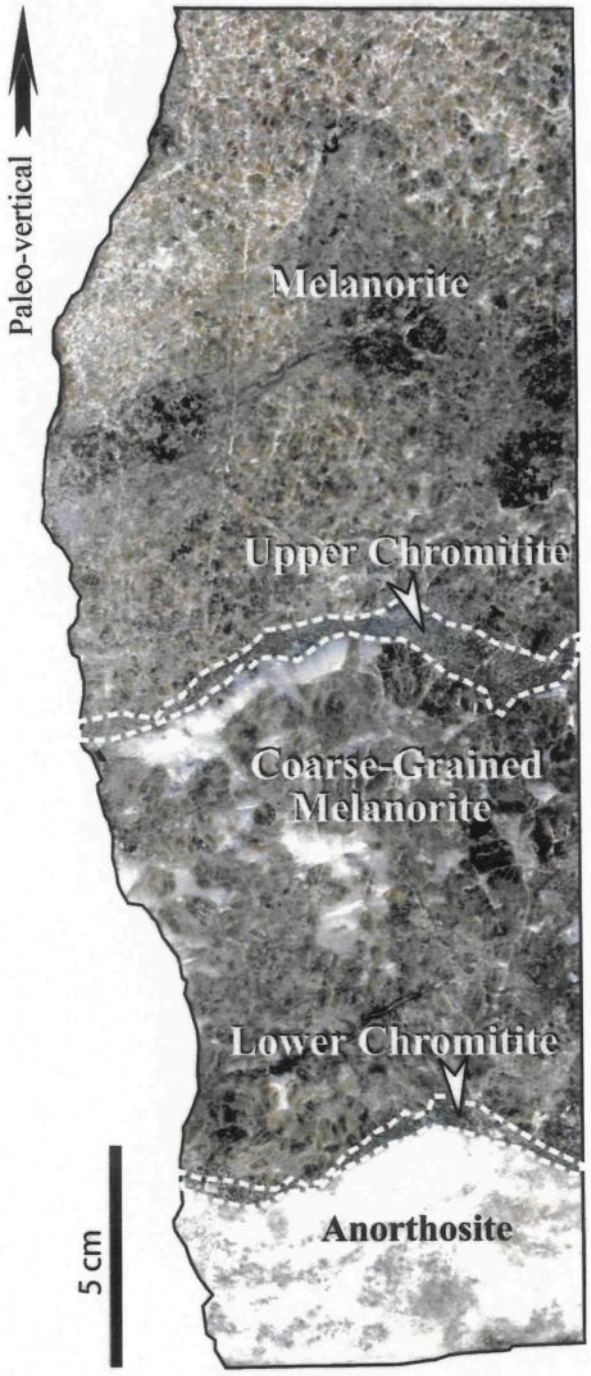

Figure 3.2: Photograph of the sample of Merensky Reef used in this study.

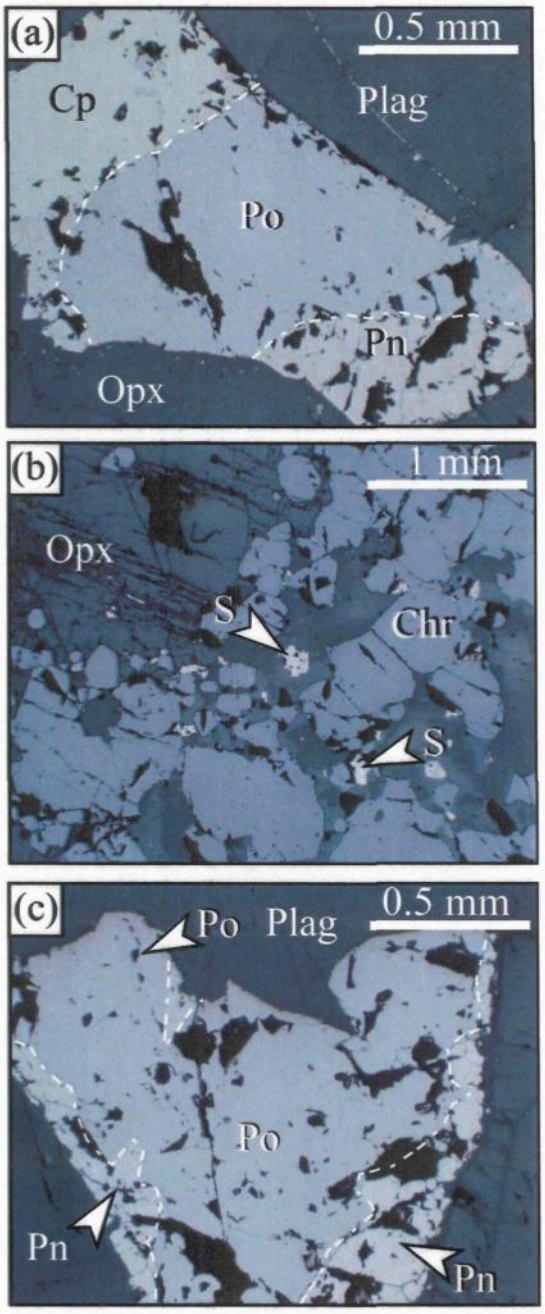

Figure 3.3: Examples of base-metal sulphides observed in our samples of Merensky Reef.

(a) Intergrowth of pyrrhotite (Po), pentlandite (Pn) and chalcopyrite (Cp) in coarse-grained melanorite (Opx: orthopyroxene; Plag: plagioclase).
(b) Disseminated base-metal sulphides (S) in the chromitite layers (Chr: chromite; Opx: orthopyroxene).
(c) Pyrrhotite (Po) surrounded by pentlandite (Pn) in the melanorite.

Major elements (S, Ni, Fe and Cu) were determined by microprobe analysis at Laval University (Quebec City) using a CAMECA SX100 electron microprobe. The microprobe was operated at 15 kV and 20 nA and a beam diameter of 2 to 5 μm and a counting time of 20 s and 10 s on peak and backgrounds, respectively. The standards used were from Astimex Microanalysis Standard: hematite for Fe; pentlandite for Ni; skutterudite for Co; marcassite for S. The standard for Cu is the chalcopyrite from P and H Developments Ltd. The results of the microprobe analyses are summarized in Table 3.1.

The concentration of the PGE, Re, Cd, Co, Au and Ag in BMS was determined at the University of Quebec, Chicoutimi (UQAC) using a laser ablation-inductively coupled plasma-quadrupole mass spectrometer along with an hexapol collision cell (LA-HEX-ICP-MS). The UQAC laser-ablation ICP-MS consists of a Thermo X7 ICP-MS with high-performance interface coupled with a New Wave Research 213 nm Nd:YAG UV laser ablation microprobe. The analyses were conducted using an 80 micron diameter spot, a laser frequency of 20 Hz and a power of 0.8 mJ/pulse. An analysis took 90 s (30 seconds of analysis of the gas background followed by 60 seconds of analysis of the minerals). A helium carrying gas mixed with argon was used. The ablated material was then analysed using the Thermo X7 ICP-MS operating in time-resolved mode using peak jumping. ^{34}S was used as internal standard to determine concentrations of PGE and other metals. The calibration was carried out using a synthetic FeS standard (Po-52) which had been doped with ~10 ppm of each of the PGE and Au. The exact concentrations of the PGE and Au in Po-52 have been determined by standard solution analysis (Table 3.2). To verify the accuracy of the calibration, the FeS standard LaFlamme-Po727 provided by CANMET has been analysed and the results are within the accepted values (Table 3.2).

Table 3.1: *Average composition of major elements of the sulphide minerals as a function of the stratigraphy.*

Rock type	Sulphide	n		S wt%	Fe wt%	Cu wt%	Ni wt%	Co wt%	Total wt%
AN	Pyrrhotite	3	Average	38.99	59.97	<0.01	0.42	<0.01	99.39
			StDev	*0.19*	*0.60*	-	*0.19*	-	
	Pentlandite	3	Average	32.58	31.18	<0.01	34.87	0.36	98.98
			StDev	*0.33*	*0.71*	-	*0.36*	*0.14*	
	Chalcopyrite	3	Average	34.20	30.43	33.98	<0.01	<0.01	98.61
			StDev	*0.11*	*0.07*	*0.06*	-	-	
LC & CGM	Pyrrhotite	2	Average	37.99	61.31	<0.01	0.30	<0.01	99.60
			StDev	*0.28*	*0.01*	-	*0.13*	-	
	Pentlandite	3	Average	32.62	32.59	<0.01	32.98	0.57	98.76
			StDev	*0.06*	*1.58*	-	*1.03*	*0.06*	
	Chalcopyrite	3	Average	34.29	30.54	34.15	<0.01	<0.01	98.97
			StDev	*0.07*	*0.10*	*0.21*	-	-	
CGM	Pyrrhotite	4	Average	37.26	61.45	<0.01	0.12	<0.01	98.83
			StDev	*0.54*	*0.29*	-	*0.06*	-	
	Pentlandite	2	Average	32.39	34.81	<0.01	30.53	0.66	98.40
			StDev	*0.11*	*0.53*	-	*1.04*	*0.19*	
	Chalcopyrite	4	Average	34.10	30.59	33.84	<0.01	<0.01	98.52
			StDev	*0.18*	*0.39*	*0.15*	-	-	
UC	Pyrrhotite	3	Average	38.03	61.27	<0.01	0.16	<0.01	99.45
			StDev	*0.16*	*0.56*	-	*0.04*	-	
	Pentlandite	3	Average	32.54	34.41	<0.01	31.52	0.67	99.14
			StDev	*0.02*	*0.44*	-	*0.43*	*0.16*	
	Chalcopyrite	2	Average	34.13	30.46	33.65	<0.01	<0.01	98.25
			StDev	*0.00*	*0.03*	*0.13*	-	-	
M	Pyrrhotite	4	Average	37.73	61.15	<0.01	0.17	<0.01	99.05
			StDev	*0.13*	*0.52*	-	*0.07*	-	
	Pentlandite	2	Average	32.42	33.88	<0.01	31.23	0.54	98.07
			StDev	*0.13*	*0.69*	-	*0.39*	*0.12*	
	Chalcopyrite	2	Average	33.99	30.21	33.70	<0.01	<0.01	97.90
			StDev	*0.05*	*0.17*	*0.20*	-	-	
M	Pyrrhotite	5	Average	37.33	61.01	<0.01	<0.01	<0.01	98.34
			StDev	*0.88*	*0.75*	-	-	-	
	Pentlandite	6	Average	32.12	32.69	<0.01	32.36	0.53	97.70
			StDev	*0.01*	*1.36*	-	*1.39*	*0.14*	
	Chalcopyrite	4	Average	34.03	30.26	33.69	<0.01	<0.01	97.98
			StDev	*0.13*	*0.40*	*0.25*	-	-	
M	Pyrrhotite	4	Average	37.95	60.58	<0.01	0.51	<0.01	99.04
			StDev	*0.16*	*0.16*	-	*0.12*	-	
	Chalcopyrite	2	Average	34.01	30.56	33.94	<0.01	<0.01	98.50
			StDev	*0.11*	*0.15*	*0.09*	-	-	
M	Pyrrhotite	4	Average	38.02	60.48	<0.01	0.44	<0.01	98.94
			StDev	*0.16*	*0.28*	-	*0.14*	-	
	Pentlandite	3	Average	32.08	31.23	<0.01	33.65	0.33	97.29
			StDev	*0.11*	*0.37*	-	*0.20*	*0.12*	
	Chalcopyrite	5	Average	33.92	30.51	33.81	<0.01	<0.01	98.23
			StDev	*0.18*	*0.28*	*0.05*	-	-	

StDev = Standard deviation for *n* different analysis.

AN: anorthosite; LC: lower chromitite; CGM: coarse-grained melanorite; UC: upper chromitite; M: melanorite.

Table 3.2: *Estimation of LA-ICP-MS precision and accuracy based on analysis of FeS standard.*

Sample	Method, Laboratory	*n*	^{101}Ru ppm	^{103}Rh ppm	^{105}Pd ppm	^{108}Pd ppm	^{192}Os ppm	^{193}Ir ppm	^{195}Pt ppm	^{197}Au ppm
PO-52	Standard addition, UQAC	6	5.32	6.53	8.67	8.67	11.60	9.71	9.01	11.28
	StDev		*0.25*	*0.50*	*0.65*	*0.65*	*1.20*	*0.45*	*0.65*	
	RSD (%)		*4.7*	*7.7*	*7.5*	*7.5*	*10.3*	*4.6*	*7.2*	
PO-52	LA-ICP-MS, UQAC	118	5.31	6.53	8.69	8.69	11.56	9.69	8.99	10.96
	StDev		*0.29*	*0.40*	*0.40*	*0.34*	*0.92*	*0.72*	*0.57*	*1.96*
	RSD (%)		*5.5*	*6.1*	*4.6*	*3.9*	*8.0*	*7.4*	*6.3*	*17.9*
LaFlamme Po727	Accepted value, CANMET	43	36.50	41.60	43.40	43.40	46.70	48.00	35.50	45.80
	StDev		*0.30*	*0.30*	*0.30*	*0.30*	*2.60*	*1.20*	*0.80*	*2.40*
	RSD (%)		*0.8*	*0.7*	*0.7*	*0.7*	*5.6*	*2.5*	*2.3*	*5.2*
LaFlamme Po727	LA-ICP-MS, UQAC	24	36.41	41.69	43.50	43.29	46.94	48.21	35.36	45.73
	StDev		*2.72*	*2.86*	*2.80*	*4.11*	*4.21*	*4.21*	*2.78*	*2.90*
	RSD (%)		*7.5*	*6.9*	*6.4*	*9.5*	*9.0*	*8.7*	*7.9*	*6.3*

StDev = Standard deviation for *n* different spot.

RSD = Relative standard deviation (StDev x 100 / average for n different spots).

The use of the collision cell reduces much of the Ni and Cu argide interferences on PGE (Mason and Kraan, 2002). Nonetheless there is still some Ni interference on Ru, and some Cu interference on Rh and Pd. These were monitored by using a synthetic $NiFeS_2$ and $CuFeS_2$ blank. On the basis of the blank results 5 ppm Ru, 2 ppm Rh and 2 ppm Pd were substracted from all chalcopyrite results and 3 ppm Ru was subtracted from all pentlandite results. The Ni and Cu concentrations were calibrated using the synthetic blanks; the concentrations for these elements having been determined by microprobe. Results for Co, Ag, Cd and Re were calculated using semi-quantitative calibration. Details of how the sulphide standards were synthesized are given in Barnes *et al.* (2006) and Peregoedova *et al.* (2006). Each standard was placed with unknowns (BMS in thin sections) in the ablation chamber and was analysed at the beginning, after each ten analyses of unknowns and at the end of each analytical session. The reduction of the data was carried out using PlasmaLab software (ThermoElemental) by subtracting gas background from each of the analysed isotopes. The results of calibrations during all analytical sessions are summarised in Table 3.2. As the analysed BMS are intergrowths of pyrrhotite, pentlandite and chalcopyrite, the concentrations of Ni and Cu were monitored to verify that the signal was generated by only one mineral. The analyses with Ni and/or Cu signals higher than the microprobe concentration (depending on BMS) were not used in further calculations. The detection limits for each BMS are summarized in Table 3.3.

In order to compare the PGE content in the BMS with the PGE content in the whole rocks, the samples (corresponding to the thin sections) were crushed in an Al-ceramic mill at UQAC. Copper and Ni associated with BMS were determined by atomic absorption spectrometry (AA) at UQAC. Sulphur was also determined at UQAC using an HORIBA EMIA-220V series analyser.

***Table 3.3**: Detection limit for the analysis of the base-metal sulphides by LA-ICP-MS*

	^{101}Ru	^{103}Rh	^{105}Pd	^{108}Pd	^{192}Os	^{193}Ir	^{195}Pt	^{197}Au
Element	ppm	ppm	ppm	ppm	ppm	ppm	ppm	ppm
Pyrrhotite	0.009	0.005	0.035	0.021	0.004	0.001	0.004	0.001
Pentlandite	0.074	0.015	0.067	0.056	0.013	0.003	0.003	0.002
Chalcopyrite	0.150	0.060	0.350	0.090	0.030	0.020	0.100	0.030

Detection limit = $3 \times (2 \times BC)^{1/2} \times C / I$

BC = background counts

C = concentration of analyte in the standard

I = peak intensity for the analyte

Table 3.4: *Comparison of certified values and values obtained in this study for the International Reference Material AMIS0007.*

	Certified values		UQAC	
Element	ppm	+/-	ppm	+/-
Cr	12817	2644	13438	436
Co	335	65	315	9
Ni	2072[a]	208	1774[c]	96
Ni	1669[b]	200	1541[b]	30
Cu	1296	150	1196[b]	34
Ru	0.45	0.06	0.421	0.024
Rh	0.25	0.04	0.265	0.008
Pd	1.5	0.2	1.457	0.064
Os	nq	nq	0.068	0.007
Ir	*0.09*		0.092	0.0004
Pt	2.48	0.28	2.633	0.045
Au	0.155	0.016	0.156	0.006

[a] Total acid digestion

[b] Aqua regia partial digestion

[c] INAA on rock powder

nq: not quantified

The precision of the S analyses based on the relative standard deviation (RDS) is < 2.5% (Bédard *et al.*, in prep). The PGE and Au in the silicate rocks were determined by Ni-sulphide fire assay followed by instrumental neutron activation analysis (INAA) on 10 g of sample using a slightly modified version of the Steele *et al.* (1975) formulas. Because of the difficulty of dissolving chromitites in the standard flux mixtures, the flux mixture for the chromitites was modified using the formula of Bédard and Barnes (2004). Results from our laboratory are in agreement with the certified values for the international reference material AMIS0007, which is a sample of Merensky Reef (Table 3.4).

3.6. – RESULTS

3.6.1. - Major elements in BMS and proportion of each BMS

Major element (S, Cu, Ni, Fe, Co) contents in the BMS are summarized in Table 3.1. These concentrations are relatively constant. The proportion of each BMS in each lithology was then calculated using the whole rock S, Cu and Ni contents (Table 3.5). The calculation is based on the following assumptions: (i) the BMS are a mixture of pyrrhotite, pentlandite and chalcopyrite; (ii) all the Cu is hosted by chalcopyrite; (iii) all the Ni is hosted by pentlandite; (iv) the remaining sulphur was allocated to pyrrhotite. Whole rock Ni contents were determined by atomic absorption (AA) after aqua regia digestion and assigning all the Ni to pentlandite assumes that the Ni in the silicates did not dissolve. The total Ni content of the rocks as determined by INAA is generally ~400 ppm higher than the Ni content determined by AA; which would suggest ~570 to ~800 ppm Ni is present in the orthopyroxene. These results are in agreement with orthopyroxene analyses of the Merensky Reef (Arndt *et al.*, 2005).

Table 3.5: *Whole rock analysis and recalculation to 100% sulphides.*

(a) Whole rock

Sample	Height	S	Ni	Cu	Co	Re	Os	Ir	Ru	Rh	Pt	Pd	Au	Ag	All PGE	Se
	mm	wt%	wt%	wt%	ppm	ppm	ppm	ppm	ppm	ppm	ppm	ppm	ppm	ppm	ppm	ppm
AN	-20	0.37	0.13	0.09	24	DL	0.10	0.12	0.50	0.42	5.34	4.03	0.33	DL	10.5	1.3
LC	0	0.47	0.22	0.13	211	DL	0.73	1.11	5.41	3.80	33.10	4.40	0.34	DL	48.6	DL
CGM-1	20	3.07	1.31	0.35	273	0.01	0.58	0.58	2.53	1.34	42.08	16.29	2.56	2.54	63.4	13.7
CGM-2	60	1.39	0.44	0.43	147	DL	0.14	0.14	0.60	0.40	8.84	5.94	4.64	1.64	16.1	4.3
UC	100	0.53	0.23	0.14	167	DL	0.26	0.35	1.70	1.00	13.45	4.27	0.31	DL	21.0	DL
M-1	135	3.21	1.37	0.28	291	0.02	0.49	0.63	2.78	1.69	16.55	11.90	1.27	3.07	34.0	15.4
M-2	180	0.74	0.29	0.10	117	0.01	0.09	0.10	0.36	0.21	3.14	2.22	0.34	DL	6.1	3.0
M-3	230	0.89	0.41	0.11	137	0.01	0.09	0.10	0.64	0.20	2.48	2.36	0.42	DL	5.9	4.0
M-4	270	0.98	0.42	0.14	137	0.01	0.07	0.07	0.32	0.17	5.21	2.16	0.22	DL	8.0	4.6

(b) Recalculated to 100% sulphide*

Sample	S	Ni	Cu	Co	Re	Os	Ir	Ru	Rh	Pt	Pd	Au	Ag	*Pt/Pd*	*Pd/Ir*	*All PGE*
	wt%	wt%	wt%	ppm	ppm	ppm	ppm	ppm	ppm	ppm	ppm	ppm	ppm			*ppm*
AN	36.1	12.7	8.4	2300	DL	9.4	11.4	48.1	40.7	515	389	31.4	DL	*1.3*	*34.2*	*1013*
LC	35.1	16.6	10.0	15872	DL	54.7	84.0	408.0	286.7	2495	332	25.3	DL	*7.5*	*3.9*	*3660*
CGM-1	36.1	15.5	4.1	3216	0.142	6.9	6.8	29.9	15.8	496	192	30.1	29.9	*2.6*	*28.3*	*747*
CGM-2	36.0	11.3	11.1	3790	DL	3.7	3.6	15.4	10.4	228	153	119.8	42.4	*1.5*	*42.1*	*415*
UC	35.5	15.2	9.4	11243	DL	17.5	23.6	114.8	67.1	906	288	20.6	DL	*3.1*	*12.2*	*1417*
M-1	36.3	15.5	3.1	3292	0.224	5.5	7.1	31.4	19.1	187	135	14.4	34.7	*1.4*	*18.9*	*385*
M-2	36.3	14.3	4.7	5743	0.246	4.3	5.0	17.6	10.5	154	109	16.7	DL	*1.4*	*21.9*	*300*
M-3	35.9	16.4	4.4	5507	0.218	3.8	4.1	25.7	8.2	100	95	17.1	DL	*1.0*	*23.0*	*237*
M-4	36.0	15.5	5.0	5022	0.192	2.7	2.7	11.6	6.2	191	79	7.9	DL	*2.4*	*29.0*	*294*

* $C_{(100\ percent\ sulphide)} = C_{WR}*100/(2.527*S+0.3408*Cu+0.4715*Ni)$, Barnes and Lightfoot (2005)

AN: anorthosite; LC: lower chromitite; CGM-1 and CGM-2: coarse-grained melanorites; UC: upper chromitite; M1, M2, M3 and M4: melanorite.

The weight fraction of chalcopyrite (F_{Cp}) is given by (Cu_{WR}/Cu_{Cp}), where Cu_{WR} is the concentration of Cu in the whole rock and Cu_{Cp} is the average concentration of Cu in the chalcopyrite. The weight fraction of pentlandite (F_{Pn}) is given by (Ni_{WR}/Ni_{Pn}), where Ni_{WR} is the concentration of Ni in the whole rock and Ni_{Pn} is the average concentration of Ni in the pentlandite. The weight fraction of pyrrhotite (F_{Po}) is calculated by ($S_{WR} - S_{Cp} \times F_{Cp} - S_{Pn} \times F_{Pn}$) / S_{Po}, where S_{WR} is the sulphur content in the whole rock, S_{Cp} is the average sulphur concentration in the chalcopyrite, S_{Pn} is the average sulphur concentration in the pentlandite and S_{Po} is the average sulphur concentration in the pyrrhotite. On average the BMS component of the rocks (Fig. 3.4) consists of ~44 wt% pentlandite, ~ 37 wt% pyrrhotite and ~ 19 wt% chalcopyrite. These results are in agreement with those obtained by Vermaak (1976) and Barnes and Maier (2002a) on other Merensky Reef samples. In our samples of Merensky Reef, BMS in the chromitite layers and the rock immediately below each chromitite layer are richer in chalcopyrite (25-30 wt%) than the silicate rocks overlying the chromitite layers (9-14 wt%).

3.6.2. - PGE and other metals in BMS

All the BMS analysed (pyrrhotite, pentlandite and chalcopyrite) (Table 3.6) contain some PGE, Re, Ag, Au, Cd, Co, Cu and Ni in solid solution. Pentlandite is the BMS which contains the highest PGE concentrations, mostly (in 80% of cases) between 200 and 500 ppm of PGE (Fig. 3.5). These values are similar to those observed by Ballhaus and Sylvester (2000) and Ballhaus and Ryan (1995). On average 90% of the pyrrhotite analyses contain between 10 and 40 ppm PGE (Table 3.6, Fig. 3.5). Chalcopyrite has the lowest PGE contents, with 85% of grains containing 4 to 10 ppm (Fig. 3.5).

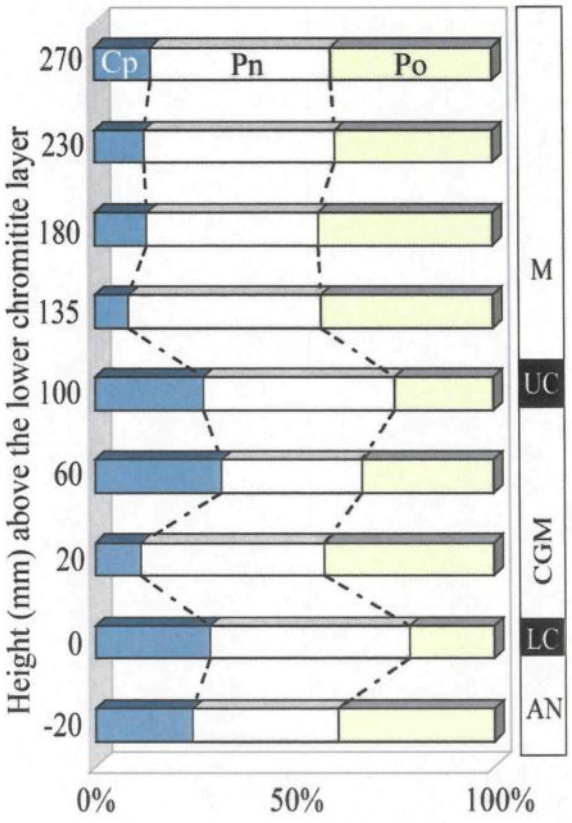

Figure 3.4: Proportions of each base-metal sulphide as a function of the stratigraphy.

Po: pyrrhotite; Pn: pentlandite; Cp: chalcopyrite.

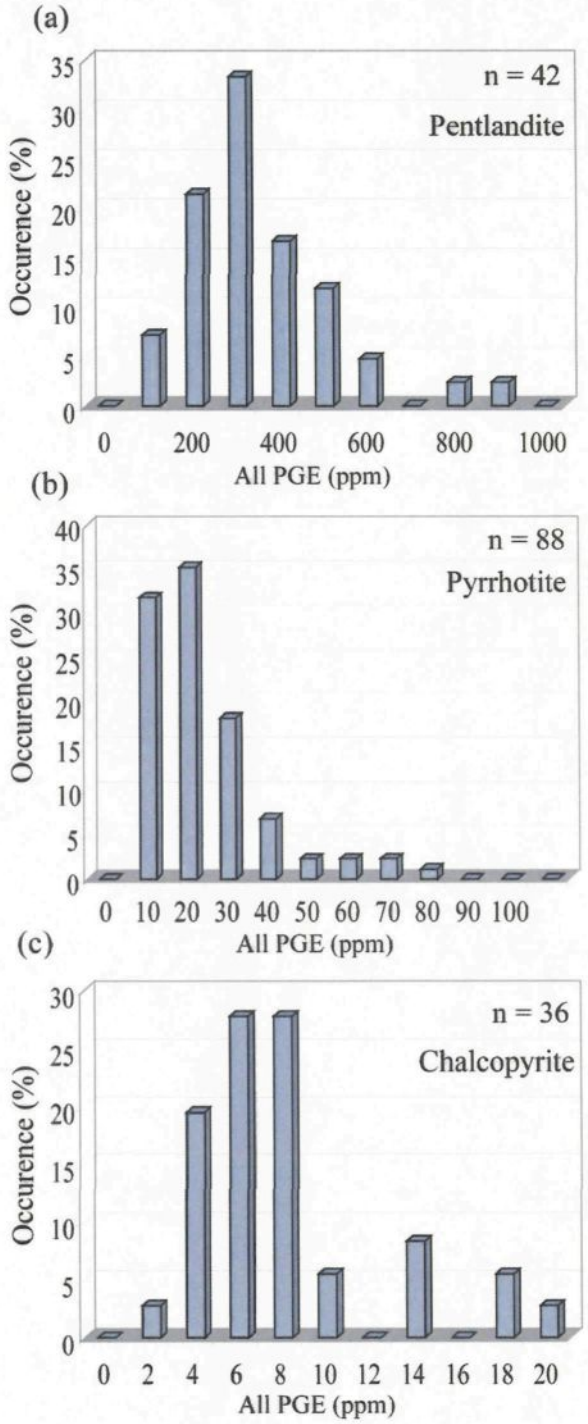

Figure 3.5: Total PGE content in base-metal sulphide minerals.

(a) in pentlandite.
(b) in pyrrhotite.
(c) in chalcopyrite.

Table 3.6: *Metal contents of the base-metal sulphides from the Merensky Reef by LA-ICP-MS.*

PENTLANDITE

Rock type	^{61}Ni	^{65}Cu	^{59}Co	^{185}Re	^{189}Os	^{193}Ir	^{101}Ru	^{103}Rh	^{195}Pt	^{105}Pd	^{197}Au	^{107}Ag	^{111}Cd
	wt%	wt%	ppm	ppm	ppm	ppm	ppm	ppm	ppm	ppm	ppm	ppm	ppm
AN	34.87	0.012	8019	0.308	1.687	2.794	4.93	6.315	9.727	222.20	0.013	1.6	1.29
AN	34.87	0.450	10930	0.631	7.244	6.985	10.92	26.21	14.75	226.50	0.017	0.8	1.41
AN	34.87	DL	12750	0.458	4.66	8.259	13.98	13.62	36.12	165.20	0.026	0.9	0.91
AN	34.87	0.157	12140	0.075	0.486	0.218	1.24	17.89	25.49	376.70	1.362	2.0	1.45
AN	34.87	0.424	8271	0.203	3.921	4.108	10.20	7.288	0.743	187.70	0.035	1.3	1.64
LC	32.98	0.003	11510	0.007	0.021	47.46	9.95	648.6	5.275	19.91	0.008	7.8	1.20
LC	32.98	0.002	9917	0.084	7.14	7.119	57.75	21.66	8.58	374.50	0.008	6.5	1.17
LC	32.98	0.087	11910	0.111	2.945	3.629	2.05	18.71	9.156	425.60	0.014	4.6	1.21
LC	32.98	0.003	12430	0.309	5.385	5.543	11.86	34.68	10.04	497.50	0.009	3.1	1.44
CGM	30.53	0.119	10030	0.065	2.88	3.729	6.77	11.15	6.217	200.10	0.015	3.6	1.26
CGM	30.53	0.005	11610	0.14	4.701	5.098	9.79	9.811	7.731	244.70	0.091	2.9	1.30
CGM	30.53	0.038	10830	1.043	2.492	1.613	2.13	14.75	3.886	191.40	0.014	2.9	1.30
CGM	30.53	0.004	12620	0.349	5.513	6.486	7.47	20.89	12.3	435.60	0.017	2.2	1.57
UC	31.52	0.003	4624	0.212	2.542	2.817	2.69	202.1	1.987	599.10	0.013	1.8	1.25
M	31.52	0.247	10890	0.197	8.026	6.176	3.34	34.3	7.208	305.30	0.007	9.6	1.56
M	31.52	0.399	9987	0.006	0.011	0.083	0.86	10.48	3.386	259.00	0.009	8.0	1.72
UC	31.52	0.921	11250	0.041	0.673	1.963	1.29	62.1	5.87	267.00	0.011	2.3	2.07
M	31.52	0.007	7291	0.069	2.178	2.25	2.09	11.08	9.01	179.80	0.010	2.3	1.34
M	31.52	0.009	14540	0.063	3.296	1.675	4.02	25.61	20.69	461.30	0.027	16.3	2.21
M	31.52	0.010	13110	0.836	4.224	3.708	5.78	44.02	7.418	310.90	0.065	3.2	2.32
M	31.52	0.022	12660	0.084	0.538	3.507	3.46	14.53	25.46	307.10	0.026	2.5	1.74
M	31.52	0.116	8010	0.15	1.565	2.735	1.40	28.85	7.3	146.30	0.012	3.6	2.39
M	31.23	0.003	11440	0.139	11.16	17.35	56.06	65.05	2.726	233.50	0.005	5.4	1.52
M	31.23	0.002	10320	0.144	2.316	3.412	1.40	24.95	5.152	219.10	DL	2.4	1.24
M	31.23	0.010	12730	0.206	5.36	7.83	3.91	44.84	3.615	237.90	DL	6.5	1.69
M	31.23	0.003	12190	0.163	3.666	5.934	2.45	25.44	3.021	233.20	0.004	6.5	1.64
M	31.23	0.003	7917	3.752	5.9	1.879	6.56	14.12	233.3	170.20	0.114	3.6	1.69
M	32.36	0.470	6505	0.012	1.963	2.186	6.56	12.34	3.535	144.80	DL	41.8	1.65
M	32.36	0.005	7184	0.202	3.577	3.048	7.15	8.644	0.017	147.10	0.015	8.3	1.77
M	32.36	0.086	3350	0.169	2.484	3.126	6.08	19.15	0.038	79.68	DL	23.4	1.50
M	32.36	0.007	7384	0.03	1.166	1.039	3.93	0.88	13.03	80.12	0.005	5.3	2.19
M	32.36	0.009	6542	0.085	2.137	2.076	7.80	11.56	0.018	83.29	0.014	2.0	1.97
M	32.36	0.007	8022	0.114	6.109	7.375	16.78	21.47	22.02	196.90	0.020	3.4	2.52
M	32.36	0.008	9042	0.043	2.416	2.815	11.18	24.29	0.045	209.70	0.006	3.7	2.46
M	32.36	0.011	10860	0.075	1.063	1.773	4.91	10.88	0.255	137.20	0.009	2.2	1.65
M	32.36	0.407	11760	0.055	1.365	1.473	3.66	5.062	151	194.20	0.081	2.5	1.68
M	33.65	0.002	8657	0.011	DL	0.203	DL	1.267	0.058	6.64	0.009	0.9	1.02
M	33.65	0.001	9096	0.025	0.398	0.87	1.99	2.729	5.76	88.70	0.007	1.0	1.04
M	33.65	0.002	9784	0.18	0.892	1.099	3.29	4.372	0.043	94.85	0.005	1.0	1.05
M	33.65	0.003	6855	0.162	0.673	1.197	2.25	4.802	0.231	62.47	0.079	2.9	1.61
M	33.65	0.003	8598	0.119	0.365	0.675	0.99	1.343	0.021	46.11	0.008	0.8	1.04
M	33.65	0.399	8869	0.277	2.263	2.165	6.37	9.539	0.198	277.40	0.006	1.5	1.19

Table 3.6 (Continued)

PYRRHOTITE

Rock type	^{61}Ni wt%	^{65}Cu wt%	^{59}Co ppm	^{185}Re ppm	^{189}Os ppm	^{193}Ir ppm	^{101}Ru ppm	^{103}Rh ppm	^{195}Pt ppm	^{105}Pd ppm	^{197}Au ppm	^{107}Ag ppm	^{111}Cd ppm
AN	0.308	0.003	140.7	0.733	3.29	5.092	8.69	1.452	9.092	1.20	0.010	0.6	1.74
AN	0.486	0.002	206	0.061	3.207	3.824	11.90	1.727	0.974	2.07	0.006	0.7	1.81
AN	0.396	0.000	151	0.237	1.787	2.395	5.39	0.116	2.402	1.48	0.003	0.7	1.20
AN	0.382	0.004	114	0.685	3.15	4.783	7.51	0.538	7.112	1.39	0.010	1.1	1.99
AN	0.532	0.001	101.5	0.007	1.269	1.13	3.06	0.096	0.405	0.32	0.057	1.0	1.22
LC	0.180	0.001	68.94	DL	0.21	3.117	2.14	0.62	0.036	0.53	0.002	0.3	0.51
LC	0.097	0.001	14.55	0.125	1.809	0.419	1.18	0.29	0.117	0.48	0.008	0.5	0.62
LC	0.250	0.000	38.07	0.155	7.347	8.78	12.76	0.82	0.575	0.46	0.004	0.3	0.72
LC	0.248	0.000	33.38	0.28	6.677	5.754	6.65	0.293	0.634	0.53	0.004	0.4	0.69
LC	0.286	0.000	30.37	0.27	5.539	5.538	5.87	0.252	0.894	0.47	0.004	0.4	0.62
CGM	0.528	0.002	135.3	DL	DL	0.003	1.66	0.541	DL	0.74	0.001	0.5	0.58
CGM	0.576	0.000	51.95	0.27	2.939	1.412	5.29	0.541	0.693	1.11	0.006	0.9	0.55
CGM	0.715	0.000	93.63	0.41	3.705	2.168	5.87	0.418	1.073	0.83	0.002	0.7	0.66
CGM	0.505	0.000	23.6	0.584	5.734	5.748	15.26	0.471	3.742	0.57	0.006	0.4	0.76
CGM	0.503	0.000	21.39	0.379	5.381	4.361	11.78	0.44	1.617	0.66	0.004	0.4	0.83
CGM	0.711	0.001	104.8	0.234	3.637	1.286	5.09	0.318	0.579	0.79	0.003	1.4	0.66
CGM	0.422	0.000	38.37	0.183	2.399	0.951	3.77	0.343	0.342	0.69	0.009	1.2	0.82
CGM	0.683	0.003	26.14	DL	0.012	0.027	1.87	0.472	0.103	2.79	0.023	1.0	0.98
CGM	0.472	0.000	24.5	0.086	3.032	2.668	3.37	0.344	0.175	0.49	0.003	0.5	0.67
CGM	0.325	0.000	20.2	0.005	0.237	0.134	2.41	0.246	0.039	0.48	0.004	0.6	0.71
CGM	0.491	0.000	26.99	0.08	2.13	1.214	2.72	0.439	0.311	0.69	0.001	0.8	0.77
CGM	0.306	0.000	17.88	0.121	2.12	1.117	2.44	0.267	0.086	0.55	0.002	0.7	0.78
CGM	0.411	0.000	19.74	0.283	4.982	5.307	4.13	0.391	0.285	0.49	0.003	0.6	0.73
CGM	0.382	0.000	20.15	0.055	2.665	1.692	3.02	0.294	0.046	0.52	0.004	0.4	0.73
CGM	0.215	0.000	10.52	DL	DL	0.016	1.48	0.212	0.009	0.35	0.001	0.4	0.61
CGM	0.243	0.000	11.62	DL	0.005	1E-03	1.43	0.183	0.023	0.44	0.001	0.4	0.59
CGM	0.535	0.002	20.6	0.127	5.597	0.597	2.63	0.28	0.064	0.88	0.004	0.3	0.82
CGM	0.509	0.000	23.07	0.134	3.187	2.447	2.83	0.29	0.061	0.40	0.004	0.3	0.64
UC	0.297	0.002	115.7	0.217	0.772	9.966	8.34	4.487	3.109	1.46	0.006	0.7	0.98
M	0.093	0.000	20.47	0.238	7.218	6.138	6.09	0.077	0.266	0.19	0.001	0.4	0.77
M	0.402	0.000	231.4	0.178	3.749	1.06	1.61	0.405	0.409	3.93	DL	1.4	0.75
M	0.080	0.001	17.77	0.684	2.71	0.784	1.77	0.09	0.174	0.26	0.002	0.7	0.92
M	0.315	0.001	145.3	0.143	2.543	0.991	2.34	0.108	0.119	3.65	0.001	1.0	0.91
M	0.139	0.003	23.92	0.255	5.288	1.704	3.34	0.178	0.144	0.66	0.007	0.6	1.27
UC	0.085	0.001	17.69	0.256	6.959	3.199	1.58	0.897	8.004	0.21	0.004	0.3	0.80
UC	0.210	0.000	32.85	0.209	4.659	4.769	4.09	0.18	0.203	0.23	DL	0.3	0.84
M	0.232	0.001	35.48	0.176	6.67	5.335	6.49	0.109	0.186	0.31	0.002	0.4	0.98
M	0.370	0.002	53.83	0.126	3.618	2.945	3.44	0.176	0.179	0.53	0.018	0.6	1.19
UC	0.414	0.002	217.4	0.041	3.173	15.73	4.15	32	4.818	2.56	0.008	0.6	1.20
UC	0.459	0.011	330	0.149	0.534	0.086	2.34	2.964	0.249	6.63	0.029	1.5	2.05
M	0.310	0.045	168.2	0.188	2.084	1.441	2.16	0.339	0.352	3.05	0.001	0.6	1.04
M	0.366	0.001	162.3	DL	0.014	0.009	1.54	0.725	0.206	5.64	0.005	1.0	1.33
M	0.188	0.001	34.12	0.178	3.098	1.337	3.44	0.212	0.145	0.41	0.002	0.5	1.26
M	0.182	0.007	47.89	0.155	0.595	0.088	3.19	0.156	0.082	1.15	0.006	0.8	1.33
M	0.108	0.000	32.85	0.1	3.791	4.226	2.75	0.494	0.078	0.40	0.002	0.5	1.01
M	0.163	0.000	114.2	0.1234	4.337	5.031	4.81	8.77	0.06	0.83	0.131	0.7	1.11
M	0.102	0.000	32.17	0.6581	2.835	2.233	3.27	0.613	0.074	0.54	0.006	4.0	1.10

Table 3.6 (Continued)

PYRRHOTITE

Rock type	^{61}Ni	^{65}Cu	^{59}Co	^{185}Re	^{189}Os	^{193}Ir	^{101}Ru	^{103}Rh	^{195}Pt	^{105}Pd	^{197}Au	^{107}Ag	^{111}Cd
	wt%	wt%	ppm	ppm	ppm	ppm	ppm	ppm	ppm	ppm	ppm	ppm	ppm
M	0.104	0.000	35.59	0.1211	6.413	6.778	5.90	0.638	0.255	0.29	0.003	0.4	0.96
M	0.104	0.008	33.74	0.0735	4.584	3.933	3.62	0.579	0.06	0.44	DL	0.5	0.99
M	0.089	0.000	30.72	0.1371	4.252	3.882	3.65	0.319	0.062	0.47	0.004	0.7	1.00
M	0.076	0.001	25.89	0.0615	2.038	0.81	2.67	0.283	0.016	0.47	0.002	0.6	1.11
M	0.098	0.000	46.05	0.1598	6.11	3.314	5.14	0.811	0.215	0.61	0.001	0.8	1.10
M	0.067	0.001	26.38	0.3664	6.33	4.544	6.08	0.254	0.242	0.54	0.002	0.6	1.13
M	0.078	0.000	37.23	0.4119	7.575	8.789	10.99	0.331	1.215	0.56	0.004	0.6	1.15
M	0.058	0.000	24.66	0.3664	6.808	5.8	5.30	0.252	0.269	0.44	0.002	0.5	1.11
M	0.058	0.001	28.79	0.4973	9.346	9.333	14.90	0.562	0.28	0.55	0.005	0.5	1.25
M	0.490	0.001	611.9	0.4054	10.86	9.27	8.76	0.259	0.493	10.13	0.001	4.0	1.19
M	0.346	DL	38.31	DL	DL	0.004	1.33	0.358	0.014	0.48	0.001	0.5	1.37
M	0.163	DL	23.84	0.287	6.055	6.688	4.67	0.313	0.303	0.47	0.008	0.5	1.39
M	0.156	DL	22.22	0.197	5.247	5.078	5.03	0.33	0.366	0.26	0.002	0.5	1.38
M	0.139	DL	18.96	0.169	3.687	3.086	3.21	0.297	0.046	0.54	DL	0.5	1.44
M	0.148	DL	22.44	0.121	3.4	1.661	3.15	0.357	0.026	0.60	DL	0.8	1.68
M	0.147	DL	20.76	0.284	4.018	2.217	2.70	0.344	0.283	0.54	DL	0.6	1.76
M	0.108	0.799	43.4	0.168	2.23	1.003	6.02	0.919	0.848	1.72	0.016	2.9	1.55
M	0.215	0.004	103	DL	4.063	4.567	9.17	1.125	0.389	2.16	0.019	2.4	1.31
M	0.250	0.136	120.3	0.004	1.738	0.63	6.19	0.854	0.553	2.12	0.001	4.4	1.73
M	0.089	0.002	29.2	0.206	2.79	2.524	8.01	1.329	0.345	1.42	0.003	1.3	1.67
M	0.310	0.002	144.9	0.207	3.944	3.663	11.35	0.982	0.074	1.92	0.004	2.5	1.71
M	0.406	0.003	206.8	0.195	4.153	3.749	11.03	0.915	0.063	2.77	0.008	2.6	1.97
M	0.217	0.008	44.56	0.283	4.365	3.337	10.90	1.226	0.131	2.75	0.013	1.4	3.33
M	0.167	0.003	32.79	0.252	4.811	3.208	10.20	1.326	0.192	1.69	0.012	1.5	2.61
Ni-rich pyrrhotite													
M	1.097	0.001	40.11	DL	0.347	0.046	2.93	0.147	0.016	0.51	DL	0.7	1.96
M	1.619	0.002	69.17	0.666	7.81	9.97	25.81	2.179	14.34	0.78	0.016	0.7	2.27
M	1.349	0.002	66.72	0.258	1.474	9.192	12.56	0.513	3.049	0.90	DL	0.9	2.21
M	1.076	0.003	50.53	0.249	2.173	2.002	7.27	0.33	0.661	1.35	0.005	1.0	2.57
M	1.170	0.002	58.67	0.914	7.107	7.114	19.96	0.397	7.572	0.78	0.007	0.9	2.39
M	1.389	0.001	87.45	0.053	0.444	0.462	1.80	0.291	0.459	1.33	0.001	0.9	2.20
M	1.328	0.002	66.95	0.362	7.006	6.29	23.03	0.325	2.103	1.06	0.009	0.8	2.44
M	1.627	0.002	49.52	0.331	3.035	1.364	11.33	0.101	0.556	0.22	0.003	0.3	0.67
M	1.366	0.001	41.55	0.141	3.805	0.794	8.89	0.114	0.545	0.27	DL	0.4	0.73
M	1.321	0.002	40.52	0.153	0.335	0.086	1.45	0.127	0.017	0.32	DL	0.4	0.85
M	1.082	0.001	38.34	0.232	0.548	0.231	1.46	0.133	0.121	0.26	0.006	0.4	0.83
M	1.246	0.001	67.86	0.034	7.501	1.879	27.26	0.156	0.595	0.37	0.004	0.4	0.82
M	1.192	0.000	66.12	0.279	2.439	0.644	5.33	0.116	0.078	0.38	DL	0.3	0.92

Table 3.6 (Continued)

CHALCOPYRITE

Rock type	^{61}Ni	^{65}Cu	^{59}Co	^{185}Re	^{189}Os	^{193}Ir	^{101}Ru	^{103}Rh	^{195}Pt	^{108}Pd	^{197}Au	^{107}Ag	^{111}Cd
	wt%	wt%	ppm	ppm	ppm	ppm	ppm	ppm	ppm	ppm	ppm	ppm	ppm
AN	0.151	33.98	79.48	0.007	0.069	0.074	DL	DL	0.313	5.79	0.01	77.0	5.91
AN	0.303	33.98	223.9	0.007	0.082	0.033	DL	DL	0.718	7.96	0.04	17.4	6.72
AN	0.493	33.98	235.2	DL	DL	0.007	DL	DL	0.995	12.00	0.07	17.5	8.90
AN	0.003	33.98	3.496	DL	DL	DL	DL	DL	0.046	5.61	DL	7.9	7.77
AN	0.009	33.98	3.851	DL	DL	DL	DL	DL	0.016	5.49	DL	4.6	14.60
AN	0.023	33.98	5.628	DL	0.005	DL	DL	DL	0.047	6.22	0.02	5.7	16.34
LC	DL	34.15	0.79	DL	DL	DL	DL	DL	0.019	2.24	DL	6.0	10.64
LC	0.004	34.15	2.085	DL	0.005	0.010	DL	DL	0.124	1.77	0.15	6.6	10.15
LC	0.016	34.15	12.13	DL	0.008	0.092	DL	DL	0.057	4.49	0.04	14.1	10.27
LC	0.007	34.15	5.397	DL	0.006	0.109	DL	DL	0.452	2.81	0.01	34.7	14.01
CGM	0.044	33.84	32.71	DL	0.008	DL	DL	DL	0.014	7.02	DL	19.8	4.27
CGM	DL	33.84	1.234	DL	DL	0.005	DL	DL	0.01	6.94	0.01	3.6	4.75
CGM	0.178	33.84	19.25	0.005	DL	0.007	DL	DL	0.017	7.23	0.01	4.1	5.77
CGM	DL	33.84	3.246	0.004	0.011	DL	DL	DL	0.011	6.97	0.01	5.2	7.44
UC	0.027	33.65	8.274	0.003	0.008	0.008	DL	DL	0.071	6.33	0.01	5.8	13.05
UC	0.139	33.65	125.9	0.005	0.028	0.102	DL	1.265	0.261	11.85	0.28	6.7	3.33
UC	0.011	33.65	8.981	0.002	0.021	0.023	DL	DL	15.72	2.95	0.1	3.7	3.42
M	0.281	33.65	192.8	0.009	0.112	0.085	DL	DL	0.291	7.93	0.06	46.0	4.60
M	0.117	33.65	73.26	DL	0.022	0.034	DL	DL	0.107	4.87	0.03	6.3	5.46
M	0.004	33.65	4.132	DL	DL	DL	DL	DL	DL	4.42	0.02	9.3	5.17
M	0.036	33.65	25.67	DL	0.005	0.007	DL	DL	0.112	4.40	0.01	4.9	13.49
M	0.028	33.65	9.651	DL	DL	0.008	DL	DL	0.495	3.55	0.01	4.1	13.89
M	0.171	33.65	102.3	0.006	0.01	0.044	DL	DL	0.246	6.57	DL	4.8	9.38
M	0.067	33.65	223.4	0.004	0.01	DL	DL	DL	DL	5.00	0.01	9.2	11.79
M	0.321	33.70	108.1	0.185	1.405	0.628	2.74	DL	0.254	11.43	0.01	5.0	4.46
M	0.406	33.70	125.2	DL	0.01	0.037	DL	DL	0.167	12.82	0.01	8.7	7.29
M	DL	33.94	DL	DL	DL	DL	DL	DL	0.009	2.46	DL	2.4	3.09
M	0.050	33.94	14.57	0.115	0.047	0.094	DL	DL	0.15	3.13	0.01	65.2	19.03
M	DL	33.94	DL	DL	DL	DL	DL	DL	0.01	2.45	0.01	2.6	3.06
M	DL	33.94	DL	DL	DL	DL	DL	DL	0.083	2.41	0.01	2.7	4.27
M	0.301	33.81	21.56	DL	0.011	0.088	DL	DL	0.201	4.01	0.05	4.6	3.95
M	0.540	33.81	27.24	0.009	0.009	0.124	DL	DL	0.577	5.83	0.1	7.2	4.96
M	0.173	33.81	10.72	DL	0.017	0.122	DL	DL	0.293	4.52	0.07	5.4	6.34
M	0.139	33.81	14.93	0.005	0.012	0.088	DL	DL	0.081	3.76	0.02	4.0	5.22
M	0.304	33.81	20.7	0.189	2.897	4.035	2.90	DL	1.747	5.80	DL	5.9	4.98
M	0.300	33.81	19.52	DL	DL	0.008	DL	DL	0.024	6.54	0.02	10.2	8.18

DL = value under the detection limit

3.6.2.1. - Controls on trace elements in the BMS

During the evolution of a Fe-Ni-Cu sulphide liquid, a monosulphide solid solution enriched in Fe (MSS) and a liquid enriched in Cu form (Kullerud *et al.*, 1969; Naldrett, 1989). Osmium, Ir, Ru, Rh and Re preferentially partition into the Fe-rich MSS whereas Cu, Pt, Pd, Ag, Au, Cd and Zn concentrate in the Cu-rich fractionated liquid (Li *et al.*, 1996; Barnes *et al.*, 2001; Mungall *et al.*, 2005). Nickel partitions almost equally between MSS and the liquid. The Cu-rich fractionated liquid crystallises as intermediate solid solution (ISS) and minor Ni-rich MSS. At temperature < 600C°, the MSS exsolves into pyrrhotite ($Fe_{1-x}S$), and pentlandite [$(Ni, Fe)_9S_8$] and the ISS exsolves to form chalcopyrite ($CuFeS_2$) $^{+}/_{-}$ cubanite ($CuFe_2S_3$). If the trace elements have not been redistributed during the exsolution of the BMS, one would expect pyrrhotite and pentlandite to be enriched in Os, Ir, Ru, Rh, Re and chalcopyrite to be enriched in the remaining elements.

3.6.2.2. - Iridium, Osmium, Ruthenium and Rhenium

Osmium, Ru and Re show a positive correlation with Ir and are largely present in pentlandite and pyrrhotite with no preference for either of the two minerals (Fig. 3.6a, b, c and Table 3.5). As explained above, this co-variance probably reflects the control of these elements by MSS and only a limited redistribution of the elements during exsolution. Osmium and Ir contents (Fig. 3.6a) in both pentlandite and pyrrhotite cover a similar range (~0.1 to ~15 ppm). Iridium and Os contents of chalcopyrite (Fig. 6a) are < 1 ppm. Pentlandite (Fig. 3.6b) contains ~4 to 20 ppm Ru (two values are higher with ~60 ppm Ru). The Ru content in the pyrrhotite (Fig. 3.6b) is slightly lower from, ~1 to ~15 ppm.

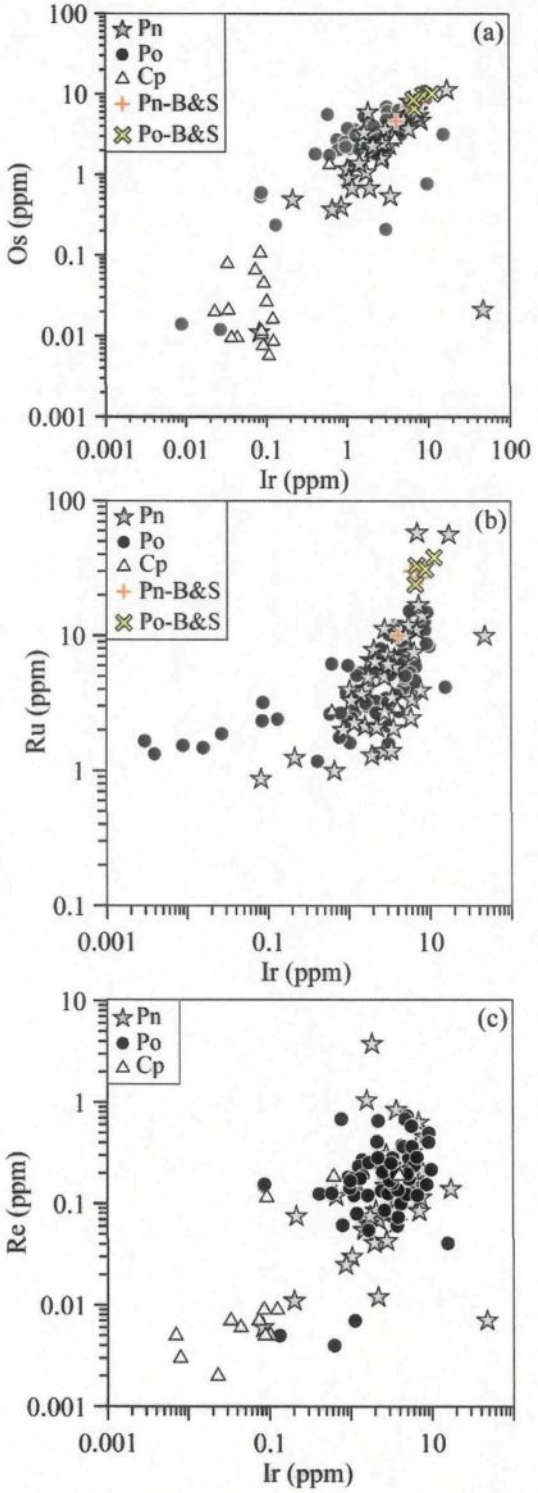

Figure 3.6: Binary variation diagrams of (a) Os vs Ir, (b) Ru vs Ir, and (c) Re vs Ir.

Results obtained by Ballhaus and Sylvester (2000) were added for comparison (Pn-B&S for pentlandite and Po-B&S for pyrrhotite).

In the chalcopyrite Ru contents are below detection limit (i.e. <0.2 ppm). Pentlandite and pyrrhotite (Fig. 3.6c) contain 0.002 to 2 ppm Re with most values <0.5 ppm. Rhenium contents are lower in chalcopyrite with values ranging from 0.003 to 0.02 ppm (Fig. 3.6c).

3.6.2.3. - Copper, Cadmium, Silver, Platinum and Gold

As would be predicted by the MSS fractionation model, Ag and Cd show a positive correlation with Cu and are concentrated in chalcopyrite (Fig. 3.7a, b and Table 3.6). Chalcopyrite contains more Ag than pentlandite and pyrrhotite with values ranging from ~3 to ~80 ppm, but most of the values are <20 ppm (Fig. 3.7a and Table 3.6). Silver contents in most pentlandite analyses are ~1 to ~7 ppm (three values were found between 15 to 40 ppm). In pyrrhotite, Ag values are ~0.3 to ~3 ppm (Fig. 3.7a and Table 3.6). Silver also occurs as inclusions; both in BMS or at the contact between BMS and silicate minerals (see description below). Chalcopyrite contains 3 to 20 ppm Cd (Fig. 3.7b and Table 3.6). Pentlandite and pyrrhotite contain ~0.5 to ~3 ppm Cd (Fig. 3.7b and Table 3.5).

In contrast to Cd and Ag, Pt and Au are not partitioned into specific BMS (Fig. 3.7c, d and Table 3.6). These results are in agreement with those of Ballhaus and Sylvester (2000). Platinum concentrations in pentlandite are 0.02 to 30 ppm (Fig. 3.7c). Pyrrhotite and chalcopyrite contain 0.01 to 10 ppm Pt (Fig. 3.7c). There are no significant correlations between Pt and other metals. During the laser ablation several inclusions enriched in platinum were observed in the BMS or at the contact between BMS and silicate (see later description). Gold is not partitioned into any particular BMS (Fig. 3.7d and Table 3.6). Gold contents in most pentlandite, pyrrhotite and chalcopyrite analyses are ~0.01 to ~0.3 ppm (Fig. 3.7d). Minor amounts of Au are associated with Ag in inclusions that are probably composed of palladian-electrum (see description below).

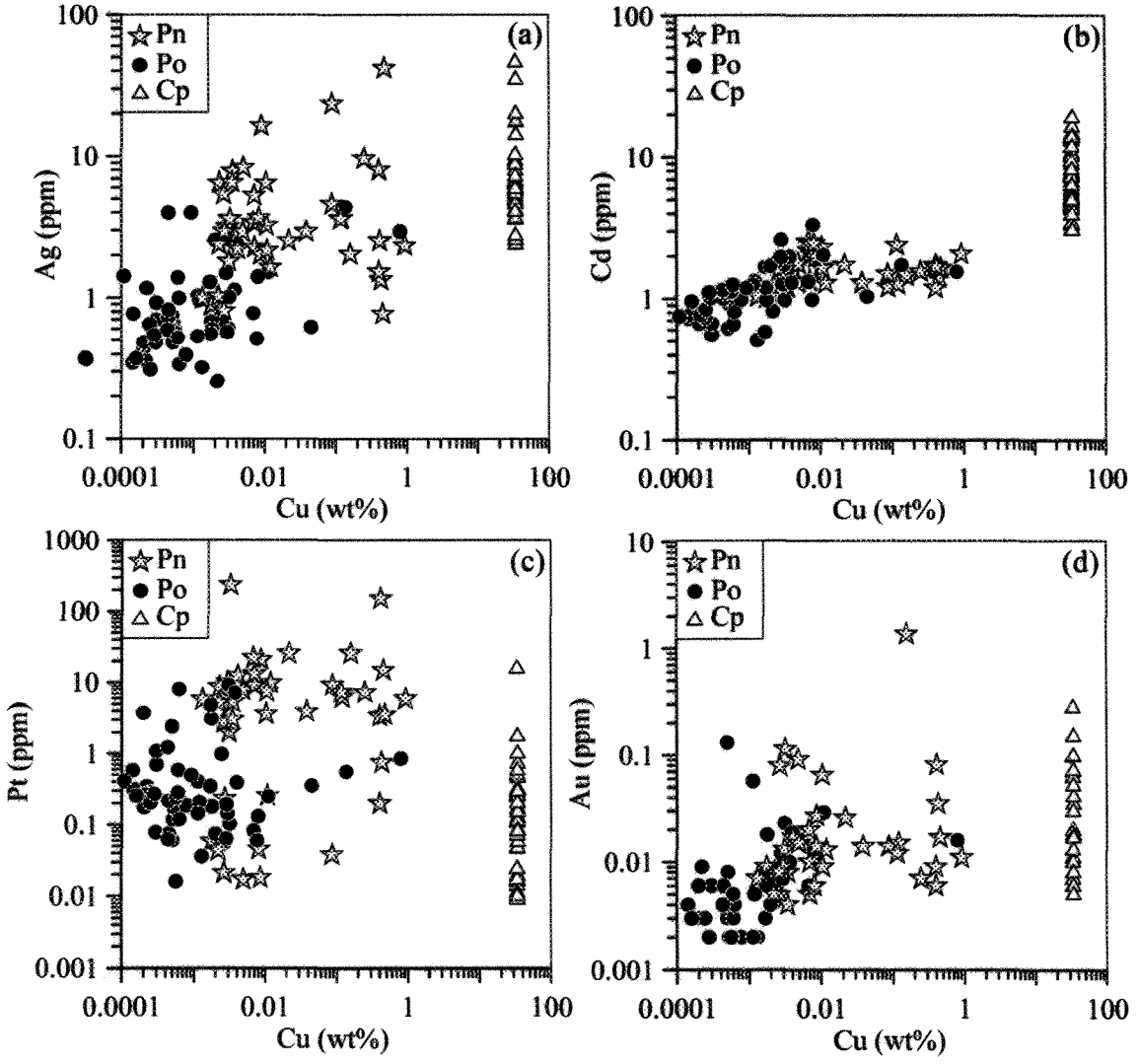

Figure 3.7: Binary variation diagrams of (a) Ag vs Cu, (b) Cd vs Cu, (c) Pt vs Cu, (d) Au vs Cu.

3.6.2.4. - Nickel, Cobalt, Palladium and Rhodium

These four elements are largely concentrated in pentlandite. Nickel, Rh, Pd and Co all show a positive correlation with each other (Fig. 3.8 and Table 3.6). The Co content in pentlandite (Fig. 3.8a, b and Table 3.6) varies from ~0.5 wt% to ~1.4 wt%, similar to the values determined by microprobe and to the values reported by Ballhaus and Sylvester (2000). Pyrrhotite contains between 10 ppm and 200 ppm Co (Fig. 3.8a, b and Table 3.6). Chalcopyrite contains ~1 to ~235 ppm of Co with most values in the 1-30 ppm level (Fig. 3.8a, b and Table 3.6).

Palladium contents of pentlandite are in the 50 to 600 ppm range (Fig. 3.8b and Table 3.6). Pyrrhotite and chalcopyrite contain less Pd with values of ~0.1 to ~10 ppm and ~3 to ~15 ppm, respectively.

Most of the Rh was found to be present in pentlandite (Fig. 3.8c and Table 3.6), with most grains containing 1 to 100 ppm Rh. In contrast, most pyrrhotites contain ~0.3 to ~1 ppm Rh. The concentration of Rh in chalcopyrite is generally <0.2 ppm.

The available data thus suggest that, during exsolution of pentlandite from MSS, Ni, Co and Pd partitioned into pentlandite. The lack of correlation between Ir and Rh and the high concentration of Rh in pentlandite suggest that Rh also diffused into the pentlandite rather than into the pyrrhotite. Pd contents in the product of MSS exsolution (pentlandite and pyrrhotite) increases with the Co content. This feature is not observed for chalcopyrite (derived from Cu-rich sulphide liquid).

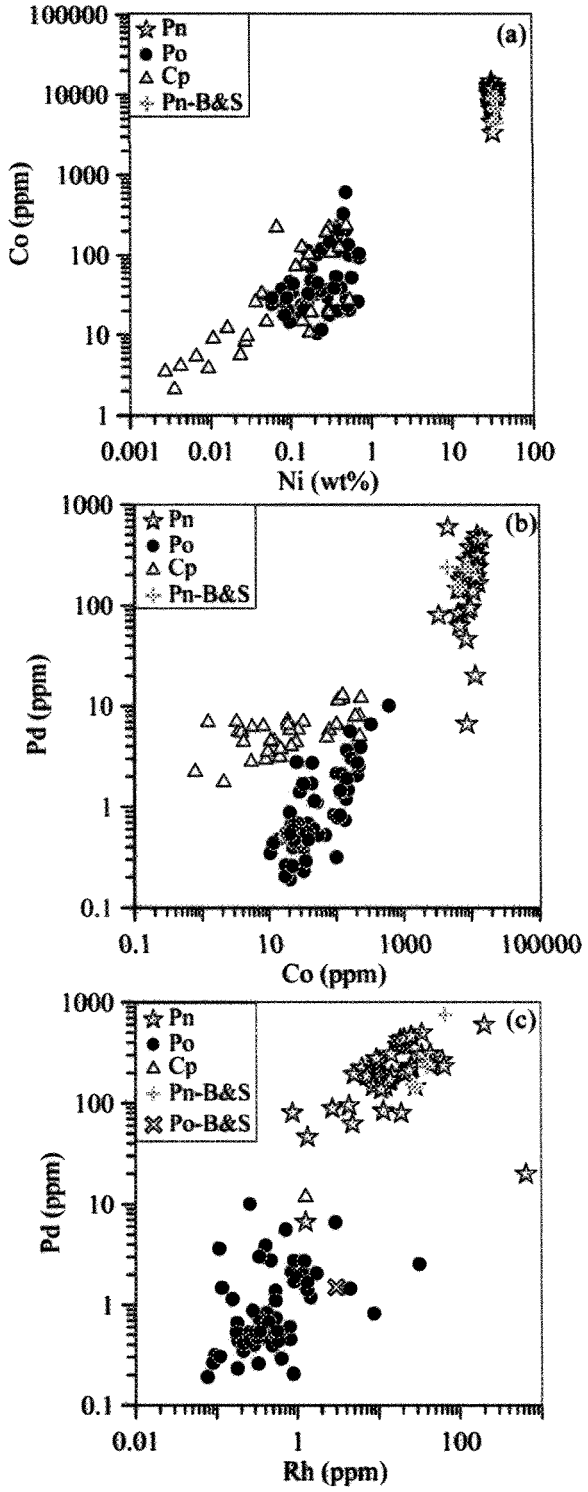

Figure 3.8: Binary variation diagrams of (a) Co vs Ni, (b) Pd vs Co, and (c) Pd vs Rh.

Results obtained by Ballhaus and Sylvester (2000) were added as comparison (Pn-B&S for pentlandite and Po-B&S for pyrrhotite).

3.6.3. - Stratigraphic variation of the PGE in the BMS

In addition to variation in PGE content between different BMS there is also some systematic variation in the PGE content of individual BMS depending on their stratigraphic position. The total PGE and more particularly the Pd content in pentlandite and pyrrhotite are highest at the level of the chromitite layers mirroring the pattern of the whole rocks (Fig. 3.9).

3.6.4. - Mass balance of PGE in BMS calculation

In order to determine what percentages of PGE are present in BMS, the whole rock concentrations of Ni, Cu, S, Co, PGE and Au have been determined (Table 3.5). The percentage ($P_{sul}i$) of each PGE (i) in a given BMS was calculated as follows:

$$P_{sul}i = (F_{sul}\, C_{sul}^{i} / C_{WR}^{i}) \times 100$$

where F_{sul} is the weight fraction of the BMS considered (same as calculation for the proportion of each BMS above), C_{sul}^{i} is the concentration of the element i in the BMS considered, C_{WR}^{i} is the concentration of the element i in the whole rock. The results obtained for each BMS in each lithology are summarized in Table 3.7.

In all lithologies relatively little (0.1 to ~10 wt%) Au and Pt are present in BMS (Table 3.7 and Fig. 3.10). In most rock types Pd and Rh are predominantly (50 up to 100 %) present in BMS (Table 3.7 and Fig. 3.10). A large proportion (35 to 72 %) of the Os, Ir, and Ru in silicate rocks is present in BMS.

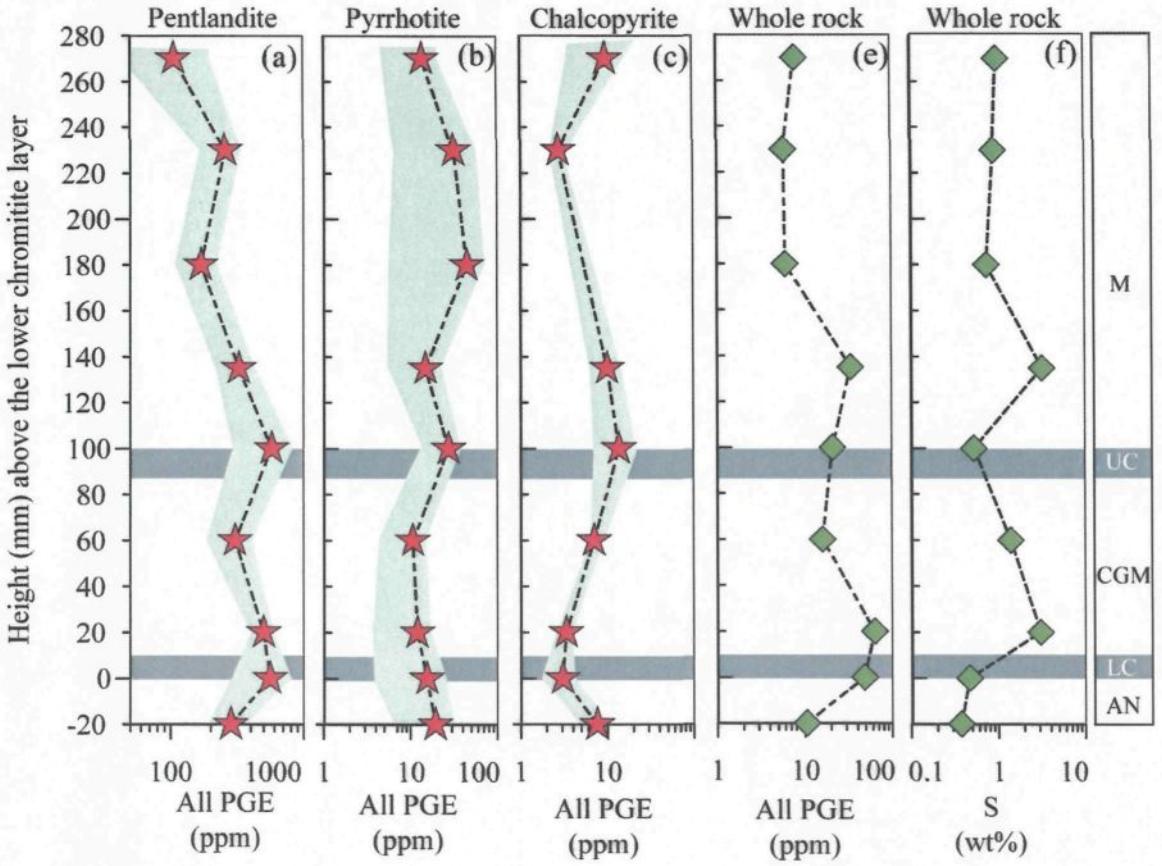

Figure 3.9: Stratigraphic variation of PGE contents in the base-metal sulphide minerals and in the whole rock.

Table 3.7: *Calculated proportions of each PGE in the base-metal sulphides.*

Sample	Sulphide	Os %	Ir %	Ru %	Rh %	Pt %	Pd %	Au %	All PGE %
AN	Pyrrhotite	10.4	11.7	5.8	0.7	0.3	0.1	0.0	0.7
	Pentlandite	13.9	14.4	6.3	12.8	1.2	22.1	0.3	10.2
	Chalcopyrite	0.1	0.0	0.0	0.0	0.0	0.5	0.0	0.2
	All sulphide	***23.7***	***25.3***	***11.8***	***13.0***	***1.5***	***21.8***	***0.4***	***10.7***
LC	Pyrrhotite	1.7	1.2	0.3	0.0	0.0	0.0	0.0	0.1
	Pentlandite	3.6	9.6	2.5	31.8	0.2	50.0	0.0	7.7
	Chalcopyrite	0.0	0.0	0.0	0.0	0.0	0.2	0.1	0.0
	All sulphide	***5.2***	***10.8***	***2.8***	***31.8***	***0.2***	***50.2***	***0.1***	***7.8***
CGM-1	Pyrrhotite	25.4	13.3	7.3	1.2	0.1	0.2	0.0	0.8
	Pentlandite	35.3	37.6	37.5	74.2	0.9	105.7	0.0	31.5
	Chalcopyrite	0.0	0.2	0.0	0.0	0.0	0.2	0.0	0.1
	All sulphide	***60.7***	***51.1***	***44.9***	***75.4***	***1.0***	***106.1***	***0.0***	***32.3***
CGM-2	Pyrrhotite	26.7	18.3	9.4	1.1	0.1	0.2	0.0	0.9
	Pentlandite	38.5	43.0	15.7	50.3	1.2	64.6	0.0	27.1
	Chalcopyrite	0.1	0.0	0.0	0.0	0.0	1.5	0.0	0.6
	All sulphide	***65.3***	***61.3***	***25.2***	***51.4***	***1.3***	***66.3***	***0.0***	***28.6***
UC	Pyrrhotite	5.2	8.1	1.0	3.4	0.1	0.2	0.0	0.6
	Pentlandite	4.4	4.9	0.8	95.3	0.2	72.8	0.0	19.6
	Chalcopyrite	0.0	0.1	0.0	0.5	0.2	0.7	0.2	0.3
	All sulphide	***9.7***	***13.1***	***1.9***	***99.2***	***0.5***	***73.7***	***0.2***	***20.5***
M1	Pyrrhotite	40.1	24.1	6.7	1.6	0.1	0.5	0.0	1.8
	Pentlandite	25.2	19.9	4.7	62.1	3.0	102.8	0.1	41.6
	Chalcopyrite	0.4	0.1	0.8	0.0	0.0	0.5	0.0	0.2
	All sulphide	***65.7***	***44.2***	***12.2***	***63.7***	***3.1***	***103.8***	***0.1***	***43.7***
M2	Pyrrhotite	69.3	40.7	53.2	16.5	0.6	4.4	0.1	7.3
	Pentlandite	28.9	27.5	21.3	59.3	1.6	54.6	0.0	24.8
	Chalcopyrite	0.0	0.0	0.0	0.0	0.0	0.0	0.0	0.0
	All sulphide	***98.2***	***68.2***	***74.5***	***75.8***	***2.2***	***59.0***	***0.1***	***32.1***
M3	Pyrrhotite	45.8	56.6	23.4	3.3	1.9	0.4	0.0	5.3
	Pentlandite	16.2	19.9	8.4	49.2	38.3	88.0	0.1	54.7
	Chalcopyrite	0.2	0.2	0.0	0.0	0.0	0.4	0.0	0.2
	All sulphide	***62.1***	***76.6***	***31.8***	***52.4***	***40.2***	***88.8***	***0.2***	***60.2***
M4	Pyrrhotite	43.7	12.5	32.8	0.8	0.1	0.2	0.0	1.9
	Pentlandite	15.4	17.5	11.8	29.9	0.3	55.8	0.1	16.6
	Chalcopyrite	3.2	4.0	3.7	0.0	0.0	0.9	0.1	0.5
	All sulphide	***62.3***	***33.9***	***48.3***	***30.7***	***0.4***	***56.9***	***0.2***	***19.0***
Average CGM	Pyrrhotite	26.0	15.8	8.4	1.2	0.1	0.2	0.0	0.8
	Pentlandite	36.9	40.3	26.6	62.3	1.0	85.2	0.0	29.3
	Chalcopyrite	0.0	0.1	0.0	0.0	0.0	0.8	0.0	0.3
	All sulphide	***63.0***	***56.2***	***35.0***	***63.4***	***1.1***	***86.2***	***0.0***	***30.4***
Average M	Pyrrhotite	49.7	33.5	29.0	5.6	0.7	1.4	0.0	4.1
	Pentlandite	21.4	21.2	11.6	50.1	10.8	75.3	0.1	34.4
	Chalcopyrite	0.9	1.1	1.1	0.0	0.0	0.4	0.0	0.2
	All sulphide	***72.1***	***55.7***	***41.7***	***55.6***	***11.5***	***77.1***	***0.2***	***38.8***
Average chromitite	Pyrrhotite	3.4	4.7	0.7	1.7	0.1	0.1	0.0	0.3
	Pentlandite	4.0	7.2	1.7	63.5	0.2	61.4	0.0	13.7
	Chalcopyrite	0.0	0.0	0.0	0.3	0.1	0.5	0.1	0.1
	All sulphide	***7.5***	***11.9***	***2.3***	***65.5***	***0.3***	***62.0***	***0.2***	***14.1***

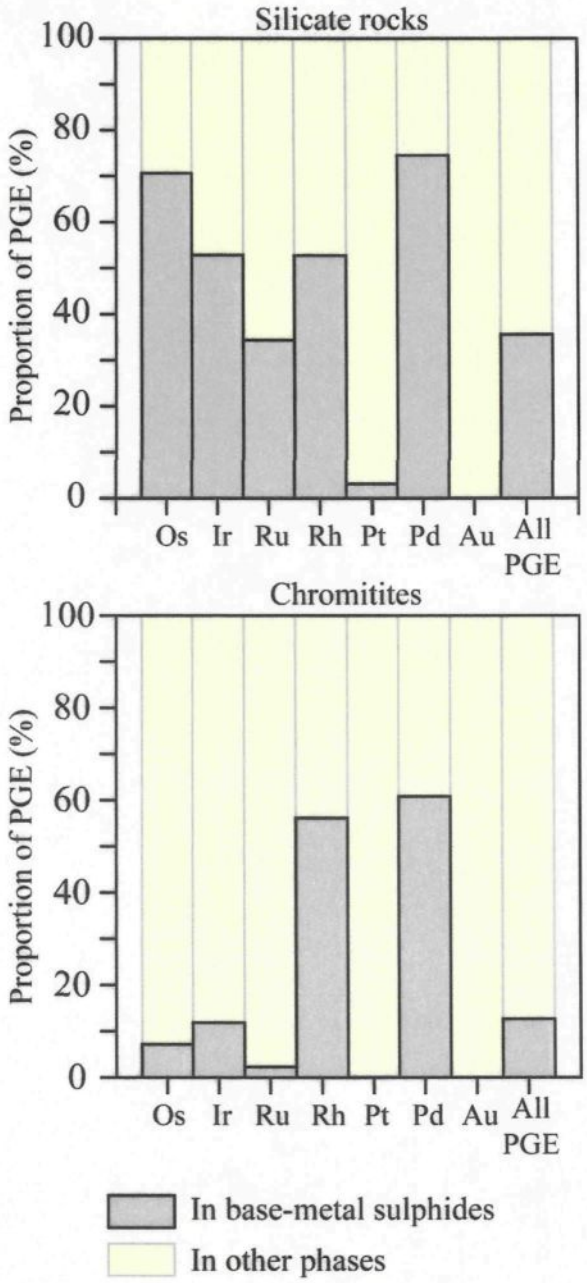

Figure 3.10: Average proportion of PGE in base-metal sulphides and other phases.

However in the chromitite layers a far smaller proportion (0.2 to ~12 %) of Os, Ir, Ru, Pt and Au is found in BMS (Table 3.7 and Fig. 3.10). If we considered all the PGE, only ~15 % (in the chromitites) to ~40 % (in the silicate rocks) of these elements are present in BMS. This indicates that phases other than the BMS accommodate the PGE.

It is well known that there are numerous platinum-group minerals (PGM) present in the Merensky Reef (Vermaal and Hendriks, 1976; Kinloch, 1982; Kinloch and Peyerl, 1990; Prichard *et al.*, 2004) and during the laser ablation we observed PGE inclusions in the BMS. To investigate whether the PGM and inclusions may account for the "missing" PGE we studied the PGM and PGE-rich inclusions present in our samples.

3.6.5. - Platinum-group minerals

Backscattered (BSE) image analysis of four sections representing different lithologies (lower chromitite, coarse-grained melanorite, upper chromitite and melanorite) was carried out using the scanning electron microprobe at Laval University (Quebec City). Two hundred and twenty two grains of PGM (Table 3.8) and a myrmekitic-like structure (Fig. 3.11) of isoferroplatinum (Pt_3Fe) were found. As these PGM are very small, quantitative analysis was done only on a few grains (Table 3.9). The other PGM were characterized using energy dispersive spectra. Only the PGM with a diameter > 0.5 μm are visible in the BSE images and are taken into account for further calculations. Six types of PGM were found (Table 3.10): (i) Pt sulphide; (ii) Pt-Pd sulphide; (iii) Pt-Pd telluride; (iv) Ru-Ir-Os sulphide; (v) Pt-Fe alloy and (vi) Pt. The distribution of the PGM varies as a function of lithology and they are found in five different textural modes (Table 3.8 and Table 3.10): at the BMS/silicate boundaries; included in BMS; included in silicate; at the chromite/BMS contact and finally, included in chromite.

Table 3.8: *Type of association of the PGM in the analysed rock types.*

	Sulphide/silicate contact	Included in sulphide	Included in silicate	Chromite/sulphide contact	Included in chromitite	Total
Melanorite (M1)						
PGM BiTe	33	53	6			92
PGM sulphide	1					1
Pt-Fe	1					1
Pt	1					1
All PGM	36	53	6			95
Upper Chromitite						
PGM sulphide	5	6		6		17
Pt-Pd-Sn-S	10					10
All PGM	15	6		6		27
Coarse-grained melanorite						
PGM BiTe	8	16	12			36
PGM sulphide	1	1				2
Pt-Fe*	13					13
Pt-Pd-Sn-S	2	1				3
All PGM	24	18	12			54
Lower Chromitite						
PGM BiTe	5	2	1			8
PGM sulphide	1	3		21	1	26
Pt-Fe		1		1		2
Pt-Pd-Sn-S				2		2
Ru-Ir-Os-S			1		1	2
Pt					1	1
All PGM	6	6	2	24	3	41
Anorthosite						
PGM sulphide	2		3			5
All PGM	2		3			5
All rock types						
PGM BiTe	46	71	19			136
PGM sulphide	10	10	3	27	1	51
Pt-Fe	14	1		1		16
Pt-Pd-Sn-S	12	1		2		15
Ru-Ir-Os-S			1		1	2
Pt	1				1	2
All PGM	***83***	***83***	***23***	***30***	***3***	***222***

* The myrmekitic-like structure (Fig. 10a) was not taken into account in this calculation.

Table 3.9: *Composition of platinum-group minerals found in the Merensky Reef at Rustenburg Platinum Mine.*

Point*	Mineral	Sulphide Host	Ni wt%	Fe wt%	Pt wt%	Cu wt%	Te wt%	Pd wt%	Bi wt%	Total wt%	Ni at%	Fe at%	Pt at%	Cu at%	Te at%	Pd at%	Bi at%
1	Pt-Fe alloy	Pyrrhotite	0.03	9.61	90.61	0.10	ND	0.01	ND	100.4	0.09	26.94	72.70	0.26	ND	0.01	ND
2	Pt-Fe alloy	Pyrrhotite	0.11	9.02	91.05	0.25	ND	ND	0.02	100.4	0.29	25.48	73.61	0.61	ND	ND	0.02
3	Pt-Fe alloy	Pyrrhotite	0.23	10.41	91.14	0.11	ND	0.09	ND	102.0	0.60	28.24	70.77	0.27	ND	0.13	ND
4	Pt-Fe alloy	Pyrrhotite	0.14	10.51	89.45	0.15	ND	0.06	ND	100.3	0.36	28.86	70.34	0.35	ND	0.09	ND
	Pt-Fe alloy	Pyrrhotite	ND	9.13	91.14	0.14	ND	0.02	ND	100.4	ND	25.83	73.79	0.36	ND	0.03	ND
	Pt-Fe alloy	Pyrrhotite	0.18	9.74	91.47	0.39	ND	0.04	0.00	101.8	0.47	26.72	71.81	0.94	ND	0.05	0.00
	Pt-Pd-BiTe	Pyrrhotite	0.19	0.01	18.60	ND	50.01	13.93	14.29	97.0	0.46	0.03	13.82	ND	56.81	18.97	9.91
	Pt-Pd-BiTe	Pyrrhotite	ND	0.05	0.48	ND	33.91	37.22	24.56	96.2	ND	0.11	0.34	ND	36.09	47.50	15.96
	Pt-Pd-BiTe	Pyrrhotite	0.29	0.34	34.27	ND	45.94	2.80	14.86	98.6	0.76	0.95	27.20	ND	55.76	4.07	11.01
	Pt-Pd-BiTe	Pentlandite	0.23	0.49	37.22	ND	42.10	ND	18.41	98.5	0.64	1.40	30.63	ND	52.96	ND	14.14
	Pt-Pd-BiTe	Pyrrhotite	0.21	0.03	18.25	ND	49.26	13.82	14.34	95.9	0.51	0.08	13.71	ND	56.60	19.05	10.06

ND: not detected.

wt%: weight percent.

at%: atomic percent.

* Position located on Fig. 3.11a.

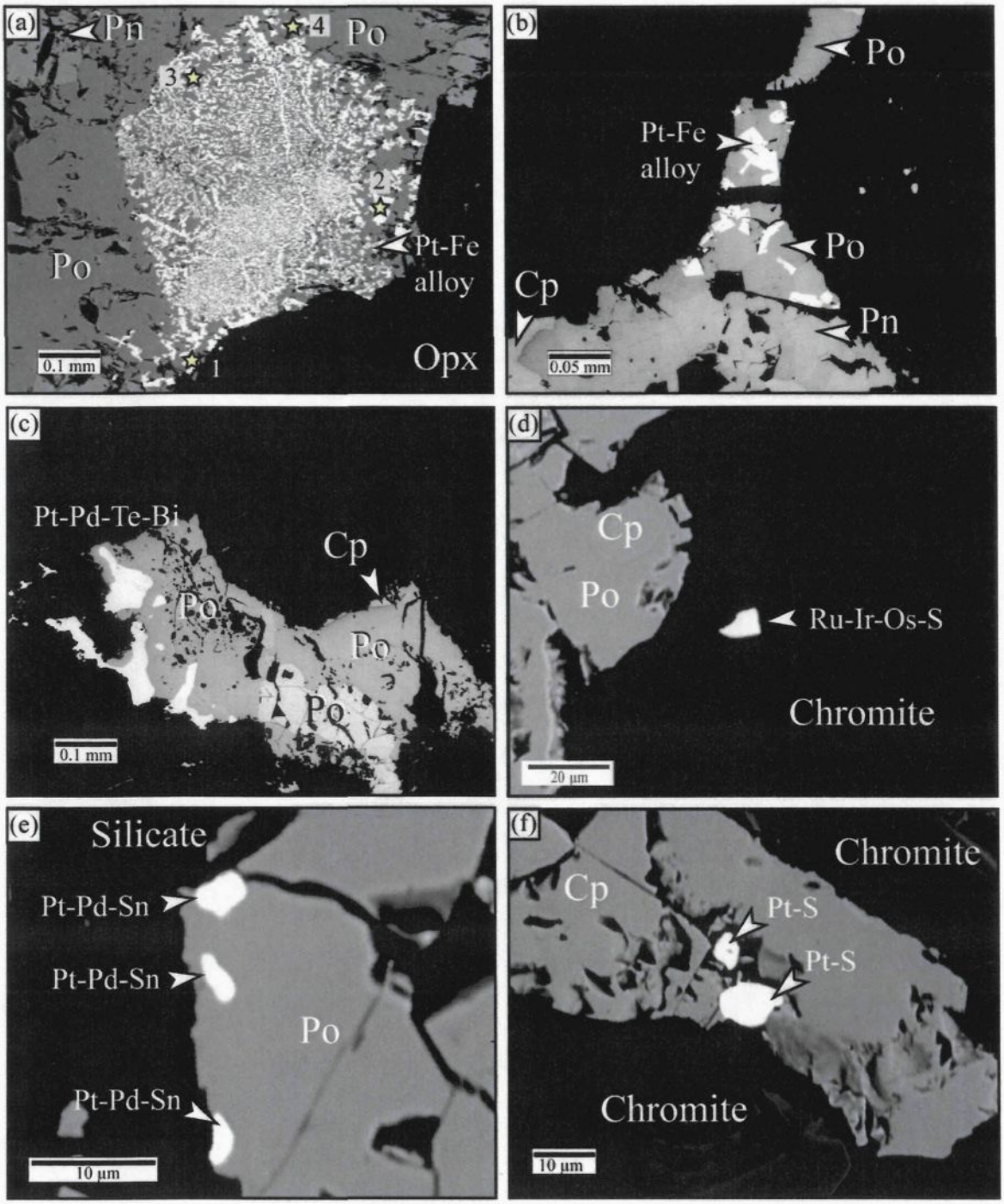
(a)
Pn
4
Po
3
2
Pt-Fe
alloy
Po
0.1 mm
1
Opx
(b)
Po
Pt-Fe
alloy
Po
Cp
Pn
0.05 mm
(c)
Pt-Pd-Te-Bi
Cp
Po
Po
Po
0.1 mm
(d)
Cp
Po
Ru-Ir-Os-S
Chromite
20 µm
(e)
Silicate
Pt-Pd-Sn
Pt-Pd-Sn
Po
Pt-Pd-Sn
10 µm
(f)
Chromite
Cp
Pt-S
Pt-S
Chromite
10 µm

Figure 3.11: Backscattered electron images of platinum-group minerals observed in our Merensky Reef sample from Rustenburg Platinum Mine.

(a) Myrmekitic and euhedral Pt-Fe alloy (isoferroplatinum) found associated with pyrrhotite (Po) and also developped at the contact between pyrrhotite and orthopyroxene (Opx). Stars represent the location of the microprobe analysis (Table 3.9).
(b) Euhedral isoferroplatinum (Pt_3Fe) included in pyrrhotite.
(c) Platinum-group bismuthotellurides found at the contact between silicate and pyrrhotite.
(d) Laurite (Ru-Ir-Os-S) included in chromite grains.
(e) Rustenburgite (Pt-Pd-Sn) included in pyrrhotite or located at the contact between pyrrhotite and silicate.
(f) Pt-sulphide (Pt-S) included in chalcopyrite or located at the contact between chromite and sulphide.
Abbreviations:
Opx: orthopyroxene; Po: pyrrhotite; Pn: pentlandite; Cp: chalcopyrite.

***Table 3.10**: Type of association of the PGM as percentages of the total of PGM in the silicate rocks and the chromitites.*

Silicate rocks*	Sulphide/silicate contact	Included in sulphide	Included in silicate	Chromite/sulphide contact	Included in chromitite	Total
PGM BiTe	32	54	14	0	0	100
PGM sulphide	50	13	38	0	0	100
Pt-Fe	100	0	0	0	0	100
Pt-Pd-Sn-S	67	33	0	0	0	100
Pt	100	0	0	0	0	100
All PGM	40	46	14	0	0	100

Chromitites**	Sulphide/silicate contact	Included in sulphide	Included in silicate	Chromite/sulphide contact	Included in chromitite	Total
PGM BiTe	63	25	13	0	0	100
PGM sulphide	14	21	0	63	2	100
Pt-Fe	0	50	0	50	0	100
Pt-Pd-Sn-S	83	0	0	17	0	100
Ru-Ir-Os-S	0	0	50	0	50	100
Pt	0	0	0	0	100	100
All PGM	31	18	3	44	4	100

* Anorthosite, coarse-grained melanorite and melanorite.

** Lower and Upper chromitites.

In the silicate rocks, most of the PGM (~83%) are Pt-Pd tellurides or bismuthotellurides (Fig. 3.11c), the majority of which are included in BMS (~53%) or located at the contact between silicate and BMS (~32%). The others (~14%) are included in silicates. In the chromitite layers Pt-Pd tellurides represent only a minority (~12%) of the PGM. Most of them are located at silicate/BMS boundaries (~63%). The remainder are included in BMS (~25%) or associated with alteration silicates (~13%).

Pt-Fe alloy (isoferroplatinum) occurs in two different forms: (i) as a myrmekitic-like structure associated with pyrrhotite (Fig. 3.11a); (ii) as euhedral grains (Fig. 3.11b). The myrmekitic-like structure is composed of small (~1-2 μm) ragged grains of isoferroplatinum, of vertical networks of isoferroplatinum of ~4 μm width in the center part of the structure and of euhedral grains (up to 10 μm) near the border of the myrmekitic-like structure. Euhedral grains of Pt-Fe alloy with a composition similar to those of the myrmekitic-like structure have also been observed in other parts of the silicate and chromite-rich rocks. In both melanorites, Pt-Fe grains are located at the contact between silicates and BMS (pyrrhotite in general). In the chromitite layers, the few Pt-Fe grains that were found are included in BMS or located at the contact between chromite and BMS.

Pt-Pd sulphides (Fig. 3.11f) were found in the all rock types. In the silicate rocks, they represent only ~5 % of the PGM observed. Most of them are located at the boundaries between BMS and silicate (~50 %). The others are surrounded by silicates (~38 %) or included in BMS (~12 %). In contrast, in the chromitite layers, Pt-Pd sulphides represent ~63 % of the PGM which are essentially (~63 %) located at the contact between the BMS and the chromites. The other grains are included in BMS (~21%) or located between BMS and silicates. Only one grain was found included in a chromite grain.

Other types of PGM were also observed, but they represent only a minor proportion of the total PGM content. Several grains of rustenburgite (Pt-Pd-Sn rich PGM, Fig. 3.11e) were observed in the chromitites (in total 10 grains located at silicate/BMS or BMS/chromite boundaries) and in the melanorite (three grains associated with or included in BMS). Two grains of laurite (Ru-Ir-Os sulphide, Fig. 3.11d) were found in the lower chromitite layer: an euhedral grain which is included in a chromite grain and another ragged grain which is associated with alteration silicates. Two small grains of platinum were also observed.

3.6.6. - Inclusions of PGE-rich phases

During laser ablation, signals from 30 micro-inclusions enriched in PGE were observed in the BMS (~ 20% of grains contain inclusions) or at the contact between the BMS and the silicates. The inclusions are found in all lithologies (anorthosite, chromitites and melanorites). Pentlandite and pyrrhotite are the principal hosts of the inclusions, however some inclusions have been observed in chalcopyrite.

The most common inclusions are Pt-rich. In many cases, Pt is associated with other PGE (Ir, Os, Re, Ru and Rh). Typical Pt-rich inclusions are: (i) Pt (Fig. 3.12b); (ii) Pt-Ir with minor Os-Rh-Re (Fig. 3.12d). Pt may also occur in minor amounts in inclusions dominated by Ir or Re (Fig. 3.12c, e and f). Most Pt inclusions are found at the contact between the BMS and the silicate minerals. Iridium in Ir-rich inclusions is found associated with Ru, Os and in some cases with Rh (Fig. 3.12e and f). These inclusions are most common in the chromitite layers. In the melanorite, one inclusion enriched in Re was found. In that case, Re was associated with minor Ir, Os and Pt (Fig. 3.12c). Another common type of inclusion consists of Ag inclusions. Silver can be found associated with Au and Pd (Fig. 3.12a). No other inclusion enriched in Pd was observed.

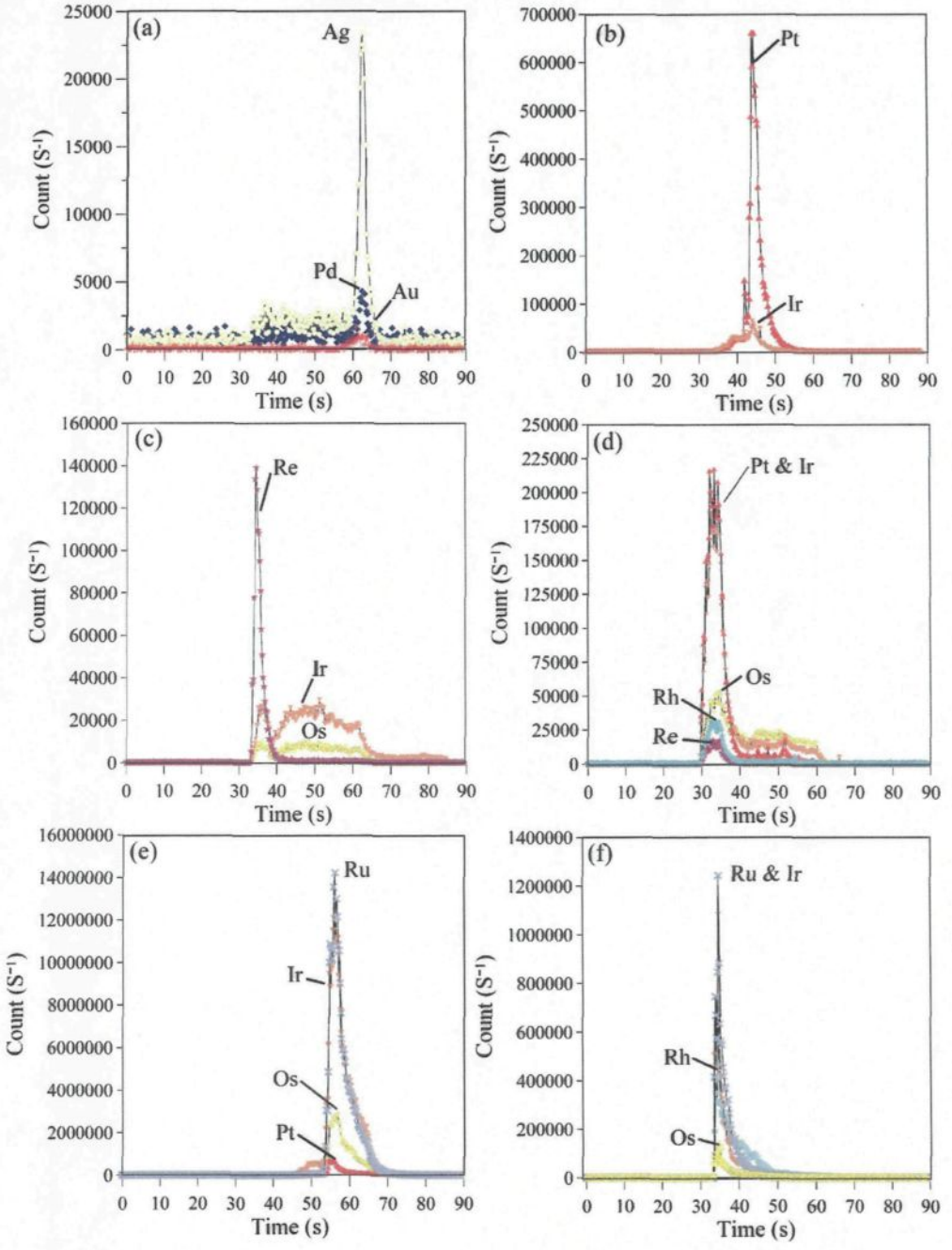

Figure 3.12: Types of PGE rich inclusions phases found associated with the base-metal sulphide minerals.

(a) Inclusion of Ag, Pd and Au in pyrrhotite.
(b) Inclusion of platinum associated with pentlandite.
(c) Inclusion of Re, Ir and minor Os and Pt associated with pyrrhotite.
(d) Inclusion of Pt-Ir, Os, Rh and Re associated with pyrrhotite.
(e) Inclusion of Ir, Ru, Os and minor Pt associated with pyrrhotite.
(f) Inclusion of Ir, Ru, Rh with minor Os associated with pyrrhotite.

By considering the PGM described above and relative abundances of PGM reported from the Merensky Reef by other authors (Kinloch, 1982; Viljoen and Hieber, 1986; Prichard *et al.*, 2004), we can infer some of the possible PGM found in the observed inclusions. The Pt-rich inclusions could be Pt-Fe alloy, Pt sulphide, Pt telluride and/or Pt arsenide commonly observed in the Merensky Reef (Vermaak and Hendriks, 1976; Kinloch, 1982; Viljoen and Hieber, 1986; Prichard *et al.*, 2004). Iridium, Ru and Os inclusions could be laurite, Pt-Ir-Rh inclusions could be the unknown Pt-Cu-Ir-Rh-S PGM of Viljoen & Hieber (1986) and Ag-Pd-Au could be palladian electrum.

The size of the inclusions (assumed to be cubic in shape, Appendix 3.A2) observed in the time-resolved analysis was roughly estimated using ablation rates in BMS and time-resolved analysis (Fig. 3.12 and Appendix 3.A2). Details of methodology and results are given in Appendix 3.A2. Most (~80 %) of the inclusions observed during laser ablation are ~1 to ~4 μm in length. These results are similar to the size of the PGM observed in the backscattered image analysis of the 222 PGM described above (Fig. 3.13). The size of our inclusions is considerably larger than those reported by Ballhaus and Sylvester (2000). Inspection of their data suggests to us that a calculation error was made in their paper and applying the method outlined in Appendix 3.A2 to their data we find that the size of their inclusions is similar to ours. This is important in the interpretation of the inclusions as we suggest that they represent exsolutions of PGM from the BMS while Ballhaus and Sylvester (2000) suggest that they represent PGE clusters or micronuggets captured by sulphide liquid.

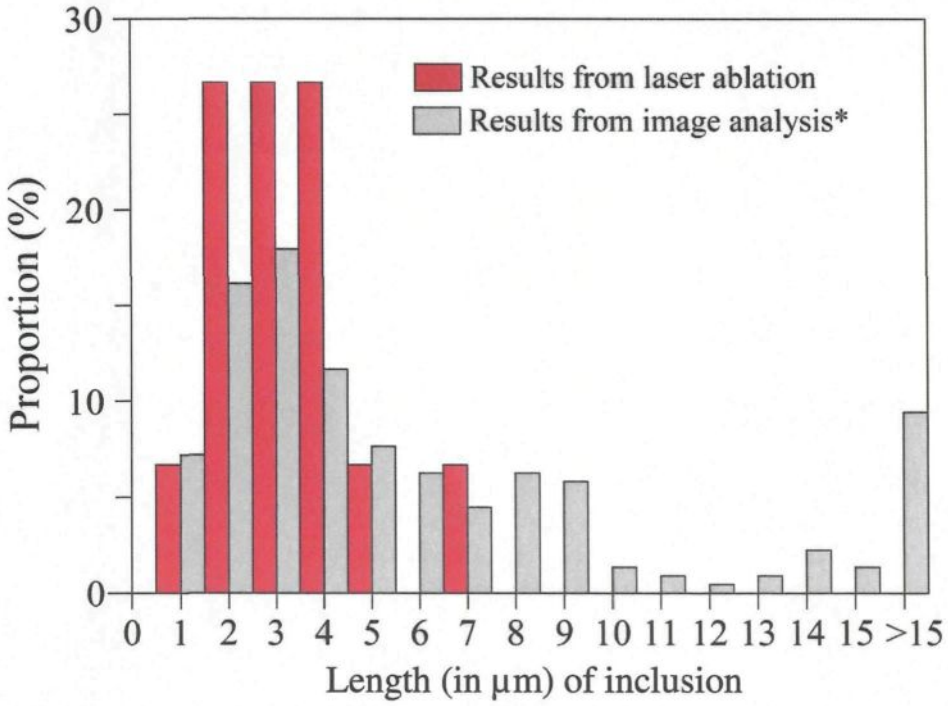

Figure 3.13: Comparison between the size of inclusions observed during laser ablation and the size of the platinum-group mineral observed in thin sections.

3.6.7. - Estimation of the contribution of the PGM

3.6.7.1. – Principle

The goal of the following calculation is to use the PGM (as determined by backscattered images and geochemical analysis) to evaluate the possible PGE mass balance between these PGM, the PGE contents in the BMS and with the whole rock data. The details of the method for the images analysis are given in Appendix 3.A1. The results of the calculations are given in Table 3.11 and Table 3.12.

3.6.7.2. – Results

The results of the mass balance calculations are summarized in Table 3.13. For all rock types Pt and Pd concentrations in the whole rock can be accounted for by combination of Pd and Pt in the BMS and PGM associated with the BMS, with most Pt present in PGM and most of the Pd present in BMS (Table 3.13). For the coarse-grained melanorite, the results do not take into account the myrmekitic-like structure. The calculation was also made including this structure and this considerably overestimates the amount of Pt present in the whole rock which probably reflects the fact that this kind of structure is rarely observed in thin section in the Merensky Reef (Kingstan and El-Dosuky, 1982).

Although in some rocks the Os, Ir, Ru and Rh present in BMS and associated PGM account for most of these elements there is a persistent tendency for a shortfall (Table 3.13). The worse case for this is the upper chromitite for Os, Ir, Ru and the lower chromitite for Rh. Some experimental work (Righter *et al.*, 2004) suggests that IPGE partition into chromite.

Table 3.11: *Summary of calculated parameters for the estimation of the PGM contribution.*

	V_{Litho}	Proportion of major phases (vol%)				Volume of each PGM ($x10^{-6}$ cm^3)							
Lithology	cm^3	Px	Plg	Chr	S	Pt-Pd sulphide	Pt sulphide	Pt-Pd-Te	Ru-Ir-Os-S	Pt-Fe	Pt-Sn-S	Pt	Gold
LC	1.24	8.8	40	50	1.2	7.17	10.96	1.98	9.68	1.5	0.2	0.07	
CGM	4.86	70	20	6.5	3.5	0.13	0.3	14.91		33.5	0.3		0.5
UC	3.96	23.5	25	50	1.5	30.68	2.55				0.53		
M1	7.01	69	20	6	5	0.11		94.4		0.04		0.6	

Table 3.12: *Calculated PGM and PGE mass from the BSE image analysis.*

	Calculated PGM mass (in µg)								Calculated PGE mass (in µg)					
Lithology	Pt-Pd S	Pt S	Pt-Pd-Te	Ru-Ir-Os-S	Pt-Fe	Pt-Sn-S	Pt	Au	Pt	Pd	Ru	Ir	Os	Au
LC	147.6	243.5	44.2	136.9	60.1	8	2.9		384.9	20.8	62.0	7.5	8.2	
CGM	0.8	1.9	94.4		380.4	3.4		5.5	388.8	0.3				5.5
UC	192.4	17.25				6.4			146.6	24.8				
M1	0.4		429.7		0.3		4.9		190.3	0.9				

Table 3.13: *Mass balance calculation between PGM image analysis, in-situ and whole rock PGE analysis.*

LOWER CHROMITITE

Data	Unit	Os	Ir	Ru	Rh	Pt	Pd	Au
Whole rock content	µg	7.30	11.10	54.10	38.00	331.00	44.00	3.40
	error	*0.37*	*0.56*	*2.71*	*1.90*	*16.55*	*2.20*	*0.17*
In-situ sulphide*	µg	0.36	1.17	1.48	11.77	0.55	21.52	0.00
	error	*0.04*	*0.12*	*0.15*	*1.18*	*0.06*	*2.15*	*0.00*
	%WR	*5.0*	*10.5*	*2.7*	*31.0*	*0.2*	*48.9*	*0.1*
PGE due to PGM analysis	µg	8.21	7.53	62.00		385.00	20.86	
	error	*1.64*	*1.51*	*12.40*		*77.00*	*4.17*	
	%WR	*112.5*	*67.8*	*114.6*		*116.3*	*47.4*	
In-situ sulphide and PGM analysis	µg	8.57	8.70	63.48	11.77	385.55	42.38	0.00
	error	*1.40*	*1.21*	*12.55*	*1.18*	*77.06*	*6.32*	*0.00*
	%WR	*117.4*	*78.3*	*117.3*	*31.0*	*116.5*	*96.3*	*0.1*
	error %	*19*	*11*	*23*	*3*	*23*	*14*	*0*

UPPER CHROMITITE

Data	Unit	Os	Ir	Ru	Rh	Pt	Pd	Au
Whole rock content	µg	2.60	3.50	17.00	10.00	134.50	42.70	3.10
	error	*0.13*	*0.18*	*0.85*	*0.50*	*6.73*	*2.14*	*0.16*
In-situ sulphide*	µg	0.11	0.17	0.14	9.31	0.49	30.64	0.01
	error	*0.01*	*0.02*	*0.01*	*0.93*	*0.05*	*3.06*	*0.00*
	%WR	*4.4*	*4.8*	*0.8*	*93.1*	*0.4*	*71.8*	*0.2*
PGE due to PGM analysis	µg					146.60	24.80	
	error					*29.32*	*4.96*	
	%WR					*109.0*	*58.1*	
In-situ sulphide and PGM analysis	µg	0.11	0.17	0.14	9.31	146.49	54.64	0.01
	error	*0.14*	*0.19*	*0.86*	*1.43*	*35.97*	*10.00*	*0.16*
	%WR	*4.4*	*4.8*	*0.8*	*93.1*	*109.4*	*129.8*	*0.2*
	error	*5*	*5*	*5*	*14*	*27*	*23*	*5*

COARSE-GRAINED MELANORITE

Data	Unit	Os	Ir	Ru	Rh	Pt	Pd	Au
Whole rock content	µg	5.8	5.8	25.3	13.4	420.8	162.9	25.6
	error	0.29	0.29	1.265	0.67	21.04	8.145	1.28
In-situ sulphide*	µg	3.34	2.83	11.03	9.96	3.94	170.32	0.01
	error	0.33	0.28	1.10	1.00	0.39	17.03	
	%WR	*57.5*	*48.8*	*43.6*	*74.4*	*0.9*	*104.6*	
PGE due to PGM analysis	µg					388.80	0.29	
	error					*77.76*	*0.06*	
	%WR					*92.4*	*0.2*	
In-situ sulphide and PGM analysis	µg	3.34	2.83	11.03	9.96	391.94	170.61	0.01
	error	*0.33*	*0.28*	*1.10*	*1.00*	*77.99*	*17.09*	*0.00*
	%WR	*57.5*	*48.8*	*43.6*	*74.4*	*93.3*	*104.7*	*0.0*
	error	*6*	*5*	*4*	*7*	*19*	*10*	*0*

Table 3.13 (Continued)

MELANORITE

Data	Unit	Os	Ir	Ru	Rh	Pt	Pd	Au
Whole rock content	µg	4.9	6.3	27.8	16.9	165.5	119	12.7
	error	*0.25*	*0.32*	*1.39*	*0.85*	*8.28*	*5.95*	*0.64*
In-situ sulphide*	µg	3.04	2.64	3.22	10.65	5.06	122.37	0.01
	error	*0.30*	*0.26*	*0.32*	*1.06*	*0.51*	*12.24*	*0.00*
	%WR	*62.0*	*42.0*	*11.6*	*63.0*	*3.1*	*102.8*	*0.1*
PGE due to PGM analysis	µg					190.30	0.91	
	error					*38.06*	*0.18*	
	%WR					*115.0*	*0.8*	
In-situ sulphide and PGM analysis	µg	3.04	2.64	3.22	10.65	195.36	123.28	0.01
	error	*0.30*	*0.26*	*0.32*	*1.06*	*38.57*	*12.42*	*0.00*
	%WR	*62.0*	*42.0*	*11.6*	*63.0*	*118.0*	*103.6*	*0.1*
	error	*6*	*4*	*1*	*6*	*23*	*10*	*0*

* Recalculated to whole rock sulphur content.
All calculation are made on the basis of 10 g of sample. Details of the calculation are given in Appendix 3.A1.

If we consider this possibility, the amount of Ir, Os, Ru and Rh required to be present in the chromite to achieve a mass balance is: ~0.1 to ~0.5 ppm Ir, ~0.3 to ~0.4 ppm Os, ~2.7 to ~2.9 ppm Ru and ~4.1 to ~4.35 ppm Rh (calculation made using both chromitite layers). Assuming that the magma from which the Merensky Reef formed contained ~0.3 ppb Os and Ir, 1.8 ppb Ru and 1 ppb Rh then these values imply partition coefficients between silicate liquid and chromite of 1000 to 2000 for Os, Ir and Ru, and ~4200 for Rh. These partition coefficients are ten times greater than those determined both experimentally (Righter *et al.*, 2004) and empirically (Puchtel *et al.*, 2004). This seems too large a discrepancy to us to accept and thus we do not consider that the "missing" IPGE are present in the chromite structure (Puchtel *et al.,* 2004).

In the lower chromitite layer two grains of laurite were observed and these could account for the balance of IPGE in this sample. However, no phases highly enriched in Ru, Ir, Os, Rh or Au (PGM or alloys) were observed in the other three rocks. Nonetheless several zones enriched in these elements (Fig. 3.12) were observed during the laser ablation of the BMS. We interpret these zones to represent laurite inclusions. Laurite has been observed in Merensky Reef samples by many authors (Kingston and El-dosuky, 1982; Kinloch, 1982; Viljoen and Hieber, 1986; Kinloch and Peyerl, 1990; Prichard et al., 2004) and only a small quantity (~65 μg) is needed to satisfy our mass balance. This represents in our samples about 10 grains of laurite of 10 μm in diameter size.

The mass balance for Au indicates only a very small quantity is accounted by the BMS. Furthermore, only one grain of Au was observed in thin section. However, zones enriched in Pd, Ag and Au were observed during laser ablation suggesting that palladian electrum is present. Kingston and El-Dosuky (1982) in their study of PGM mineralogy of the Rustenburg Mine report 1 vol% of this mineral. Our mass balance requires ~50 μg of electrum (Au-Ag alloy) equivalent in our samples to 3 grains of 10 μm in diameter size.

In summary, 88% by volume of the PGM are included in or at the contact with BMS. The mass balance works considering the PGM and the BMS accounts for most Pt, Pd and Rh. To account for the Os, Ru, Ir and Au requires that some laurite and palladian electrum is present but rarely observed in thin section. There is evidence for these minerals in the time-resolved analysis from the laser ablation of the BMS. However, as the thin sections scanned for PGM analyses are not necessarily those that were used for the laser ablation and that we have probably not "ablated" all the inclusions. We cannot conclude on their exact influence on mass balance.

3.6.8. - Modeling the role of sulphide liquid on PGE distribution

3.6.8.1. – Principle

The model of collection of the PGE by a sulphide liquid presented by Campbell & Naldrett (1979) is based on the assumption that PGE and others metals have a large partition coefficient with respect to the sulphide liquid and that the PGE concentration in sulphides is dependent on the relative volume of magma which interacted with the sulphide liquid. In a closed system, the concentration of an element in the sulphide (C_{Sul}) is given by the following equation (Campbell and Naldrett, 1979):

$$C_{Sul} = C_{Sil}\, D^{sul/sil}\, (R+1)/(R+D^{sul/sil})$$

where C_{Sil} is the concentration in the silicate liquid, $D^{sul/sil}$ is the partition coefficient (for each metal) between the sulphide and the silicate liquids, and R is the ratio of silicate to sulphide liquid.

As sulphide liquid sinks throughout the magma column, Brügmann *et al.* (1993) have proposed that the sulphide liquid composition may be adequately modelled using the zone-refining equation. In this case, the concentration of an element in the sulphide (C_{Sul}) is given by :

$$C_{Sul} = C_{Sil} [D^{sul/sil} - (D^{sul/sil} - 1) e^{-(1/ Dsul/sil. N)}]$$

where N is the mass ratio of silicate to sulphide liquid (similar to R-factor).

These two equations can be applied to our data as follows: if the PGE were initially in the sulphide liquid, the contents of the PGE and others metal in the whole rock can be modelled with the equation above. In the case where PGE crystallised directly as PGM, the PGE content would not be well modelled with these equations and consequently, other processes are needed to explain the observed features.

3.6.8.2. - Initial magma

The Merensky Reef occurs in the Upper Critical Zone of the Bushveld Complex. According to Davis and Tredoux (1985) and Harmer and Sharpe (1985), the rocks from the Merensky Reef can be formed from two possible silicate liquids: a Mg-rich basaltic andesite and a tholeiitic basalt. The composition of magma taken for the calculation is the mixed magma proposed by Barnes and Maier (2002a). The composition is given in Table 3.14.

3.6.8.3. - Results of the modelling

The two equations described above give relatively similar results. Parameters and results of the modelling using the equations proposed by Brügmann *et al.* (1993) are summarized in Table 3.14.

Table 3.14: *Results of sulphide liquid modelisation.*

(a) Parameters

	Ni ppm	Os ppb	Ir ppb	Ru ppb	Rh ppb	Pt ppb	Pd ppb	Au ppb	Cu ppm
Initial magma[a]	249	0.29	0.28	1.8	1.08	16.6	9.8	3	60
$D^{sil/sul}$	550	40000	40000	40000	40000	40000	40000	20000	1000

(b) Modelled compositions for the silicate rocks

	Ni wt%	Os ppb	Ir ppb	Ru ppb	Rh ppb	Pt ppb	Pd ppb	Au ppb	Cu wt%
R= 45 000	13.70	7834	7564	48626	29175	448436	264739	81043	6

(c) Modelled compositions for the chromitite layers

	Ni wt%	Os ppb	Ir ppb	Ru ppb	Rh ppb	Pt ppb	Pd ppb	Au ppb	Cu wt%
Lower chromitite									
R= 45 000 sulphide + 0.4 PGM%*	13.70	69434	84844	577266	191095	2478676	278739	53676	6.11
Upper chromitite									
R= 45 000 sulphide+ 0.1 PGM%*	13.70	23234	26884	180786	69655	955996	268239	53676	6.03

* Composition of the platinum-group minerals used in the calculation

	Ni wt%	Os wt%	Ir wt%	Ru wt%	Rh wt%	Pt wt%	Pd wt%	Au wt%	Cu wt%	Proportion %
Cooperite[b]	0.7					84	0.7			50
Laurite[b]		5.5	6.9	47.2						28
Malanite[c]					18.4	39.8			12.4	22

[a] Mixed magma (Barnes and Maier, 2002),

[b] Kingston and El-Dosuku (1982),

[c] Cabri (2002),

$D^{sil/sul}$: partition coefficient between silicate and suphide liquids.

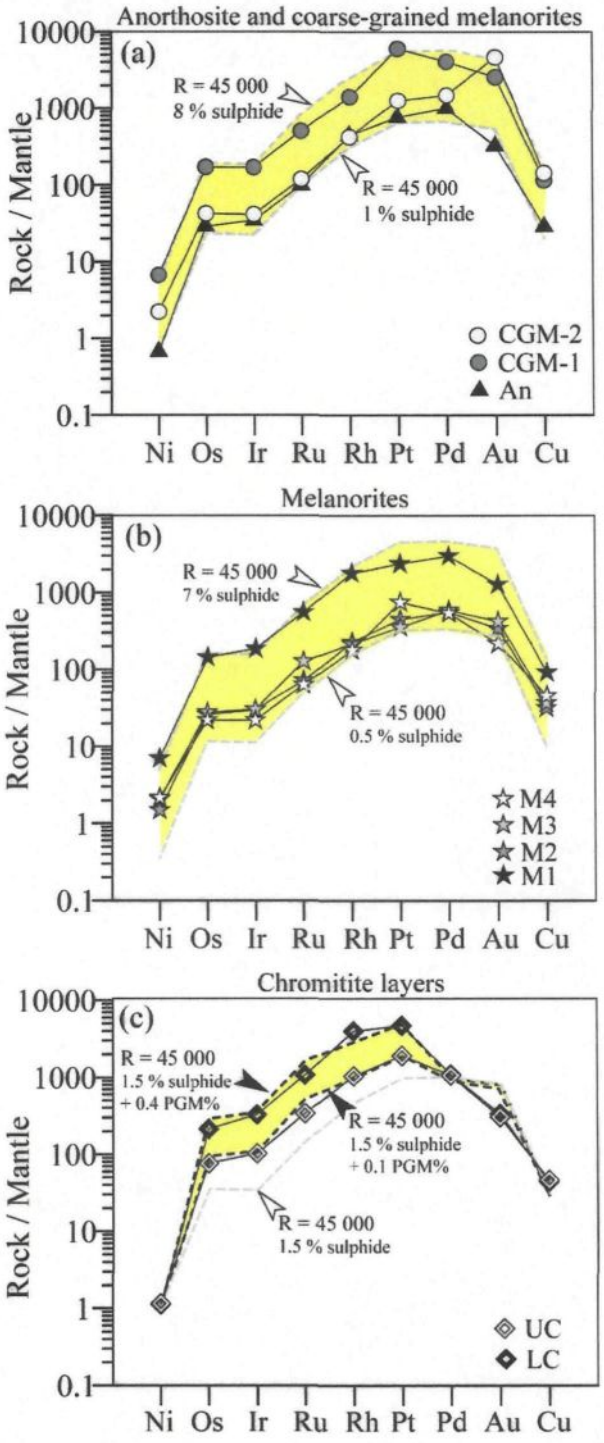

Figure 3.14: Comparison of observed and modeled metal patterns of rock types in the Merensky Reef.

(a) and (b) The PGE contents of the silicate rocks can be modelled by assuming that they are hosted by base-metal sulphide that segregated at an N-factor of 45000.

(c) The PGE contents of the chromitite layers are mostly too high to be explained by base-metal sulphide collection alone, but can be modelled by assuming crystallization of 0.1-0.4% PGM (see text for explanation).

The composition of the BMS in the silicate rocks of the Rustenburg Merensky Reef sample can be modelled with using a N-factor of 45 000 and by considering that these rocks contain 1 to 8 % sulphides (Fig. 3.14a and Table 3.14). These sulphide contents are consistent with the whole rock data (Table 3.6) and the results of X-ray tomography (Godel *et al.*, 2006).

Contrary to the silicate rocks, the PGE budget of the chromitite layers cannot be modelled by sulphide segregation alone. Using a N-factor of 45 000 and 1.5 % sulphides (as observed in the whole rocks), there is a mismatch between the model composition and the composition of the chromitites (Fig. 3.14c). The calculated composition contains lower Pt, Os, Ir, Ru, and Rh than the observed composition. It is possible to model the composition of the chromitite layers to contain 1.5% sulphide liquid (with N= 45 000) and 0.4 % PGM for the lower chromitite layer and 0.1 % PGM for the upper chromitite layer (Table 3.14). The assemblage of PGM used in the calculation consists of cooperite, laurite and malanite (Table 3.14). These PGM have to crystallize before an immiscible sulphide liquid has formed. Barnes and Maier (2002a) found a similar problem in matching the PGE content of the chromitite from the Impala Platinum Mine.

3.7. – DISCUSSION

In the light of our results any model for the formation of the reef needs to consider: the association of the PGE and PGM with BMS, the tendency of the BMS to distribute preferentially in the direction of the paleovertical, the enrichment of IPGE, Rh and Pt relative to S, Ni, Pd, and Au in the chromitite layers.

Five possible processes, which are not necessarily mutually exclusive, could be considered as important in the origin of the Merensky Reef: (i) collection of the PGE by an immiscible sulphide liquid; (ii) partitioning of the IPGE into chromite; (iii) crystallisation of the

PGM directly from the magma; (iv) loss of S, Pd and base metals from the BMS in the chromitite layer; and (v) redistribution of the PGE by a fluid rising from the underlying cumulate pile. The implication of each of these processes will be considered and a possible model for the formation of the Merensky Reef will then be proposed.

3.7.1. - Collection of the PGE by an immiscible sulphide liquid

The model is based on the suggestion that when a new magma enters the chamber, it mixes with the resident magma to form a mixed magma which becomes saturated in an immiscible sulphide liquid (Campbell and Naldrett, 1979; Li and Ripley, 2005). As PGE have a large partition coefficient into sulphide liquid, the immiscible sulphide liquid collects the PGE then settles onto the cumulate pile (Campbell *et al.*, 1993; Naldrett *et al.*, 1986). The BMS occur as interstitial phases in vertical networks developed along the silicate grain boundaries in the melanorites and as droplets in the chromitite layers (Godel *et al.*, 2006). Based on our modeling, the PGE in the silicate rocks can all be accommodated in a sulphide liquid which interacted with a large volume of silicate magma (N-factor = 45 000).

In contrast, in the chromitite layers, as previously described by Barnes and Maier (2002b) at Impala Platinum Mine, it is not possible to explain the PGE content by considering only the model of collection of the PGE by a sulphide liquid.

3.7.2. - Partitioning of PGE in the Cr-spinel

Another possibility is that the IPGE and Rh partitioned into chromite during crystallisation. Experimental work on partitioning of Ir, Ru, Rh and Pd between spinel and

silicate melt (Capobianco and Drake, 1990; Capobianco *et al.*, 1994; Sattari *et al.*, 2002; Righter *et al.*, 2004) have shown that Ir, Rh and Ru could partition into spinel phases.

Applying this to our dataset, the mass balance calculations for this model requires that the partition coefficients for the IPGE and Rh are considerable higher than those that have been determined experimentally, although it should be mentioned that the experimental data are sparse and the possibility of collection of IPGE and Rh by chromite cannot be entirely ruled out. The main problem with this model is that it does not account for the high Pt values in the chromite layer.

3.7.3. - Crystallisation of the PGM directly from the magma

Some workers (*e.g.* Hiemstra, 1979) have suggested that PGM could have crystallized directly from the Bushveld magma and been precipitated from the magma by minerals on the liquidus such as chromite. Due to the low concentration of the PGE, the grains would be very small and in order to collect them in the cumulate pile they would have to be incorporated in the other crystallizing phases such as chromite and olivine. Empirical evidence for the formation of PGM directly from mafic magmas has been provided by many authors from Keays and Campbell (1981) to Fiorentini *et al.* (2004). Barnes (1993) has suggested the PGM could be included in BMS liquid. However, because of the very low concentrations of PGE in the magma at the time of saturation (0.1-0.5 ppb for IPGE to 10 to 20 ppb for Pt) and the presence of BMS some debate has arisen as to how this could occur. In order to overcome the kinetic problem that arise in nucleating PGM in a magma with such low PGE concentrations a model whereby PGE and metalloids atoms form clusters of 100 to 1000 atoms in the silicate magma was proposed by Tredoux *et al.* (1995). The clusters have no structure and are not minerals or nuclei. These

clusters are then physically captured by whatever phase is crystallising. This is not an equilibrium process and partition coefficients are not applicable. A variation of this model has been applied to formation of the Merensky Reef by Ballhaus and Sylvester (2000).

The crystallisation of PGM from the silicate magma has remained controversial because it is difficult to determine the solubility of PGE in mafic magma at fO_2 approaching natural systems.

Early experiments were plagued by the formation of micronugget (*e.g.* Borisov and Palme, 1997). The presence of the micronuggets has been used as evidence that clusters exist. However, recent experimental work suggests that micronuggets are an experimental artefact (Fortenfant *et al.*, 2003; Pruseth and Palme, 2004; Blaine *et al.*, 2005). Based on the experimental database and thermodynamic calculations, Borisov and Palme (1997) calculated that at fO_2 at or just below FMQ, Fe-bearing mafic magmas become saturated in Pt-Ru and Ir-Fe alloys at 0.4 to 14 ppb. These concentrations are similar to those observed in the Bushveld magma and many other mafic magmas. If the magmas are saturated in Fe-PGE alloys then clusters are no longer required. It could be argued that the high values of these elements in the chromitite layers are due to the crystallization of the Fe-PGE alloys which have been incorporated into the chromite and collected onto the crystal pile with chromite. Mungall (2002) suggests a reduction front around chromite grains may trigger PGM formation. This model has a difficulty in that our PGM study has shown that the PGM contained the chromitite layers are commonly associated with the BMS and only few PGM are included in chromite grains. This observation is in agreement with other PGM studies of the Merensky Reef samples (*e.g.* Kinloch, 1982; Lee and Parry, 1988; Prichard *et al.*, 2004) all of whom suggested that the PGM exsolved from BMS. The association of the PGM sulphides is also problematic because Brenan and Andrews (2001) calculate that at fO_2 and fS_2 at

which a BMS liquid segregate from a mafic magma, Fe-PGE alloys are not stable. They suggest that the PGM crystallized and were subsequently absorbed by the infiltration of the BMS liquid.

3.7.4. - Sulphur, Pd and base metal loss from the chromitite layers

Naldrett and Lehmann (1988) suggest that Fe-sulphide could react with chromite producing a Fe-rich chromite and removing S from the system, thereby triggering PGM crystallisation by lowering the fS_2. This suggestion could explain the fact that BMS in the chromitite layers of the Bushveld Complex have a high PGE/S ratio and are generally rich in Cu and Ni (Fig. 3.4). By this argument, the chromitite layers originally contained 5 times more BMS than they do now and the PGE were originally collected by these BMS. However, it does not explain why the chromitite layers are not as rich in Pd as the other PGE or Au.

Peregoedova *et al.* (2004) have shown that the desulphidization of MSS results in the formation of an IPGE rich MSS, Fe-Pt alloys and a Cu-Pd(+/-) Au sulphide liquid. Applying this process to our data one could suggest that a cumulate pile formed and consisted of a semi-consolidated chromitite layer and melanorite. The silicate magma became saturated in base-metal suphide liquid which collected the PGE. The sulphide liquid percolated downwards through the cumulate pile. The highest concentration of the sulphide liquid collected in the chromitite layer. During cooling Fe from the BMS was lost to the chromite and S was released (Naldrett and Lehmann, 1988). This resulted in the formation of PGM-alloys, MSS and Cu-Pd-Au sulphide melt (Peregoedova *et al.*, 2004). The loss of S may be evaluated by using the S/Se ratios of the whole rock (*e.g.* Lorand *et al.*, 2003). Selenium substitutes for S in BMS and primary magmas have S/Se ratios of ~3000. During alteration, S is more mobile during alteration than Se and consequently the S/Se decreases strongly (*e.g.* ~1400 for the J-M reef samples of the Stillwater

complex, Godel and Barnes (2007). In our samples of Merensky Reef, the S/Se ratios (Table 6) are ~2500-3000 which implies that no extensive S removal has occurred. These S/Se results are similar to those calculated from the data of Barnes and Maier (2002a) for the Merensky Reef at Impala Platinum Mine, thus S loss does not seem probable.

3.7.5. - Redistribution of the PGE by a fluid rising from the underlying cumulate pile

Some authors have proposed that PGE enrichment in some portions of layered intrusions was caused by upward migration of fluid enriched in Cl (Boudreau and McCallum, 1992; Boudreau and Meurer, 1999; Willmore *et al.*, 2000). In this model, the fractionated intercumulus liquid became saturated in hydrous Cl-rich fluid and PGE partitioned into the fluid which migrated upward in the cumulate pile. The fluid (enriched in S, base metal and possibly some PGE) migrated upward until it encountered a layer where the intercumulate silicate liquid was undersaturated in fluid. The fluid then dissolved in the silicate liquid and the metals and S that the fluid was transporting precipitated as BMS among the silicate grains.

If we apply this model to our data one would have to argue that the rising fluid started to dissolve into the interstitial silicate liquid at the level of the chromitite layer and deposited most of its Cu, IPGE, Rh and Pt at this point. Not all the fluid dissolved in the chromitite layer and the remainder continued to rise through the melanorite and encouraged grain growth resulting in the layer being coarse grained. As more fluid dissolved into the interstitial silicate liquid, the S and metals it was carrying were deposited along the fluid pathways, and the amount of PGE and Au deposited decreased as the fluid became depleted upsection.

This model has a number of weaknesses. It is possible to argue that this occurred for the first chromitite layer and overlying melanorite, assuming that the cumulate pile below the

chromitite is depleted in PGE. For the second chromitite layer and the overlying melanorite, however it is not clear to us where the metals and S come from since the fluid should have been depleted in these elements by the time it reached the second chromitite layer and yet the chromitite is enriched in PGE. It is also impossible to test the model numerically because experimental work determining the solubility of the PGE in magmatic fluids are sparse and only values for Pt and Au are available (Hanley *et al.*, 2005). Barnes and Maier (2002b) considered this model on a much larger scale for the Bushveld and concluded that it is the rocks above the reefs that are depleted in PGE and not the rocks below the reef. Therefore it seems more likely that the PGE were collected from the magma above the reef than the cumulate pile below.

3.7.6. - Proposed model of formation for the Merensky Reef

Integration of the above considerations allows us to propose the following model for the formation of the Merensky Reef at the Rustenburg Platinum mine. A crystal pile consisting of plagioclase and trapped melt (proto-anorthosite) overlain by a fractioned silicate liquid formed. A new injection of magma (possibly high-Mg basalt) entered the chamber and mixed with the resident magma bringing chromite, orthopyroxene and PGE alloys onto the liquidus (Fig. 3.15a). These minerals settled onto the protoanorthosite. Chromite grains and associated PGM were concentrated immediately above the protoanorthosite to form a layer consisting of chromite, PGM and trapped melt (protochromite layer) while the orthopyroxene was concentrated immediately above this to form a layer consisting mainly of orthopyroxene and trapped melt (protomelanorite). The fractionated melt become saturated in a base-metal sulphide liquid (Fig. 3.15b), immiscible sulphide droplets formed and collected the remaining PGE by extensive interaction with the silicate magma (N-factor = 45 000).

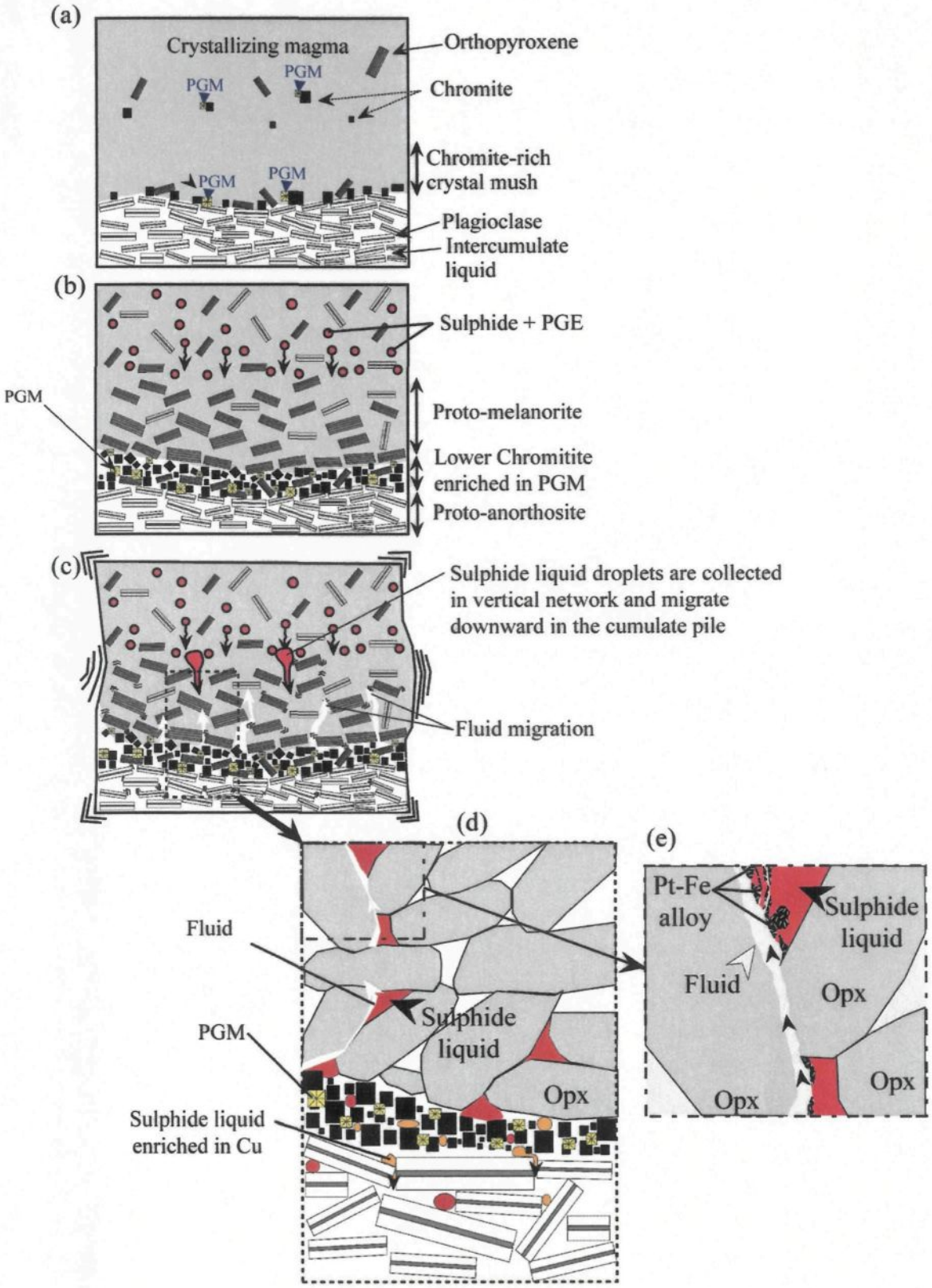
(a)
Crystallizing magma
PGM
PGM
PGM
PGM
Orthopyroxene
Chromite
Chromite-rich crystal mush
Plagioclase
Intercumulate liquid
(b)
Sulphide + PGE
PGM
Proto-melanorite
Lower Chromitite enriched in PGM
Proto-anorthosite
(c)
Sulphide liquid droplets are collected in vertical network and migrate downward in the cumulate pile
Fluid migration
(d)
Fluid
Sulphide liquid
PGM
Opx
Sulphide liquid enriched in Cu
(e)
Pt-Fe alloy
Sulphide liquid
Fluid
Opx
Opx
Opx

Figure 3.15: Proposed model of formation for the Merensky Reef at Rustenburg Platinum Mine.

(a) A new injection of magma entered the chamber and mixed with the resident magma. Chromite associated with PGM and orthopyroxene crystallised and settled on the top of the underlying proto-anorthosite overlying by proto-melanorite.
(b) After chromite and orthopyroxene crystallisation, the magma became saturated in an immiscible sulphide liquid which collected the remaining PGE.
(c) Magma chamber instabilities (possibly movements due to earthquakes) triggered the collection of the sulphide droplets to networks facilitating its downward migration along vertical dilatancies formed during compaction. The downward migration of the sulphide liquid is slowed when it reaches the chromitite layer (due to a change in sulphide liquid wetting properties in chromitite).
(d) As temperature decreases, fluid interacts with the base-metal sulphides triggering their partial desulphurisation.
(e) Pt-Fe alloy form by partial desulphurisation of the system. The fluid triggers locally a disequilibrium of the base-metal sulphide leading to crystallisation of myrmekitic Pt-Fe alloy.

During the evolution of the sulphide liquid, a monosulphide solid solution enriched in Fe (MSS) and a fractionated sulphide liquid enriched in Cu formed. The Fe-Ni-Cu-PGE sulphide liquid collected along vertical networks along the dilatancies formed during the compaction (Barnes and Maier, 2002a; Godel *et al.*, 2006) of the cumulate pile (Fig. 3.15c). Magma chamber instabilities may improve the downward migration of the sulphide liquid. As Cu-rich sulphide liquid has an higher wetability against silicate and oxides than Cu-poor sulphide liquid (Ebel and Naldrett, 1996; Ebel and Naldrett, 1997), some of the Cu-rich liquid migrated through the chromitite. The liquid dissolved some of the PGE alloys that had earlier crystallised and collected in the chromitite layer when the silicate liquid was sulphide undersaturated. The BMS now observed in the chromitite layer occur as droplets, thus the sulphides which escape downward into the silicates rocks below the chromitites were probably not interconnected and were trapped rapidly in the silicate matrix as temperature decreased (Fig. 3.15d). This phenomenon would explain the BMS in the chromitite layers and the rocks immediately below each chromitite layer are richer in chalcopyrite. Magma chamber instabilities may also trigger fluid (magmatic, aqueous or even vapour) migration. This fluid may react with the BMS and lead to their partial desulfurisation triggering formation Pt-Fe alloy (isoferroplatinum) as in experiments (*e.g.* Peregoedova *et al.*, 2004).

A second magma injection entered into the magma chamber, similarly triggering the formation of the upper chromitite. The magma chamber was heated by this new influx of magma so that orthopyroxene in the protomelanorite was maintained close to its solidus temperature and could recrystallise to form large grains (Cawthorn and Boerst, 2006). Furthermore, compaction appears to have forced some orthopyroxene grains together resulting in a fusion of the grains, with small chromite grains marking the old grain boundaries (Barnes and Maier, 2002). The

combination of these processes could have resulted in coarsening of grain size and the formation of the coarse grained melanorite (Merensky pegmatoid).

As the temperature fell, the MSS exsolved to pyrrhotite and pentlandite and the ISS exsolved to chalcopyrite and cubanite. Most of the PGM (*e.g.* sulphides or bismutho-tellurides) exsolved from the BMS. Pentlandite and pyrrhotite are preferentially enriched in IPGE and Rh as would be expected if these minerals exsolved from MSS. However pentlandite is also enriched in Pd and this requires that during exsolution of sulphides, Pd diffused into the pentlandite from the Cu-rich minerals.

3.8. – CONCLUSION

The majority (~65 up to ~85%) of the PGE in the Merensky Reef at Rustenburg Platinum Mine are not found in solid-solution within the BMS, but are essentially found as PGM closely associated with the BMS (included in BMS or located at the BMS/silicate or oxide grain boundaries). Amongst the BMS, pentlandite is the principal host of Pd, Rh, Os, Ir and Ru. Platinum and gold are not partitioned in sulphide minerals, but occur as PGM or electrum. The BMS in the chromitite layers are slightly enriched in PGE (by a factor of 2), but it cannot explain the strong (by a factor of 5) enrichment of the chromitite in PGE. The data suggest that some PGE are hosted by BMS (principally pentlandite), but the majority is hosted by PGM. Our modeling has shown that the PGM found in the chromitite layers are unlikely to be solely the results of exsolution from a sulphide liquid. A primary (*i.e.* before immiscible sulphide formed) crystallisation of PGM is needed to account for the PGE mass balance.

So in light of our results, the collection of the PGE in chromitite layers of the Merensky Reef at Rustenburg Pt Mine may have happened in two steps: (i) some PGM (essentially laurite,

cooperite and malanite) crystallised from the magma during the formation of chromite and before sulphide saturation; (ii) an immiscible sulphide liquid formed and the remaining PGE were collected by this liquid and then percolated downward in the crystal pile until it encountered the chromitite layers. In the silicate rocks, only one step is needed; the PGE are collected by an immiscible sulphide liquid which percolated in the silicate rocks. On cooling, some PGMs exsolve from the Mss and Iss in both chromitites and silicate rocks.

3.9. – ACKNOWLEDGMENTS

Rustenburg Platinum Mine is thanked for allowing access to their properties and allowing sampling of the Merensky Reef. Dr. Richard Cox (UQAC) is thanked for his assistance with the LA-ICP-MS analysis. Dr. Paul Bédard and Mr. Dany Savard (UQAC) are thanked for their advice and assistance during the whole rock analysis. Dr. Marc Choquette (Laval University) is thanked for his assistance with the microprobe analysis. Pr. Christian Ballhaus, Dr. Stephen Barnes, and Pr. James Mungall are thanked for their constructive reviews. This work was funded by a Discovery Grant from the Natural Science and Engineering Research Council of Canada and the Canadian Research Chair in Magmatic Metallogeny.

3.10. – REFERENCES

Arndt, N., Jenner, G., Ohnenstetter, M., Deloule, E. & Wilson, A. (2005). Trace elements in the Merensky Reef and adjacent norites Bushveld Complex South Africa. *Mineralium Deposita* **40**, 5, 550-575.

Ballhaus, C. & Ryan, C. G. (1995). Platinum-group elements in the Merensky reef. I. PGE in solid solution in base metal sulfides and the down-temperature equilibration history of Merensky ores. *Contributions to Mineralogy and Petrology* **122**, 3, 241-251.

Ballhaus, C. & Sylvester, P. (2000). Noble Metal Enrichment Processes in the Merensky Reef, Bushveld Complex. *Journal of Petrology* **41**, 4, 545-561.

Barnes, S.-J. & Maier, W. D. (2002a). Platinum-Group Element Distributions in the Rustenburg Layered Suite of the Bushveld Complex, South Africa. In: Cabri, L. J. (ed.) *Geology, Geochemistry, Mineralogy and Mineral benefication of Platinum Group Element.* Canadian Institute of Mining, Metallurgy and Petroleum, **Special Volume 54**, 553-580.

Barnes, S.-J. & Maier, W. D. (2002b). Platinum-group elements and microstructures of Normal Merensky Reef from Impala Platinum Mines, Bushveld Complex. *Journal of Petrology* **43**, 1, 103-128.

Barnes, S.-J. & Lightfoot, P. C. (2005). Formation of Magmatic Nickel Sulfide Deposits and Processes Affecting their copper and Platinum Group Element Contents. *Economic Geology* **100th Anniversary Volume**, 179-213.

Barnes, S.-J., Cox, R. & Zientek, M. (2006). Platinum-group element, Gold, Silver and Base Metal distribution in compositionally zoned sulfide droplets from the Medvezky Creek Mine, Noril'sk, Russia. *Contributions to Mineralogy and Petrology* **152**, 2, 187-200.

Barnes, S.-J., van Achterbergh, E., Makovicky, E. & Li, C. (2001). Proton microprobe results for the partitioning of platinum-group elements between monosulphide solid solution and sulphide liquid. *South African Journal of Geology* **104**, 4, 275-286.

Barnes, S. J. (1993). Partitioning of the Platinum Group Elements and Gold between Silicate and Sulfide Magmas in the Munni-Munni Complex, Western-Australia. *Geochimica Cosmochimica Acta* **57**, 6, 1277-1290.

Bédard, L. P. & Barnes, S. J. (2004). Improved platinum-group element extraction by NiS Fire assay from chromitite ore samples using a flux containing sodium metaphosphate. *Geostandards and Geoanalytical Research* **28**, 2, 311-316.

Blaine, F. A., Linnen, R. L., Holtz, F. & Brugmann, G. E. (2005). Platinum solubility in a haplobasaltic melt at 1250°C and 0.2 GPa: The effect of water content and oxygen fugacity. *Geochimica Cosmochimica Acta* **69**, 5, 1265-1273.

Borisov, A. & Palme, H. (1997). Experimental determination of the solubility of platinum in silicate melts. *Geochimica Cosmochimica Acta* **61**, 20, 4349-4357.

Boudreau, A. E. & Mc Callum, I. S. (1992). Infiltration Metasomatism in Layered Intrusions - an Example from the Stillwater Complex, Montana. *Journal of Volcanology and Geothermal Research* **52**, 1-3, 171-183.

Boudreau, A. E. & Meurer, W. P. (1999). Chromatographic separation of the platinum-group elements, gold, base metals and sulfur during degassing of a compacting and solidifying igneous crystal pile. *Contributions to Mineralogy and Petrology* **134**, 2-3, 174-185.

Brenan, J. M. & Andrews, D. R. A. (2001). High-temperature stability of laurite and Ru-Ir-Os alloy and their role on PGE fractionation in mafic magmas. *Canadian Mineralogist* **39**, 341-360.

Brenan, J. M.; McDonough, W. F. & Dalpé, C. (2003) Experimental constraints on the partitionning of rhenium and some platinum-group elements between olivine and silicate melt. *Earth and Planetary Science Letters*, **212**, 1-5, 135-150.

Brügmann, G. E., Naldrett, A. J., Asif, M., Lightfoot, P. C., Gorbachev, N. S. & Fedorenko, V. A. (1993). Siderophile and chalcophile metals as tracers of the evolution of the Siberian Trap in the Noril'sk region, Russia. *Geochimica Cosmochimica Acta* **57**, 9, 2001-2018.

Cabri, L. J. (2002). The Platinum-Group Minerals. In: Cabri, L. J. (ed.) *Geology, Geochemistry, Mineralogy and Mineral benefication of Platinum Group Element.* Canadian Institute of Mining, Metallurgy and Petroleum, **Special Volume 54**, 13-129.

Campbell, I. H. & Naldrett, A. J. (1979). The influence of silicate silicate: sulphide ratios on the geochemistry of magmatic sulphides. *Economic Geology* **74**, 1503-1505.

Campbell, I. H., Naldrett, A. J. & Barnes, S. J. (1983). A Model for the Origin of the Platinum-Rich Sulfide Horizons in the Bushveld and Stillwater Complexes. *Journal of Petrology* **24**, 2, 133-165.

Capobianco, C. J. & Drake, M. J. (1990). Partitioning of ruthenium, rhodium, and palladium between spinel and silicate melt and implications for platinum group element fractionation trends. *Geochimica Cosmochimica Acta* **54**, 3, 869-874.

Capobianco, C. J., Hervig, R. L. & Drake, M. J. (1994). Experiments on crystal/liquid partitioning of Ru, Rh and Pd for magnetite and hematite solid solutions crystallized from silicate melt. *Chemical Geology* **113**, 1-2, 23-43.

Cawthorn, R. G. (1999). The platinum and palladium resources of the Bushveld Complex. *South African Journal of Science* **95**, 11/12, 481.

Cawthorn, R. G. (2002). Platinum-Group Element Deposits in the Bushveld Complex, South Africa. In: Cabri, L. J. (ed.) *Geology, Geochemistry, Mineralogy and Mineral benefication of Platinum Group Element.* Canadian Institute of Mining, Metallurgy and Petroleum, **Special Volume 54**, 389 - 429.

Cawthorn, R. G. & Boerst, K. (2006). Origin of the Pegmatitic Pyroxenite in the Merensky Unit, Bushveld Complex, South Africa. *Journal of Petrology* **47**, 1509-1530.

Davies, G. & Tredoux, M. (1985). The platinum-group element and gold contents of the marginal rocks and sills of the Bushveld Complex. *Economic Geology* **80**, 838-848.

Eales, H. V. & Cawthorn, R. G. (1996). The Bushveld Complex. In: Cawthorn, R. G. (ed.) *Layered Intrusions.* Amsterdam, The Nederlands: Elsevier, 181-230.

Ebel, D. S. & Naldrett, A. J. (1996). Fractional Crystallisation of sulfide ore liquids at high temperature. *Economic Geology* **91**, 607-621.

Ebel, D. S. & Naldrett, A. J. (1997). Crystallization of sulfide liquids and the interpretation of ore composition. *Canadian Journal of Earth Sciences* **34**, 4, 352-365.

Fiorentini, M. L., Stone, W. E., Beresford, S. W. & Barley, M. E. (2004). Platinum-group element alloy inclusions in chromites from Archaean mafic-ultramafic units: evidence from the Abitibi and the Agnew-Wiluna Greenstone Belts. *Mineralogy and Petrology* **82**, 3 - 4, 341-355.

Fortenfant, S. S., Gunther, D., Dingwell, D. B. & Rubie, D. C. (2003). Temperature dependence of Pt and Rh solubilities in a haplobasaltic melt. *Geochimica Cosmochimica Acta* **67**, 1, 123-131.

Godel, B. & Barnes, S.-J. (in press). Platinum-group elements in sulfide minerals and whole rocks of the J-M reef (Stillwater Complex, U.S.A.): Implication for the formation of the reef. Chemical Geology

Godel, B., Barnes, S.-J. & Maier, W. D. (2006). 3-D Distribution of Sulphide Minerals in the Merensky Reef (Bushveld Complex, South Africa) and the J-M Reef (Stillwater Complex, USA) and their Relationship to Microstructures Using X-Ray Computed Tomography. *Journal of Petrology* **47**, 1853-1872.

Hanley, J. J., Pettke, T., Mungall, J. E. & Spooner, E. T. C. (2005). The solubility of platinum and gold in NaCl brines at 1.5 kbar, 600 to 800°C: A laser ablation ICP-MS pilot study of synthetic fluid inclusions. *Geochimica Cosmochimica Acta* **69**, 10, 2593-2611.

Harmer, R. E. & Sharpe, M. R. (1985). Field relations and strontium isotope systematic of the marginal rocks of the eastern Bushveld Complex. *Economic Geology* **80**, 813-837.

Hiemstra, S. A. (1979). The role of collectors in the formation of the platinum deposits in the Bushveld Complex. *Canadian Mineralogist 17, Nickel-sulfide and platinum-group-element deposits,* 469-482.

Keays, R. R. & Campbell, I. H. (1981). Precious metals in the Jimberlana Intrusion, Western Australia: Implications for the genesis of platiniferous ores in layered intrusions. *Economic Geology* **76**, 1118-1141.

Kingston, G. A. & El-Dosuky, B. T. (1982). A contribution on the Platinum-Group Mineralogy of the Merensky Reef at the Rustenburg Platinum Mine. *Economic Geology* **77**, 6, 1367-1384.

Kinloch, E. D. (1982). Regional trends in the platinum-group mineralogy of the Critical Zone of the Bushveld Complex, South-Africa. *Economic Geology* **77**, 6, 1328-1347.

Kinloch, E. D. & Peyerl, W. (1990). Platinum-Group minerals in various rock types of the Merensky Reef: Genetic Implications. *Economic Geology* **85**, 537-555.

Kullerud, G., Yund, R. A. & Moh, G. H. (1969). Phase relations in the Cu-Fe-S, Cu-Ni-S and Fe-Ni-S systems. *Economic Geology*, **Monograph no. 4**, 323-343.

Lee, C. A. & Parry, S. J. (1988). Platinum-Group Element geochemistry of the lower and middle group chromitites of the eastern Bushveld Complex. *Economic Geology* **83**, 6, 1127-1139.

Leeb-Du Toit, A. (1986). The Impala Platinum Mines. In: Anhaeusser, C. R. & Maske, S. (ed.) *Mineral Deposits of Southern Africa. Johannesburg:* Geological Society of South africa, I and II, 1901-1106.

Li, C. & Ripley, E. M. (2005). Empirical equations to predict the sulfur content of mafic magmas at sulfide saturation and applications to magmatic sulfide deposits. Mineralium Deposita -46.

Li, C., Ripley, E. M., Merino, E. & Maier, W. D. (2004). Replacement of base metal sulfides by actinolite, epidote, calcite, and magnetite in the UG2 and Merensky Reef of the Bushveld Complex, South Africa. *Economic Geology* **99**, 1, 173-184.

Li, C., Barnes, S.-J., Makovicky, E., Rose-Hansen, J. & Makovicky, M. (1996). Partitioning of Ni, Cu, Ir, Rh, Pt, and Pd between monosulfide solid solution and sulfide liquid: Effects of composition and temperature. *Geochimica Cosmochimica Acta* **60**, 7, 1231-1238.

Lorand, J. P., Alard, O., Luguet, A. & Keays, R. R. (2003). Sulfur and selenium systematics of the subcontinental lithosperic mantle: Inferences from the Massif Central xenolith suite (France). *Geochimica Cosmochimica Acta* **67**, 21, 4137-4151.

Maier, W. D., Barnes, S. J., Gartz, V. & Andrews, G. (2003). Pt-Pd reefs in magnetites of the Stella layered intrusion, South Africa: A world of new exploration opportunities for platinum group elements. *Geology* **31**, 10, 885-888.

Mason, P. R. D. & Kraan, W. J. (2002). Attenuation of spectral interferences during laser ablation inductively coupled plasma mass spectrometry (LA-ICP-MS) using an rf only collision and reaction. *Journal of Analytical Atomic Spectrometry* **17**, 8, 858-867.

Mungall, J. E. (2002) A model for co-precipitation of platinum-group minerals with chromite from silicate melts. *9th International Platinum symposium. Billings, U.S.A.*

Mungall, J. E., Andrews, D. R. A., Cabri, L. J., Sylvester, P. J. & Tubrett, M. (2005). Partitioning of Cu, Ni, Au, and platinum-group elements between monosulfide solid solution and sulfide melt under controlled oxygen and sulfur fugacities. *Geochimica Cosmochimica Acta* **69**, 17, 4349-4360.

Naldrett, A. J. (1989). Magmatic Sulfide Deposits. (ed.) Oxford University Press, 189.

Naldrett, A. J. & Lehmann, J. (1988). Spinel non-stoichiometry as an explanation for Ni-, Cu-, and PGE-enriched sulphides in chromitites. In: Prichard, H. M., Potts, P. J., Bowles, J. F. W. & Cribb, S. J. (ed.) *Geo-Platinum 87*. Amsterdam: Elsevier, 113-143.

Naldrett, A. J., Gasparrini, E. C., Barnes, S. J., Von Gruenewaldt, G. & Sharpe, M. R. (1986). The Upper Critical Zone of the Bushveld Complex and the Origin of Merensky-Type Ores. *Economic Geology* **81**, 5, 1105-1117.

Peregoedova, A., Barnes, S.-J. & Baker, D. R. (2004). The formation of Pt-Ir alloys and Cu-Pd-rich sulfide melts by partial desulfurization of Fe-Ni-Cu sulfides: results of experiments and implications for natural systems. *Chemical Geology* **208**, 1-4, 247-264.

Peregoedova, A., Barnes, S.-J. & Baker, D. R. (2006). An experimental study of mass transfer of platinum-group elements, gold, nickel and copper in sulfur-dominated vapor at magmatic temperatures. *Chemical Geology* **235**, 1-2, 59-75.

Polovina, J. S., Hudson, D. M. & Jones, R. E. (2004). Petrographic and geochemical characteristics of postmagmatic hydrothermal alteration and mineralization in the J-M Reef, Stillwater Complex, Montana. *Canadian Mineralogist* **42**, 261-277.

Prichard, H. M., Barnes, S.-J., Maier, W. D. & Fisher, P. C. (2004). Variations in the nature of the platinum-group minerals in a cross-section through the Merensky Reef at Impala Platinum: Implications for the mode of formation of the reef. *Canadian Mineralogist* **42**, 423-437.

Pruseth, K. L. & Palme, H. (2004). The solubility of Pt in liquid Fe-sulfides. *Chemical Geology* **208**, 1-4, 233-245.

Puchtel, I. S., Humayun, M., Campbell, A. J., Sproule, R. A. & Lesher, C. M. (2004). Platinum group element geochemistry of komatiites from the Alexo and Pyke Hill areas, Ontario, Canada. *Geochimica Cosmochimica Acta* **68**, 6, 1361-1383.

Righter, K., Campbell, A. J., Humayun, M. & Hervig, R. L. (2004). Partitioning of Ru, Rh, Pd, Re, Ir, and Au between Cr-bearing spinel, olivine, pyroxene and silicate melts. Geochimica Cosmochimica Acta **68**, 4, 867-880.

Sattari, P., Brenan, J. M., Horn, I. & McDonough, W. F. (2002). Experimental constraints on the sulfide- and chromite- silicate melt partitioning behavior of rhenium and platinum-group elements. *Economic Geology* **97**, 2, 385-398.

Steele, T. W., Levin, J. & Copelowitz, I. (1975). Preparation and certification of a reference sample of a precious metal ore. National Institute for Metallurgy Report, 1696-1975.

Tredoux, M., Lindsay, N. M., Davies, G. & McDonald, I. (1995). The fractionation of platinum-group elements in magmatic systems, with the suggestion of a novel causal mechanism. *South African Journal of Geology* **98**, 157-167.

Vermaak, C. F. (1976). Merensky Reef - Thoughts on Its Environment and Genesis. *Economic Geology* **71**, 7, 1270-1298.

Vermaak, C. F. & Hendriks, L. P. (1976). Review of Mineralogy of Merensky Reef, with Specific Reference to New Data on Precious Metal Mineralogy. *Economic Geology* **71**, 7, 1244-1269.

Viljoen, M. J. & Hieber, R. (1986). The Rustenburg section of the Rustenburg Platinum Mines Limited, with reference to the Merensky Reef. In: Anhaeusser, C. R. & Maske, S. (ed.)

Mineral Deposits of Southern Africa. Johannesburg: Geological Society of Southern Africa, II, 1107-1034.

Viljoen, M. J., Theron, J., Underwood, B. M., Walters, J. & Peyerl, W. (1986). The Amandelbult section of Rustenburg Platinum Mines Limited, with reference to the Merensky Reef. In: Anhaeusser, C. R. & Maske, S. (ed.) *Mineral Deposits of Southern Africa.* Johannesburg: Geological Society of Southern Africa, II, 1041-1060.

Von Gruenewaldt, G. (1986). Platinum-group element-chromitite associations in the Bushveld Complex. *Economic Geology* **81**, A third issue devoted to platinum deposits, 1067-1079.

Von Gruenewaldt, G. (1989). Contrasting platinum-group element concentration patterns in cumulates of the Bushveld Complex. *Mineralium Deposita* **24**, 3, 219-229.

Willmore, C. C., Boudreau, A. E. & Kruger, F. J. (2000). The halogen geochemistry of the Bushveld Complex, Republic of South Africa: Implications for chalcophile element distribution in the lower and critical zones. *Journal of Petrology* **41**, 10, 1517-1539.

Zientek, M. L., Cooper, R. W., Corson, S. R. & Geraghty, E. P. (2002). Platinum-Group Element Mineralization in the Stillwater Complex, Montana. In: Cabri, L. J. (ed.) *Geology, Geochemistry, Mineralogy and Mineral benefication of Platinum Group Element.* Canadian Institute of Mining, Metallurgy and Petroleum, **Special Volume 54**, 459 - 481.

APPENDIX 3-A1: METHOD OF CALCULATION OF PGM CONTRIBUTION ON THE PGE CONTENT

IMAGE ANALYSIS

BSE images were collected for all the PGM described previously. The first step is to determine the area represented by each PGM. Automated PGM boundaries extraction from BSE images was done using in-house IDL (ITT Visual Information Solutions) code and new 8-bit images of the PGM were created. The scales on the BSE images were used to calculate the real image sizes. These new images of the PGM were then import into ImageJ software (a PC version of NIH image) and were analysed using particle measurement function which calculate many parameter such as the area, the major and minor axis, the orientation and the position of each PGM. The summary of the results are given in Table 3.11 and 3.12. In a second hand, the area represented by each lithology (V_{Litho}) was calculated using high-resolution scans of corresponding thin sections. Mask image of each lithology was created and then analysed using the same method as for the PGM. The proportion of each non-sulphide minerals was also determined by image analysis and the proportions of each sulphide minerals (pyrrhotite, pentlandite and chalcopyrite) used in the further calculation are given in Fig. 3.4. As no information is available on the 3D distribution or size of the PGM, in the further calculation, we made the assumption that the volume represented by each phase or lithology can be approximated by the area calculated on the 2D images. In other words, the thickness considered to calculate a volume from an area is considered to be infinitely small, so that area and volume are almost identical.

EQUATIONS FOR THE CALCULATION

Mass of each lithology

The first step of the calculation is to calculate the mass of each lithology by taking into account: the volume of each lithology, the proportions of each mineral, the volume of PGM and the densities of each phase. All the parameters, their abbreviations, the units and the constant used in the further calculation are summarized in Table 3.A1.

The mass of the non-PGM phase (m_{Oth}) is given by the following equations:

$$m_{Oth} = m_{Px} + m_{Plg} + m_{Chr} + m_{Sul}$$

with

$$V_{Oth} = (V_{Litho} - V_{PGM})$$

$$m_{Px} = V_{Oth} \times X_{Px} \times D_{Px}$$

$$m_{Plg} = V_{Oth} \times X_{Plg} \times D_{Plg}$$

$$m_{Chr} = V_{Oth} \times X_{Chr} \times D_{Chr}$$

$$m_{Sul} = V_{Oth} \times X_{Sul} \times D_{Sul}$$

The mass of the PGM (M_{PGM}) is given by the following equations:

$$m_{PGM} = m_{Braggite} + m_{Cooperite} + m_{Moncheite} + m_{Laurite} + m_{Isoferroplatinum} + m_{Rustenburgite} + m_{Pt}$$

with

$$m_{Braggite} = V_{Braggite} \times D_{Braggite}$$

$$m_{Cooperite} = V_{Cooperite} \times D_{Cooperite}$$

$$m_{Moncheite} = V_{Moncheite} \times D_{Moncheite}$$

$$m_{Laurite} = V_{Laurite} \times D_{Laurite}$$

$$m_{Isoferroplatinum} = V_{Isoferroplatinum} \times D_{Isoferroplatinum}$$

$$m_{Rustenburgite} = V_{Rustenburgite} \times D_{Rustenburgite}$$

$$m_{Pt} = V_{Pt} \times D_{Pt}$$

The total mass of the sample (M_{Sam}) is given by:

$m_{Sam} = m_{PGM} + m_{Oth}$

Calculation of the PGM content

The second step is to calculate the content (in ppm) of each PGM in a mass of sample equal to the mass of sample used for the geochemical analysis (*i.e.* 10 g).

For example, the braggite content ($C_{Braggite}$) is given by the equation:

$C_{Braggite} = (m_{Braggite} \times 10^6) / m_{Sam} \times 10$

The 10^6 corresponds to the conversion from g to μg

The structure of the equation is similar for the others PGM. The results of the calculation are given in Table 3.12.

Calculation of each PGE content

The final step is to calculate the total mass of each PGE due to the PGM using the PGM composition (Table A2) and the PGM content calculated just above.

The Pt content due to PGM (Pt_{Rec}) is given by:

$Pt_{Rec} = C_{Braggite} \times X_{PtBraggite} + C_{Coooperite} \times X_{PtCooperite} + C_{Moncheite} \times X_{PtMoncheite} + C_{Isoferroplatinum} \times X_{PtIsoferroplatinum} + C_{Rustenburgite} \times X_{PtRustenburgite} + C_{Pt} \times X_{PtPt}$

The Pd content due to PGM (Pd_{Rec}) is given by:

$Pd_{Rec} = C_{Braggite} \times X_{PdBraggite} + C_{Cooperite} \times X_{PdCoopertite} + C_{Moncheite} \times X_{PdMoncheite} + C_{Rustenburgite} \times X_{PdRustenburgite}$

The Ru content due to PGM (Ru_{Rec}) is given by:

$Ru_{Rec} = C_{Laurite} \times X_{RuLaurite}$

The Os content due to PGM (Os_{Rec}) is given by:

$Os_{Rec} = C_{Laurite} \times X_{OsLaurite}$

The Ir content due to PGM (Ru_{Rec}) is given by:

$Ru_{Rec} = C_{Laurite} \times X_{IrLaurite}$

The results are summarized in Table 3.12.

Table 3.A1: *Parameter, abbreviation and unit used in the calculation*

Abbreviation	Description	Unit
Px	Pyroxene	
Plg	Plagioclase	
Chr	Chromite	
Po	Pyrrhotite	
Pn	Pentlandite	
Cp	Chalcopyrite	
V_z	Volume of Z	cm^3
X_z	Fraction of the phase Z	
X_{yz}	Fraction of y in z	
D_z	Density of phase Z	g/cm^3
D_{Sul}	Density of sulphides with: $D_{sul} = D_{Po} \times X_{Po} + D_{Pn} \times X_{Pn} + D_{Cp} \times X_{Cp}$	g/cm^3
m_z	Mass of the phase Z with $m_z = D_z \times V_z$	g

Table 3.A2: *Composition of PGM and density of PGM and other minerals used in the calculation*

PGM	Mineral	Density	Pt	Pd	Ru	Ir	Os	Au
		g/cm^3	wt%	wt%	wt%	wt%	wt%	wt%
Pt-Pd-S	Braggite	9.4	66.5	12.4				
PtS	Cooperite	10.1	84	0.6				
Pt-Te	Moncheite	10.2	43	0.2				
Ru-IrOsS	Laurite	6.4			47.2	5.5	6.9	
PtFe	Isoferroplatinum	18.2	91					
Pt-Sn-S	Rustenburgite	18.2	69	12.5				
Pt	Platinum	19.1	100					
	Gold	17.6						100
	Chromite	4.5						
	Pyroxene	3.3						
	Plagioclase	2.7						
	Pentlandite	4.8						
	Pyrrhotite	4.6						
	Chalcopyrite	4.2						

APPENDIX 3-A2: ESTIMATION OF THE SIZE OF THE INCLUSIONS OBSERVED DURING LASER ABLATION

During laser ablation, signals from 30 micro-inclusions enriched in PGE were observed in the base-metal sulphides (BMS) or at the contact between the BMS and the silicates of our samples of the Merensky Reef at Rustenburg Pt Mine. The precise volumes of these inclusions are difficult to calculate as their shapes and orientation relative to laser beam remain unknown. However, one can try to estimate the size (or length) of these inclusions making some assumptions or estimations. Thus, if we considered that these inclusions are cubic, one can estimate the minimal and maximal size of the inclusions using: minimal, maximal and average ablation rates; two different (Fig. A2-1) grains orientations (relative to laser beam); and the laser ablation spectra (time resolved).

ESTIMATION OF ABLATION RATES

As pointed out by Ballhaus and Sylvester (2000), the ablation rate may be calculated using the depths of the ablation pits (in μm) and the duration (in s) of the ablation. Our analyses indicate that the ablation rate varies as a function of the composition of the BMS ablated. Calculation based on 48 measurements gives an ablation rate averaging 2.5 $^{+}/_{-}$ 1 μm/s. Consequently in order to more closely consider this variation and its implications on the calculation of inclusion sizes, we will use in the following three different ablation rates: at 1.5 μm/s; at 2.5 μm/s and at 3.5 μm/s.

GRAIN ORIENTATIONS

Laser ablation allows to access the distribution of element in 3-D and allow to detect inclusions (platinum-group mineral for example). Nevertheless, it remains difficult to infer the orientation or size of the grains and it is impossible to know whether the whole inclusion was ablated. However, by approximating the shape of the inclusions to a cube and by considering that the whole grains are ablated, one can consider two "extreme" cases to calculate minimal and maximal inclusions diameter.

CASE 1:

The laser strikes the grains perpendicular to the crystal faces. Consequently, the distance (in μm) covered by the laser throughout the inclusion (DI) corresponds to the distance AB (Fig. A2-1). This represents the length of the inclusion (LI).

CASE 2:

The laser strikes the grains along the diagonal of the cube. Consequently, DI corresponds to the distance CE (Fig. A2-1) and this represents the diagonal of the cube and is given by the formula:

$$CE^2 = 3 \times (LI)^2$$

where LI is the length of the inclusion.

The length of the inclusion is inferred as follows:

$$LI = [1/3 \times CE^2]^{1/2}$$

The estimation of the distances covered by the laser throughout an inclusion (distance AB and CE) is detailed below.

ESTIMATION OF THE LENGTH OF GRAINS ABLATED

The distance covered by the laser throughout the inclusion (DI) can be calculated using the ablation rates and the time of the inclusion ablation deducted from the laser spectra of the analysis and DI (in μm) given by:

$$DI = AR \times T_{IA}/1000$$

where AR is the ablation rate (in μm/s) and T_{IA} is the time of inclusion ablation (in ms).

The time of the inclusion ablation (T_{IA}) is evaluated by considering the peak observed on the spectra (Fig. A2-2) and is given by:

$$T_{IA} = T_f - T_i$$

where T_f and T_i are the time (in ms) at the end and at the beginning of the inclusion ablation, respectively. These values are accurately obtained with PlasmaLab software.

RESULTS OF INCLUSION SIZE ESTIMATION

The calculations explained above were carried out for the 30 inclusions observed during the laser ablation of the BMS of the Merensky Reef. The results obtained for the different ablation rates and the different cases are summarized in Table A2-1. The length of the inclusions calculated varies from ~ 0.3 to ~12 μm. In order to access whether the size of the inclusions calculated from the laser spectra are realistic and representative of our samples, we compared these results with those obtained from the backscattered images analysis of the platinum-group minerals (described in the manuscript). Both results are in good agreement (Fig. 3.13). The distribution of the size of the 222 platinum-group minerals observed on the backscattered images is similar to that calculated from the average laser ablation data (Table A2-1 and Fig. 3.13). This

implies that the inclusions hit during the laser ablation of the BMS are micron scale in size and are not <100 nm (Ballhaus and Sylvester, 2000).

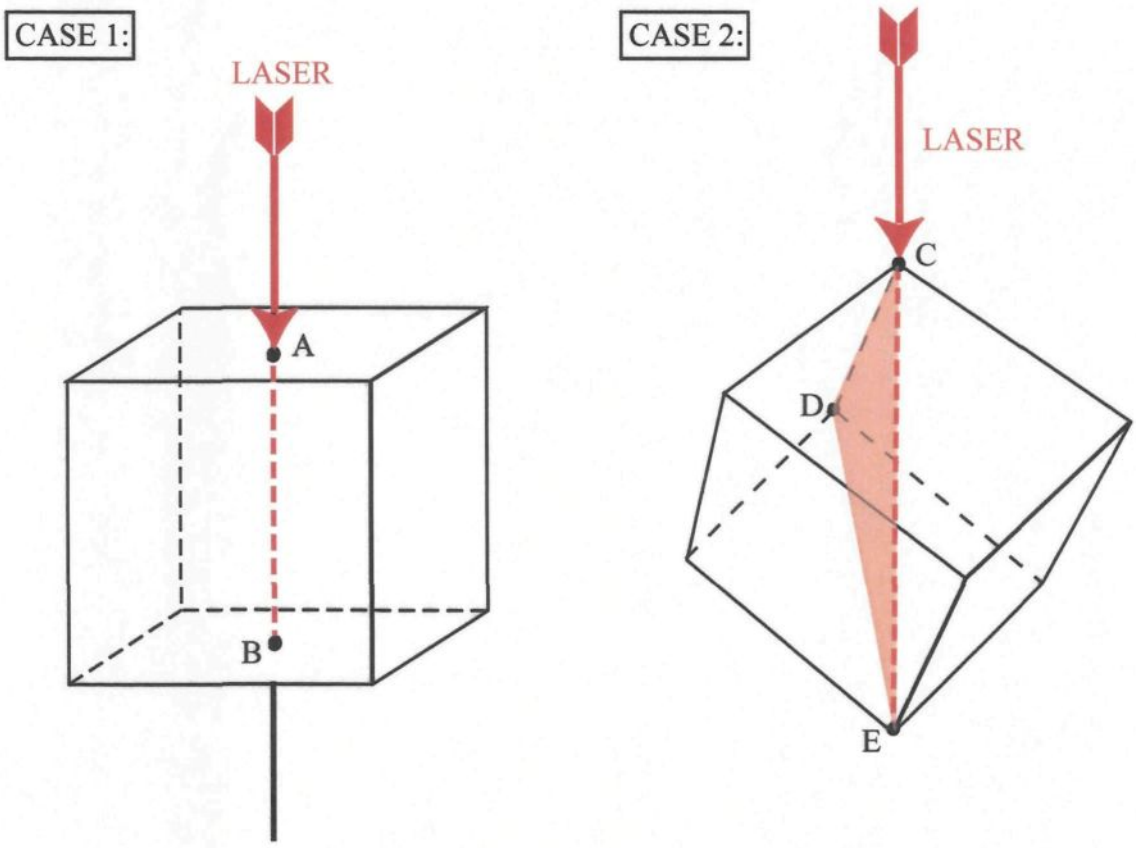

Figure A2-1: Orientation of inclusions (cubic) relative to laser beam

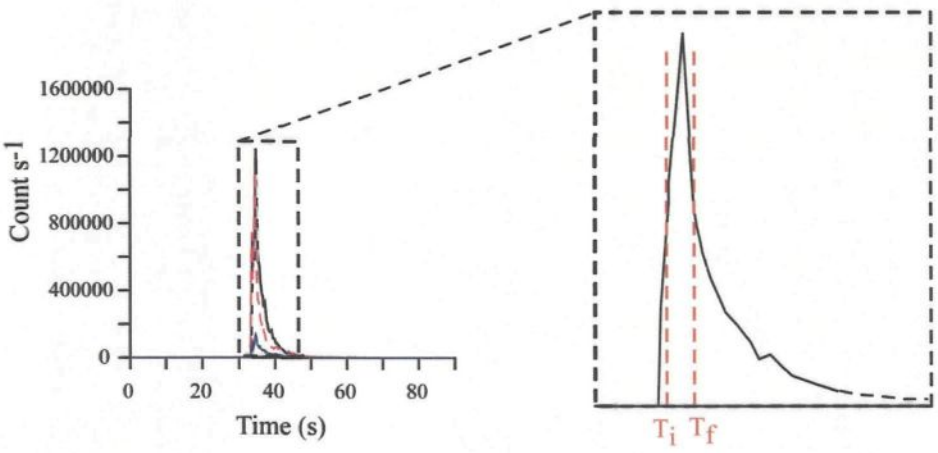

Figure A2-2: Example of calculation of the time of inclusion ablation

***Table A2-1**: Results of the calculation of the length of the inclusions observed during the laser ablation of the base metal sulphides*

				Ablation rate: 1.5 µm/s			Ablation rate: 2.5 µm/s			Ablation rate: 3.5 µm/s			Summary		
					Case 1	Case 2		Case 1	Case 2		Case 1	Case 2	*Length (µm) of inclusion*		
	T_f	T_i	T_{IA}	DI	LI	LI	DI	LI	LI	DI	LI	LI			
Nb	*ms*	*ms*	*ms*	*µm*	*µm*	*µm*	*µm*	*µm*	*µm*	*µm*	*µm*	*µm*	Minimal	Maximal	Average
1	35422	34635	787	1.18	1.18	0.68	1.97	1.97	1.14	2.75	2.75	1.59	0.68	2.75	1.55
2	35029	34329	700	1.05	1.05	0.61	1.75	1.75	1.01	2.45	2.45	1.41	0.61	2.45	1.38
3	42638	41195	1443	2.16	2.16	1.25	3.61	3.61	2.08	5.05	5.05	2.92	1.25	5.05	2.85
4	35885	34635	1250	1.88	1.88	1.08	3.13	3.13	1.80	4.38	4.38	2.53	1.08	4.38	2.46
5	39941	39613	328	0.49	0.49	0.28	0.82	0.82	0.47	1.15	1.15	0.66	0.28	1.15	0.65
6	35291	34766	525	0.79	0.79	0.45	1.31	1.31	0.76	1.84	1.84	1.06	0.45	1.84	1.04
7	67303	66253	1050	1.58	1.58	0.91	2.63	2.63	1.52	3.68	3.68	2.12	0.91	3.68	2.07
8	52740	51034	1706	2.56	2.56	1.48	4.27	4.27	2.46	5.97	5.97	3.45	1.48	5.97	3.36
9	33848	32274	1574	2.36	2.36	1.36	3.94	3.94	2.27	5.51	5.51	3.18	1.36	5.51	3.10
10	39358	38833	525	0.79	0.79	0.45	1.31	1.31	0.76	1.84	1.84	1.06	0.45	1.84	1.04
11	40014	39227	787	1.18	1.18	0.68	1.97	1.97	1.14	2.75	2.75	1.59	0.68	2.75	1.55
12	53265	51428	1837	2.76	2.76	1.59	4.59	4.59	2.65	6.43	6.43	3.71	1.59	6.43	3.62
13	43556	41720	1836	2.75	2.75	1.59	4.59	4.59	2.65	6.43	6.43	3.71	1.59	6.43	3.62
14	34985	34460	525	0.79	0.79	0.45	1.31	1.31	0.76	1.84	1.84	1.06	0.45	1.84	1.04
15	59956	58644	1312	1.97	1.97	1.14	3.28	3.28	1.89	4.59	4.59	2.65	1.14	4.59	2.59
16	56807	54460	2347	3.52	3.52	2.03	5.87	5.87	3.39	8.21	8.21	4.74	2.03	8.21	4.63
17	33192	31618	1574	2.36	2.36	1.36	3.94	3.94	2.27	5.51	5.51	3.18	1.36	5.51	3.10
18	35160	32011	3149	4.72	4.72	2.73	7.87	7.87	4.55	11.02	11.02	6.36	2.73	11.02	6.21
19	50379	48804	1575	2.36	2.36	1.36	3.94	3.94	2.27	5.51	5.51	3.18	1.36	5.51	3.11
20	42769	41457	1312	1.97	1.97	1.14	3.28	3.28	1.89	4.59	4.59	2.65	1.14	4.59	2.59
21	32142	30699	1443	2.16	2.16	1.25	3.61	3.61	2.08	5.05	5.05	2.92	1.25	5.05	2.85
22	34897	33586	1311	1.97	1.97	1.14	3.28	3.28	1.89	4.59	4.59	2.65	1.14	4.59	2.58
23	35816	33848	1968	2.95	2.95	1.70	4.92	4.92	2.84	6.89	6.89	3.98	1.70	6.89	3.88
24	55364	54664	700	1.05	1.05	0.61	1.75	1.75	1.01	2.45	2.45	1.41	0.61	2.45	1.38
25	45787	43425	2362	3.54	3.54	2.05	5.91	5.91	3.41	8.27	8.27	4.77	2.05	8.27	4.66
26	37244	36807	437	0.66	0.66	0.38	1.09	1.09	0.63	1.53	1.53	0.88	0.38	1.53	0.86
27	38702	37645	1057	1.59	1.59	0.92	2.64	2.64	1.53	3.70	3.70	2.14	0.92	3.70	2.08
28	46501	45699	802	1.20	1.20	0.69	2.01	2.01	1.16	2.81	2.81	1.62	0.69	2.81	1.58
29	46705	43294	3411	5.12	5.12	2.95	8.53	8.53	4.92	11.94	11.94	6.89	2.95	11.94	6.73
30	63498	61530	1968	2.95	2.95	1.70	4.92	4.92	2.84	6.89	6.89	3.98	1.70	6.89	3.88

CHAPITRE 4

PLATINUM-GROUP ELEMENTS IN SULFIDE MINERALS AND THE WHOLE ROCKS OF THE J-M REEF (STILLWATER COMPLEX): IMPLICATIONS FOR THE FORMATION OF THE REEF

BELINDA GODEL and SARAH-JANE BARNES

UNIVERSITE DU QUEBEC A CHICOUTIMI, SCIENCES DE LA TERRE, CHICOUTIMI, G7H 2B1, CANADA

Chemical Geology
DOI:10.1016/j.chemgeo.2007.05.006

4.1. – RESUMÉ

La concentration des éléments du groupe du platine (PGE) ainsi que Ni, Cu, Co, Re, Au et Ag a été déterminée dans les sulfures enrichis en métaux de base (BMS : pyrrhotite, pentlandite, chalcopyrite) et les échantillons d'une section du J-M Reef (Complexe de Stillwater, E.U.).

Le but de l'étude est d'établir : (i) si les sulfures enrichis en métaux de base (pyrrhotite, pentlandite et chalcopyrite) sont les hôtes principaux de ces éléments ; (ii) si ces éléments se concentrent préferentiellement dans les BMS ; (iii) si la concentration de ces éléments varie en fonction de la lithologie et/ou de l'altération.

Les résultats de ces analyses permettront d'évaluer : (1) la composition d'un magma parent pour le J-M reef ; (2) le rôle d'un liquide sulfuré immiscible sur la collection des PGE et (3) le rôle de l'altération sur la formation des minéralisations du J-M Reef.

Les roches du mur et du toit du J-M Reef contiennent très peu de PGE (~10 à 140 ppb) ainsi que très peu de soufre (~140 à 400 ppm). Au contraire, les roches enrichies en sulfures (i.e. le J-M Reef) contiennent des teneurs élevées en PGE (entre 49 et 419 ppm). Les teneurs en S, Ni, Cu et PGE suivent la même tendance. Cela reflète problablement le fait que les BMS sont les principales phases qui contrôlent ces éléments. Le palladium et le platine sont les PGE les plus abondants (teneurs atteignant 244 ppm pour Pd et 166 ppm pour Pt). Les spectres normalisés au manteau, les rapports Pd/Pt et les rapports Pd/Ir indiquent que le palladium des roches est fortement enrichi par rapport au platine ainsi que par rapport aux autres PGE. La pentlandite est le sulfure qui contient la plus grande quantité de PGE en solution solide. Le palladium représente ~95% des PGE trouvés en

solution dans les sulfures et est principalement contenu dans la pentlandite. Au contraire, le platine ne ce concentre pas dans les sulfures, il se retrouve uniquement sous la forme de minéraux du groupe du platine. Les autres PGE sont en grande partie contenu dans les sulfures (principalement la pentlandite).

La variation du rapport S/Se et la présence de magnétite secondaire observée dans certains échantillons indiquent que ces échantillons ont perdu 20 à 50 % de leur contenu originel en soufre. Les teneurs les plus élevées en Pd (et par analogie les teneurs en PGE) se retrouvent dans les échantillons qui contiennent de la magnétite secondaire. Ces échantillons ne sont pas nécessairement ceux qui ont subi la plus grande perte de soufre. Par conséquent, cela indique probablement que le processus qui a engendré la perte de soufre est différent de celui qui a engendré la formation de magnétite secondaire.

Les résultats des modélisations suggèrent que l'enrichissement en PGE observés dans le J-M Reef peut être résumé en trois étapes différentes et successives :

(a) un liquide sulfuré immmiscible intéragit avec une grande quantité de magma silicaté (ayant une composition en PGE similaire à celles des basaltes enrichis en Mg) et collecte les PGE. Ce liquide sulfuré enrichi en PGE percole vers le bas dans la pile de cumulats et s'arrête là ou la perméabilité est trop faible pour qu'il puisse continuer à migrer.

(b) Pendant le refroissement de l'intrusion, des instabilités dans la chambre magmatique provoquent une désulfurisation partielle des sulfures et un enrichissement de ces derniers en PGE.

(c) Finalement, dans certaines parties de la zone minéralisée, un fluide enrichi en Pd (Pd certainement lessivé des cumulats sous-jacents) dépose Pd et altère partiellement les sulfures en magnétite. Le palladium précipite sous forme d'alliage et diffuse également dans la pentlandite formant ainsi des pentlandites très riches en Pd.

La variabilité des teneurs en PGE observées dans le J-M Reef pourrait ainsi être expliquées par des contributions plus ou moins importantes de ces différents processus.

4.2. - ABSTRACT

The concentration of platinum-group elements (PGE), Co, Ni, Cu, Re, Au and Ag were determined in base metal sulfides (BMS) minerals and whole rocks of the J-M Reef (footwall, reef and hanging wall) of the Stillwater Complex (U.S.A.). The aims of the study were to establish: (i) whether the BMS minerals (pyrrhotite, pentlandite, and chalcopyrite) are the principal host of these elements; (ii) whether these elements preferentially partition into a specific BMS mineral. The results of this study allowed us to consider and evaluate the possible parental magma composition, the role of sulfide liquid and the role of alteration in the formation of the J-M Reef.

Only a minor quantity of PGE (~10 to 140 ppb) were found in the footwall and hanging wall samples of the J-M Reef, which contain only small amounts of sulfur (~140 to 400 ppm). In contrast, the reef samples enriched in sulfides contain higher values of PGE (49 to 419 ppm). The S, Ni, Cu, and PGE contents follow the same trends indicating that

BMS minerals are the principal phases controlling these elements. Palladium and Pt are the most abundant PGE (up to 244 ppm for Pd and 166 ppm for Pt) with an average Pd/Pt ratio of 3.3. Similarly, the Pd/Ir ratio and the mantle normalized PGE patterns indicate that Pd is more strongly enriched in the reef relative to surrounding rocks than the other PGE.

Pentlandite is the BMS mineral that contains the largest weight fraction of PGE. Palladium represents ~95% of the PGE found in solution in BMS minerals and is mainly partitioned in pentlandite. In contrast, Pt is almost exclusively found as platinum-group minerals and appear not to have partitioned into any BMS minerals. The other PGE are largely found in the BMS minerals, mainly pentlandite.

The variation of S/Se ratios and the presence of secondary magnetite in some samples indicate that these samples may have lost 20 to 50% of their original S. The highest Pd (and by analogy PGE contents) are found in samples containing secondary magnetite, but these are not necessarily those which have experienced the highest S removal. This indicates that the processes which caused the removal of S and the alteration to magnetite are probably distinct.

Our modeling results suggest that PGE (and to a greater extent Pd) enrichment may be summarized into two different steps. First, an immiscible sulfide liquid interacted with a large volume of magma with PGE composition close to high Mg basalt and collected the PGE. The sulfide liquid percolated down through the crystal mush to collect at a level where the porosity did not permit any further migration. During cooling, magma chamber instabilities triggered the partial desulfurization of the sulfides and the enrichments of the remaining sulfides in PGE. Finally, in some parts of reef, a fluid deposited Pd (possibly

removed from the footwall) and altered the BMS minerals to magnetite. During this step, Pd was precipitated as an alloy in the most Pd-enriched samples and Pd possibly diffused into pentlandite forming a high Pd-bearing pentlandite. The different contributions of each of the above processes may explain the variability of the Pd grade observed along the J-M Reef.

4.3. - INTRODUCTION

The Stillwater Complex (Montana, U.S.A.) is a layered ultramafic to mafic intrusion, which contains several PGE-rich layers. One of these layers, the J-M Reef has the highest Pt+Pd grade (~18 ppm) of all known PGE reefs (Zientek *et al.*, 2002). The J-M Reef is altered and has been affected by several hydrothermal events, which could have remobilized the base metal sulfide (BMS) minerals and modified the platinum-group element (PGE: Pt, Pd, Ir, Os, Ru, and Rh) content of the reef (Bow *et al.*, 1982; Boudreau and McCallum, 1992a; Czamanske and Loferski, 1996; Polovina *et al.*, 2004).

Several processes are proposed to explain the enrichment of the PGE and the other siderophile elements in the cumulate portions of layered intrusions. One school of thought (Campbell *et al.*, 1983, Naldett *et al.*, 1986) suggests that PGE are collected by an immiscible sulfide liquid that segregated from the magma. These sulfides enriched in PGE and base metals can then be connected and percolated downward in the cumulate pile along vertical dilatancies that form during the compaction of the cumulate pile (Barnes and Maier, 2002; Godel *et al.*, 2006). The percolation of the sulfide liquid is stopped as it reaches a layer with a permeability which is too low to allow it to further migrate (Godel *et*

al., 2006). Other authors proposed that the PGE are collected by magmatic fluids enriched in Cl (Boudreau and McCallum, 1992; Willmore *et al.*, 2000). In this case, the authors proposed that BMS minerals are (partially or completely) dissolved by magmatic fluid (collecting base metal and PGE) which percolated upwards in the cumulate pile and the fluid-saturated-intercumulus liquid. When the Cl-rich fluid encountered a layer undersaturated in fluid, the BMS minerals and the PGE precipitate forming a layer enriched in PGE-rich sulfides. In addition, the cumulate and the BMS minerals could also undergo a subsequent low temperature alteration which may modified the PGE distribution (Li *et al.*, 2004; Polovina *et al.*, 2004).

In many cases, the PGE in reefs are found associated with BMS minerals and in PGM that are associated with the sulfides (Kinloch, 1982; Barnes and Naldrett, 1985; Zientek *et al.*, 2002; Prichard *et al.*, 2004). Previous authors (Cabri *et al.*, 1984; Polovina *et al.*, 2004; Li and Ripley, 2006) reported high Pd concentration in pentlandites from the J-M Reef of the Stillwater Complex. These microprobe analysis showed that pentlandites may contain ~ 1870 to ~98 000 ppm Pd (Cabri *et al.*, 1984; Zientek and Oscarson, 1986; Polovina *et al.*, 2004; Li and Ripley, 2006). In a recent work, Polovina *et al.* (2004) characterized the postmagmatic alteration for borehole samples from the J-M Reef and discussed its possible implications on the PGE mineralization. The authors concluded that the highest Pd contents in pentlandite (up to ~7800 ppm in their samples) are found in the least altered samples and that Pt and Pd may have been leached out of altered pentlandite by low-temperature (~250-300°C) hydrothermal fluids. No data are available for the other PGE (Ir, Os, Ru and Rh).

In the current work we have attempted to establish which minerals host the PGE in order to consider and evaluate: (i) the possible parental magma composition; (ii) the role of sulfide liquid and (iii) the role of alteration in the formation of the J-M Reef. The aim of this study is to determine the concentration of PGE, Re, Ag, Au, Cd, Co, and Zn in the BMS minerals (pentlandite, pyrrhotite, and chalcopyrite) and in the whole rocks of the J-M Reef in order to establish: (i) whether these sulfides are the principal host of these elements, and (ii) whether these elements preferentially partition into a specific BMS minerals.

4.4. - GEOLOGICAL SETTINGS

The Stillwater Complex is a layered ultramafic to mafic intrusion (Fig. 4.1a and b) which is located in the southwestern Montana. The complex is 2705+/- 4 Ma old (U-Pb age, Premo *et al.*, 1990) and has intruded middle to late Archean metasedimentary rocks. The original size of the complex is unknown as only a part (~42 km in length and ~6 km in thickness) of the complex is exposed along the Beartooth uplift (Page and Zientek, 1985). The layered rocks of the complex are divided into five series, from bottom to top (Fig. 4.1b): the Basal series consists of norites and bronzitites which contain minor amount of BMS minerals; the Ultramafic series is formed essentially of harzburgite and bronzitite, with minor chromite seems; the Lower, Middle, and Upper Banded series contain mainly norite, gabbronorite, olivine gabbronorite, and anorthosite (McCallum *et al.*, 1980; Page and Zientek, 1985; Zientek *et al.*, 1985; Barnes and Naldrett, 1986; Zientek et al., 2002). The Stillwater Complex is the host of several layers enriched in PGE, amongst them the John Manville Reef (J-M Reef) and the Picket Pin deposit (Fig. 4.1). The samples studied

in this work are from the J-M Reef package. The J-M Reef is a PGE-enriched layer with disseminated base-metal sulfide minerals in the Lower Banded series. In most cases, the mineralization is found in the olivine gabbronorite containing disseminated sulfides known as the Olivine-bearing cumulate zone I (OB-1) (Turner *et al.*, 1985; Zientek *et al.*, 1985; Barnes and Naldrett, 1986; Zientek *et al.*, 2002). The complex has been affected by several metamorphic and /or hydrothermal processes which have triggered alteration of the silicate and BMS minerals (Page, 1976; Czamanske and Lferski, 1996; Polovina et al., 2004). The alteration commonly observed in the Stillwater complex may notably be related to: (i) the initial crystallisation or cooling of the complex; (ii) the intrusion of quartz monzonite near the base of the complex (Nunes and Tilton, 1971); (iii) the intrusion of mafic dikes and sills that crosscut the complex (Czamanske and Zientek, 1985); (iv) the greenschist facies metamorphism at 1.7 to 1.6 Ga (Nunes and Tilton, 1971; Page, 1977).

4.5. - PETROGRAPHY

Twelve samples from across the J-M Reef "package" (footwall, reef, and hanging wall) from the East Boulder Mine were studied. Two reef samples (ST16 and ST17) are from underground level 2400N 65W+0E. The remaining samples are from drill cores that cross the reef (in the same area). Because the samples are from different boreholes the exact distance between samples is unknown and only their relative position is given on the stratigraphic section.

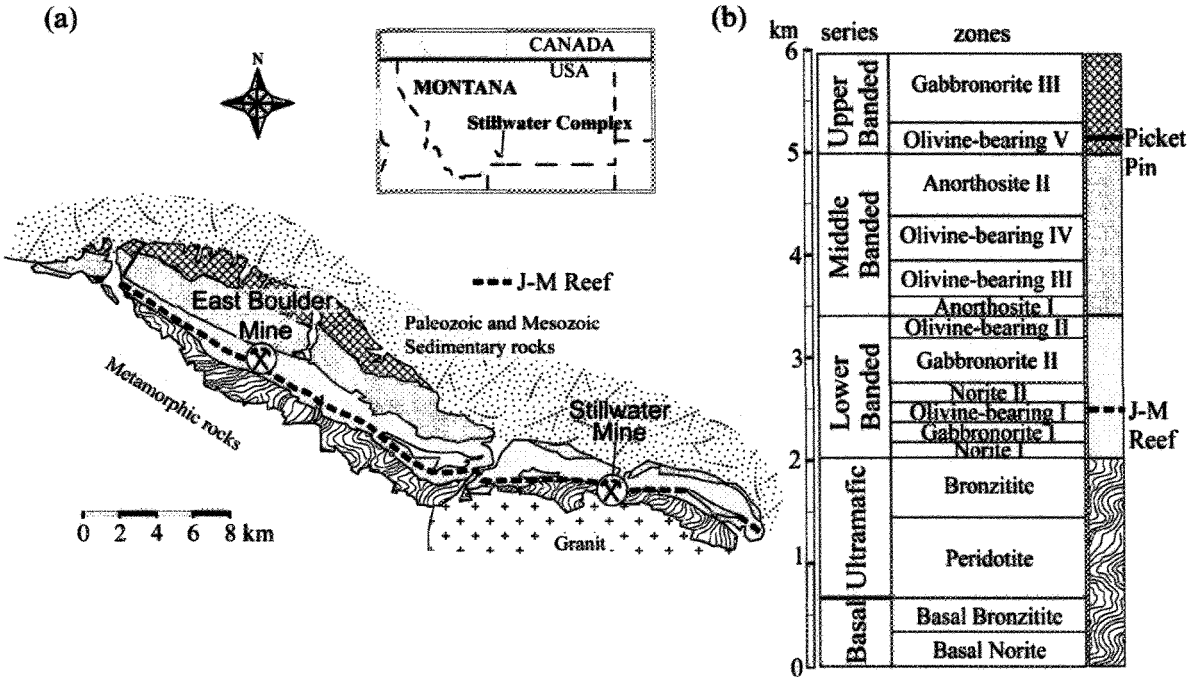

Figure 4.1: Geology and stratigraphy of the Stillwater Complex, Montana, U.S.A.

(a) Simplified geological map of the Stillwater Complex (modified after McCallum *et al.*, 1980; Zientek *et al.*, 2002).
(b) Stratigraphy of the Stillwater Complex (modified after Zientek *et al.*, 2002).

The J-M Reef footwall samples consist of anorthosite (ST04), melanorite (ST05), and leuconorite (ST06 and ST07). The anorthosite (ST04) contains ~95 modal% plagioclase and 5 modal % orthopyroxene. All mineral percentages below reported as modal values. Plagioclase occurs as randomly orientated euhedral and lobate grains of ~0.5 to 3 mm in diameter. Orthopyroxene is interstitial to plagioclase. Alteration minerals (tremolite-actinolite) occur locally at plagioclase or plagioclase-orthopyroxene grain boundaries. A few veinlets filled with calcite crosscut the sample. No BMS minerals are present in the sample.

The melanorite (ST05) consists of ~70 % euhedral orthopyroxene, ~28 % plagioclase, and ~2 % of clinopyroxene. Cumulus orthopyroxene occurs as euhedral grains ~ 1 mm to 7 mm in diameter. Clinopyroxene exsolutions with a spindle shape occur along cleavage planes in almost all the orthopyroxene grains. Plagioclase occurs as an intercumulus phase between orthopyroxene grains. Several high-temperature deformation features (deformation twins in plagioclase and indented-contacts in orthopyroxene) are observed. No BMS minerals were found in the sample.

The leuconorite (ST06) is composed of ~85 % subhedral to lobate plagioclase, ~ 13 % interstitial orthopyroxene, and ~2 % of interstitial clinopyroxene. No BMS were observed on the sections.

The leuconorite (ST07) is composed of ~85 % euhedral to lobate plagioclase, ~15 % pyroxene and, ~5 % olivine. The sample contains only minor amounts of small BMS minerals (mainly chalcopyrite) which are usually associated with alteration minerals (chlorite and epidote) of plagioclase and few tiny grains of secondary magnetite.

The reef samples are melatroctolites (ST08, ST12), anorthosite (ST14), leuconorite (ST16), and olivine melagabbronorite (ST17).

The troctolite ST08 contain ~70 % highly serpentinized olivine, and ~30 % of strongly altered interstitial plagioclase. The alteration silicates consist of chlorite, actinolite, serpentine and to a lesser extent talc. In addition, secondary magnetite occurs as small grains which crosscut all the primary silicate minerals and define a foliation. This foliation may be related to one of the deformation events that affected the Stillwater Complex.

The troctolite ST12 is also highly altered and serpentinized. The sample is composed of ~60 % olivine, ~30 % plagioclase, ~6 % clinopyroxene, ~2 % interstitial BMS minerals, and ~2 % chromite. The BMS minerals occur as vertical networks extending 1 or 2 cm along silicate grain boundaries. The BMS minerals are composed of intergrowths of pyrrhotite and pentlandite in many cases surrounded by chalcopyrite (Fig. 4.2a). Secondary magnetite commonly replaces the BMS minerals where they are in contact with silicate minerals, forming a halo of magnetite with secondary chalcopyrite associated with the alteration minerals (mainly chlorite, actinolite and tremolite) (Fig. 4.2b). Secondary magnetite defines a foliation which crosscuts the primary silicate and the BMS minerals.

The sample ST14 is an anorthosite at its base containing ~95 % euhedral plagioclase, ~3 % interstitial pyroxene, and ~2 % BMS minerals. The sample grades into norite containing ~58 % pyroxene and ~40 % plagioclase and ~2 % BMS minerals. The BMS minerals occur as disseminated grains closely associated with alteration minerals (tremolite and actinolite) (Fig. 4.2c).

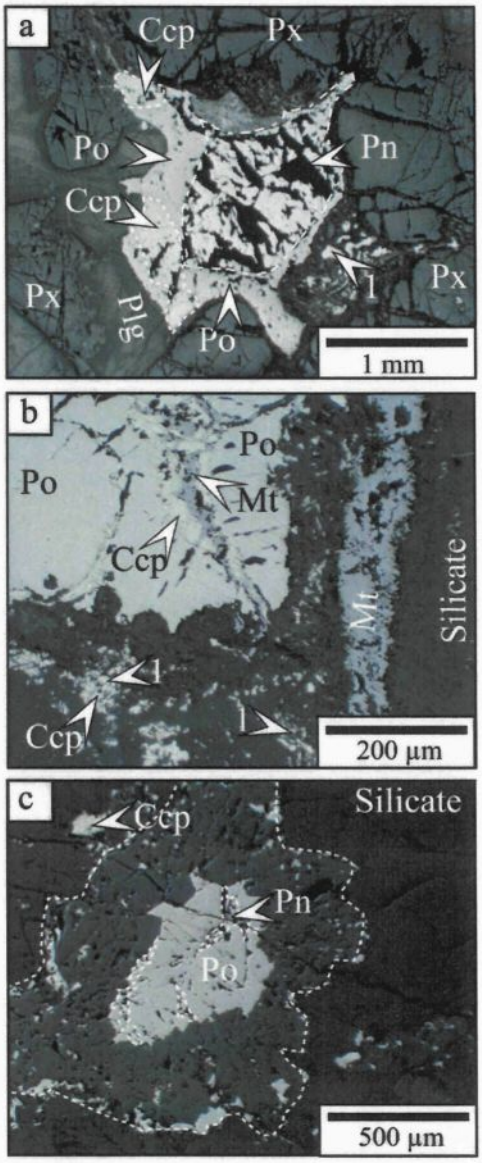

Figure 4.2: Base-metal sulfide minerals in the studied samples of the J-M Reef.

(a) Intergrowth of pyrrhotite, pentlandite and chalcopyrite surrounded by silicate minerals (Px and Plg). Some of the chalcopyrite is found associated with alteration minerals (1).
(b) Magmatic pyrrhotite associated with secondary magnetite and chalcopyrite. The magmatic sulfides are replaced by alteration minerals (1) which are associated with secondary chalcopyrite.
(c) Intergrowth of magmatic pentlandite and pyrrhotite which are partially replaced by alteration minerals (area inside dashed line).
Po: pyrrhotite; Pn: pentlandite; Ccp: chalcopyrite; Mt: magnetite; Px: pyroxene; Plg: plagioclase

The leucogabbronorite (ST16) contains ~70 % subhedral plagioclase, ~25 % interstitial clinopyroxene, and ~5 % BMS minerals. The BMS minerals occur as vertical networks along silicate grain boundaries. Alteration minerals (chlorite-tremolite-actinote) are present at the contact between silicate and BMS minerals.

The ST17 sample is an olivine melagabbronorite composed of ~ 45 % pyroxene, ~ 40 % olivine, ~ 7 % plagioclase and ~ 5 % BMS minerals. All silicate phases have undergone extensive alteration (serpentinization). The BMS minerals occur as patches ~1 cm located between the silicate grains. They are composed of intergrowth of pyrrhotite, pentlandite, and chalcopyrite. The BMS minerals located at the contact with the silicate are altered to secondary magnetite. Secondary chalcopyrite is also found associated with alteration silicates which are located as halos mainly around pyroxenes and olivine (similar to Fig. 7c in Godel *et al.*, 2006).

The J-M Reef hanging wall samples consist of leuconorite (ST10) and olivine melagabbronorite (ST11 and ST13). The leuconorite (ST10) consists of ~90 % plagioclase and ~10 % pyroxene. Dihedral angles between plagioclase are ~120 degrees which implies that extensive recrystallization of plagioclase has occurred. Pyroxene consists of small disseminated "patches" (~5 mm x ~5 mm) located between plagioclase grains and are usually surrounded by alteration minerals and secondary magnetite. Only tiny (<50 μm) secondary BMS minerals (essentially chalcopyrite) were observed and these are present along orthopyroxene cleavage planes.

The olivine melagabbro ST11 is extensively altered and is composed of ~62 % serpentinized olivine, ~12 % altered clinopyroxene, and ~16 % altered plagioclase. The

olivine mela-gabbronorite ST13 is also strongly altered and is composed of ~47 % olivine, ~31 % pyroxene, and ~22 % plagioclase. In both case (ST11 and ST13), the silicates are almost entirely replaced by serpentine, talc, and calcite. Secondary magnetite defines a foliation which crosscut the silicate phases and, in some cases are associated with calcite. No BMS minerals are observed.

4.6. - METHODOLOGY

4.6.1. - Whole rock analysis

The twelve samples were analysed for PGE, Ni, Cu, S and Se. The samples were crushed in an Al-ceramic mill at the University of Quebec at Chicoutimi (UQAC). All analyses were carried out at UQAC. Results for the international reference materials are shown in Table 4.1. Copper was determined by atomic absorption spectrometry (AA) after aqua regia digestion. Nickel, Co, and others trace elements were determined by instrumental neutron activation on ~3 g of sample using the method of Bédard and Barnes (2002). Sulfur was determined using an HORIBA EMIA-220V series C and S analyser. The PGE and Au in the rocks were determined by Ni-sulfide fire assay followed by instrumental neutronic activation analysis (INAA) on 15 g of sample using a slightly modified version of the Steele *et al.* (1975) formula (Bédard and Barnes, 2002).

Table 4.1: *Values obtained for the standard used for the whole rock PGE analysis.*

Name	Laboratory		Pt ppb	Pd ppb	Rh ppb	Ru ppb	Ir ppb	Os ppb	Re ppb	Au ppb	Ni ppm	Co ppm	Cu* ppm	S wt%	Se ppm
AMIS0007	African Mineral Standarts		2480	1500	250	450	90	n-d	n-d	155	2072	335	1296	-	-
		SD	280	200	40	60	n-d			16	208	65	150	-	-
AMIS0007	UQAC, INAA or AA		2633	1457	265	421	91.7	68	2.3	156	1774	315	1196	-	-
		SD	45	64	2	24	0.3	7	2.1	6	96	9	34	-	-
KPT-1	GeoPT18		-	-	-	-	-	-	-	-	-	-	-	1.1	2.93
		SD	-	-	-	-	-	-	-	-	-	-	-	0.03	n-d
KPT-1	UQAC		-	-	-	-	-	-	-	-	-	-	-	1.06	2.68
		SD	-	-	-	-	-	-	-	-	-	-	-	0.12	0.24

*Aqua regia partial digestion.

SD : Standard deviation.

n-d: not determined.

4.6.2. - In situ analysis of the base-metal sulfide minerals

Only four of the reef samples (ST12, ST14, ST16, and ST17) contain visible BMS minerals (pyrrhotite, pentlandite, and chalcopyrite). Polished sections or polished thin sections (100 μm thick) were prepared and examined with a petrographic microscope to select sites for analysis. Major element composition of the sulfides (S, Fe, Ni, Cu) was determined by electron microprobe at Laval University, Quebec City (Table 4.2). Platinum-group elements, Re, Au, Ag, Cd, Ni, Cu, and Co concentrations in BMS minerals were determined by laser ablation inductively coupled mass-spectrometry (LA-ICP-MS). The UQAC laser-ablation ICP-MS consists of a Thermo X7 ICP-MS with high-performance interface coupled with a New Wave Research 213 nm Nd:YAG UV laser ablation microprobe. The analyses were conducted using 80 μm diameter spot and a laser frequency of 20 Hz. The ablated material was carried using hydrogen gas and then analysed using the Thermo X7 ICP-MS operating in time resolved mode using peak jumping and a dwell time of 10 ms/peak. The instrument was operated using a collision cell which reduces much of the argide interferences on the PGE (Mason and Kraan, 2002) and was tuned to minimize them. In addition, Ni_3S_2 and $CuFeS_2$ blanks were used to monitor Ni interferences on Ru, and some Cu interferences on Rh and Pd. On the basis of the blank results, 1 ppm Ru, 0.5 ppm Rh, and 0.5 ppm Pd was subtracted from all the chalcopyrite results and 3 ppm Ru was subtracted from all the pentlandite results. ^{34}S was used as internal standard to determine concentrations of PGE and other metals.

Table 4.2: *Major element concentrations in the BMS of the Stillwater Complex samples.*

Section	Mineral	n	S	Fe	Cu	Ni	Co	Total
			wt%	wt%	wt%	wt%	wt%	wt%
ST12a*	Pentlandite	8	32.77	36.26	<0.1	27.31	1.17	97.52
	Pyrrhotite	4	38.13	61.51	0.04	0.04	<0.1	99.72
	Chalcopyrite	3	34.56	34.11	29.31	0.01	0.08	98.07
ST12b*	Pentlandite	7	32.55	35.98	<0.1	27.19	1.24	96.96
	Pyrrhotite	4	38.33	61.40	<0.1	0.01	0.11	99.85
	Chalcopyrite	1	34.35	30.64	32.53	0.14	<0.1	97.65
ST14a**	Pentlandite	5	32.76	30.25	<0.1	34.93	0.75	98.68
	Pyrrhotite	5	39.27	59.54	<0.1	0.67	<0.1	99.48
	Chalcopyrite	2	34.44	30.55	32.75	0.05	<0.1	97.79
ST14b**	Pentlandite	6	32.46	31.57	<0.1	33.02	0.65	97.71
	Pyrrhotite	6	38.95	59.60	0.03	0.37	0.11	99.05
	Chalcopyrite	2	34.12	30.62	32.72	0.03	<0.1	97.48
ST16	Pentlandite	3	31.80	31.45	<0.1	33.30	0.48	97.03
	Pyrrhotite	4	38.23	59.39	0.04	0.57	0.03	98.27
	Chalcopyrite	2	33.63	30.03	32.72	0.03	<0.1	96.40
ST17	Pentlandite	3	31.69	37.47	0.32	27.25	0.50	97.24
	Pyrrhotite	6	35.27	63.42	<0.1	0.03	0.10	98.82
	Chalcopyrite	2	33.85	35.98	27.31	0.04	0.17	97.35

* Two sections (ST12a and ST12b) were cut for the sample ST12.

** Two sections (ST14a and ST14b) were cut for the sample ST14.

The reduction of all the data was carried out using PlasmaLab software (ThermoElemental) by subtracting gas background from each of the analysed isotopes. The calibration of the ICP-MS was carried out using the reference material Laflamme Po727 supplied by CANMET. The "Laflamme" reference material is a synthetic FeS which contains ~ 45 ppm PGE and Au (Table 4.3). To check the homogeneity of this material and the stability of the LA-ICP-MS, Po727 was run twice after each batch of approximately 15 analyses, once as calibration and once as unknown. The average of Po727 run as an unknown and the standard deviation is shown in Table 4.3 and indicates that the relative standard deviation for the PGE and Au is ~4%. To check the accuracy of the calibration Po62 an in-house synthetic FeS doped with ~2 ppm PGE, Au and Re was used. The description of Po62 synthesis is identical to those of Barnes *et al.* (2006). The results as determined by laser ablation for this sample are similar to those obtained by isotope dilution (Table 4.3). Nickel and Cu were calibrated using the semi-quantification option of PlasmaLab software. This appear to work well for Re as the results estimated for Po62 are similar to the results obtained by isotope dilution on this material (Table 4.3). We have no independent check of the Ag and Cd values. As a further check on our analyses we would point out that our results for Pd, Ru and Rh compare well with results from other analytical methods such as proton microprobe (Cabri *et al.,* 1984), trace electron probe and micro-PIXE (Gervilla et al., 2004) and electron microprobe (Li and Ripley, 2006).

Table 4.3: *Estimates of precision and accuracy for the LA-ICP-MS analysis.*

Standard	Laboratory	Method	n	^{101}Ru ppm	^{103}Rh ppm	^{105}Pd ppm	^{108}Pd ppm	^{192}Os ppm	^{193}Ir ppm	^{195}Pt ppm	^{197}Au ppm	^{185}Re ppm
LaFlamme	CANMET		43	36.5	41.6	43.5	43.5	46.7	48	35.5	45.8	-
Po727			SD	0.3	0.3	0.3	0.3	2.6	1.2	0.8	2.4	-
LaFlamme	UQAC	LA-ICP-MS	12	36.45	41.49	43.36	43.37	46.73	48.01	35.57	45.84	-
Po727			SD	1.46	1.71	1.64	1.64	1.98	1.92	1.36	1.92	-
Po-62	Loeben	Isotope dilution	4	1.43	1.7	1.6	1.57	1.59	1.53	1.64	n-d	-
				0.05	0.1	0.13	0.13	0.27	0.04	0.13		
Po-62	UQAC	LA-ICP-MS	6	2.53	1.54	1.82	1.6	1.86	1.75	1.7	1.95	-
			SD	1.09	0.66	0.76	0.76	0.89	0.73	0.49	1.14	-
MSS-1	Loeben	Isotope dilution		1.75	n-d	1.26	1.26	1.9	1.37	1.66	n-d	0.09
			SD	0.026		0.015	0.015	0.007	0.011	0.013		0.003
MSS-1	UQAC	LA-ICP-MS	3	2.88	0.98	1.37	1.82	1.77	1.55	1.61	1.50	0.099
			SD	0.39	0.15	0.45	0.68	0.58	0.46	0.22	0.82	0.020

n: number of analysis.
n-d: not determined.
SD: standard deviation.

4.7. - PGE AND OTHER METALS IN THE WHOLE ROCKS

The rocks of the footwall and hanging wall of the J-M Reef contain only minor PGE (~10 to 140 ppb, Table 4.4). Only four rocks (ST12, ST14, ST16, and ST17) contain significant values (49 to 419 ppm) of PGE (Table 4.4). Palladium and Pt are the major PGE found in these rocks and represents ~ 60 to ~83 % and ~23 to ~40 % of the total PGE content, respectively.

In the whole rock, the Ni, Cu, and PGE contents follow the same trend as S content (Fig. 4.3 and Table 4.4) indicating that BMS minerals are the principal phases controlling these elements. In the footwall of the J-M Reef, the rocks contain only a small amount of sulfur (140 to 400 ppm). The Pt, Pd, Ir, and Rh contents (Fig. 4.3 and Table 4.4) decrease slightly from bottom to top (reaching a minimal value in the unmineralized reef sample). The mineralized samples contain 0.26 to 1 wt% of S and 37 to 248 ppm Pd, and 7.8 to 166 ppm Pt (Fig. 4.3 and Table 4.4).

For the mineralized rocks, the mantle normalized metal patterns (Fig. 4.4) show a strong enrichment in PGE relative to Ni and Cu, giving "double arch-shaped" patterns. The rocks are enriched in Os relative to Re, Ir, and Ru with Ir/Os ratios ranging from 0.2 to 0.5. The concentration increases sharply from Ru to Pd (Pd being the PGE the most enriched in the rocks). This increase is followed by a decrease in concentration from Au to Cu. The shape and level of mantle normalized pattern of our reef samples is very similar to the average obtained by Barnes and Naldrett (1985) for a larger data set (40 samples) from the Minneapolis Adit area, Stillwater Complex.

Table 4.4: *Whole rock analysis and recalculation to 100% sulfide.*

(a) Whole rock

Sample	Stratigraphy	S	Ni	Cu	Co	Re	Os	Ir	Ru	Rh	Pt	Pd	Au	All PGE	Se	S/Se	Pd/Pt	Pt/Ir	Pd/Ir	Cu/Pd	Cu/Pt
		wt%	*wt%*	*wt%*	*ppm*	*ppb*	*ppb*	*ppb*	*ppb*	*ppb*	*ppb*	*ppb*	*ppb*	*ppm*	*ppm*						
ST-04	Footwall	0.014	0.003	0.002	3.5	<1	1.52	0.74	5.6	4.4	61	32	1.5	0.11	n-d	n-d	0.5	83	43	605	313
ST-05	Footwall	0.023	0.008	0.002	59.8	<1	<0.02	0.34	<3	5.22	63	43	0.9	0.11	n-d	n-d	0.7	187	127	552	375
ST-06	Footwall	0.014	0.003	0.001	18.0	<1	1.38	0.24	<4	4.36	48	17	0.4	0.07	n-d	n-d	0.3	200	70	833	290
ST-07	Footwall	0.040	0.071	0.002	65.7	<1	<0.1	0.37	<3.9	3.3	33	10	0.8	0.05	n-d	n-d	0.3	89	26	1701	502
ST-08	Reef Unmineralized	0.065	0.164	0.004	100.6	<1	<0.6	0.04	3.2	3.34	8	10	2.1	0.02	n-d	n-d	1.3	195	243	3999	5001
ST-12	Reef	0.752	0.226*[1]	0.181	191.0	29	1155	383	785	2400	166355	248678	3489	419.8	5.33	1412	1.5	434	649	7	11
ST-14	Reef	0.332	0.087	0.060	22.4	1	68	36	113	313	7811	40757	669	49.1	1.47	2269	5.2	217	1132	15	77
ST-16	Reef	1.009	0.335	0.171	59.8	6	156	30	132	201	23007	45007	727	68.5	6.03	1673	2.0	780	1526	38	75
ST-17	Reef	0.269	0.063*[2]	0.039	17.3	<1	91	32	68	281	11391	37134	498	49.0	1.23	2196	3.3	355	1157	10	34
ST-10	Hanging wall	0.042	0.016	0.002	19.2	<1	<0.1	0.02	<6	<1	4	4	0.3	0.01	n-d	n-d	1.0	225	225	4053	4042
ST-11	Hanging wall	0.072	0.129	0.001	111.5	<1	<0.1	0.07	<5	<1	21	60	3.2	0.08	n-d	n-d	2.9	291	843	199	576
ST-13	Hanging wall	0.125	0.087	0.004	89.5	<1	<0.5	0.12	<4.3	1.1	47	83	1.7	0.13	n-d	n-d	1.8	409	722	477	842

(b) Recalculation** to 100% sulfide for the reef sample

Sample	Stratigraphy	S	Ni	Cu	Co	Re	Os	Ir	Ru	Rh	Pt	Pd	Au	All PGE
		wt%	*wt%*	*wt%*	*ppm*	*ppm*	*ppm*	*ppm*	*ppm*	*ppm*	*ppm*	*ppm*	*ppm*	*ppm*
ST-12	Reef	36.35	10.93	8.77	9230	1.40	55.82	18.51	37.94	116.0	8040	12018	169	20287
ST-14	Reef	36.87	9.69	6.67	2486	0.13	7.54	3.99	12.53	34.7	866	4520	74	5445
ST-16	Reef	36.48	12.12	6.20	2164	0.21	5.64	1.07	4.77	7.3	832	1627	26	2478
ST-17	Reef	37.21	8.76	5.39	2395	n-d	12.59	4.44	9.41	38.9	1576	5136	69	6777

*[1] and *[2] Ni corrected for Ni in olivines. For [1] $Ni_{Initial}$ = 0.406 wt% and for [2] $Ni_{Initial}$ = 0.183 wt%

** $C_{100\ \%\ sulfide} = C_{WR} \times 100/(2.527 \times S + 0.3408 \times Cu + 0.4715 \times Ni)$ Barnes and Lightfoot (2005)

where C_{WR} is the concentration of the elements in the whole rocks and S, Cu and Ni are the concentration in the whole rock of sulfur, copper and nickel, respectively.

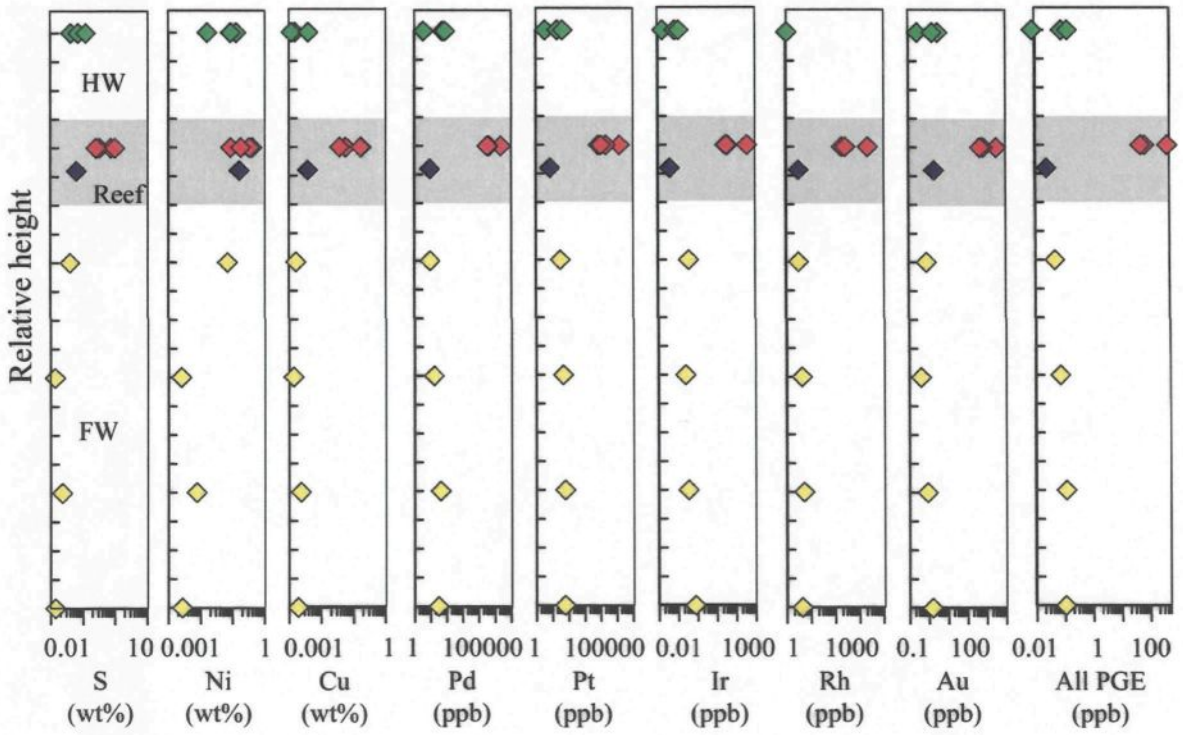

Figure 4.3: Stratigraphic variation of platinum-group elements in the whole rocks of the J-M Reef package.

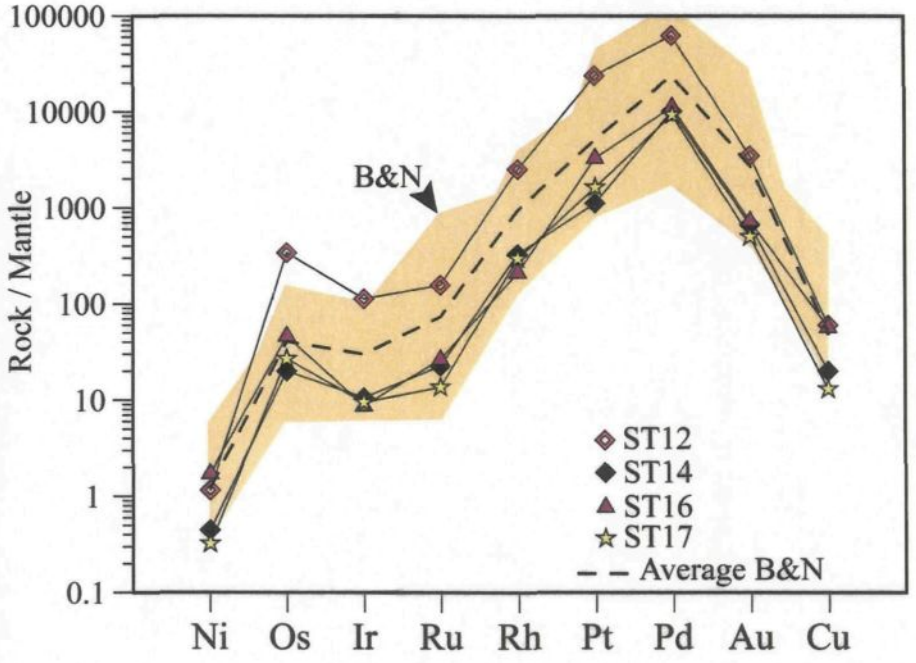

Figure 4.4: Mantle normalized metal pattern for the mineralized samples.

B&N curve corresponds to the values obtained by Barnes and Naldrett (1985).

The Pd/Pt and Pd/Ir ratios are lowest just below the reef (0.3 and 26 respectively, Table 4.4 and Fig. 4.5). These ratios increase strongly in the reef samples (from 1.3 to 5.2 for Pd/Pt and from 243 to 1526 for Pd/Ir).

In the hanging wall samples, the values decrease upward from 2.9 to 1 for Pd/Pt and from 722 to 225 for Pd/Ir. These results indicate that Pd is more strongly enriched in the reef than the other PGE, which raises the possibility that Pd was enriched in the magma pulse that formed OB-1, or that Pd was concentrated in the reef during magmatic or alteration processes.

These possibilities will be investigated by determining which phases host the PGE and by discussing each of the processes and by calculating for each case the possible parental magma of the J-M Reef.

4.8. - PGE AND OTHER METALS IN THE BASE-METAL SULFIDE MINERALS

All of the BMS minerals (pentlandite, pyrrhotite, and chalcopyrite) contain various amount of PGE. The total PGE content varies as a function of the BMS minerals (Table 4.5). Pentlandite is the principal BMS mineral host of the PGE with concentrations ranging from ~350 ppm to more than 2.8 wt%. Most of the pyrrhotite (~80%) contains between 50 and 150 ppm PGE. Some Ni-rich pyrrhotite (0.136 to 0.533 wt% Ni) contains more PGE (up to 500 ppm). Chalcopyrite contains 2 to ~100 ppm PGE. Examples of typical time resolved analysis (TRA) spectra for pentlandite, pyrrhotite and chalcopyrite are given in Fig. 4.6.

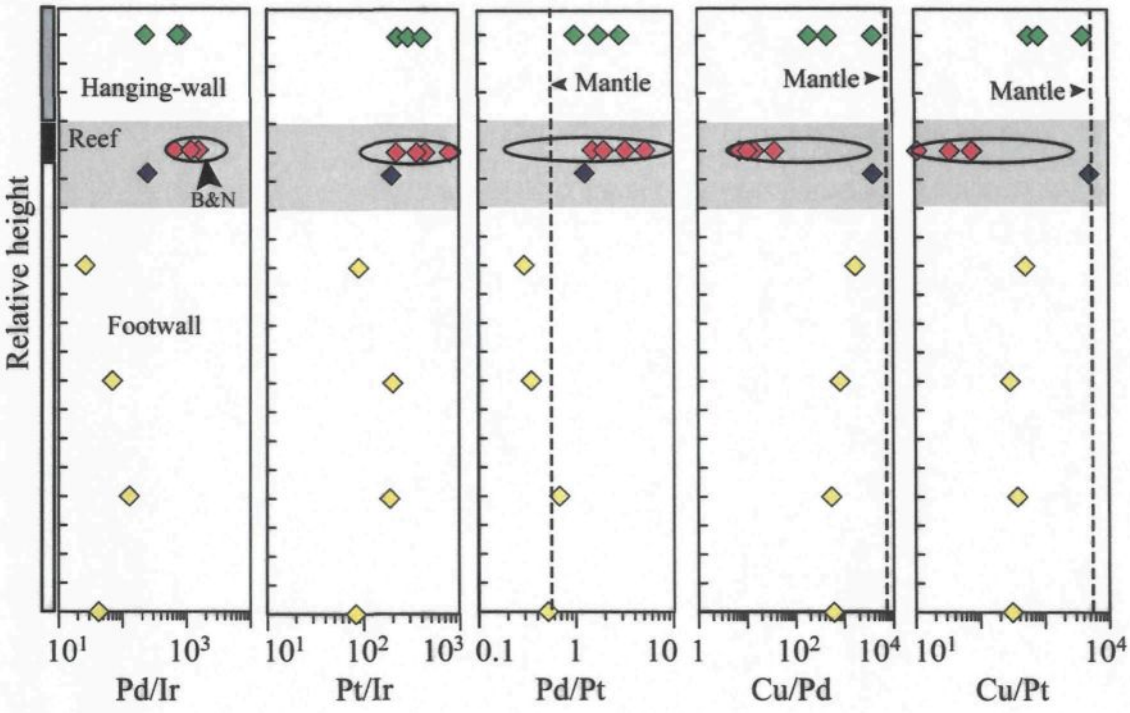

Figure 4.5: Stratigraphic variations of whole rock Pd/Pt, Pd/Ir, Pt/Ir, Cu/Pd and Cu/Pt ratios of the J-M Reef samples.

B&N ellipses corresponds to the values obtained by Barnes and Naldrett (1985).

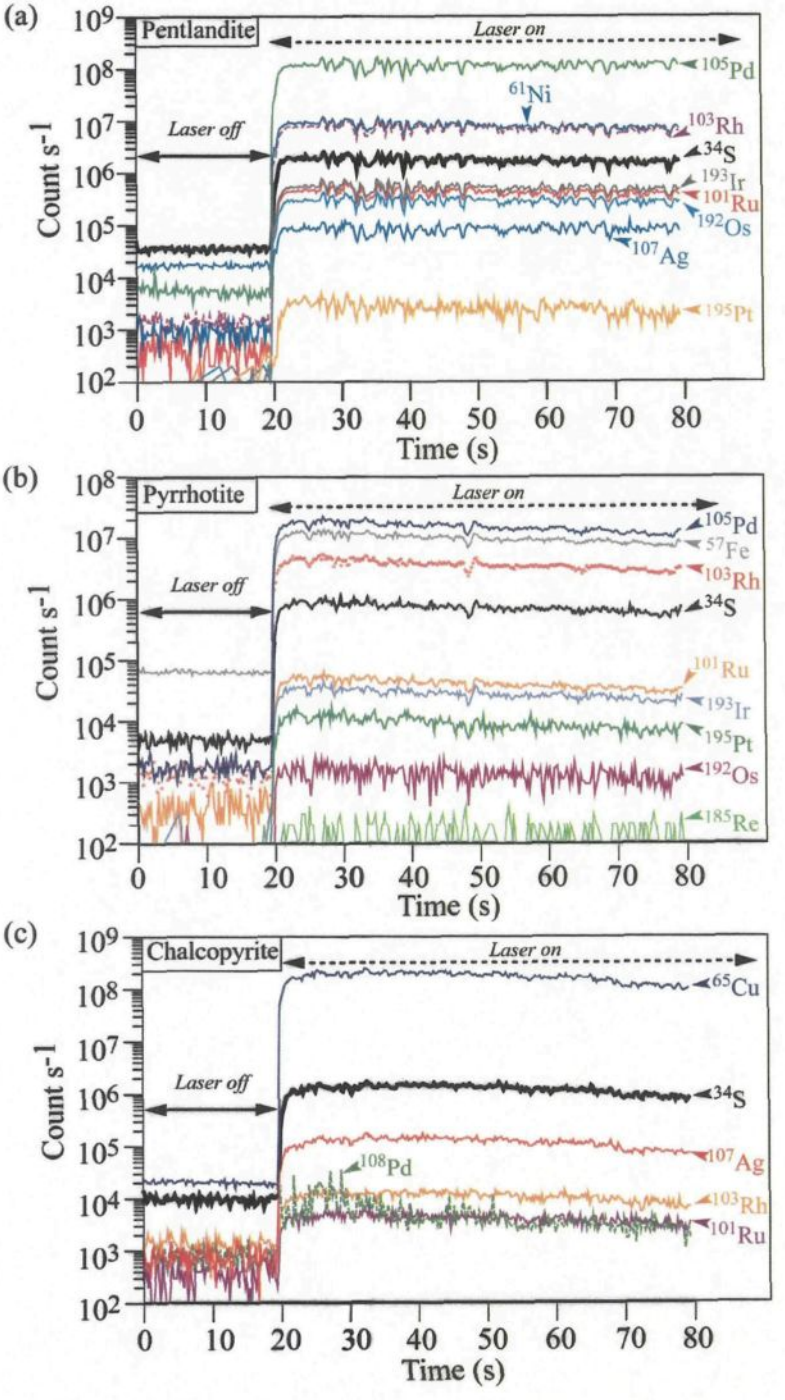
(a)
Pentlandite
Laser on
Laser off
105Pd
61Ni
103Rh
34S
193Ir
101Ru
192Os
107Ag
195Pt
Count s-1
Time (s)
(b)
Pyrrhotite
Laser on
Laser off
105Pd
57Fe
103Rh
34S
101Ru
193Ir
195Pt
192Os
185Re
Count s-1
Time (s)
(c)
Chalcopyrite
Laser on
Laser off
65Cu
34S
107Ag
108Pd
103Rh
101Ru
Count s-1
Time (s)

Figure 4.6: Time-resolved analysis spectra of (a) pentlandite, (b) pyrrhotite and (c) chalcopyrite.

4.8.1. - Controls on trace elements in the base-metal sulphide minerals

As a Fe-Ni-Cu sulfide liquid cools, a monosulfide solid solution enriched in Fe (MSS) crystallizes and is in equilibrium with a liquid enriched in Cu (Kullerud *et al.*, 1969; Naldrett, 1989). Nickel partitions equally between MSS and liquid (Li *et al.*, 1996). As temperature decreases, the Cu-rich fractionated liquid crystallizes as intermediate solid solution (ISS) and minor MSS. At temperature < 600°C, the MSS exsolves into pyrrhotite ($Fe_{1-x}S$), and pentlandite [$(Ni, Fe)_9S_8$] and the ISS exsolves to form chalcopyrite ($CuFeS_2$) +/- cubanite ($CuFe_2S_3$). According to the partition coefficient between sulfide liquid and the MSS in alloy-free system, Cu, Pt, Pd, Ag, Au, and Cd would be expected to concentrate in the Cu-rich fractionated liquid, now represented by chalcopyrite. In contrast, Os, Ir, Ru, Rh, and Re preferentially partitionned into the MSS, now represented by pyrrhotite and pentlandite (Li *et al.*, 1996; Barnes *et al.*, 1997; Mungall *et al.*, 2005). If the trace elements have not been redistributed during the exsolution process, pyrrhotite and pentlandite would be rich in Os, Ir, Ru, Rh, and Re whereas chalcopyrite would be rich in the remaining elements.

4.8.2. - Variation and correlation between metals

4.8.2.1. - Nickel, Cobalt, Palladium and Rhodium

Palladium show strong correlations with Ni, Co, and Rh content (Fig. 4.7). In the pentlandite, for all types of lithologies, Pd represents ~98 % of the PGE found in this mineral (Table 4.5 and Fig. 4.7b). Pentlandite from the troctolite (ST12) contains ~18 800 to 26 800 ppm Pd. The pentlandite of the anorthosite (ST14) contains ~ 300 to ~ 13 000 ppm, with one exception, a grain which reaches 28 280 ppm Pd. The pentlandite in the gabbronorite (ST16) contains ~1850 to 5450 ppm Pd. In the olivine gabbronorite (ST17), the Pd content in the pentlandite varies from ~5670 to 9260 ppm. These values are in agreement with those reported by Cabri *et al.* (1984) and Gervilla *et al.* (2004) and are lower than those reported by Li and Ripley (2006) on highly enriched pentlandite. In the pyrrhotite, the Pd content varies from 1 to 160 ppm and Pd represents 63% to 95% of the PGE found in the BMS minerals (Table 4.5). The Pd content is lower in the chalcopyrite and varies from 1 to ~50 ppm (Table 4.5).

Like Pd, Rh also shows a positive correlation with Ni and Co (Fig. 4.7c). Pentlandite is the mineral which contains most of the Rh found in BMS minerals. Rhodium content in pentlandite varies from ~1 to 400 ppm. These values are similar to those determined by Cabri *et al.* (1984) using proton microprobe (Fig. 4.7c). Rh varies from ~0.03 to ~ 4 ppm and ~0.03 to ~2 ppm in pyrrhotite and chalcopyrite, respectively.

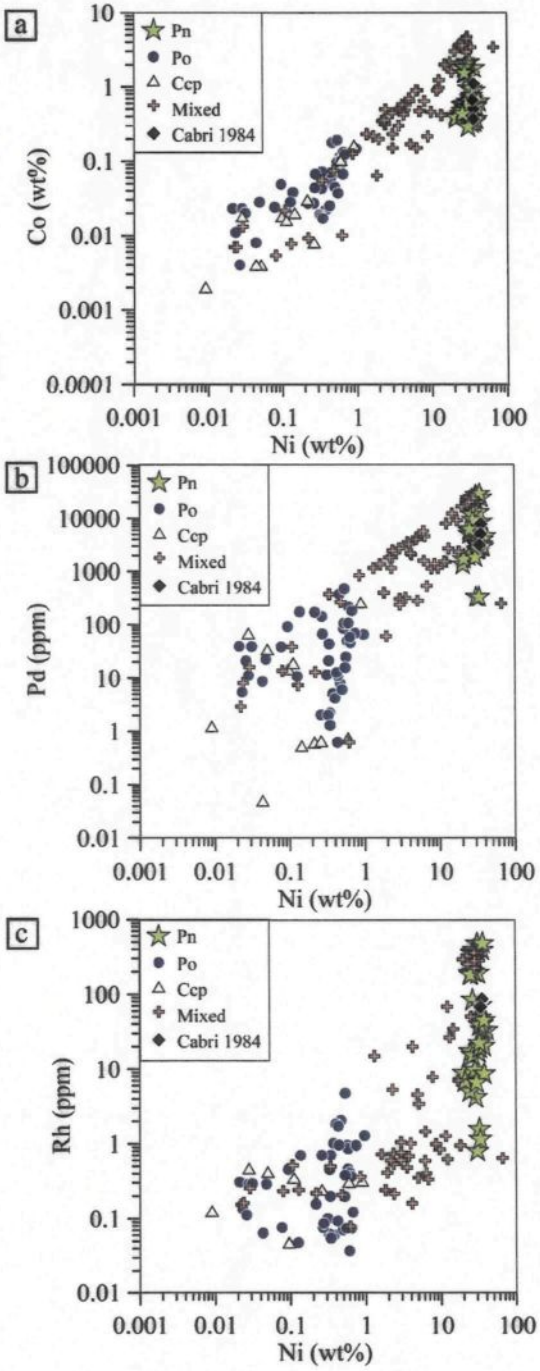

Figure 4.7: Binary variation diagrams, plotting: (a) Co vs Ni; (b) Pd vs Ni and (c) Rh vs Ni.

The values obtained for pentlandite by Cabri et al. (1984) are labelled as Cabri (1984).
Pn: pentlandite; Po: pyrrhotite; Ccp: chalcopyrite; Mixed: mixed values

Table 4.5: *Average metals content of the BMS minerals from the J-M Reef package obtained by LA-ICP-MS analysis.*

Section	*n*		^{61}Ni wt%	^{65}Cu wt%	^{59}Co wt%	^{185}Re ppm	^{192}Os ppm	^{193}Ir ppm	^{101}Ru ppm	^{103}Rh ppm	^{195}Pt ppm	$^{105/108}$Pd ppm	^{197}Au ppm	^{107}Ag ppm	^{111}Cd ppm	^{67}Zn ppm
PENTLANDITE																
ST12	12	GM	28.88	0.247	1.785	0.352	31.135	32.778	110.22	318.69	0.629	21720	0.01	11.77	2.47	381.4
		SD	*0.91*	*0.308*	*0.863*	*0.095*	*0.445*	*0.712*	*0.43*	*0.64*	*0.799*	*0.9*	*0.50*	*0.65*	*0.45*	*0.2*
ST14	11	GM	29.87	0.018	0.682	0.065	0.389	2.465	2.64	11.21	2.727	3693	0.02	3.78	1.49	17.5
		SD	*0.84*	*0.133*	*0.777*	*0.148*	*0.502*	*0.479*	*0.20*	*0.15*	*0.354*	*0.2*	*0.45*	*0.58*	*0.65*	*0.4*
ST16	13	GM	32.33	0.017	0.438	0.017	0.659	1.153	1.57	17.20	1.077	2992	0.01	1.36	1.01	30.2
		SD	*0.83*	*0.123*	*0.784*	*0.178*	*0.596*	*0.628*	*0.43*	*0.46*	*0.119*	*0.7*	*0.44*	*0.46*	*0.72*	*0.1*
ST17	4	GM	27.14	0.710	0.488	0.013	2.562	4.846	20.13	189.59	1.715	6721	0.00	6.79	0.88	94.0
		SD	*0.90*	*0.891*	*0.900*	*0.849*	*0.784*	*0.886*	*0.83*	*0.96*	*0.685*	*0.8*	*0.82*	*0.72*	*0.91*	*0.4*
PYRRHOTITE																
ST12	9	GM	0.074	0.092	0.039	0.015	0.090	0.366	1.00	0.53	0.014	56.41	0.00	1.38	0.65	35.0
		SD	*0.287*	*0.266*	*0.377*	*0.112*	*0.327*	*0.629*	*0.63*	*0.33*	*0.319*	*0.22*	*0.28*	*0.44*	*0.74*	*0.2*
ST14	17	GM	0.490	0.003	0.076	0.012	0.199	1.531	1.83	0.75	0.035	18.76	0.01	0.72	0.63	7.2
		SD	*0.723*	*0.278*	*0.641*	*0.138*	*0.430*	*0.545*	*0.60*	*0.52*	*0.127*	*0.19*	*0.33*	*0.55*	*0.72*	*0.2*
ST16	8	GM	0.417	0.013	0.028	0.110	0.498	0.404	1.70	0.07	0.064	8.01	0.00	0.80	0.59	
		SD	*0.771*	*0.482*	*0.608*	*0.339*	*0.559*	*0.623*	*0.55*	*0.81*	*0.489*	*0.27*	*0.25*	*0.39*	*0.88*	
ST17	10	GM	0.173	0.145	0.015	0.032	0.061	0.561	0.74	0.07	0.017	12.99	0.01	0.30	0.71	530.7
		SD	*0.338*	*0.193*	*0.194*	*0.142*	*0.282*	*0.323*	*0.74*	*0.45*	*0.488*	*0.07*	*0.28*	*0.37*	*0.69*	*0.3*
CHALCOPYRITE																
ST12	3	GM	0.028	26.04	0.003	0.003	0.261	0.330	0.66	0.24	0.038	5.02	0.01	2.74	1.23	415.3
		SD	*0.000*	*0.79*	*0.188*	*0.422*	*0.200*	*0.759*	*0.63*	*0.39*	*0.158*	*0.09*	*0.22*	*0.73*	*0.67*	*0.6*
ST14	6	GM	0.117	32.78	0.018	0.008	0.011	0.021	0.66	0.21	0.048	11.44	0.02	19.21	2.05	719.4
		SD	*0.186*	*0.97*	*0.177*	*0.437*	*0.570*	*0.366*	*0.61*	*0.43*	*0.290*	*0.11*	*0.56*	*0.66*	*0.67*	*0.5*
ST16	1	GM	0.001	30.28	0.001	0.004	0.013	0.009	0.08	0.00	0.004	0.17	0.00	1.69	12.13	802.3
ST17	4	GM	0.136	31.92	0.012	0.010	0.014	0.027	0.03	0.24	0.054	0.32	0.00	2.46	1.62	1355.2
		SD	*0.446*	*0.90*	*0.404*	*0.281*	*0.161*	*0.064*	*0.30*	*0.10*	*0.313*	*0.29*	*0.67*	*0.55*	*0.54*	*0.5*

GM: geometric mean of *n* values
SD: standard deviation around geometric mean

4.8.2.2. - Iridium, Osmium, Ruthenium and Rhenium

Iridium and Os show a good positive correlation for all the BMS minerals (Fig. 4.8a and Table 4.5). Iridium contents in the pentlandite are highest in the troctolite (ST12) and vary from 16 to ~50 ppm. Osmium content in this lithology varies from 15 to 150 ppm. The pentlandite hosted by the other lithologies (ST14, ST16, and ST17) contain less Ir (1 to 7 ppm) and Os (0.1 to ~3.3 ppm). In the pyrrhotite and the chalcopyrite, the Ir content varies from 0.2 to 3 ppm and 0.01 to ~1 ppm, respectively. Osmium values are similar in both BMS minerals (0.01 to ~3 ppm). No variation of Os and Ir contents with lithology were observed for either pyrrhotite or pentlandite.

Ruthenium strongly correlates with Ir in the pentlandite and the pyrrhotite (Fig. 4.8b and Table 4.5). In the pentlandite of the troctolite (ST12), the ruthenium content is higher (50 to 200 ppm, with two other values higher at ~500 ppm) than in the other lithologies (2 to 30 ppm of Ru). These values are in good agreement with those found by Cabri *et al.* (1984) on other Stillwater pentlandites. As for Os, and Ir, the Ru content in the pyrrhotite is independent of the host lithologies. Pyrrhotite contains ~0.5 to ~5 ppm Ru. In the chalcopyrite, most Ru values were less than the detection limit. However, for the remaining values the Ru variation is low with values ranging from ~0.8 to ~2 ppm.

Rhenium values are higher in the pentlandite (0.003 to 20 ppm, Fig. 8c, and Table 4.5) and the pyrrhotite (0.003 to 2 ppm, Fig. 4.8c, and Table 4.5) than in the chalcopyrite (0.003 to 0.1 ppm, Fig. 4.8c, and Table 4.5).

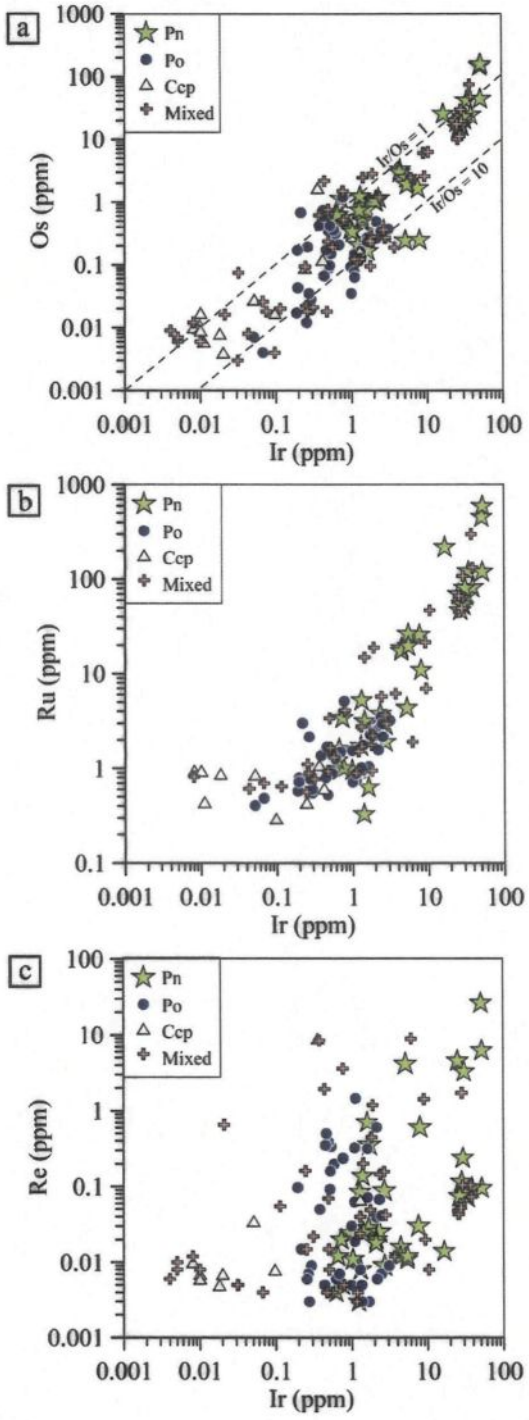

Figure 4.8: Binary variation diagrams of: (a) Os vs Ir; (b) Ru vs Ir and (c) Re vs Ir.

Pn: pentlandite; Po: pyrrhotite; Ccp: chalcopyrite; Mixed: mixed values.

The ICP-MS signal shows that rhenium content can vary strongly within a single sulfide grain, i.e. without variation in either Ni or Cu observed (Fig. 4.9). This variation in the Re content is commonly found in the pyrrhotite and may be due to heterogeneous diffusion of Re during pyrrhotite exsolution from the MSS, or to the ablation of Re-bearing minerals (triggering peaks on the ICP-MS Re signal). However, no Re bearing minerals were found during the platinum-group minerals analysis.

4.8.2.3. - Copper, Platinum, Gold, Cadmium, Silver, and zinc

The BMS minerals contain only a minor amount of Pt, more than 75 % of the BMS minerals contain less than 1 ppm Pt (Table 4.5). Platinum content in pentlandite ranges from 0.035 ppm to 8 ppm, with ~75 % of the values being < 5 ppm. Pyrrhotite and chalcopyrite contain less Pt with values between 0.001 to 2 ppm (with ~95 % of the values < 0.2 ppm). Platinum does not show any correlation with base metals (Fig. 4.10a).

Gold also does not partition into a specific sulfide mineral (Table 4.5). All the sulfides (pentlandite, pyrrhotite, and chalcopyrite) contain 0.05 to 0.1 ppm Au.

Silver behaves slightly differently, and is preferentially partitioned in both chalcopyrite and pentlandite (~1 to 30 ppm) relative to the pyrrhotite (~0.05 to 5 ppm) (Table 4.5 and Fig. 4.10b).

Cadmium shows a weak correlation with Cu content (Fig. 4.10d). Pentlandite and chalcopyrite contain 0.5 to 12 ppm Cd. The Cd content is slightly lower in the pyrrhotite, with values of 0.5 to 2 ppm (Table 4.5).

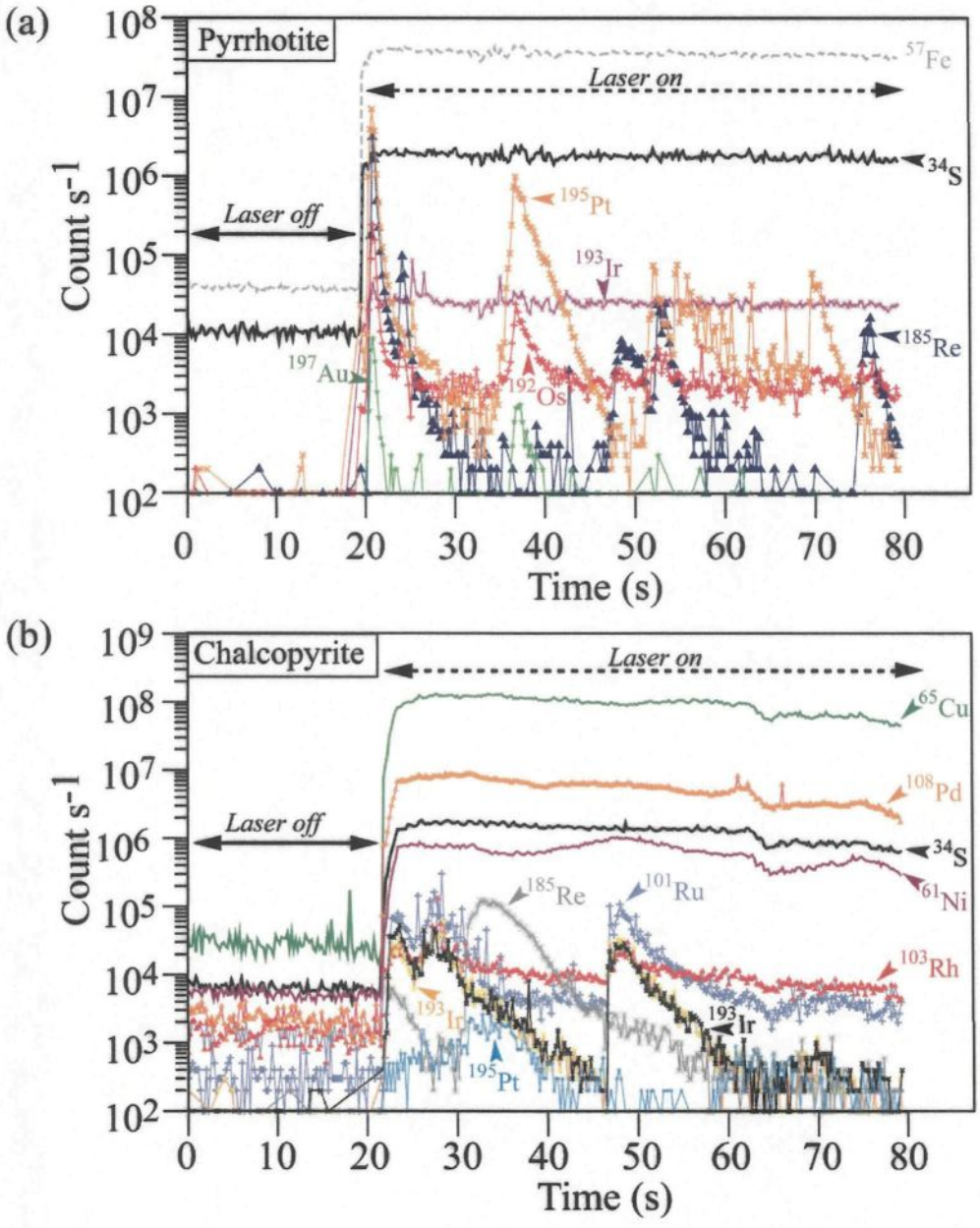

Figure 4.9: Examples of inclusions observed during laser ablation.

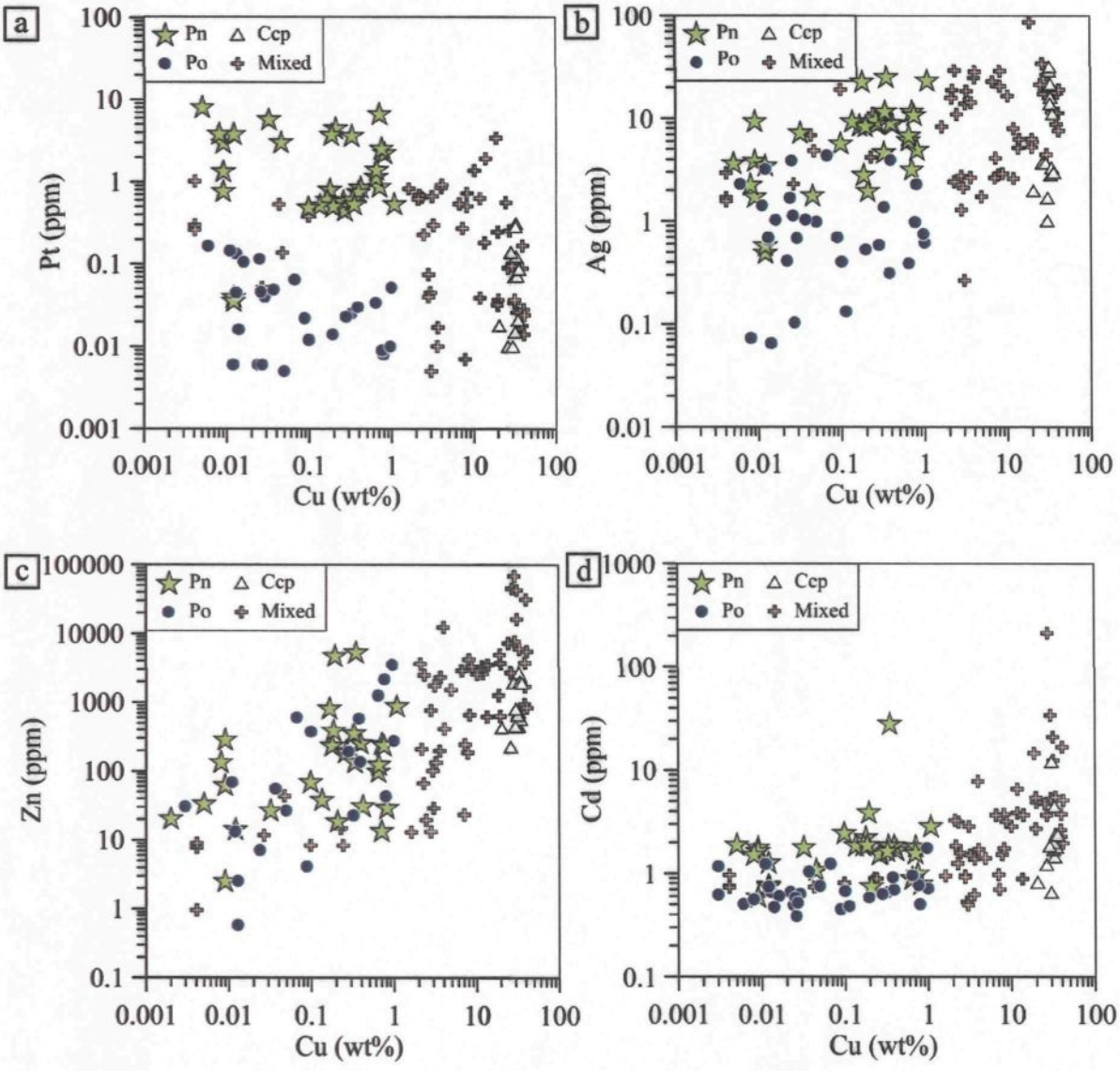

Figure 4.10: Binary variation diagrams of: (a) Pt vs Cu; (b) Ag vs Cu ; (c) Zn vs Cu and (d) Cd vs Cu.

Pn: pentlandite; Po: pyrrhotite; Ccp: chalcopyrite; Mixed: mixed values.

Zinc content correlates with the Cu content in pyrrhotite and pentlandite. As predicted by the empirical observation, Zn partitions more efficiently into Cu-rich phases. Zinc values vary from 0.4 to 5 000 ppm in pentlandite and pyrrhotite and from 100 ppm to 5000 ppm in the chalcopyrite (Table 4.5 and Fig. 4.10c).

4.9. - MASS BALANCE OF PGE

In the following, we will evaluate the proportions of each element in each BMS minerals in order to assess whether the BMS minerals are indeed the principal host of PGE observed in the J-M Reef samples, or whether other phases control the PGE distribution.

4.9.1. Method of calculation

The percentage of each PGE associated with each BMS mineral was calculated using the whole rock concentrations of Ni, Cu, S, Co, PGE, and Au (Table 4.4) and the results of the in-situ PGE analysis of BMS minerals (Table 4.5).

The percentage (P_{sul}^{i}) of each PGE (i) in a given BMS minerals was calculated as follows:

$$(P_{sul}^{i}) = (F_{sul} \times C_{sul}^{i} / C_{WR}^{i}) \times 100$$

where F_{sul} is the weight fraction of the BMS minerals considered, C_{sul}^{i} is the concentration of the element i in the BMS minerals considered, C_{WR}^{i} is the concentration of the element i in the whole rocks.

The weight fraction of chalcopyrite (F_{Ccp}) is calculated by assuming that all the Cu in the whole rock is hosted by chalcopyrite. F_{Ccp} is given by (Cu_{WR}/Cu_{Ccp}) where Cu_{WR} is

the concentration of Cu in the whole rocks and Cu_{Ccp} is the average concentration of Cu in the chalcopyrite. The weight fraction of pentlandite (F_{Pn}) is calculated by assuming that Ni is hosted by pentlandite and olivine (Barnes and Naldrett, 1985). F_{Pn} is given by (Ni_{WR} – X_{Ol} Ni_{Ol}) / Ni_{Pn} where Ni_{WR} is the concentration of Ni in the whole rock, X_{Ol} is the fraction of olivine in the rock, Ni_{Ol} is the concentration of Ni in olivine, and Ni_{Pn} is the concentration of Ni in pentlandite. The concentration of Ni in olivine used in the calculation is 3000 ppm Ni, it corresponds to the average values found by Barnes and Naldrett (1985) in olivines from the J-M Reef. The weight fraction of pyrrhotite (F_{Po}) is calculated by considering that the remaining S (i.e. after the weight fractions of pentlandite and chalcopyrite are estimated) is given by (S_{WR} – F_{Pn} S_{Pn} – F_{Ccp} S_{Ccp}) / S_{Po} where S_{WR} is the S content in the whole rock, S_{Pn} is the average sulfur content in the pentlandite, S_{Ccp} the average sulfur content in the chalcopyrite and S_{Po} the average S concentration in the pyrrhotite. The weight fraction and the proportion of each BMS mineral are given in Table 4.6.

4.9.2. - Results of the mass balance calculation

In all the samples, almost no Pt and Au (<0.1 %) are present in the BMS minerals (Table 4.7). These elements are found as platinum-group minerals or as electrum. Several inclusions enriched in these elements were observed during laser ablation (Fig. 4.8 and Table 4.9). The results are similar to those obtained for a mass balance study of the Merensky Reef of the Bushveld Complex (Godel *et al.*, 2007) and for the sulfide droplets from the Medvezky Creek Mine of Noril'sk, Russia (Barnes et al., 2006).

Table 4.6: *Weight fraction and proportion of each BMS minerals in the whole rock.*

Section	Weight fraction			Percentage (%)		
	Chalcopyrite	Pentlandite	Pyrrhhotite	Chalcopyrite	Pentlandite	Pyrrhhotite
ST12	0.0062	0.0083	0.007	28.8	38.6	32.6
ST14	0.0018	0.0025	0.0048	20.2	27.4	52.4
ST16	0.0052	0.0101	0.0134	18.2	35.1	46.7
ST17	0.0014	0.0023	0.0042	18	29.4	52.6

Table 4.7: *Calculated proportion of each element in each BMS mineral.*

Section	Mineral*	^{61}Ni	^{65}Cu	^{59}Co	^{185}Re	^{109}Os	^{193}Ir	^{101}Ru	^{103}Rh	^{195}Pt	^{108}Pd/^{105}Pd	^{197}Au
ST12	Pn	105.8	1.1	77.2	10.0	22.3	70.9	116.3	109.9	0.003	72.3	0.002
ST12	Po	0.2	0.4	1.4	0.4	0.1	0.7	0.9	0.2	0.000	0.2	0.001
ST12	Ccp	0.1	88.8	0.1	0.7	0.1	0.5	0.5	0.1	0.000	0.0	0.002
ST12	*All sulfide*	*106.1*	*90.3*	*78.7*	*11.1*	*22.5*	*72.1*	*117.7*	*110.2*	*0.003*	*72.5*	*0.005*
ST14	Pn	85.4	0.4	75.8	101.0	1.9	22.2	13.2	47.9	0.126	45.7	0.010
ST14	Po	2.7	0.0	16.2	4.7	1.4	20.3	7.7	1.1	0.002	0.2	0.004
ST14	Ccp	0.2	100.2	1.0	0.9	0.0	0.1	1.0	0.1	0.001	0.0	0.007
ST14	*All sulfide*	*88.3*	*100.7*	*93.0*	*106.7*	*3.3*	*42.5*	*21.9*	*49.1*	*0.129*	*45.9*	*0.021*
ST16	Pn	97.1	0.1	74.0	3.0	4.2	39.3	11.9	86.1	0.047	66.9	0.008
ST16	Po	1.7	0.1	6.2	25.8	4.3	18.4	17.2	0.5	0.004	0.2	0.008
ST16	Ccp	0.0	92.5	0.1	0.4	0.0	0.2	0.3	0.0	0.000	0.0	0.003
ST16	*All sulfide*	*98.8*	*92.7*	*80.3*	*29.2*	*8.6*	*57.9*	*29.5*	*86.6*	*0.051*	*67.2*	*0.019*
ST17	Pn	117.9	4.2	65.9	n-d	6.6	35.1	68.9	157.0	0.035	42.1	0.002
ST17	Po	1.1	1.5	3.5	n-d	0.3	7.3	4.5	0.1	0.001	0.1	0.007
ST17	Ccp	0.3	117.0	1.0	n-d	0.0	0.1	0.1	0.1	0.001	0.0	0.001
ST17	*All sulfide*	*119.3*	*122.8*	*70.4*	*n-d*	*6.9*	*42.5*	*73.4*	*157.2*	*0.036*	*42.3*	*0.010*

*The proportion of each BMS mineral is given in Table 4.6

In all four samples, pentlandite is the BMS mineral that contains the largest weight fraction of the siderophile elements. Pyrrhotite contains 0.1 to 20 % of the IPGE and Rh and negligible amounts of the other siderophile elements. Chalcopyrite accounts for <1 % of any siderophile element in the rock. A large part (~45 to 100%) of the Pd, Ir, Rh are present in the BMS minerals. The amount of Ru and Re in BMS minerals covers a large range (11 to 100%) from rock to rock. The weight fractions of Os, Pt, and Au in BMS minerals are low (3 to 20 % for Os and <0.1 % for Pt and Au). There may be a correlation between the degree of alteration of the sulfides and the amount of PGE in the BMS minerals. For example, sample ST14 contains the sulfides with the greatest degree of recrystallization and also has the lowest weight fraction of PGE in BMS minerals. However, the sample does not appear to have lost S as it has the highest S/Se ratio of the samples.

The results indicate that phases other than BMS minerals must also be present in order to accommodate approximatively half the Pd, Ir, Rh, and Ru and almost all the Os, Pt, and Au. Numerous platinum-group mineral (PGM) are reported from the J-M Reef (Zientek and Oscarson, 1986; Polovina *et al.*, 2004) which could be the host of these PGE. We have examined the four reef samples and found more than 850 grains of PGM. These will be described in more detail in another manuscript.

Table 4.8: *Inclusions observed during laser ablation.*

Type	Sulfide	Number	Length (μm) Min.	Max.
Ru+/-Ir+/-Os	Po	4	0.38	2.63
	Pn	3	0.24	1.75
Pt-rich	Po	2	0.40	1.53
	Pn	2	0.30	1.58
	Cp	2	0.81	4.08
Re-rich	Po	12	0.19	2.98
	Pn	20	0.32	6.43
	Cp	1	0.45	1.31
Au-rich	Po	2	0.23	0.95
	Pn	7	0.24	6.89
	Cp	1	0.25	0.73
Ag-rich	Po	2	0.30	4.59
	Pn	3	0.27	3.68
	Cp	4	0.51	3.28
Ir-rich	Pn	2	0.42	1.33
Pd-rich	Po	5	0.28	4.44
Rh-rich	Po	1	0.30	0.88
	Pn	1	0.45	1.31
Os-rich	Pn	1	0.32	0.93
Total		*75*		

Po: pyrrhotite, Pn: pentlandite, Cp: chalcopyrite

4.10. – DISCUSSION

As previously described, two principal models have been proposed to explain the PGE enrichments of some layers in the Stillwater Complex (and other intrusions *e.g.* the Bushveld Complex): (i) the collection of PGE by immiscible sulfide liquid (Campbell *et al.*, 1983; Naldrett *et al.*, 1986) and (ii) the collection of PGE by magmatic fluid (Boudreau and McCallum, 1992; Willmore *et al.*, 2000).

In the following, we will discuss the possible PGE content of the parental magma of the J-M Reef by taking into account the collection of the PGE by sulfide liquid and the possible redistribution of PGE by fluids. The different results obtained will then be considered to propose a possible model of formation for this PGE reef.

4.10.1. - Modeling of the collection of PGE by a sulfide liquid

4.10.1.1. - Principle

The model of collection of the PGE by an immiscible sulfide liquid presented by Campbell and Naldrett (1979) is based on the idea that when a new magma enters the chamber and mixes with the resident magma, a mixed magma saturated in an immiscible sulfide liquid may form. As PGE have a high partition coefficient into sulfide liquid, as soon as immiscible sulfide droplets have formed, they interact with the silicate magma and collect all the PGE that they encounter (Campbell *et al.*, 1983; Naldrett *et al.*, 1986). Campbell and Naldrett (1979) have shown that the PGE concentrations in the sulfide (C_{Sul}) is dependent on the volume of silicate which interacted with the sulfide liquid (referred to

as R-factor). More recently, Brügmann et al. (1993) proposed that the composition of sulfide droplets sinking in the magma chamber may be calculated using the zone refining equation. In this case, the concentration of each metal in the sulfide (C_{Sul}) is given by the following equation (Brügmann *et al.*, 1993):

$$C_{Sul} = C_{Sil} [D^{Sul/Sil} - (D^{Sul/Sil} - 1) \times e^{-(1/ DSul/Sil \times N)}]$$

where C_{Sil} is the concentration in the original silicate liquid, $D^{Sul/Sil}$ is the partition coefficient between the sulfide and the silicate liquids and N is the ratio of mass of silicate to sulfide liquid (similar to R-factor).

4.10.1.2 - Role of sulfur removal

The BMS minerals in our samples have undergone some alteration with the development of secondary magnetite and recrystallization of the BMS in one of the samples. This may result in the loss of S from the rocks. Sulfur/Se ratios are commonly use to determine whether rocks containing disseminated BMS minerals have lost S (e.g. Lorand *et al.*, 2003). The reason for this is that Se substitutes for S in many BMS mineral. However S is more mobile than Se during alteration. The ratio of S/Se in the mantle is ~3000 (McDonough and Sun, 1995). Assuming that primary magmas have S/Se ratio of 3000, and that the saturation of the Stillwater magma in base metal sulfide liquid occurred at approximately 500 ppm S, and that the partition coefficient of Se into sulfide liquid is 1000, the S/Se ratio of the sulfide liquid is approximately ~3000. The Merensky Reef has a S/Se

ratio close to 3000 (Barnes and Maier, 2002, Godel *et al.*, 2007). In contrast, in our samples of J-M reef, the S/Se ratios in the samples range from ~1400 to ~2300.

This implies that S was removed during post-sulfide liquid collection and/or alteration processes. The concentration of S before sulfur removal, termed S_{Origin} (in wt%) may be calculated as:

$$S_{Origin} = 0.3 \times Se_{WR}$$

where Se_{WR} is the Se content (in ppm) in the whole rock. The average sulfide mineral contents of the whole rock (initial or observed) were calculated by assuming an average of 36 wt% of S in the BMS minerals. Results for the mineralized samples are summarised in Table 4.9. The samples that have undergone the maximum sulfur removal are not necessarily those that have the highest Pd/Pt, Pd/Ir or Pt/Ir ratios. These observations imply that the processes that triggered the S removal and the Pt and/or Pd enrichment or remobilization are complex and probably distinct.

4.10.1.3. - Results of the modeling

In contrast to the Bushveld Complex, South Africa, no well-defined initial magma has been proposed for the Stillwater Complex. Consequently, the PGE composition of the parental magma which has formed the Stillwater Complex is not well known, and values are available for only a few PGE (Zientek et al., 1986). Some authors (Barnes and Naldrett, 1985) considered that the magmas present at Stillwater Complex had similar composition to those found for the Bushveld Complex.

Table 4.9: *Observed and recalculated sulfide contents.*

S_{WR}	S_{Origin}	Sulfide WR	Sulfide Origin
wt%	wt%	%	%
0.752	1.598	2.1	4.4
0.332	0.440	0.9	1.2
1.009	1.809	2.8	5.0
0.269	0.368	0.7	1.0

We have evaluated the possible composition of the parental magma of the J-M Reef using the zone refining equation (Brügmann *et al.*, 1993), both sulphide contents (observed and recalculated) and ranges of N-factor and partition coefficients $D^{Sul/Sil}$. Calculations were made for each of our samples and for the average values (based on 40 samples) obtained by Barnes and Naldrett (1985) on other J-M reef samples. The calculated parental magma compositions were compared to those of the Bushveld parental magma (Barnes and Maier, 2002) and to those of most basalts (Crocket, 2002 and reference therein). Examples of results are given in Table 4.10 and summarized in Fig. 4.11.

Our modelling indicates that the calculated Ir, Os, Ru, Rh, Ni and Cu composition of the parental magma are comparable with those observed for the Bushveld Complex or for most basalts (Table 4.10 and Fig. 4.11). In contrast, calculated Pt and Pd values are much higher (up to more than 10 times) than those observed in most basalts (Fig. 4.10 and Table 4.11). These results suggest that all the PGE and the base metals could have been initially collected by a sulphide liquid but that Pd, and to a lesser extent Pt, were added to the rock after the sulfide liquid collection event.

Table 4.10: *Estimation of PGE and base metal contents of the parental magma of the J-M Reef of the Stillwater Complex using whole rock metal contents.*

(a) Example of calculations

Sample	Ni ppm	Os ppb	Ir ppb	Ru ppb	Rh ppb	Pt ppb	Pd ppb	Au ppb	Cu ppm	
N-factor= 45 000										
$D^{sul/Sil}$	550	40 000	40 000	40 000	40 000	40 000	40 000	20 000	1 000	% Sulfide
ST12	110	1	0.3	0.7	2.1	130	190	4.5	50	4.5
	200	1.8	0.7	1.4	3.8	320	450	9	70	2
ST14	130	0.2	0.11	0.35	1	22	110	3	55	1.5
	140	0.23	0.15	0.4	1.1	28	150	3.5	70	1
ST16	120	0.15	0.03	0.12	0.2	18	34	1	55	4.5
	200	0.21	0.05	0.2	0.4	36	65	2	70	2.5
ST17	120	0.3	0.12	0.24	1	42	135	2.7	50	1
	145	0.5	0.18	0.33	1.4	60	200	3	50	0.7
B&N	130	0.16	0.11	0.4	1	38	100	4	50	4
	200	0.28	0.2	0.7	1.7	70	180	8	75	2
N-factor= 30 000										
$D^{sul/Sil}$	550	20 000	20 000	20 000	20 000	20 000	20 000	15 000	1 000	% Sulfide
ST12	100	1.7	0.6	1.2	3.5	220	340	6	40	4.5
	190	3.7	1.4	2.6	8	550	780	14	90	2
ST14	110	0.32	0.18	0.5	1.5	36	190	3.5	45	1.5
	160	0.47	0.25	0.7	1.9	50	250	5.7	60	1
ST16	120	0.22	0.04	0.18	0.3	32	60	1.2	40	4.5
	240	0.44	0.08	0.35	0.52	50	115	2.5	70	2.5
ST17	110	0.6	0.21	0.43	1.9	73	230	4	60	1
	160	0.85	0.31	0.63	2.6	105	350	5.8	55	0.7
B&N	120	0.25	0.18	0.63	1.6	65	180	5.8	45	4
	240	0.45	0.38	1.2	3	120	320	11	80	2

Table 4.10 (continued)

(b) Minimal, maximal and average values obtained from all calculations

N-factor	$D^{sul/Sil}$		Ni ppm	Os ppb	Ir ppb	Ru ppb	Rh ppb	Pt ppb	Pd ppb	Au ppb	Cu ppm
45000	40000	Min	110	0.15	0.03	0.12	0.2	18	34	1	50
		Max	200	1.8	0.7	1.4	3.8	320	450	9	75
		Average	149.5	0.483	0.195	0.484	1.37	76.4	161.4	4.07	59.5
45000	30000	Min	114	0.43	0.166	0.398	1.2	54	121.8	2.86	50
		Max	200	3	1	2	5.5	600	800	10	90
		Average	147	0.665	0.252	0.594	1.68	106.4	200.4	4.16	59.5
45000	20000	Min	100	0.2	0.04	0.16	0.25	28	50	1.2	45
		Max	220	3.5	1.3	2.2	7	480	750	12	90
		Average	151	0.813	0.321	0.737	2.168	115.4	250	4.99	59
30000	30000	Min	100	0.17	0.035	0.15	0.23	25	50	1.2	38
		Max	230	2.9	1.2	2.1	6	480	700	14	90
		Average	152.5	0.713	0.2965	0.6955	1.975	112	239	5.83	56.1
30000	20000	Min	100	0.22	0.04	0.18	0.3	32	60	1.2	40
		Max	240	3.7	1.4	2.6	8	550	780	14	90
		Average	155	0.9	0.363	0.842	2.482	130.1	281.5	5.95	58.5

B&N: average values on 40 samples of Barnes and Naldrett (1985)

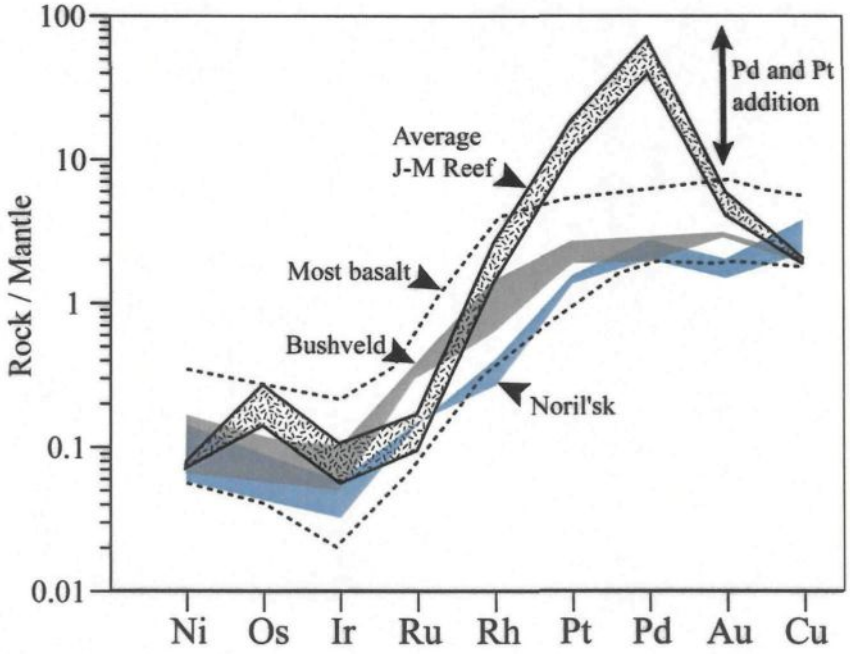

Figure 4.11: Mantle-normalized metal patterns for the calculated parental magma of the J-M Reef.

4.10.2. Redistribution of palladium and platinum by fluid

Experimental work (Pan and Wood, 1994; Wood, 2002; Hanley *et al.*, 2005a; Hanley *et al.*, 2005b) have shown that Pd and Pt can be soluble in high temperature hydrothermal fluid. Results of our modelling indicate that Pd and to a lesser extend Pt were added to the whole rock after the collection of the PGE by immiscible sulfide liquid. The addition of Pd and Pt may probably be due to fluid percolation during one of the alteration events.

4.10.2.1. - Estimation of the proportion of Pt and Pd added

The minimum proportion of Pd and Pt added to the whole rock by fluid may be estimated using the whole rock content and the zone refining equation (Brügmann et al., 1993) and a range of Pt and Pd compositions in the initial silicate magma (C_{Sil}) that are characteristic of most basalts (Barnes and Maier, 2002; Crocket, 2002 and reference therein). The minimum proportion of Pt (Pt_{Min} in %) or Pd (Pd_{Min} in %) added to the whole rock is given by:

$$(C_{WR} - C_{Sul}^{Calc}) \times 100 / C_{WR}$$

where C_{WR} is the concentration of the element considered in the whole rock, C_{Sul}^{Calc} is the concentration of the element in the sulfide calculated with the zone refining equation (Brügmann *et al.*, 1993) and using the recalculated sulfide contents (Table 9). Results of the calculation for $D^{Sul/Sil}$ varying from 20 000 to 40 000, N-factor varying from 45 000 to

30 000 and Pt and Pd contents in the silicate magma varying from 10 to 25 ppb are summarized in Table 4.11.

The proportions of Pt and Pd added vary as a function of the samples considered (Fig. 4.12 and Table 4.11). In highly mineralized sample (such as ST12, Fig. 4.12a and b), the minimum proportions of Pt or Pd added are higher than 80% or 90%, respectively. If we consider the calculation made on the average composition (based on 40 samples) of the J-M Reef obtained by Barnes and Naldrett (1985), a minimum of 40% of Pt and 70% of Pd addition after the sulfide liquid collection is needed to account for the whole rock Pt and Pd contents (Fig. 4.12 and Table 4.11).

4.10.2.2. - Evidence of Pd remobilisation

Backscattered electron (BSE) image analysis of our mineralized samples was done using a scanning electron microprobe at Laval University (Quebec City). More than 850 platinum-group minerals (PGM) were found in the thin sections. The PGM consist mainly of Pd+/-Pt sulfides, Pt-Fe alloy, Pd+/-Pt tellurides, Pd alloys and minor laurite (Ru (Ir, Os) S_2) and palladian electrum (Au-Ag-Pd) that are in many cases associated with BMS minerals. In the samples containing secondary magnetite replacing BMS minerals, Pd alloys and Pd sulfides were found either as interstitial phase between magnetite crystal or as small veinlets crosscutting the BMS minerals (Fig. 4.13a). This observation suggests that Pd was mobile after the solidification of BMS minerals and possibly added to the system

during alteration or metamorphic processes which lead to the oxidation of the BMS minerals to magnetite.

Table 4.11: *Minimum proportion of Pt and Pd added by fluid.*

	Proportion of Pt added (%)				Proportion of Pd added (%)			
Initial magma	10 ppb	15 ppb	20 ppb	25 ppb	10 ppb	15 ppb	20 ppb	25 ppb
Sample								
N= 45 000 and D= 40 000								
ST12	93	89	85	82	95	93	90	88
ST14	48	22	-4	-30	90	85	80	75
ST16	47	21	-6	-32	73	59	46	32
ST17	76	64	53	41	93	89	85	82
B&N	73	59	45	32	90	85	79	74
N= 45 000 and D= 30 000								
ST12	94	91	87	84	96	94	92	89
ST14	55	33	10	-12	91	87	83	79
ST16	54	32	9	-14	77	65	53	42
ST17	80	69	59	49	94	91	87	84
B&N	76	65	53	41	91	87	82	78
N= 45 000 and D= 20 000								
ST12	95	93	90	88	97	95	94	92
ST14	66	48	31	14	93	90	87	84
ST16	65	48	30	13	82	73	64	55
ST17	84	76	69	61	95	93	90	88
B&N	82	73	64	55	93	90	86	83
N= 30 000 and D= 30 000								
ST12	95	92	90	87	97	95	93	91
ST14	64	45	27	9	93	90	86	83
ST16	63	44	26	7	81	72	62	53
ST17	83	75	67	58	95	92	90	87
B&N	81	71	62	52	93	89	86	82
N= 30 000 and D= 20 000								
ST12	96	94	92	89	97	96	94	93
ST14	70	55	40	25	94	91	89	86
ST16	70	54	39	24	84	77	69	61
ST17	86	80	73	66	96	94	92	90
B&N	84	76	69	61	94	91	88	85

B&N: average values on 40 samples of Barnes and Naldrett (1985).

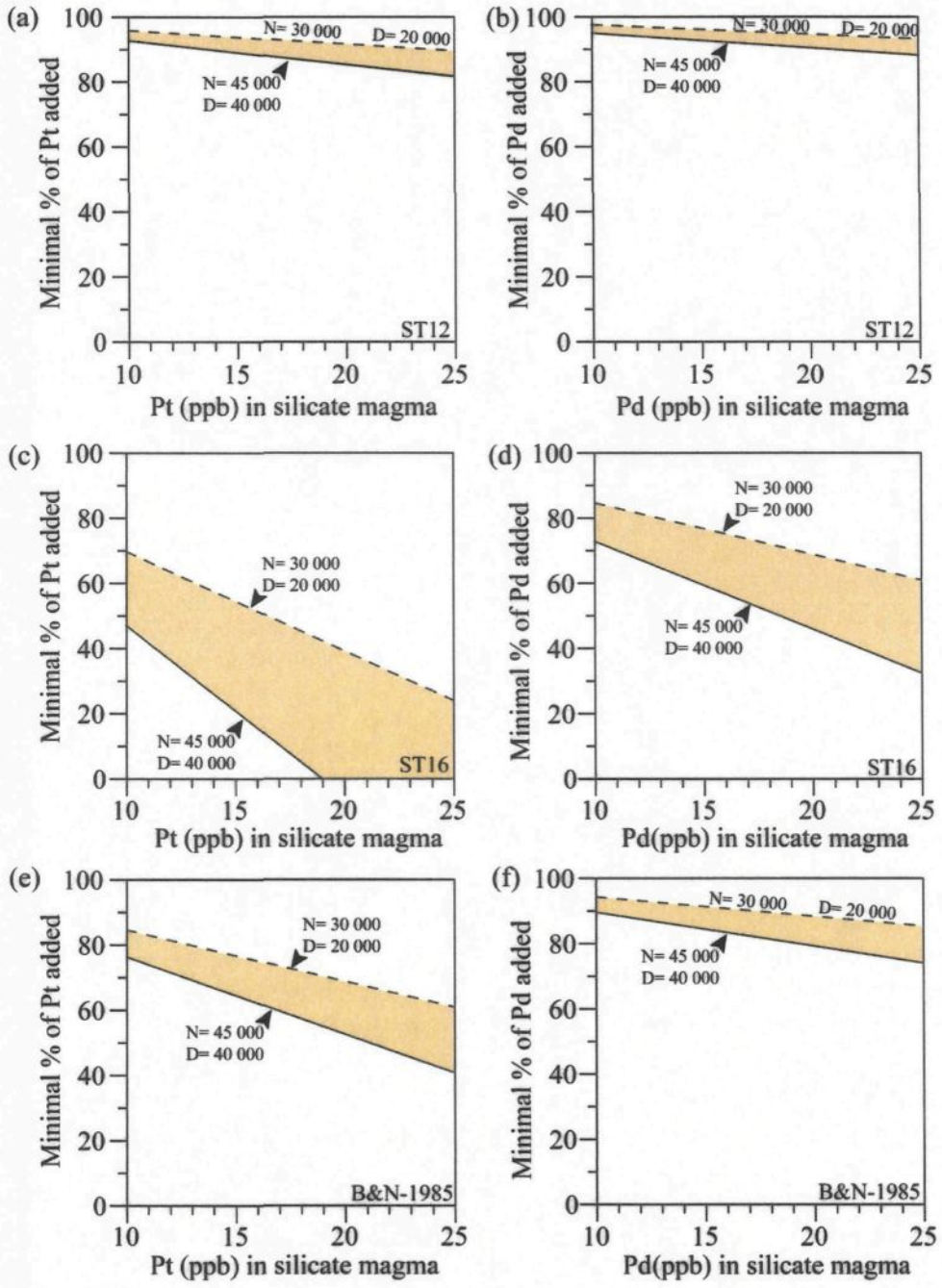

Figure 4.12: Estimation of the Pd and Pt addition for samples of the J-M Reef.

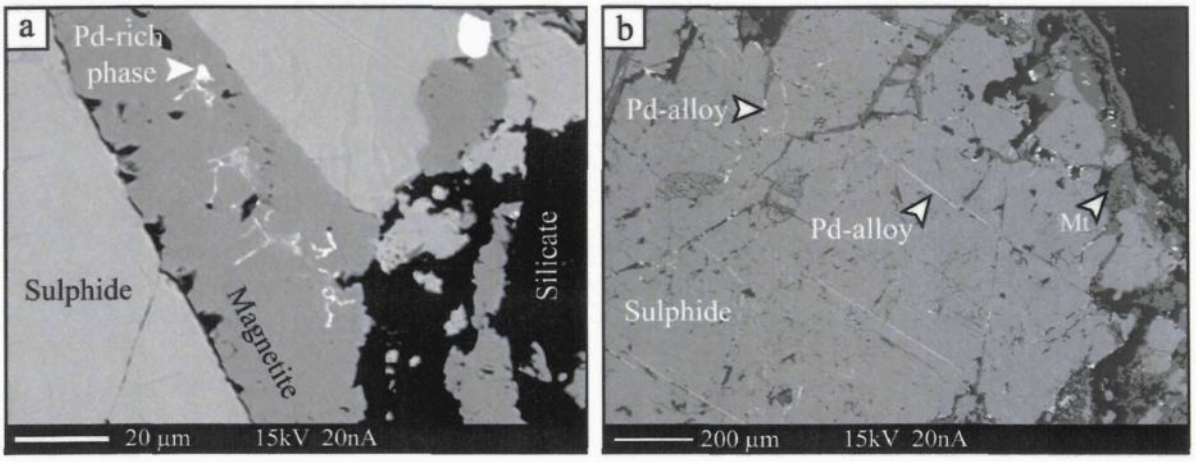

Figure 4.13: Magnetite formation and redistribution of Pd by fluid.

(a) Pd-rich phase (in white) included in magnetite.
(b) Example of textural association of Pd-rich phases which appear as white veinlets in sulfides or included in magnetite.

No textural evidence of Pt addition in our sample was observed in thin section. The origin of the reprecipitated Pd is difficult to constrain. The Pd may originally have been close to its present location (cm scale), or it may have been transported much further (m or km scale) by the fluids. Hanley *et al.* (2005) have shown that volatiles may have removed S, Cu, Pd, and some Pt from the cumulates below the J-M Reef. So, one possibility is that some of the remobilized Pd and Pt observed in our sample are from the cumulate below the reef.

Lead isotopic data (McCallum et al., 1999) and oxygen isotopes analyses (Lechler *et al.*, 2002) indicate that a post-emplacement hydrothermal event coeval to the recrystallization of the sulfides at low temperature has occurred. Alteration of the silicate minerals by non magmatic fluid has also been reported. Page (1977) described a foliation defined by magnetite and serpentine similar to the foliation observed in our samples. The author interpreted this foliation and the common occurrence of secondary chlorite and epidote in the samples as evidence of greenschsit facies metamorphism between 1.7 Ga and 1.6 Ga (Nunes and Tilton, 1971).

In addition, Polovina *et al.* (2004) observed Cl-rich amphibole in their samples of J-M Reef and indicated that the alteration may have not exceeded 350°C. To date, our data does not place constraints on the temperature or on the possible composition of the fluid.

4.10.3. - Implications on the model of formation of the J-M Reef

Integration of the above considerations for all of our samples allow us to propose the following model for the formation of the J-M Reef.

A new magma (high-Mg basalt) entered into the magma chamber which contained a crystal mush overlain by a fractionated silicate liquid. The new magma mixed vigorously with the resident magma. As olivine, pyroxene, and/or plagioclase crystallize the magma became sulfide saturated which triggered the formation of immiscible sulfide droplets (Fig. 4.14a). These droplets interacted with a large volume of magma (N-factor up to 45 000) and collected the PGE and base metals to form PGE-rich sulfide droplets (Fig. 4.14a). Magma chamber instabilities (*e.g.* earthquakes) triggered the collection of these droplets of sulfides to a vertical network (Godel *et al.*, 2006) and possibly augmented the downward migration of the sulfide liquid into the cumulate pile. As temperature dropped, the BMS minerals were partially desulfurized. The partial desulfurization of the BMS minerals triggered the removal (25 to 50 wt%) of the initial sulfur content. The sulfur removal triggered an enrichment of the remaining sulfide in PGE. The partial desulfurization of the BMS minerals may be due to percolation of fluid (possibly S-undersaturated intercumulate liquid or vapor formed during degassing of the magma chamber). The magma chamber instabilities could have triggered a heterogeneous upward migration of the fluid creating some channelways enriched in fluid (as in sand volcanoes formed during earthquakes). We could imagine that the amount of sulfur removed depended on the volume of fluid which

had interacted with the BMS minerals (highest content for ST12 and ST16, the rocks which have the lowest S/Se ratio). As temperature dropped, the MSS enriched in PGE formed pyrrhotite and pentlandite and the ISS formed chalcopyrite and some PGM exsolved and migrated to BMS grains boundaries. However, this simple model does not explain the reason why the samples more enriched in Pd (high Pd/Pt or Pd/Ir ratios, e.g. ST14) are not necessarily those which have undergone the highest sulfide removal (ST12 and ST16). So, other processes are necessary to explain the high Pd (and to a lesser extent Pt enriched) samples. We could imagine that during alteration or metamorphism processes, a new fluid percolated through the cumulate pile (Fig. 4.14d) and removed Pd and Pt from the footwall. As the fluid migrated it could have reacted with the sulfides to form secondary magnetite (Fig. 4.14e), Pd-enriched pentlandite and precipitated Pd-rich phases which were trapped by the magnetite (Fig. 4.14f). The S released during the alteration of the sulfide to magnetite could have reacted with Cu to form secondary chalcopyrite which is commonly found associated with the alteration minerals or found as tiny grains along cleavage planes in the minerals. The variability of the Pd (or PGE) grade observed along the J-M Reef of the Stillwater Complex would probably reflect the different contribution of each process in different parts of the reef.

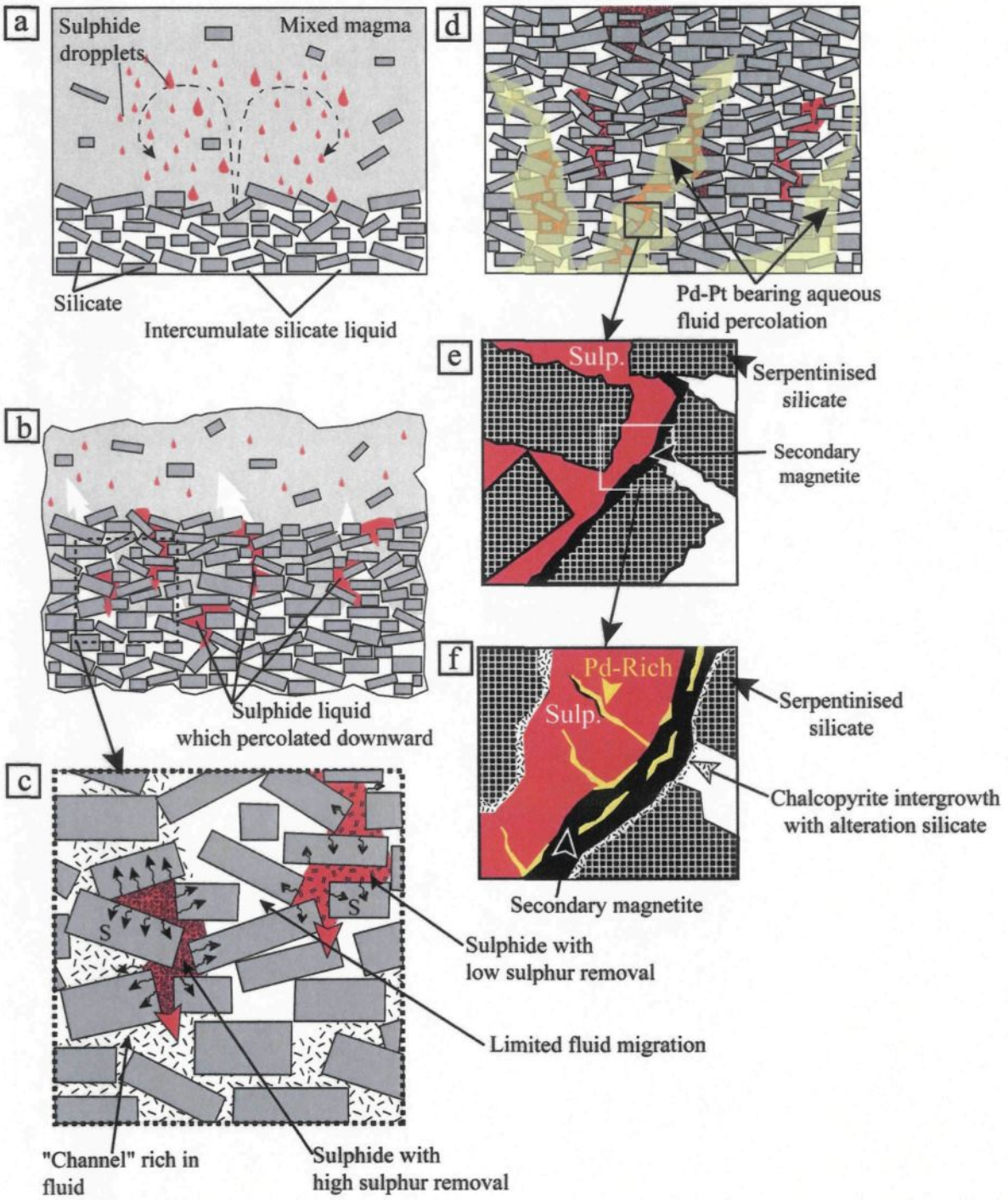
a
Sulphide dropplets
Mixed magma
Silicate
Intercumulate silicate liquid
b
Sulphide liquid which percolated downward
c
S
S
"Channel" rich in fluid
Sulphide with high sulphur removal
Limited fluid migration
Sulphide with low sulphur removal
d
Pd-Pt bearing aqueous fluid percolation
e
Sulp.
Serpentinised silicate
Secondary magnetite
f
Pd-Rich
Sulp.
Serpentinised silicate
Chalcopyrite intergrowth with alteration silicate
Secondary magnetite

Figure 4.14: Model of formation for the J-M Reef.

(a) As a new magma entered the chamber it mixed with the resident magma and became progressively saturated in an immiscible sulfide liquid. Droplets of immiscible sulfide liquid formed, interacted with a large quantity of silicate magma (N-factor = 45 000) and collected the PGE they encountered.
(b) Magma chamber instabilities triggered the connection of the sulfide droplets into vertical networks facilitating the downward percolation of the sulfide liquid in the cumulate pile.
(c) Fluid interacted with the BMS minerals and triggered their partial desulfurization. The desulfurization is more pronounced in zone where the fluid content is greater (upward migration channelways). The PGE content is enriched in the remaining BMS minerals due to the sulfur removal.
(d) As the system cooled, new Pd-bearing fluid percolated in the cumulate pile
(e) These aqueous fluids triggered the alteration of the BMS minerals to magnetite. Sulfur is released and then reprecipitated as secondary chalcopyrite around silicate in an alteration zone.
(f) Palladium may be precipitated as alloy, and is found enclosed in the secondary magnetite, or found as veinlets crosscutting the BMS minerals (see Fig. 10) and may enhance the Pd content of the BMS minerals by diffusion of Pd into the pentlandite lattice.

4.11. - CONCLUSION

Palladium and Pt are the PGE which are the most abundant in our mineralized J-M Reef samples (up to 244 ppm for Pd and 166 ppm for Pt) with an average Pd/Pt ratio of 3.3. Palladium and Pt have a different behaviour in BMS minerals. Palladium is mainly partitioned into pentlandite whereas Pt is almost exclusively found as PGM and does not partition in BMS. The other PGE are essentially found in BMS minerals.

The S/Se ratios and the presence of secondary magnetite in some samples, suggest that some samples have lost 20 to 50% of their original S. But the samples which have undergone the highest S removal are not necessarily those which contain extensive secondary magnetite. In other words, the processes which have triggered the removal of S and the alteration to magnetite are probably different. Our modeling results suggest that the PGE (and more precisely the Pd enrichment) of the J-M Reef can be summarized in three steps. First, the PGE are collected by an immiscible sulfide liquid which interacted with a large volume of magma with a composition similar to the Bushveld Complex magmas, or to most high-Mg basalts. Then magma chamber instabilities trigger the partial desulfurization of the BMS minerals and the enrichment of the remaining BMS minerals in PGE. In a final step, an aqueous fluid leached Pd, and to a lesser extent Pt, from the footwall of the reef. This fluid precipitated Pd in the reef and altered the BMS minerals to magnetite. During this step Pd may crystallize as Pd-alloy and/or substitute for Ni in pentlandite to form a high-Pd bearing pentlandite.

4.12. – ACKNOWLEDGMENTS

Stillwater Mining Company is thanked for hosting the "9th International Platinum Symposium" field trip and allowing sampling of the J-M Reef cores. Richard Cox (UQAC) is thanked for his assistance with the LA-ICP-MS analysis. Paul Bédard and Dany Savard (UQAC) are thanked for their advice and assistance during the whole rock analysis. Marc Choquette (Laval University) is thanked for his assistance with the microprobe analysis. Michael Zientek and an anonymous reviewer are thanked for their constructive comments. This work was funded by a Discovery Grant from Natural Science and Engineering Research Council of Canada and the Canadian Research Chair in Magmatic Metallogeny.

4.13. - REFERENCES

Barnes, S.-J. & Maier, W. D. 2002. Platinum-group elements and microstructures of Normal Merensky Reef from Impala Platinum Mines, Bushveld Complex. Journal of Petrology 43, 1, 103-128.

Barnes, S.-J. & Lightfoot, P. C. 2005. Formation of Magmatic Nickel Sulfide Deposits and Processes Affecting their copper and Platinum Group Element Contents. Economic Geology 100th Anniversary Volume, 179-213.

Barnes, S.-J., Cox, R. & Zientek, M. 2006. Platinum-group element, Gold, Silver and Base Metal distribution in compositionally zoned sulfide droplets from the Medvezky Creek Mine, Noril'sk, Russia. Contributions to Mineralogy and Petrology 152, 2, 187-200.

Barnes, S. J. & Naldrett, A. J. 1985. Geochemistry of the J-M Howland Reef of the Stillwater Complex, Minneapolis Adit Area. I. Sulfide Chemistry and Sulfide-Olivine Equilibrium. Economic Geology 80, 627-645.

Barnes, S. J. & Naldrett, A. J. 1986. Geochemistry of the J-M Reef of the Stillwater Complex, Minneapolis Adit Area II. Silicate Mineral Chemistry and Petrogenesis. Journal of Petrology 27, 4, 791-825.

Barnes, S.-J., Makovicky, E., Makovicky, M., RoseHansen, J. & KarupMoller, S. 1997. Partition coefficients for Ni, Cu, Pd, Pt, Rh, and Ir between monosulfide solid solution and sulfide liquid and the formation of compositionally zoned Ni-Cu sulfide bodies by fractional crystallization of sulfide liquid. Canadian Journal of Earth Sciences 34, 4, 366-374.

Bédard, L. P. & Barnes, S. J. 2002. A comparison of the capacity of FA-ICP-MS and FA-INAA. Journal of Radioanalytical and Nuclear Chemistry 254, 2, 319-329.

Boudreau, A. E. & Mc Callum, I. S. 1992a. Concentration of Platinum-Group Elements by Magmatic Fluids in Layered Intrusions. Economic Geology 87, 7, 1830-1848.

Boudreau, A. E. & Mc Callum, I. S. 1992b. Infiltration Metasomatism in Layered Intrusions - an Example from the Stillwater Complex, Montana. Journal of Volcanology and Geothermal Research 52, 1-3, 171-183.

Bow, C., Wolfgram, D., Turner, A. R., Barnes, S. J. & Evans, J. 1982. Investigations of the Howland Reef of the Stillwater Complex, Minneapolis Adit area: stratigraphy, structure, and mineralization. Economic Geology 77, 1481-1492.

Brügmann, G. E., Naldrett, A. J., Asif, M., Lightfoot, P. C., Gorbachev, N. S. & Fedorenko, V. A. 1993. Siderophile and chalcophile metals as tracers of the evolution of the Siberian Trap in the Noril'sk region, Russia. Geochimica et Cosmochimica Acta 57, 9, 2001-2018.

Cabri, L. J., Blank, H., El Goresy, A., Laflamme, J. H. G., Nobiling, R., Sizgoric, M. B. & Traxel, K. 1984. Quantitative trace-element analyses of sulfides from Sudbury and Stillwater by proton microprobe. Canadian Mineralogist 22, 521-542.

Campbell, I. H. & Naldrett, A. J. 1979. The influence of silicate silicate: sulfide ratios on the geochemistry of magmatic sulfides. Economic Geology 74, 1503-1505.

Campbell, I. H., Naldrett, A. J. & Barnes, S. J. 1983. A Model for the Origin of the Platinum-Rich Sulfide Horizons in the Bushveld and Stillwater Complexes. Journal of Petrology 24, 2, 133-165.

Crocket, J. H. 2002. Platinum-Group Element Geochemistry of Mafic and Ultramafic Rocks. In: Cabri, L. J. ed. Geology, Geochemistry, Mineralogy and Mineral benefication of Platinum Group Element. Canadian Institute of Mining, Metallurgy and Petroleum, Special Volume 54, 553-580.

Czamanske, G. K. & Zientek, G. K. 1985. The Stillwater Complex, Montana : geology and guide. ed. Butte, Montana: Montana College of Mineral Science and Technology, Special publication / Montana Bureau of Mines and Geology, no. 92, 396.

Czamanske, G. K. & Loferski, P. J. 1996. Cryptic trace-element alteration of anorthosite, Stillwater Complex, Montana. Canadian Mineralogist 34, 559-579.

Gervilla, F., Cabri, L. J., Kojonen, K., Oberthür, T., Weiser, T. W., Johanson, B., Sie, S. H., Campbell, J. L., Teesdale, W. J. & Laflamme, J. H. G. 2004. Platinum-Group Element Distribution in Some Ore Deposits: Results of EPMA and Micro-PIXE Analyses. Microchimica Acta 147, 3, 167-173.

Godel, B., Barnes, S.-J. & Maier, W. D. 2006. 3-D Distribution of Sulfide Minerals in the Merensky Reef Bushveld Complex, South Africa and the J-M Reef Stillwater Complex, USA and their Relationship to Microstructures Using X-Ray Computed Tomography. Journal of Petrology 47, 1853-1872.

Godel, B., Barnes, S.-J. & Maier, W. D. in press. Platinum-group elements in sulfide minerals, platinum-group minerals and the whole rock of the Merensky Reef Bushveld Complex, South Africa: Implication for the formation of the reef. Journal of Petrology

Hanley, J. J., Mungall, J. E. & Spooner, E. T. C. 2005a. Fluid and melt inclusion evidence for platinum-group element transport by high salinity fluids and halide melts below the J-M Reef, Stillwater Complex, Montana, U.S.A. 10th International Platinum Symposium "Platinum-Group Elements - from Genesis to Beneficiation and Environmental Impact", Törmänen, T. O. & Alapieti, T. T., Oulu, Finland, Geological Survey of Finland, Extended Abstract, 94-97.

Hanley, J. J., Pettke, T., Mungall, J. E. & Spooner, E. T. C. 2005b. The solubility of platinum and gold in NaCl brines at 1.5 kbar, 600 to 800°C: A laser ablation ICP-MS pilot study of synthetic fluid inclusions. Geochimica et Cosmochimica Acta 69, 10, 2593-2611.

Kinloch, E. D. 1982. Regional Trends in the Platinum-Group Mineralogy of the Critical Zone of the Bushveld Complex, South-Africa. Economic Geology 77, 6, 1328-1347.

Kullerud, G., Yund, R. A. & Moh, G. H. 1969. Phase relations in the Cu-Fe-S, Cu-Ni-S and Fe-Ni-S systems. Economic Geology Monograph no. 4, 323-343.

Lechler, P. J., Arehart, G. B. & knight, M. 2002. Multielement and isotopic geochemistry of the J-M Reef, Stillwater Intrusion, Montana. 9th International Platinum symposium, Billings, Abstract Programm, 245-248.

Li, C. & Ripley, E. M. 2006. Formation of Pt-Fe alloy by desulfurization of Pt-Pd sulfide in the J-M Reef of the Stillwater Complex, Montana. Canadian Mineralogist 44, 895-903.

Li, C., Ripley, E. M., Merino, E. & Maier, W. D. 2004. Replacement of base metal sulfides by actinolite, epidote, calcite, and magnetite in the UG2 and Merensky Reef of the Bushveld Complex, South Africa. Economic Geology 99, 1, 173-184.

Li, C., Barnes, S.-J., Makovicky, E., Rose-Hansen, J. & Makovicky, M. 1996. Partitioning of Ni, Cu, Ir, Rh, Pt, and Pd between monosulfide solid solution and sulfide liquid: Effects of composition and temperature. Geochimica et Cosmochimica Acta 60, 7, 1231-1238.

Lorand, J. P., Alard, O., Luguet, A. & Keays, R. R. 2003. Sulfur and selenium systematics of the subcontinental lithosperic mantle: Inferences from the Massif Central xenolith suite France. Geochimica et Cosmochimica Acta 67, 21, 4137-4151.

Mason, P. R. D. & Kraan, W. J. 2002. Attenuation of spectral interferences during laser ablation inductively coupled plasma mass spectrometry LA-ICP-MS using an rf only collision and reaction. Journal of Analytical Atomic Spectrometry 17, 8, 858-867.

McCallum, I. S., Raedeke, L. D. & Mathez, E. A. 1980. Investigations of the Stillwater Complex: Part I. Stratigraphy and Structure of the Banded Zone. American Journal of Science 280-A, 59-87.

McCallum, I. S., Thurber, M. W., O'Brien, H. E. & Nelson, B. K. 1999. Lead isotopes in sulfides from the Stillwater Complex, Montana: evidence for subsolidus remobilization. Contributions to Mineralogy and Petrology 137, 3, 206-219.

McDonough, W. F. & Sun, S. S. 1995. The composition of the Earth. Chemical Geology 120, 223-253.

Mungall, J. E., Andrews, D. R. A., Cabri, L. J., Sylvester, P. J. & Tubrett, M. 2005. Partitioning of Cu, Ni, Au, and platinum-group elements between monosulfide solid solution and sulfide melt under controlled oxygen and sulfur fugacities. Geochimica et Cosmochimica Acta 69, 17, 4349-4360.

Naldrett, A. J. 1989. Magmatic Sulfide Deposits. ed. Oxford University Press, 189.

Naldrett, A. J., Gasparrini, E. C., Barnes, S. J., Von Gruenewaldt, G. & Sharpe, M. R. 1986. The Upper Critical Zone of the Bushveld Complex and the Origin of Merensky-Type Ores. Economic Geology 81, 5, 1105-1117.

Nunes, P. D. & Tilton, G. R. 1971. Uranium-lead ages of minerals from the Stillwater Complex and associated rocks, Montana. Geological Society of America Bulletin 82, 2231-2250.

Page, N. J. 1976. Serpentinization and alteration in an olivine cumulate from the Stillwater Complex, southwestern Montana. Contributions to Mineralogy and Petrology 54, 127-137.

Page, N. J. 1977. Stillwater Complex, Montana: rock succesion, metamorphism and structure of the complex and adjacent rocks. U.S. Geological Survey Professional paper, 999,

Page, N. J. & Zientek, M. L. 1985. Geologic and Structural setting of the Stillwater Complex. In: Czamanske, G. K. & Zientek, M. L. ed. The Stillwater Complex, Montana: geology and guide. Butte, Montana: Montana Bureau of Mines and Geology, Special Publication, no. 92, 1-8.

Pan, P. & Scott, S. A. 1994. Solubility of Pt and Pd sulfides and Au metal in aqueous bisulfide solutions. Mineralium Deposita 29, 5, 373-390.

Polovina, J. S., Hudson, D. M. & Jones, R. E. 2004. Petrographic and geochemical characteristics of postmagmatic hydrothermal alteration and mineralization in the J-M Reef, Stillwater Complex, Montana. Canadian Mineralogist 42, 261-277.

Premo, W. R., Helz, R. T., Zientek, M. L. & Langston, R. B. 1990. U-Pb and Sm-Nd ages for the Stillwater Complex and its associated sills and dikes, Beartooth Mountains, Montana: Identification of a parent magma? Geology 18, 1065-1068.

Prichard, H. M., Barnes, S.-J., Maier, W. D. & Fisher, P. C. 2004. Variations in the nature of the platinum-group minerals in a cross-section through the Merensky Reef at Impala Platinum: Implications for the mode of formation of the reef. Canadian Mineralogist 42, 423-437.

Steele, T. W., Levin, J. & Copelowitz, I. 1975. Preparation and certification of a reference sample of a precious metal ore. National Institute for Metallurgy Report, 1696-1975.

Turner, A. R., Wolfgram, D. & Barnes, S. J. 1985. Geology of the Stillwater County sector of the J-M Reef, including the Minneapolis Adit. In: Czamanske, G. K. & Zientek, M. L. ed. The Stillwater Complex, Montana : geology and guide. Butte, Montana: Montana Bureau of Mines and Geology, Special Publication, no. 92, 210-230.

Willmore, C. C., Boudreau, A. E. & Kruger, F. J. 2000. The halogen geochemistry of the Bushveld Complex, Republic of South Africa: Implications for chalcophile element distribution in the lower and critical zones. Journal of Petrology 41, 10, 1517-1539.

Wood, S. A. 2002. The Aqueous Geochemistry of the Platinum-Group Elements with Applications to Ore Deposits. In: Cabri, L. J. ed. Geology, Geochemistry, Mineralogy and Mineral benefication of Platinum Group Element. Canadian Institute of Mining, Metallurgy and Petroleum, Special Volume 54, 211-249.

Zientek, M. L. & Oscarson, R. L. 1986. Textural association of platinum-group minerals from the J-M Reef, Stillwater Complex, Montana. U.S. Geological Survey Circ. 995, 75-76.

Zientek, M. L., Czamanske, G. K. & Irvine, T. N. 1985. Stratigraphy and nomenclature for the Stillwater Complex. In: Czamanske, G. K. & Zientek, M. L. ed. The Stillwater Complex, Montana : geology and guide. Butte, Montana: Montana Bureau of Mines and Geology, Special Publication, no. 92, 21-32.

Zientek, M. L., Foose, M. P. & Mei, L. 1986. Palladium, Platinum, and Rhodium Contents of Rocks near the Lower Margin of the Stillwater Complex, Montana. Economic Geology 81, 1169-1178.

Zientek, M. L., Cooper, R. W., Corson, S. R. & Geraghty, E. P. 2002. Platinum-Group Element Mineralization in the Stillwater Complex, Montana. In: Cabri, L. J. ed. Geology, Geochemistry, Mineralogy and Mineral benefication of Platinum Group Element. Canadian Institute of Mining, Metallurgy and Petroleum, Special Volume 54, 459 - 481.

CHAPITRE 5

IMAGES ANALYSIS AND COMPOSITION OF PLATINUM-GROUP MINERALS IN THE J-M REEF OF THE STILLWATER COMPLEX (U.S.A.)

BELINDA GODEL and SARAH-JANE BARNES

SCIENCES DE LA TERRE, UNIVERSITE DU QUEBEC A CHICOUTIMI, QC, G7H 2B1, CANADA

Economic Geology

5.1. – RESUMÉ

Une étude detaillée des minéraux du groupe du platine (analyse géochimique et analyse d'image) a été réalisée sur des échantillons minéralisés du J-M Reef (contenant de 49 à 419 ppm de Pt+Pd avec un rapport Pd/Pt de 3.3). Le J-M Reef est un des niveaux enrichis en EGP du Complexe de Stillwater (Montana, Etats-Unis) qui a subit un métamorphisme au faciès schiste vert.

Cette étude est un complément à l'analyse antérieure par LA-ICP-MS de la concentration en EGP dans les sulfures (pyrrhotite, pentlandite et chalcopyrite) du J-M Reef.

Le but de ces études était de déterminer quelles sont les phases qui contiennent la plupart des EGP, d'examiner les relations texturales qui existent entre les différentes phases, et d'utiliser ces observations pour développer un modèle de formation pour le J-M Reef.

Les minéraux du groupe du platine (MGP) observés dans les échantillons sont composés essentiellement de : sulfures de Pd+/-Pt ; d'alliages de Pt-Fe (isoferroplatinum) ; de tellures de Pd+/-Pt et d'alliages de Pd-Cu (Skaergaardite). Quelques autres MGP plus rares ont été observés : Pd natif, des sulfures de Ru-Ir-Os (laurite) et des alliages de Au-Pd-Ag (électrum riche en Pd).

La plupart des MGP observés sont associés à des sulfures: soit inclut dans ces sulfures ou localisés au contact entre les sulfures et les silicates ou les oxydes. Les textures des MGP contenus dans les sulfures ou localisés à leurs bordures suggèrent que ces MGP se sont exsolvés à partir des sulfures. Pour ces minéraux, nous suggérons que les EGP, Ni,

Cu et Te avaient été initialement colléctés par un liquide sulfuré et se soient « dissous » dans les sulfures qui ont cristallisé à partir de ce liquide.

L'isoferroplatinum (alliage de Pt-Fe) et certains des sulfures de Pd se seraient exsolvés à partir des sulfures lors d'un épisode de désulfurisation à haute température. Au contraire, la skaergaaardite (alliage de Pd-Cu) et certains sulfures de Pd sont associés à de la magnétite secondaire et se seraient formés à plus basse température (~250-465°C). Ces minéraux auraient pu se former pendant l'épisode de métamorphisme de faciès schiste vert qui a affecté le complexe.

Le rapport Pd/Pt des roches minéralisés (moyenne de 3.3) sont supérieurs à ceux de la plupart des magmas mafiques alors que le rapport Pd/Pt des roches situées sous la zone minéralisée est beaucoup plus faible (0.3 à 0.7). Il est possible qu'une partie du Pd dans la zone minéralisée ait été lessivée des roches sous-jacentes et déposée au niveau du reef durant la formation de magnétite secondaire.

5.2. – ABSTRACT

Detailed image and geochemical analysis of the platinum-group minerals were conducted on mineralized samples of the J-M reef, Stillwater complex (Montana, U.S.A.). This study complements a LA-ICP-MS investigation of the platinum-group element (PGE) concentrations in the base metal sulfide minerals (pyrrhotite, pentlandite and chalcopyrite) of the reef. The aims of both studies were: to determine which phases are the main hosts of the PGE, to examine the textural relationships of these phases; and to use the observations to develop a model for the genesis of the reef. The platinum-group minerals (PGM) observed in our samples consist of: Pd+/-Pt sulfides; Pt-Fe alloy (isoferroplatinum); Pd+/-tellurides and Pd-Cu alloy (skaergaardite) with minor Pd alloy; Ru-Ir-Os sulfides (laurite) and Au-Pd-Ag alloy (palladian electrum). Most of these platinum-group minerals are closely associated with base metal sulfide (BMS) minerals: either included in the BMS or located at the contact between the BMS and the silicates or oxides. The texture of the PGM within the BMS and at the margins of BMS suggests that they exsolved from the BMS. We suggest for these minerals that the PGE, Ni, Cu and Te partitioned into a magmatic sulfide liquid and that these elements were accommodated in the BMS that crystallized from the sulfide liquid. The Pt-Fe alloys and some of the Pd sulfides exsolved from the BMS during desulfidization at fairly high temperatures. In contrast the skaergaardite and some Pd sulfides are found in association with secondary magnetite and formed at lower temperatures (~250-465 °C). These minerals could have formed during greenschist facies metamorphism or late magmatic cooling. The Pd/Pt ratio of the reef (3.3) is higher than most mafic magmas and Pd/Pt ratio of the footwall is lower (0.3 to 0.7). It is possible that

some of the Pd in the reef was leached from the underlying rocks and deposited in the reef as the Pd-rich PGM that is associated with the secondary magnetite.

5.3. – INTRODUCTION

Large mafic and ultramafic layered intrusions, such as the Bushveld Complex (South Africa) or the Stillwater Complex (Montana, U.S.A.) contain stratiform layers which are enriched in platinum-group element (PGE). These layers are referred to as "reef". In both Bushveld and Stillwater complexes, the PGE are found associated with disseminated (usually 0.5 to 5 vol%) base-metal sulfide minerals (BMS) consisting mainly of pyrrhotite, pentlandite and chalcopyrite. The PGE are found either in solid solution in BMS or as platinum-group minerals (PGM). In many cases, the PGM are associated with the BMS or found in alteration halos around the sulfides (Godel et al., 2007; Zientek et al., 1986; Li et al., 2004; Polovina et al., 2004; Prichard et al., 2004). Several processes have been proposed to explain the local concentration of the PGE: (i) the direct crystallization from the magma as platinum-group mineral (Hiemstra, 1979); (ii) the collection of PGE by an immiscible sulfide liquid which interacted with a large volume of silicate magma (Campbell et al., 1983; Naldrett et al., 1986); (iii) the collection of the PGE by magmatic fluids enriched in Cl (Boudreau and McCallum, 1992a; Boudreau, 1999; Willmore et al., 2000). Low temperature alteration of the reefs and PGE redistribution is known to have occurred (Li et al., 2004; Polovina et al., 2004).

Contrary to the Bushveld Complex, the Stillwater Complex has been affected by several hydrothermal events which have altered the rocks (Czamanske and Loferski, 1996) and possibly remobilize the BMS and modify the PGE content found in the reef (Bow et al., 1982; Boudreau and McCallum, 1992; Godel and Barnes, 2007; Polovina et al., 2004).

Heyse (1983) in their estimation of the host of Pd and Pt in the Stillwater mine area (Fig.1) reported: (i) for Pd, 80 % of Pd in pentlandite; 15% of Pd hosted in Pd-sulfides and 5% of Pd as tellurides; (ii) for Pt, 67% as Pt-sulfides, 25% as Pt-Fe alloy and the remaining Pt as tellurides. Zientek and Oscarson (1986) studied the platinum-group minerals from a sample (~5 cm^2) of the J-M Reef and reached a similar conclusion. They found ~160 PGM grains (mostly Pd-Pt telluride and Pt-Fe alloy) and concluded that the entire Pt budget is hosted by PGM and that ~20 % of Pd is contained in PGM with the remaining Pd hosted by Pd-rich pentlandite.

In a recent work, Godel and Barnes (2007) studied the PGE and chalcophile element contents in BMS and the whole rock of the J-M Reef package (footwall, reef and hanging wall) from the East Boulder Mine (Fig. 5.1). For the mineralized samples, we have found that: (i) almost all (99.9%) of Pt and Au are hosted by phases other than BMS; (ii) a large portion (~45 to 100%) of Pd, Ir and Rh are present in BMS and (iii) ~3 to 20% of Os is found in BMS. Consequently, phases other than BMS must accommodate almost all the Pt, Au and to a lesser extent Os and ~40-50 % of the remaining PGE (Pd, Ir, Ru and Rh). Numerical modeling using PGE contents in BMS and whole rocks (Godel and Barnes, in press) of the J-M Reef indicate that these elements were initially collected by a sulfide liquid which had interacted with a magma having a PGE content close to that of a high-Mg basalt, but were then redistributed by fluids during alteration events.

Thus, a detailed analysis of the platinum-group minerals (PGM) was conducted on the samples used by Godel and Barnes (in press) in order to test whether the PGM have recorded the same alteration events. The aims of this paper are to determine: (1) which

PGM are present in the samples; (2) the size of the PGM; (3) the relationship between the PGM and the others phases (alteration silicates, magnetite, sulfide etc.); (4) whether there is a variation in type of PGM and/or textural occurrence as a function of host lithologies or alteration. These observations are then used to suggest an origin of the PGM and the possible role of fluid on PGE and other metal redistribution.

5.4. - GEOLOGY, PETROLOGY AND GEOCHEMISTRY

The 2705 +/- 4 Ma old (U-Pb age, Premo et al., 1990) Stillwater Complex (Montana, U.S.A.) is a layered ultramafic to mafic intrusion which intruded middle to late Archean metasediments (Fig. 5.1). The Stillwater Complex is the host to two layers enriched in PGE: the J-M Reef and the Picket Pin Deposit (Fig. 5.1). The samples studied in this work are from the J-M Reef package at the East Boulder mine. The J-M Reef is a disseminated PGE-enriched sulfide mineralization which contains the highest Pt+Pd grade (~18 ppm) of all known PGE deposits (Zientek et al., 2002). This layer is associated with the olivine-bearing cumulate (OB-1) of the Lower Banded Series (Turner et al., 1985; Zientek et al., 1985; Barnes and Naldrett, 1986).

Detailed descriptions of the samples are presented in Godel and Barnes (2007) thus only a brief description of the samples is outlined below. Our samples are troctolite, anorthosite, leuconorite and olivine meta-gabbronorite with ~1 to ~ 5 wt% BMS. The samples contain ~49 to 419 ppm PGE. Palladium and Pt represent more than 95 % of the whole rock PGE content with a Pd/Pt ratio which varying from 1.3 to 5.2 (average 3). In

many cases, the disseminated BMS are found as network along silicates (plagioclase, pyroxene and olivine) boundaries (Godel et al., 2006). The proportion of each sulfide varies between the samples: pyrrhotite represents ~32 to 52 wt%; pentlandite represents 27 to 38 wt% and chalcopyrite represents ~18 to 28 wt%. Pentlandite is the BMS which hosts most of the PGE in solid-solution. Palladium is essentially concentrated in pentlandite and it represents ~98% of the PGE found in the BMS. Almost all (99.9%) of Pt and Au are hosted by phases other than BMS. A large portion (~45 to 100%) of Pd, Ir and Rh are present in BMS and ~3 to 20% of Os is found in BMS. Consequently, other phases must accommodate almost all the Pt, Au and to a lesser extent Os and ~ 40-50 % of the remaining PGE (Pd, Ir, Ru and Rh).

The samples are strongly altered (~20 to ~60%). Primary silicates are partially replaced by chlorite, actinolite, tremolite, serpentine and talc. In many cases, these alteration silicates are found associated with tiny grains of chalcopyrite and secondary magnetite. In some cases, the secondary magnetite may crosscut the primary silicate defining a "foliation" but does not necessarily crosscut the BMS.

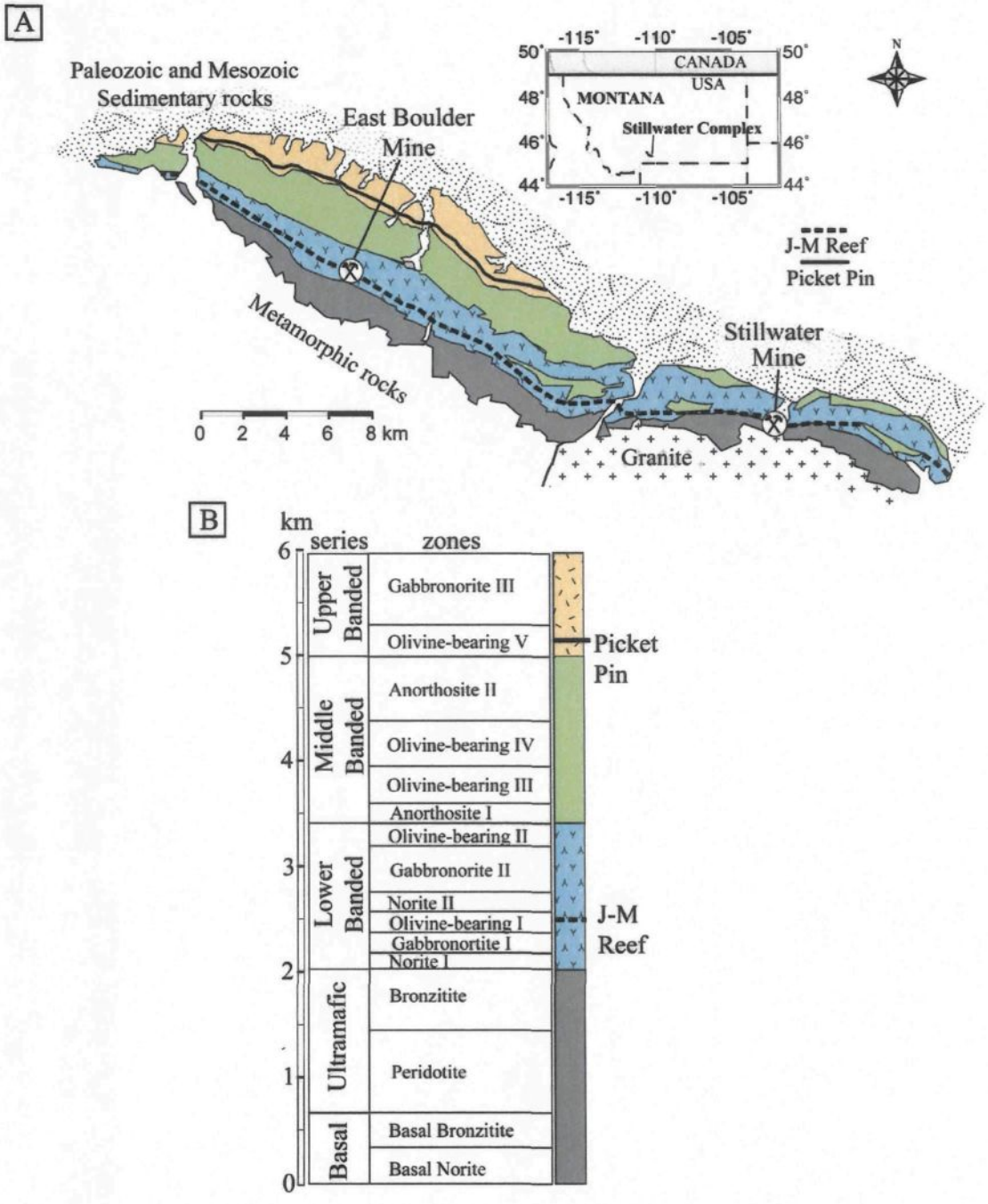

Figure 5.1: Simplified geological and stratigraphy of the Stillwater Complex, Montana, U.S.A. Modified from Zientek et al. (2002).

5.5. - METHODOLOGY

5.5.1. - Quantitative and qualitative analysis of PGM

Backscattered (BSE) image analysis of four sections representing the different lithologies of the J-M Reef of the Stillwater Complex at the East Boulder Mine was carried out using the scanning electron microprobe at Laval University (Quebec City). As these PGM are very small, determining the exact composition of PGM could be carried out only on a few grains. The other PGM were characterized using energy dispersive spectra. The microprobe was operated at 15 kV and 20 nA with a beam diameter of 2 μm with counting time of 20 s and 10 s on peak and backgrounds. The results of the quantitative analysis are summarized in Table 1. The standards used were from Astimex Microanalysis Standard and from P and H Developments Ltd: pure Pt, pure Au, G2Ir for Ir, hematite for Fe, pure Sn, Au80Ag20 for Ag, pyrite for S, G2Os for Os, AgTe for Te, PdS for Pd, pure Ru, BiTe for Bi, and Galena As for As.

5.5.2. - Image analysis of the PGM

Backscattered images were collected for each PGM. The measurement of each PGM was carried out using automated PGM boundaries extraction from the BSE images followed by analysis with ImageJ software (a PC version of NIH image). Firstly, for each image, the boundaries of each PGM were calculated using in-house IDL (ITT Visual Information Solutions) code and new black and white scaled 8-bit images (masks) of the PGM were created. The PGM are in black on the images. The real size of each image was

calculated using the scales on the BSE images. Secondly, each mask was imported into ImageJ and analysed using particle measurements function, which calculates many parameters such as the area; the position, the perimeter, the major and minor axis and, the orientation of each PGM. An example of PGM extraction and area calculation is shown in Fig. 5.2. The textural association of each PGM with other phases was noted and included in the database. The results of all analyses are summarized in Tables 5.2, 5.3 and 5.4.

5.6. - RESULTS

More than 850 grains of PGM were located, identified and measured on four sections of ~ 10 cm^2 each. Eight types of PGM were found: (i) Pd +/-Pt telluride; (ii) Pd +/-Pt sulfide; (iii) Pt-Fe alloy; (iv) Ru-Ir-Os sulfide; (v) Pd electrum; (vi) Pd-Pb alloy; (vii) Pd-Cu alloy and (viii) native Pd. These PGM occur in different textural settings and are described in detail below (Table 5.3 and 5.4).

Three sections contain a similar group of PGM and will be described first. One thin section contained Pd-Cu alloy, native Pd and only four other PGM grains (2 grains of Pt-Fe alloy and 2 of Pd-Pt tellurides). As the paragenesis of this sample appears different it will be described and treated separately.

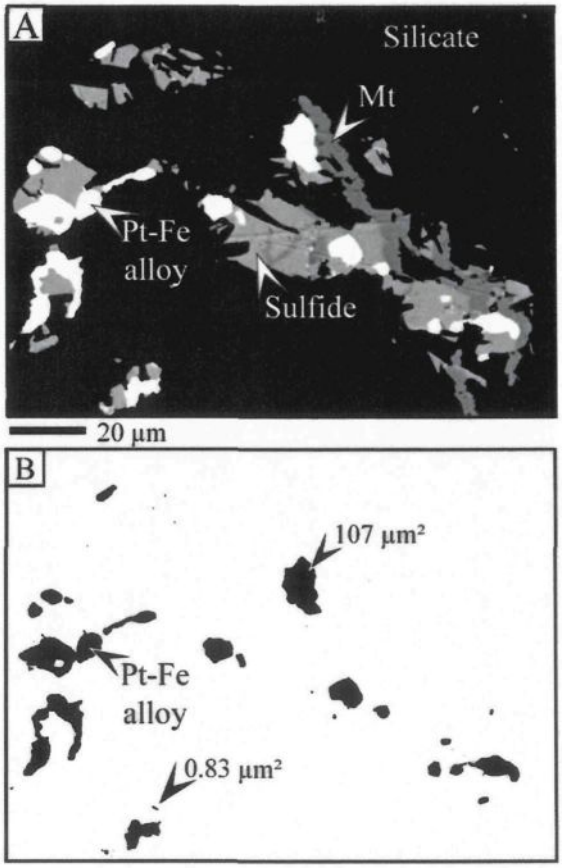

Figure 5.2: Example of automated PGM boundaries extraction from BSE images.

a) Backscattered images of Pt-Fe alloy associated with base metal sulfides and/or magnetite (Mt).
b) "Mask" after the PGM boundaries extraction. The areas of some Pt-Fe grain calculated are given as examples.

Table 5.1: *Quantitative analysis of platinum-group minerals found in our section of J-M Reef at the East Boulder mine (Stillwater Complex).*

		Pd-Pt telluride											
Section		ST12	ST12	ST12	ST12	ST15	ST16	ST 16	ST12	ST12	ST12	ST12	ST15
Mineral		TP	TP	TP	TP	TP	TP	TP	KE	KE	MO	KE	KE
Ni	wt%	-	-	-	-	-	-	-	-	0.26	0.09	-	-
Cu	wt%	-	-	-	-	-	-	-	-	2.02	-	-	-
Au	wt%	-	0.76	0.06	-	0.36	-	-	0.00	-	-	-	1.26
Pt	wt%	0.41	0.71	-	0.66	0.71	-	-	0.07	0.01	31.88	0.25	0.35
Ir	wt%	0.46	0.07	0.19	-	-	0.69	-	0.00	-	-	0.00	0.01
Fe	wt%	1.72	0.24	0.17	0.20	0.42	1.43	1.26	0.22	3.73	0.14	0.37	0.23
Sn	wt%	0.03	0.02	-	0.02	-	-	-	0.01	-	-	0.57	0.67
Ag	wt%	-	-	-	8.22	6.80	-	-	-	-	-	-	-
S	wt%	0.15	0.02	0.03	0.05	0.03	0.03	0.02	0.04	3.12	0.05	0.05	0.02
Os	wt%	-	0.03	0.01	0.07	-	-	-	0.02	-	-	0.07	6.00
Te	wt%	31.53	30.34	32.18	32.18	39.12	33.03	32.77	27.45	29.98	53.39	14.24	24.69
Pd	wt%	62.02	63.01	63.47	60.03	51.64	64.63	64.32	66.60	58.55	8.42	69.88	66.62
Ru	wt%	-	-	-	-	-	-	-	-	-	-	-	-
Bi	wt%	3.37	4.12	0.77	0.15	0.05	0.13	0.53	1.95	0.87	1.13	3.28	0.44
As	wt%	0.36	0.60	0.45	0.37	0.05	0.52	0.30	0.32	-	-	5.94	0.13
Pb	wt%	-	-	-	-	-	-	-	-	-	-	-	-
Total	wt%	100.05	99.92	97.33	101.94	99.18	100.47	99.20	96.68	98.53	95.08	94.65	94.43
Ni	*at%*	-	-	-	-	-	-	-	-	*0.45*	*0.22*	-	-
Cu	*at%*	-	-	-	-	-	-	-	-	*3.21*	-	-	-
Au	*at%*	-	*0.44*	*0.04*	-	*0.21*	-	-	-	-	-	-	*0.76*
Pt	*at%*	*0.24*	*0.42*	-	*0.37*	*0.42*	-	-	*0.04*	*0.01*	-	*0.15*	*0.21*
Ir	*at%*	*0.27*	*0.04*	*0.11*	-	-	*0.40*	-	-	-	*24.33*	*0.00*	*5.00*
Fe	*at%*	*3.45*	*0.50*	*0.35*	*0.39*	*0.86*	*2.84*	*2.53*	*0.45*	*6.74*	*0.37*	*0.76*	*0.49*
Sn	*at%*	*0.02*	*0.02*	-	*0.02*	-	-	-	*0.01*	-	-	*0.55*	*0.67*
Ag	*at%*	-	-	-	*8.40*	*7.25*	-	-	-	-	-	-	-
S	*at%*	*0.52*	*0.08*	*0.09*	*0.16*	*0.10*	*0.12*	*0.05*	*0.14*	*9.82*	*0.21*	*0.16*	*0.09*
Os	*at%*	-	*0.02*	*-7.00*	*0.04*	-	-	-	*0.02*	-	-	*0.04*	*5.00*
Te	*at%*	*27.73*	*27.30*	*29.20*	*27.80*	*35.25*	*28.63*	*28.83*	*25.01*	*23.74*	*62.29*	*12.71*	*22.97*
Pd	*at%*	*65.42*	*68.00*	*69.08*	*62.19*	*55.81*	*67.18*	*67.86*	*72.76*	*55.61*	*11.78*	*74.82*	*74.35*
Ru	*at%*	-	-	-	-	-	-	-	-	-	-	-	-
Bi	*at%*	*1.81*	*2.26*	*0.43*	*0.08*	*0.03*	*0.07*	*0.29*	*1.09*	*0.42*	*0.80*	*1.79*	*0.25*
As	*at%*	*0.54*	*0.92*	*0.69*	*0.55*	*0.07*	*0.77*	*0.45*	*0.49*	-	-	*9.03*	*0.20*
Pb	*at%*	-	-	-	-	-	-	-	-	-	-	-	-

TP: telluropalladinite; KE: keithconnite; MO: moncheite
at% : atomic percent

Table 5.1 (Continued)

		Pd-Pt sulfide											
Section		ST15	ST16	ST16	ST16	ST15	ST15	ST12	ST12	ST12	ST12	ST15	ST15
Mineral		KE	KE	KE	CO	BR	VY	BR	BR	BR	BR	BR	BR
Ni	wt%	0.03	-	0.12	-	2.45	10.7	6.15	6.44	4.11	5.73	4.86	5.49
Cu	wt%	0.01	0.19	-	-	0.02	-	-	-	-	-	0.02	-
Au	wt%	-	-	-	0.47	-	-	-	-	-	-	-	-
Pt	wt%	-	-	7.00	81.46	49.34	9.21	35.87	20.44	43.65	19.91	34.43	27.28
Ir	wt%	-	-	-	-	-	-	-	-	-	-	-	-
Fe	wt%	0.35	0.47	0.30	0.73	0.01	-	0.51	0.27	0.22	0.02	0.09	-
Sn	wt%	-	-	-	0.01	-	-	-	-	-	-	-	-
Ag	wt%	-	-	-	0.3	-	-	-	-	-	-	-	-
S	wt%	0.02	0.03	0.02	14.37	18.33	23.43	20.66	21.72	19.46	21.81	20.14	21.33
Os	wt%	-	-	-	0.05	-	-	-	-	-	-	-	-
Te	wt%	32.85	31.48	31.74	-	-	-	-	-	-	-	-	-
Pd	wt%	61.57	61.33	61.38	2.18	28.1	52.62	34.57	48.21	29.68	48.98	36.03	43.33
Ru	wt%	-	-	-	0.01	-	-	-	-	-	-	-	-
Bi	wt%	-	0.91	0.61	-	-	-	0.02	-	-	-	-	-
As	wt%	-	-	-	-	-	-	-	-	-	-	-	-
Pb	wt%	-	-	-	-	-	-	-	-	-	-	-	-
Total	wt%	94.83	94.41	94.19	99.58	98.25	95.96	97.78	97.08	97.12	96.45	95.57	97.43
Ni	*at%*	*0.07*	-	*0.25*	-	*3.69*	*12.53*	*8.27*	*8.13*	*5.91*	*7.28*	*6.75*	*7.17*
Cu	*at%*	*0.01*	*0.36*	-	-	*0.03*	-	-	-	-	-	*0.03*	-
Au	*at%*	-	-	-	*0.27*	-	-	-	-	-	-	-	-
Pt	*at%*	-	-	*5.00*	*46.14*	*22.36*	*3.24*	*14.51*	*7.76*	*18.91*	*7.61*	*14.37*	*10.71*
Ir	*at%*	-	-	-	-	-	-	-	-	-	-	-	-
Fe	*at%*	*0.74*	*1.00*	*0.65*	*1.44*	*0.02*	-	*0.72*	*0.36*	*0.33*	*0.03*	*0.13*	-
Sn	*at%*	-	-	-	*0.01*	-	-	-	-	-	-	-	-
Ag	*at%*	-	-	-	*0.31*	-	-	-	-	-	-	-	-
S	*at%*	*0.08*	*0.12*	*0.08*	*49.52*	*50.55*	*50.23*	*50.86*	*50.19*	*51.29*	*50.74*	*51.15*	*50.94*
Os	*at%*	-	-	-	*0.03*	-	-	-	-	-	-	-	-
Te	*at%*	*30.51*	*29.38*	*29.72*	-	-	-	-	-	-	-	-	-
Pd	*at%*	*68.59*	*68.63*	*68.94*	*2.27*	*23.35*	*34*	*25.64*	*33.57*	*23.57*	*34.33*	*27.58*	*31.19*
Ru	*at%*	-	-	-	*0.02*	-	-	-	-	-	-	-	-
Bi	*at%*	-	*0.52*	*0.35*	-	-	-	-	-	-	-	-	-
As	*at%*	-	-	-	-	-	-	*0.01*	-	-	-	-	-
Pb	*at%*	-	-	-	-	-	-	-	-	-	-	-	-

CO: cooperite, BR: braggite, VY: vysotskite

Table 5.1 (continued)

Section		ST16	ST16	ST12	ST12	Pt-Fe alloy ST12	ST15	ST15	ST16	ST16	Au-Pd ST12
Mineral		VY	BR	Isoferroplatinum							Pd-electrum
Ni	wt%	8.54	4.06	-	-	-	-	-	-	-	-
Cu	wt%	-	0.21	-	-	-	-	-	-	-	-
Au	wt%	-	-	1.38	0.04	0	0.17	0.78	0	0	87.9
Pt	wt%	2.96	36.49	80.48	84.41	86.12	81.57	84.15	81.34	84.2	-
Ir	wt%	-	-	-	-	-	-	-	-	-	-
Fe	wt%	0.01	0.12	11.35	10.12	9.75	11.76	10.66	10.52	11.29	0.61
Sn	wt%	-	-	0	0	0.04	0	0	0.04	0	-
Ag	wt%	-	-	0.43	0.35	0.34	0.38	0	0.7	0	1.36
S	wt%	23.44	20.1	0.1	0.09	0.09	0.09	0.11	0.08	0.1	0.04
Os	wt%	-	-	0.03	0.14	0.18	0.11	0.13	0.06	0.08	-
Te	wt%	-	-	0.04	0	0	0	0.02	0.04	0	-
Pd	wt%	61.29	36.26	3.63	2.39	2.44	3	3.61	5.59	1.42	8.35
Ru	wt%	-	-	0	0.03	0.06	0	0	0.02	0.03	-
Bi	wt%	-	-	0.01	0	0.03	0.07	0.01	0	0.01	0.31
As	wt%	-	-	0	0	0	0.03	0	0	0	-
Pb	wt%	-	-	-	-	-	-	-	-	-	-
Total	wt%	96.24	97.24	97.45	97.57	99.05	97.18	99.47	98.39	97.13	98.57
Ni	*at%*	*9.91*	*5.62*	-	-	-	-	-	-	-	-
Cu	*at%*	-	*0.26*	-	-	-	-	-	-	-	-
Au	*at%*	-	-	*1.06*	*0.03*	*0*	*0.13*	*0.6*	*0*	*0*	*80.98*
Pt	*at%*	*1.03*	*15.22*	*62.09*	*67.24*	*68.24*	*62.86*	*64.91*	*62.43*	*66.3*	-
Ir	*at%*	-	-	-	-	-	-	-	-	-	-
Fe	*at%*	*0.02*	*0.17*	*30.58*	*28.16*	*26.99*	*31.64*	*28.73*	*28.2*	*31.05*	*1.97*
Sn	*at%*	-	-	-	-	*0.06*	-	-	*0.06*	-	-
Ag	*at%*	-	-	*0.6*	*0.51*	*0.48*	*0.53*	-	*0.97*	*0*	*2.29*
S	*at%*	*49.8*	*51*	*0.47*	*0.43*	*0.41*	*0.4*	*0.52*	*0.36*	*0.48*	*0.24*
Os	*at%*	-	-	*0.02*	*0.12*	*0.15*	*0.09*	*0.1*	*0.05*	*0.06*	-
Te	*at%*	-	-	*0.05*	-	-	-	*0.02*	*0.04*	-	-
Pd	*at%*	*39.24*	*27.73*	*5.13*	*3.48*	*3.54*	*4.24*	*5.11*	*7.87*	*2.05*	*14.25*
Ru	*at%*	-	-	-	*0.04*	*0.1*	*0.01*	*0*	*0.03*	*0.04*	*0.01*
Bi	*at%*	-	-	-	-	*0.02*	*0.05*	*0.01*	-	*0.01*	*0.27*
As	*at%*	-	-	-	-	-	*0.06*	-	-	-	-
Pb	*at%*	-	-	-	-	-	-	-	-	-	-

Table 5.1 (continued)

		Ru-Ir-Os sulfide			Pd-Cu alloy					Pd-Pb alloy	
Section		ST12			ST17					ST12	ST12
Mineral		Laurite			Skaergaardite					Zvyagintsevite	
Ni	wt%	-	-	-	-	-	-	-	0.10	-	-
Cu	wt%	-	-	-	30.76	26.56	30.47	33.08	27.86	-	0.07
Au	wt%	-	-	-	-	-	-	-	-	2.36	1.98
Pt	wt%	-	-	-	0.08	-	-	0.05	-	0.47	0.14
Ir	wt%	13.71	9.89	14.24	-	-	-	-	-	-	-
Fe	wt%	2.42	2.75	3.39	14.61	5.51	7.88	9.25	7.11	0.41	0.28
Sn	wt%	-	-	-	-	-	-	-	-	-	-
Ag	wt%	0.04	-	-	-	-	-	-	-	-	-
S	wt%	27.23	30.43	27.51	-	-	-	-	0.08	-	-
Os	wt%	33.01	8.6	23.54	-	-	-	-	-	-	-
Te	wt%	0.01	-	-	-	-	-	-	-	-	-
Pd	wt%	0.94	1.66	1.09	55.28	61.49	62.39	59.98	60.56	57.54	58.04
Ru	wt%	22.75	45.51	27.69	-	-	-	-	-	-	-
Bi	wt%	-	-	-	-	-	-	-	-	-	-
As	wt%	0.46	-	0.69	-	-	-	-	-	-	-
Pb	wt%	-	-	-	-	-	-	-	-	35.19	35.35
Total	wt%	100.57	98.84	98.15	100.73	93.56	100.74	102.35	95.70	95.98	95.85
Ni	*at%*	-	-	-	-	-	-	-	*0.15*	-	-
Cu	*at%*	-	-	-	*38.24*	*38.19*	*39.73*	*41.64*	*38.49*	-	*0.16*
Au	*at%*	-	-	-	-	-	-	-	-	*1.64*	*1.37*
Pt	*at%*	-	-	-	*0.03*	-	-	*0.02*	-	*0.33*	*0.1*
Ir	*at%*	*5.18*	*3.3*	*5.26*	-	-	-	-	-	-	-
Fe	*at%*	*3.15*	*3.16*	*4.31*	*20.68*	*9.01*	*11.68*	*13.25*	*11.18*	*1.013*	*0.672*
Sn	*at%*	-	-	-	-	-	-	-	-	-	-
Ag	*at%*	*0.02*	-	-	-	-	-	-	-	-	-
S	*at%*	*61.69*	*60.91*	*60.9*	-	-	-	-	*0.22*	-	-
Os	*at%*	*12.61*	*2.9*	*8.79*	-	-	-	-	-	-	-
Te	*at%*	*0.01*	-	-	-	-	-	-	-	-	-
Pd	*at%*	*0.64*	*1*	*0.72*	*41.05*	*52.80*	*48.58*	*45.09*	*49.97*	*73.83*	*74.43*
Ru	*at%*	*16.25*	*28.72*	*19.3*	-	-	-	-	-	-	-
Bi	*at%*	-	-	-	-	-	-	-	-	-	-
As	*at%*	*0.45*	-	*0.65*	-	-	-	-	-	-	-
Pb	*at%*	-	-	-	-	-	-	-	-	-	-

In the three thin sections with a similar PGM association, the percentages represented by each PGM or each type of textural association (taking into account all types of PGM) were calculated in both cases in two different ways: firstly by using the area represented by each PGM and secondly by using the number of PGM grains (Tables 5.2, 5.3 and 5.4). These two types of calculation demonstrate that considering only the number of PGM grains in the calculation may trigger a false estimate of the real volume PGM (or by analogy PGE) abundance. The PGM which are the most numerous are not necessarily those which represent the greatest area (e.g. Pd-Pt sulfides in Table 5.2). Thus, in order to obtain a better estimate of the PGM abundance we will use the percentage calculated using the area represented by each PGM. However, the percentage calculated using the number of PGM is given for reader information and for ease of comparison with other studies.

5.6.1. - Pd-Pt sulfides

Palladium +/- Pt sulfides observed in our J-M Reef samples consists mainly of braggite, cooperite and vysotskite (Table 5.1). These Pd-Pt sulfides are the most common PGM observed in our J-M Reef samples (Table 5.2) and represent 58.9 area% of the PGM found. Most of them (47.8 %) are located as vermicular structures within BMS, but close to the edge of the BMS (Fig. 5.5a). The most common BMS that the PGM are associated with is chalcopyrite (Fig. 5.5a). These Pd-Pt sulfides are interpreted to have exsolved from the chalcopyrite (Fig. 5.5a). Palladium+/- Pt sulfides are also commonly (35 %) found enclosed in alteration silicates (Fig. 5.5b).

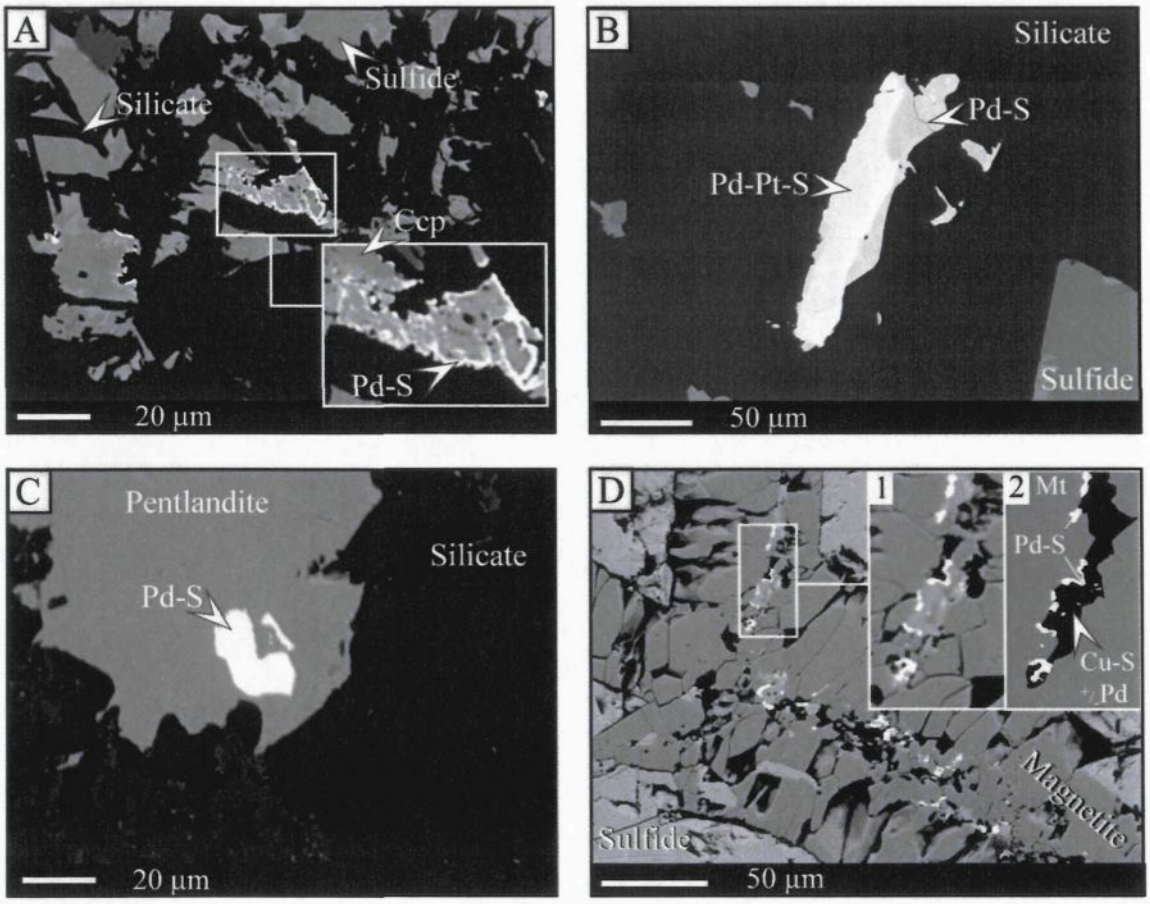

Figure 5.3: Photomicrographs of Pd-Pt sulfides observed in our J-M Reef samples.

a) Pd sulfides found as ragged grains or network associated with chalcopyrite. The Pd sulfides are more common at the contact between the chalcopyrite and the silicates.
b) Pd-Pt sulfide and Pd sulfide closely associated and surrounded by silicates.
c) Ragged Pd sulfide grain included in pentlandite.
d) Pd sulfide found associated with Cu +/- Pd +/- S and included in the central part of secondary magnetite veinlets.

Table 5.2: *Summary of each type of platinum-group mineral found in our samples of J-M Reef at East Boulder mine.*

Type of PGM	Area (μm²)	Number	% Area	% Number
Pd-Pt sulfide	22785	382	58.9	43.8
Pt-Fe alloy	9033	271	23.4	31.1
Pd-Pt telluride	4627	159	12	18.2
Pd-Pb alloy	1067	5	2.8	0.6
Au-Ag-Pd	727	37	1.9	4.2
Ru-Ir-Os sulfide	425	18	1.1	2.1
All PGM	*38664*	*872*	*100*	*100*

Table 5.3: *Summary of each type of textural association of the platinum-group mineral found in our samples of J-M Reef at East Boulder Mine.*

Type of association	Area (μm²)	Number	% Area	% Number
Contact BMS/silicate	16435	272	42.5	31.2
Included in BMS	9077	137	23.5	15.7
Included in silicate	10056	156	26	17.9
Included in magnetite	2095	271	5.4	31.1
Contact BMS/magnetite	302	7	0.8	0.8
Contact magnetite/silicate	689	29	1.8	3.3
All associations	*38654*	*872*	*100*	*100*

Table 5.4: *Textural association of platinum-group mineral found in our samples of the J-M Reef at East Boulder Mine.*

Textural association	Contact BMS/silicate	Included in BMS	Included in silicate	Included in magnetite	Contact magnetite/silicate	Contact magnetite/BMS	All types of association
Pd-Pt sulphides							
Area (μm²)	10884	3240	7969	691	n-o	n-o	22784
Number	95	8	51	228	n-o	n-o	382
% Area	*47.8*	*14.2*	*35*	*3*	*n-o*	*n-o*	*100*
% Number	*24.9*	*2.1*	*13.4*	*59.7*	*n-o*	*n-o*	*100*
Pt-Fe alloy							
Area (μm²)	3525	4369	217	6	298	618	9033
Number	111	108	19	3	5	25	271
% Area	*39*	*48.4*	*2.4*	*0.1*	*3.3*	*6.8*	*100*
% *Number*	*41*	*39.9*	*7*	*1.1*	*1.8*	*9.2*	*100*
Pd-Pt tellurides							
Area (μm²)	1606	53	1567	1397	3.4	n-o	4627
Number	33	4	80	40	2	n-o	159
% Area	*34.7*	*1.1*	*33.9*	*30.2*	*0.1*	*n-o*	*100*
% *Number*	*20.8*	*2.5*	*50.3*	*25.2*	*1.3*	*n-o*	*100*
Pd-Pb alloy							
Area (μm²)	220	847	n-o	n-o	n-o	n-o	1067
Number	4	1	n-o	n-o	n-o	n-o	5
% Area	*20.6*	*79.4*	*n-o*	*n-o*	*n-o*	*n-o*	*100*
% *Number*	*80*	*20*	*n-o*	*n-o*	*n-o*	*n-o*	*100*
Au-Pd-Ag alloy							
Area (μm²)	199	226	302	n-o	n-o	n-o	727
Number	29	2	6	n-o	n-o	n-o	37
% Area	*27.4*	*31.1*	*41.5*	*n-o*	*n-o*	*n-o*	*100*
% *Number*	*78.4*	*5.4*	*16.2*	*n-o*	*n-o*	*n-o*	*100*

Table 5.4 (continued)

Textural association	Contact BMS/silicate	Included in BMS	Included in silicate	Included in magnetite	Contact magnetite/silicate	Contact magnetite/BMS	All types of association
Ru-Ir-Os							
Area (μm^2)	n-o	341	n-o	n-o	n-o	70	425
Number	n-o	14	n-o	n-o	n-o	4	18
% Area	*n-o*	80.2	*n-o*	*n-o*	*n-o*	16.4	100
% Number	*n-o*	77.8	*n-o*	*n-o*	*n-o*	22.2	100

Note: as Pd-Cu alloy occurs in particular ways, this PGM was not taken into account in the calculation and is described in a later section.

n-o: not observed

In this case, these PGM occur as subhedral to ragged grains of ~30-40 μm^2 (ranging from ~1 μm^2 up to 4600 μm^2). The remaining Pd-Pt sulfides are found as subhedral to ragged grains of various size (1 up to 2700 μm^2, geometric mean ~45 μm^2) enclosed by BMS (Fig. 5.5c) and to a lesser extent (3 %) as small (<20 μm^2) ragged grains which are associated with secondary magnetite (Fig. 5.5d). In this case, the Pd-Pt sulfides are located in the central part of secondary magnetite veins (Fig. 5.5d) which crosscut the BMS and are in many cases associated with Cu-S-Pd phases (Fig. 5.5d inset 1 and 2).

5.6.2. - Pt-Fe alloy

Platinum-Fe alloy (Table 5.1 and Fig. 5.6) is the second most abundant PGM observed in our sample and represent 23.4 area% of the PGM observed. The Pt-Fe alloy consists of isoferroplatinum (Pt_3Fe) and contains ~3.2 wt% (ranging from 1.42 to 5.59 wt%) Pd. These results are similar to those of Todd et al. (1982). Isoferroplatinum is in many cases associated with BMS. Most of the grains (48.4 %) are included in BMS (mainly pyrrhotite and pentlandite) where they occur as rounded to ragged grains (Figs. 5.4a, b and c) or are found at the contact between the BMS and silicate minerals (39.0 %). In both cases, the isoferroplatinum grains are large relative to other PGM (~4 up to 1700 μm^2, average ~50 μm^2). The remaining isoferroplatinum grains occur: (i) at the contact between magnetite and BMS (6.8 %); (ii) at the contact between magnetite and silicate (3.3 %, Fig. 5.4); (iii) as inclusion in alteration silicates (2.4 %, Fig. 5.4c) or (iv) as inclusion in magnetite (0.1 %).

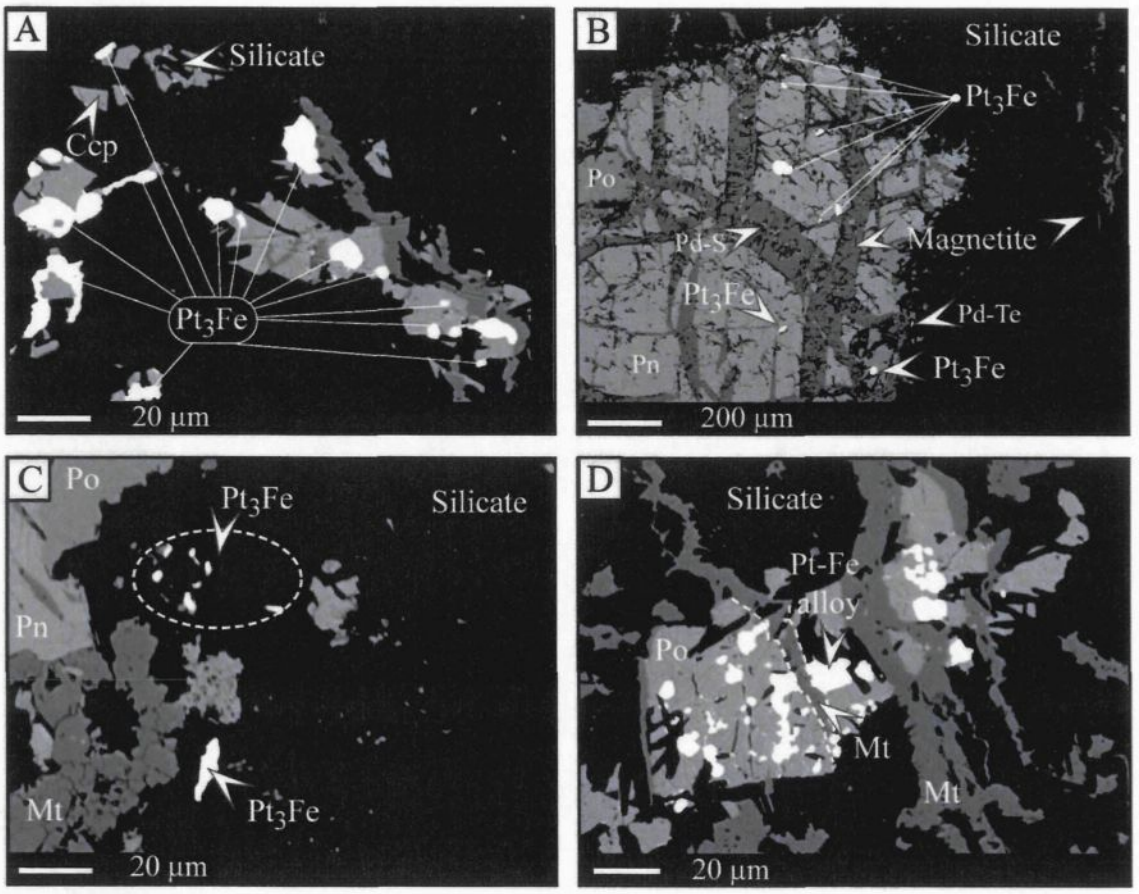

Figure 5.4: Photomicrographs of Pt-Fe alloy observed in our J-M Reef samples.

a) Pt-Fe alloys found associated with base metal sulfides.
b) Euhedral to subhedral grains of Pt-Fe alloy included in base metal sulfides.
c) Ragged grains of Pt-Fe alloys surrounded by alteration silicates.
d) Ragged grains of Pt-Fe alloys included in pyrrhotite and crosscut by secondary magnetite (Mt) stringers.

5.6.3. - Pd-Pt tellurides

The Pd-Pt tellurides represent 12 area% of the all the PGM found in our samples (Table 5.2). These PGM consist of telluropalladinite, keithconnite and kotulskite with minor merenskiite and moncheite (Table 5.1). Palladium-Pt tellurides are in many cases associated with alteration silicates (chlorite, tremolite, actinolite) either located at the contact between BMS and alteration silicates (34.7 %, Fig. 5.5a) or completely enclosed in alteration silicates (33.9 %, Fig. 5.5b). In both cases, the Pd-Pt tellurides occur as subhedral to ragged grains of small size (Fig. 5.5). The mean area (geometric mean) represented by a PGM grain varies from ~ 2.3 to 7.6 μm^2. Only a few large grains (up 610 μm^2 for PGM at contact between silicate/sulfide and up 218μm^2 for those included in alteration silicate) were observed. Some Pd-Pt tellurides (~30.2 %) are found included in secondary magnetite which in many cases replace the BMS, or more rarely, forms a corona around few chromite grains (Fig. 5.5c). These Pt-Pd telluride occur as subhedral to ragged grains which are larger (~8.4 μm^2) than those associated with the silicate minerals. Only four subhedral grains (~1.1 area%) of Pd-Pt telluride were observed as inclusions in BMS (Fig. 5.5d).

5.6.4. - Pd-Pb rich phases

Zvyagintsevite, a Pd-Pb alloy (Fig. 5.6 and Table 5.1) was observed in our sections and represents 2.8 area% of the PGM found. Only one large (~850 μm^2) grain of zvyagintsevite was found included in BMS (pentlandite surrounded by chalcopyrite).

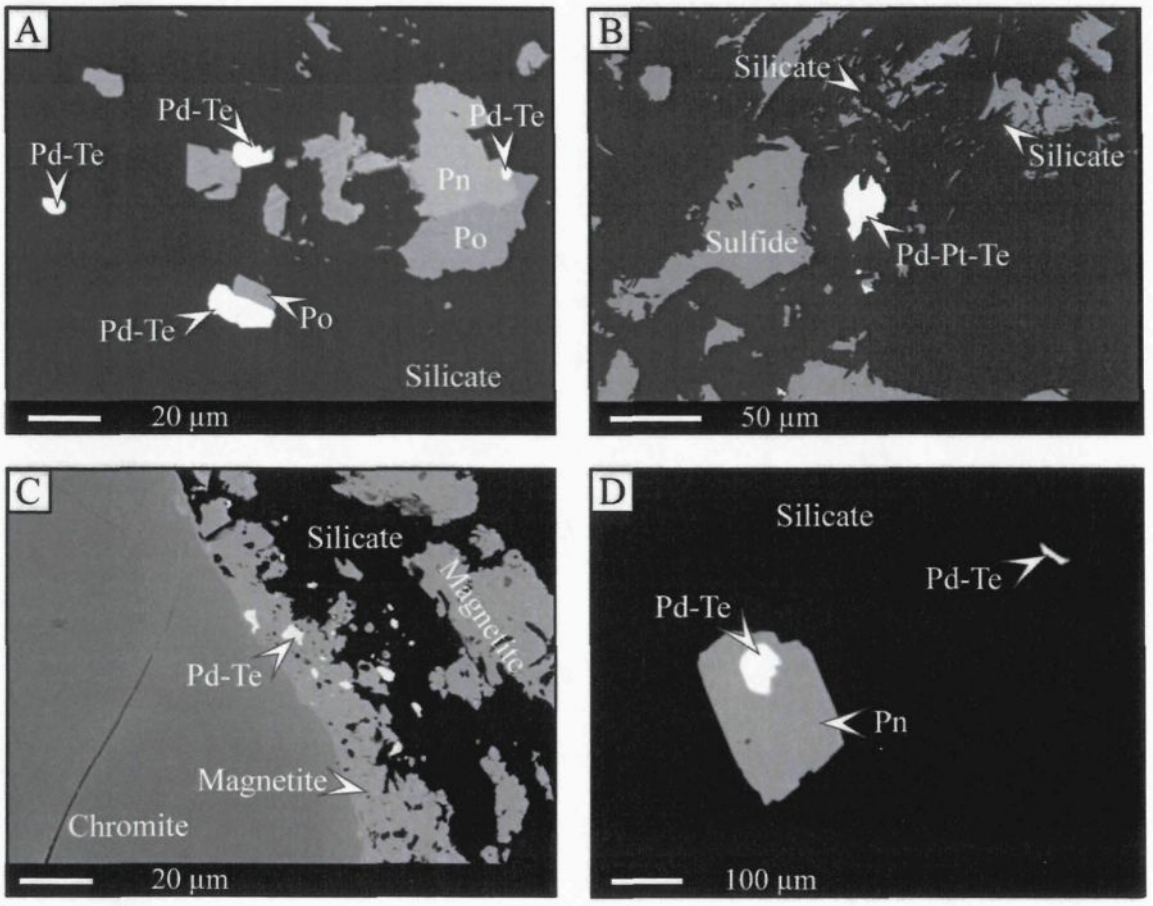

Figure 5.5: Photomicrographs of Pd-Pt tellurides observed in our J-M Reef samples.

a) Pd tellurides located at the contact between the sulfide and silicate minerals.
b) Pd-Pt tellurides surrounded by alteration silicate.
c) Pd tellurides included in secondary magnetite developed around a chromite grain.
d) Pd telluride included in pentlandite (Pn), or surrounded by silicates.

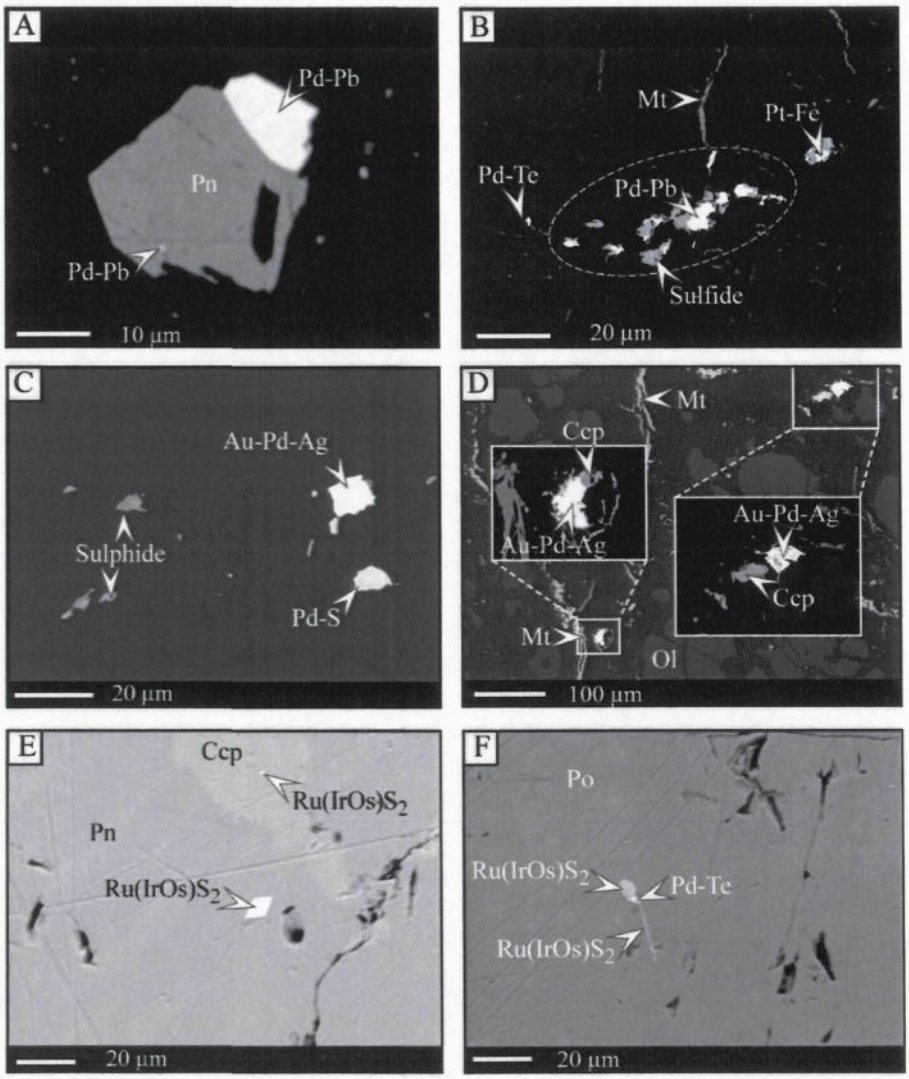

Figure 5.6: Photomicrographs of minor PGM observed in our J-M Reef samples.

a) Subedral grains of Pd-Pb alloy located at the contact between base metal sulfides and silicates or included in the sulfide.
b) Pd-Pb alloy associated with sulfide, Pd telluride, Pt-Fe alloy and secondary magnetite stringers.
c) Ragged grain of Au-Pd-Ag alloy included in silicate and also associated with Pd sulfide.
d) Altered grains of Au-Pd-Ag alloy associated with chalcopyrite and secondary magnetite stringers.
e) Euhedral Ru(Ir,Os) sulfide (Laurite) grain included in pentlandite and tiny laurite grain included in chalcopyrite.
f) Ragged and stringer-shaped grains of laurite associated with Pd telluride, both included in pyrrhotite.

The other grains of zvyagintsevite were observed at the contact between the silicate minerals and the BMS (Fig. 5.8a and b). These grains are smaller (up to 119 μm^2 with a geometric mean of 6.1 μm^2). The zvyagintsevite observed in the J-M reef contains elevated gold content (up to 2.4 wt%). Zvyagintsevite with similar compositions were observed in samples from Noril'sk, Russia (Cabri and Traill, 1966).

5.6.5. - Au-Pd-Ag alloy

Palladian electrum (Au-Pd-Ag alloy, Table 5.1 and Fig. 5.8c and d) represents 1.9 area% of the PGM observed. Most of the palladian electrum (41.5 area%) occurs as ragged patches (up to ~300 μm^2) surrounded by alteration silicates. The remaining palladian electrum are associated with BMS either located at the contact between the silicate and the BMS (27.4 area%) or included in the BMS (31.1 area%). In both case, the palladian electrum occurs as ragged grains of ~100 μm^2 which are, in many cases, associated with chalcopyrite. Elevated content of Pd in Au-rich alloy is also reported from the Lac des Iles complex, Ontario (Cabri and Laflamme, 1981).

5.6.6. - Ru-Ir-Os sulfide

Laurite ($Ru(Ir,Os)S_2$) represents 1.1 area% of the PGM found in our sections (Table 5.2). Most laurite grains (80.2 %) occur as inclusions in BMS as laths, or as ragged or as euhedral grains (Fig. 5.8). The size of the grains of laurites varies from 0.3 to 114 μm^2 (geometric mean of 6.9 μm^2).

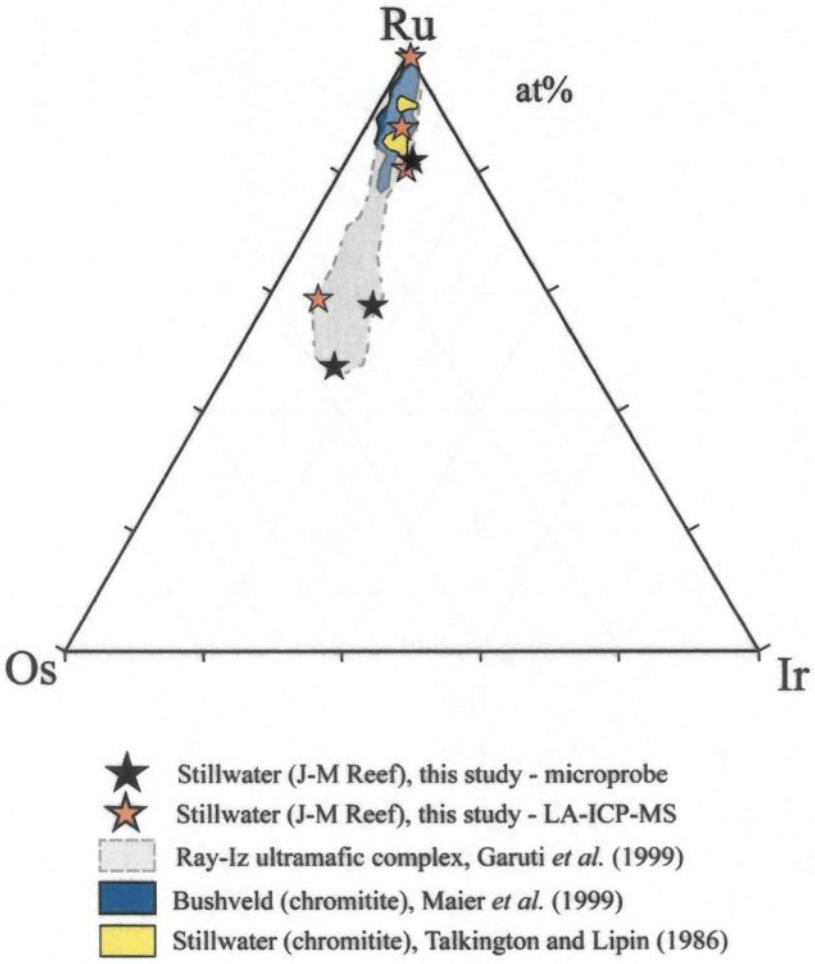

Figure 5.7: Ru-Ir-Os ternary diagram.

Composition of laurite found in the J-M Reef sample (this study), in chromitites of the Union section of the Bushveld complex (Maier et al., 1999), in the chromitite of the Stillwater Complex (Talkington and Lipin, 1986) and in chromitite of ophiolites (Garuti et al., 1999).

The other laurite grains (16.5 %) are observed at the contact between secondary magnetite and BMS and are typically smaller (from 0.3 to 51 μm^2, geometric mean of 5.6 μm^2). The laurites found in our sample of the J-M Reef (Table 5.2, Fig. 5.9) contain various amount of Ru (22.75 to 45. 51 wt%) and are rich in Ir (9.89 to 14.24 wt%) and Os (8.60 to 33.01 wt%). These values are close to values (Fig. 5.9) observed from the Union Section and the Rustenburg Mine in the Western Bushveld Complex (Kingston and El-dosuky, 1982; Maier et al., 1999), the Stillwater Complex (Talkington and Lipin, 1986) or, for the laurite enriched in Os, to values observed in chromitites of the Ray-Iz Complex in Russia (Garuti et al., 1999).

5.6.7. - Pd-Cu alloy

The Pd-Cu alloy (Fig. 5.3 and Fig. 5.4) observed in our sections has compositions similar (Table 5.1 and Fig. 5.4) to skaergaardite recently characterized in the Kangerdlusgssuaq area of the Skaergaard intrusion in East Greenland (Rudashevsky et al., 2004) and also reported for the South Kawishiwi Intrusion of the Duluth Layered Intrusion Complex, Minnesota, U.S.A. (Komppa, 1998). The Pd-Cu alloy observed at Stillwater is composed of: 55.28 to 62.39 wt% Pd, 25.56 to 33.08 wt% Cu and 5.51 to 14.61 wt% Fe (Table 5.1 and Fig. 5.4). In our sample, skaergaardite is in many cases found associated with secondary magnetite, either included in the magnetite (Fig. 5.3a) or located at the contact between magnetite and silicate or BMS (Fig. 5.3b).

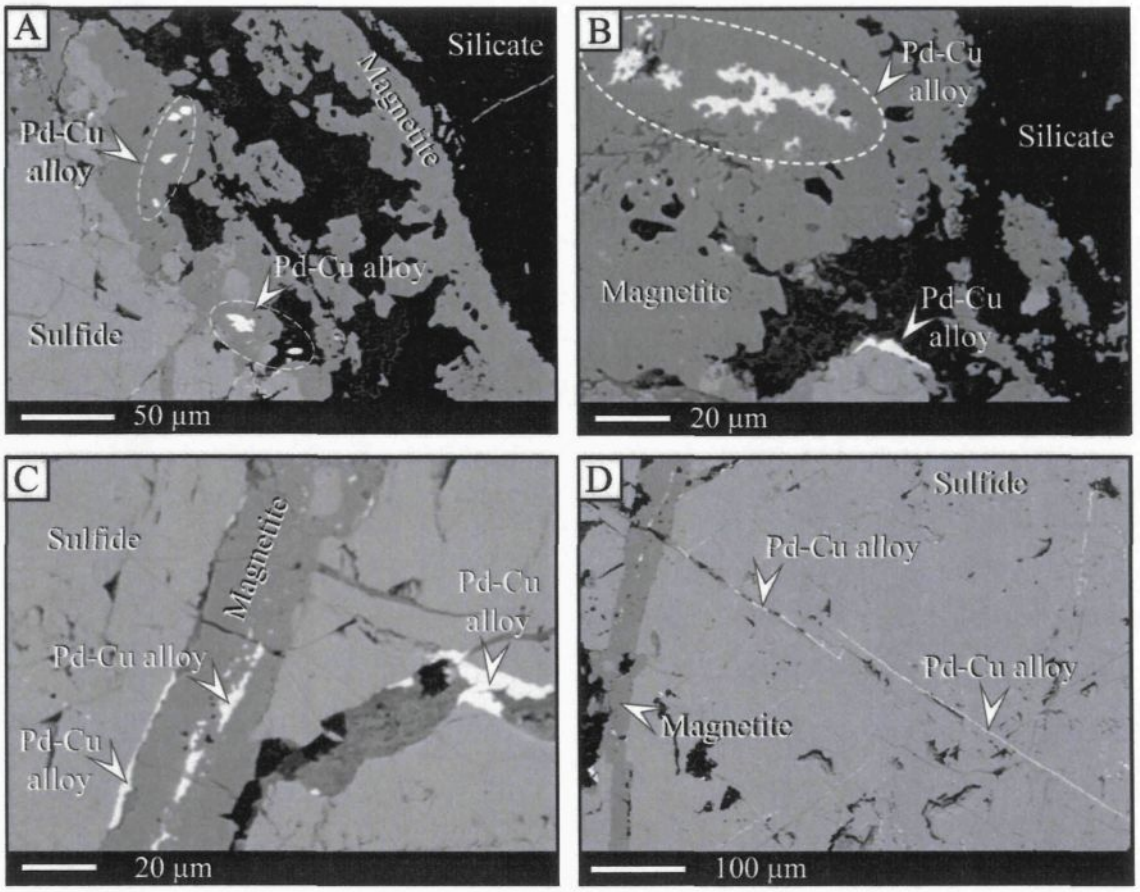

Figure 5.8: Photomicrographs of Pd-Cu alloy observed in our J-M Reef samples.

a) Ragged to subhedral grains of Pd-Cu alloy included in secondary magnetite.
b) Patches of Pd-Cu alloy included in secondary magnetite or located at the contact between alteration silicate and base metal sulfides.
c) Pd-Cu alloy associated with veinlets of secondary magnetite which crosscut the base metal sulfides. Pd-Cu is observed either in the central part of the veinlets or at the wall between the base metal sulfide and the magnetite.
d) Pd-Cu alloy found as narrow veinlets of up to 1 mm in length which crosscut the base metal sulfides.

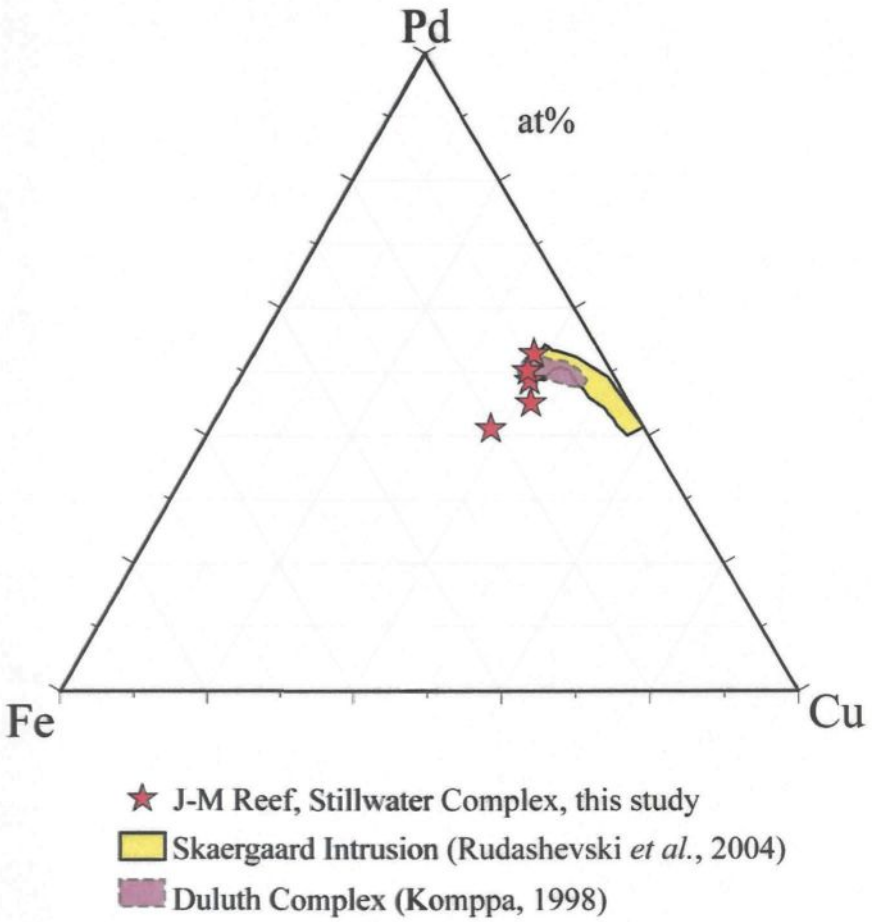

Figure 5.9: Pd-Cu-Fe ternary diagram.

Composition of Pd-Cu found in the J-M Reef sample (this study), compared with examples from the Skaergaard intrusion (Rudashevski et al., 2004) and the Duluth Complex (Komppa, 1998).

Skaergaardite which is found associated with magnetite, occurs in three different forms: as subhedral grains of ~5 to 20 μm (Fig. 5.3a); as networks or disseminated patches (up to 10 μm in width and up to 50 μm in length) which are in many cases found in the central part of magnetite veins and oriented parallel to the vein wall (Fig. 5.3c and d) or, finally, as thin networks (up to 5 μm in width and 50 μm in length) which are located at the boundaries between veins of magnetite and its host BMS (Fig. 5.3c). Skaergaardite may also occur as veinlets (up to 500 μm in length) which crosscut the BMS and which are not necessarily associated with secondary magnetite (Fig. 5.3d). Recently, Barkov et al. (2005) reported rare grains of Pt-rich skaergaardite (skaergaardite-hongshiite series) at the Kirakkajuppura PGE deposit in the Penikat intrusion in Finland. In that case, the skaergaardite was observed in narrow (<10 μm) alteration zones.

5.7. - DISCUSSION

Our PGM analysis indicate that the great majority (~82 area%) of the PGM found in the three thin sections of the J-M Reef consists of Pd (with minor Pt) sulfides and Pt-Fe alloy. The remaining (~18 area%) PGM consist of Pd+/-Pt tellurides and minor electrum, laurite and Pd-Pb alloy. These PGM are in most cases found (68 %) associated with BMS (included in the BMS or located at the contact between silicate and BMS). As previously pointed out by Zientek and Oscarson (1986), the PGM included in the BMS are larger than that found in the other textural modes (Fig. 5.10).

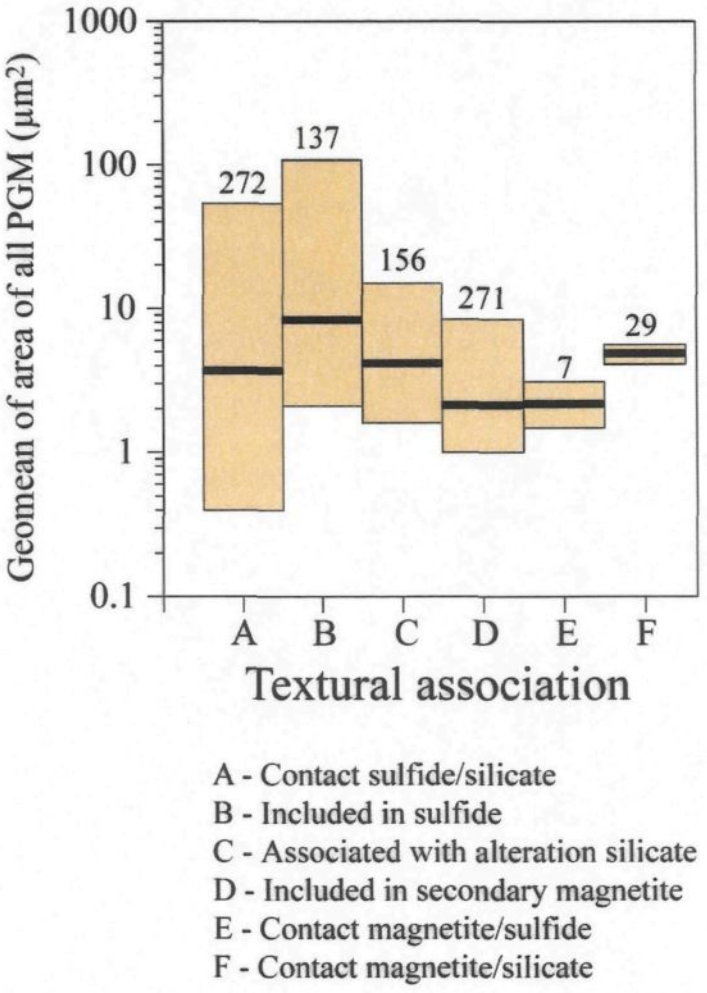

Figure 5.10: Statistics on size of PGM as a function of the textural association.

The other PGM (26 %) are located in alteration zones around sulfides with secondary alteration silicates (mainly chlorite, tremolite, actinolite, serpentine) or secondary magnetite. In the samples which contain secondary magnetite, some PGM are included in magnetite (example of Pd-Cu alloy or Pd sulfide, Fig. 5.3), some are located at the contact between magnetite/silicates and magnetite/sulfides or crosscuting the BMS. Godel and Barnes (in press) have shown that the S, Cu, Ni and PGE contents in the whole rock follow the same trend and this probably reflects the fact that BMS are the principal phases controlling these elements. In addition, the authors concluded that the variation of S/Se ratios and the presence of secondary magnetite in some samples indicate that these samples may have lost 20 to 50% of their original S content.

By considering these results, we infer that sulfides have played an important role in PGE collection (either in solid solution or as PGM). The possible origin (early crystallization, exsolution from sulfide liquid or magma, fluid precipitation etc.) of each type of PGM will be discussed in the light of all results and this allows us to place some constraints on the formation of the J-M Reef.

5.7.1. - Ru-Ir-Os sulfide, Pd-Pt sulfide and Pd-Pt tellurides: PGM exsolution from BMS

In our study, laurite grains are always included in BMS. So there are two possibilities for their formation: (i) either laurite crystallized prior sulfide liquid formation and then was trapped by a newly formed immiscible sulfide liquid or (ii) laurite grains

formed by exsolution from BMS on cooling. Textural evidence indicates that laurite found in the J-M Reef are the result of exsolution from the BMS (Fig. 5.6).

Laurite grains observed in the J-M Reef contain various amounts of Ir and Os (Table 5.1 and Fig. 5.7). Experiments have shown that the Os and Ir content in laurite increases with increasing fS_2 (Brenan and Andrews, 2001) and decreasing temperature. The variation in our laurite compositions may reflect variations in these parameters.

Palladium-Pt sulfides, and to a lesser extent Pd-Pt tellurides, are in many cases associated with BMS (either included in or located at the edge of BMS and other minerals). These elements (Pd, Pt, Te, Bi) were initially partitioned in a sulfide liquid. Godel and Barnes (in press) have modelled the sulfide liquid compositions as follows. As olivine, pyroxene and/or plagioclase crystallized, the possible parental magma (high-Mg basalt) of the J-M reef became sulfide saturated. This may have triggered the formation of immiscible sulfide droplets which interacted with a large volume of magma (N-factor = 45 000) and collected the PGE, Ni and Cu (and possibly Te and Bi). The Pd-Pt sulfide and Pd-Pt tellurides observed in our samples could have exsolved from the BMS during cooling. Experimental studies (Hoffman and MacLean, 1976) have shown that these PGM form at temperature below 760°C. The BMS should be solid and thus the telluride exsolve and migrate to the grain boundaries of the BMS.

5.7.2. - Pt-Fe alloy: Role of sulfur removal

Almost all (~95%) the grains of isoferroplatinum (Pt_3Fe) observed in our samples are associated with BMS (pyrrhotite and pentlandite). This suggests that Pt was initially partitioned into a sulfide liquid. We suggest that the Pt_3Fe is an exsolution product from monosulfide-solid solution (MSS). In one thin section, we found that one Pt_3Fe grain in BMS is crosscut by secondary magnetite veinlets (Fig. 5.6d). This observation implies that Pt_3Fe formed after BMS solidification, but prior to the secondary magnetite.

Experimental work (Peregoedova and Ohnenstetter, 2002; Peregoedova et al., 2004; Peregoedova et al., 2006) has shown that the desulfurization of monosulfide solid solution may trigger the formation of Pt-Fe, IPGE rich MSS and Cu-Pd-Au rich liquid. Modelling based on S/Se ratio of the whole rock and on in situ BMS analysis (Godel and Barnes, in press) indicates that our samples have lost 20 to 50% of their initial S. If we consider that the Pt-Fe alloy formed by desulfurization of the BMS, then one would expect that the "residual MSS" enriched in IPGE would be depleted in Pt. Thus, pyrrhotite and pentlandite which form by exsolution from MSS on cooling would also be depleted in Pt relative to IPGE. Mantle normalized metal patterns for both pyrrhotite and pentlandite show negative Pt anomalies (Fig. 5.11) which reflects the fact that Pt is depleted relative to the other PGE in these minerals. The diagram S/Se vs Pt/Pt* (Fig. 5.11) allows us to more closely consider the effect of desulfurization (indicated by the S/Se ratio in the whole rock) on the Pt anomaly observed for each sulfide. The Pt anomaly (noted Pt/Pt*) is calculated for each sulfide as follows:

$$Pt/Pt^* = Pt_N / (Rh_N \times Pd_N)^{1/2}$$

where Pt_N, Rh_N and Pd_N are for each sulfide the concentrations of Pt, Rh and Pd normalized to mantle value. Normalization values are those of Barnes and Maier (1999). In order to more closely consider the effect of sulfur removal on the PGE content of the BMS, data for BMS and whole rock of the Merensky Reef of the Bushveld Complex (Godel et al., 2007) are plotted in addition to those of the J-M Reef. For both complexes, the size of negative Pt anomaly observed for pyrrhotite (Fig. 5.12a) and pentlandite (Fig. 5.12b) increases (decreasing Pt/Pt*) with decreasing S/Se (increasing desulfurization). These results are in agreement with what is expected for the formation of Pt-Fe alloy from BMS desulfurization. This result is confirmed by the analysis of the platinum-group minerals (Godel et al., 2007) which indicates that the grains of Pt-Fe alloy grains are more abundant (relative to other PGM) in the J-M Reef (~24 area%, Godel and Barnes, 2007) than in the Merensky Reef (~9 area%, Godel, unpublished data). Consequently, the negative Pt anomaly observed in BMS may be the result of the partial desulfurization of the MSS which has led to Pt-Fe alloy formation.

Another line of evidence for desulfurization is that Pd sulfide exsolutions in the chalcopyrite are more abundant at the contact between the silicate and the Cu sulfides (Fig. 5.5a). These textural associations may be another result of the partial desulfurization of the initial MSS. The Pd sulfides developed preferentially at the contact between silicate and BMS, i.e. in a location where the desulfurization would have been favoured.

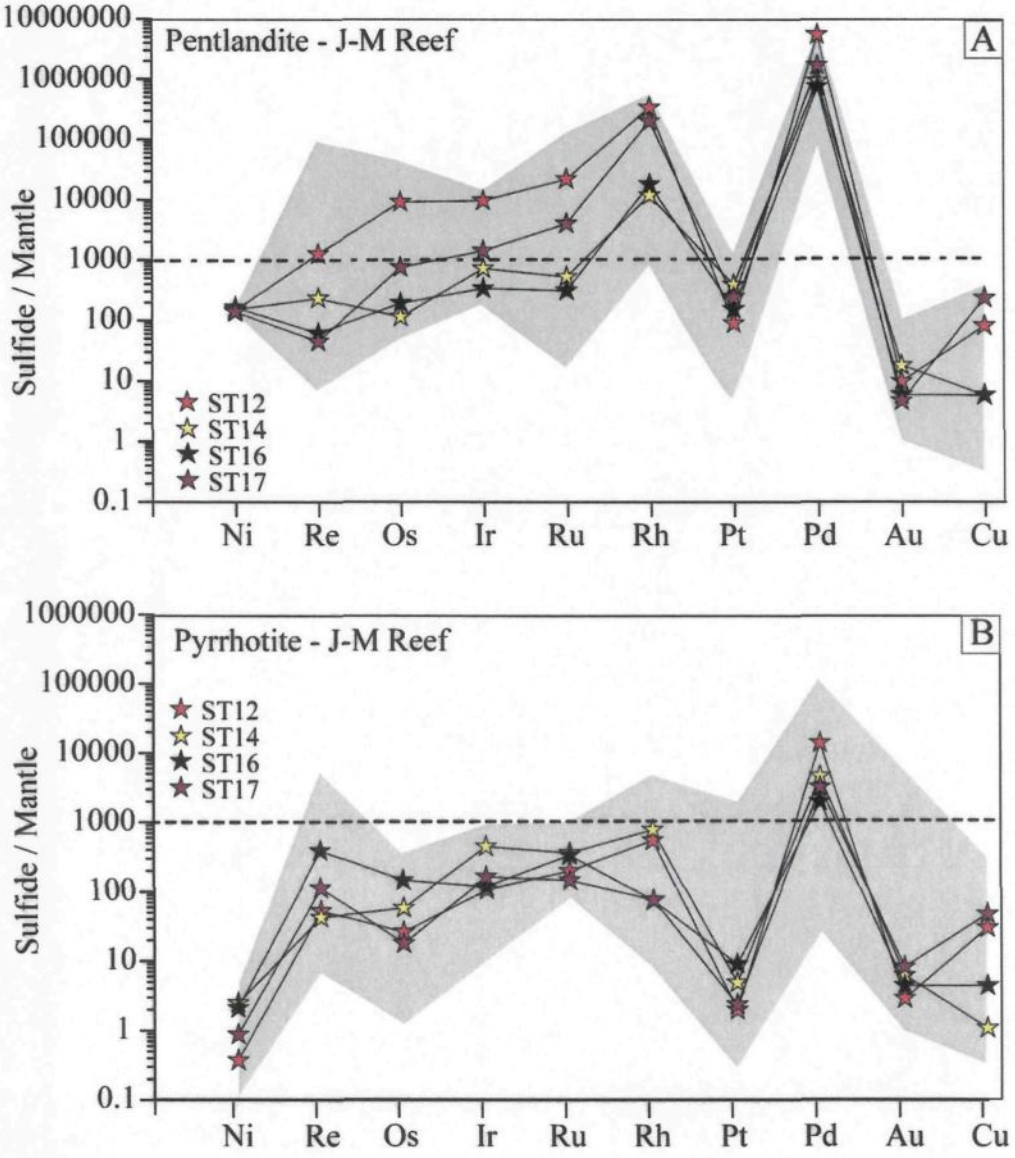

Figure 5.11: Mantle normalized metal patterns for the pyrrhotite and pentlandite of the J-M Reef of the Stillwater Complex.

Data are from Godel and Barnes (2007). The grey areas represent the range of values obtained by considering all analyses. The curves represent the geometric mean of all the values obtained for a given sample.

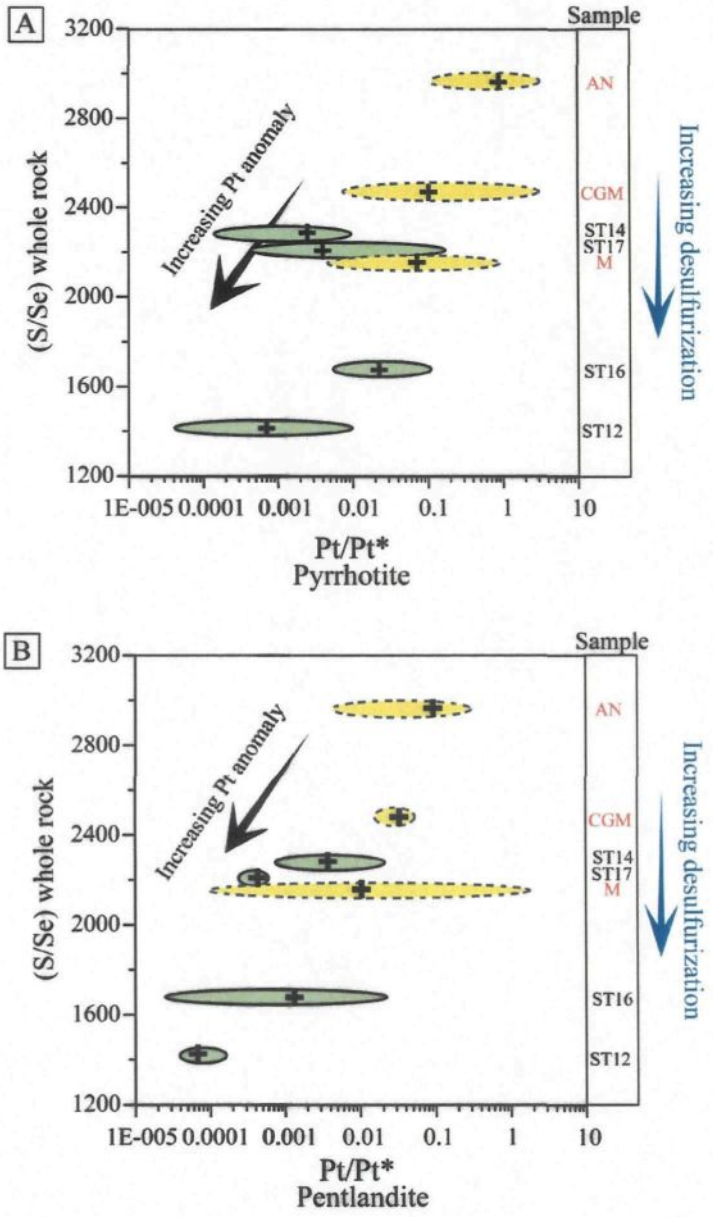

Figure 5.12: Diagram S/Se in the whole rock vs Pt/Pt*.
Each ellipse represents the range of values obtained for each sample and the black cross represents the geometric mean calculated from all the analyses.
The J-M Reef samples are: ST12; ST14; ST16 and ST17. A detailed description and geochemistry of these samples is given in Godel and Barnes (in press).
The samples noted AN, CGM and M are samples from the Merensky Reef of the Bushveld Complex (Godel et al., in press). These refer to anorthosite (AN); coarse-grained melanorite (CGM) and melanorite (M) as described in Godel et al. (2006) and Godel et al. (in press).

5.7.3. - Pd-Cu alloy: Remobilisation of PGE and noble metals

Rudashevsky et al. (2004) characterized the skaergaardite in the Skaergaard intrusion. They found that skaergaardite occurs as droplets and as subhedral to euhedral or irregular grains (from 2 to 75 μm in size) and is, in many cases, associated with bornite, chalcocite, digenite and chalcopyrite. Experimental work (Baker et al., 1992; Karup-Möller and Makovicky, 1999; Makovicky, 2002), the shape of grains and their textural association allowed the authors to conclude that two immiscible melts formed: (i) a Cu-rich sulfide liquid and (ii) a Pd-rich sulfide liquid. They suggested that the Pd-Cu alloy crystallized from the Pd-rich sulfide melt.

In our case, skaergaardite occurs in a very different form. Skaergaardite was found as irregular patches included in secondary magnetite or as veinlets crosscutting the BMS (Fig. 5.3). This indicates that the BMS were already solid when the Pd-Cu alloy formed and that the formation of skaergaardite is probably coeval with the formation of the secondary magnetite. Phase relations in the Cu-Fe-Ni-S system (Craig and Kullerud, 1969) indicate that at temperatures below ~780 °C the BMS would have been completely solidified.

Rudashevsky et al. (2004) determined that skaergaardite has a CsCl-type structure (also called β-PdCu). According to the Pd-Cu phase diagram (Subramanian and Laughlin, 1991), the skaergaardite of the composition observed in our sample, orders to a CsCl-type structure between ~250 and 465 °C (Fig. 5.13). These values are only estimates, but they are in agreement with our textural observations. These observations imply that: (i) either Pd

and Cu were remobilized by fluid from the surrounding BMS and precipitated as Pd-Cu with magnetite or (ii) Pd and Cu were added to the rocks during alteration and/or metamorphism.

Whole rock data (Godel and Barnes, in press) indicate that Pd is enriched in the J-M reef relative to the other PGE (reef Pd/Pt ratio of 3.3, Pd/Pt ratio above and below the reef <1). Assuming that the silicate/sulfide liquid partition coefficient for Pd and Pt are approximately equal (Fleet et al., 1999), this small-scale remobilization of Pd-Cu from the BMS on a small scale (mm to cm) is not likely to be the cause of Pd enrichment as all Pd would have been initially in the sulfide liquid and thus would have been modelled from whole rock data. In addition, only minor PGM alteration was observed in our section (Fig. 5.14) and consequently, this slight PGM alteration likely redistributed only a minor quantity of PGE. Thus the Pd-Cu redistribution may have occurred on a larger scale and these elements may have been introduced from outside the reef package.

In our J-M Reef section, the footwall cumulates have much lower Pd/Pt ratios (0.3 to 0.7) than the reef and the proposed initial magma (Godel and Barnes, 2007). One possibility is that some Pd was remobilized from the cumulate rocks in the footwall. These results are in agreement with those of Hanley et al. (2005) who have shown that volatiles may have removed S, Cu, Pd and some Pt from the cumulates below the J-M Reef. We suggest that the skaergaardite observed from the J-M Reef at East Boulder mine could have precipitated from Pd-Cu rich fluids that have migrated upward and leached Cu and Pd from the footwall and bring Pd up to the level of the reef. The fluid may have percolated in the cumulate pile, precipitated skaergaardite and in many cases desulfidized the BMS to

magnetite. This process could explain the occurrence of skaergaardite (+/- magnetite) veinlets crosscutting BMS and the alteration of the BMS to form magnetite (e.g. Fig. 5.4 b and d).

Some of the PGM (Pd-Pt telluride essentially) are completely surrounded by alteration silicates, but are usually found associated with secondary chalcopyrite or secondary magnetite. In this case, the PGM were probably associated with BMS (included in or located at the contact between the BMS and the silicate) but some S may have been removed during alteration leaving PGM behind. The primary BMS could have been replaced by a mixture of alteration silicate, magnetite or secondary chalcopyrite (crystallized almost in situ from the remobilized S). This replacement may result in the formation of "alteration patches" rich in PGM which are no longer associated with BMS. The alteration silicates consist mainly of chlorite, tremolite, actinolite and serpentine. These minerals are characteristic of greenschist facies metamorphism (i.e. temperature up to 500 °C). These temperatures are in agreement with those obtained for the formation of the skaergaardite.

Although the origin and the characteristics of the fluid which lead to Pd enrichment in the J-M Reef are difficult to constrain, the occurrence of skaergaardite and the textural association of PGM indicate that the fluid would have precipitated Pd at temperatures below 500°C (250°C to 465°C according to experimental studies on Pd-Cu alloy). This alteration may be related to the cooling of the intrusion or to the regional metamorphism greenschist facies event which affected the Stillwater Complex between 1.7 and 1.6 Ga (U-Pb age on apatite, Nunes and Tilton, 1971).

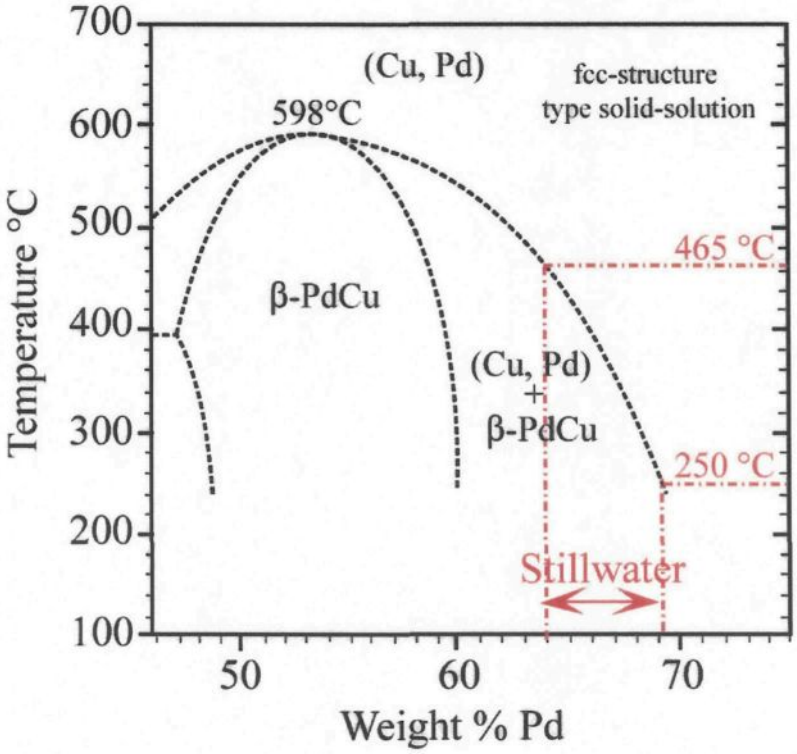

Figure 5.13: Pd-Cu phase diagram for the Pd-Cu alloy found in our samples of J-M Reef , After Subramanian and Laughlin (1991).

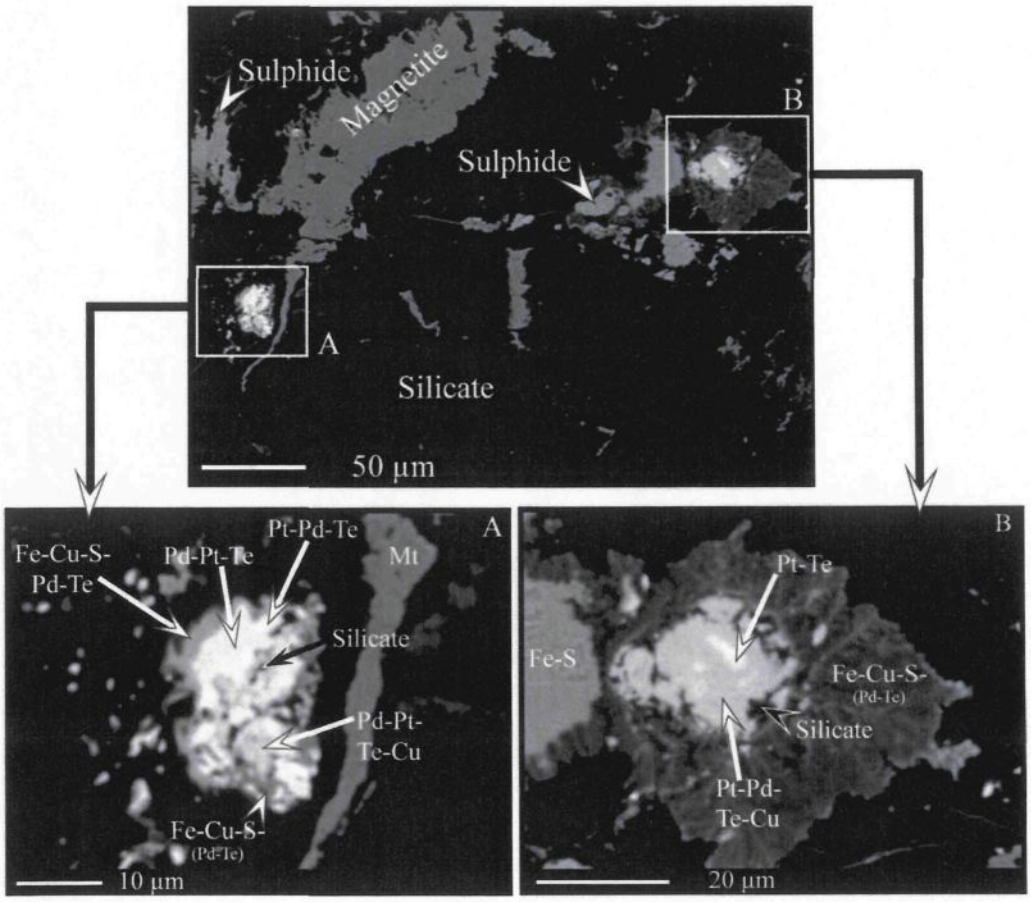

Figure 5.14: Example of the alteration of platinum-group element minerals.

5.7.4. - A possible scenario for the formation of the J-M Reef

Integration of the above informations allows us to more closely constrain the possible model for the formation of the J-M reef of the Stillwater Complex proposed by Godel and Barnes (2007). The enrichments in PGE at the level of the J-M reef may have occurred in four steps:

(i) A new magma (high-Mg basalt) entered the magma chamber which contained a crystal mush overlain by a fractionated silicate liquid and mixed vigorously with the resident magma. As the silicates crystallized, the magma became saturated in an immiscible sulfide liquid droplets which interacted with the large volume of silicate magma and collected the PGE, Ni, Cu, Te and Bi to form a sulfide liquid highly enriched in these elements (Fig. 5.15a).

(ii) Instabilities of the crystal pile (possibly due to earthquakes) triggered the collection of these droplets into vertical network (Godel et al., 2006) and possibly enhanced the downward percolation of the sulfide liquid (Fig. 5.15b).

(iii) As the temperature dropped, fluids (possibly S-undersaturated intercumulate liquid or vapour formed during the degassing of the magma chamber) interacted with the newly formed sulfides, triggered their partial desulfurization and removed (25 up to 50%) of the initial sulfur content (Fig. 5.15c). The desulfurization caused the formation of Pt-Fe alloy and a Pd-Cu-S rich liquid (Fig. 5.15d). During cooling, the Pd-Cu-S rich liquid form intergrowth of Pd sulfide and chalcopyrite (Fig. 5.5a).

(iv) As the temperature dropped, the MSS enriched in PGE formed pyrrhotite and pentlandite and the ISS formed chalcopyrite. The PGM, mainly laurite, Pd-Pt telluride and Pd-Pt sulfide exsolved during these steps.

(v) At temperature <500°C, another fluid percolated in the cumulate pile (possibly during cooling of the intrusion or during later greenschist facies metamorphism), and removed Pd from the footwall (Fig. 5.15e). This fluid now enriched in Pd migrated upwards to the level of the actual J-M reef, reacted with the base metal sulfides and, precipitated skaergaardite (Fig. 15f and g). The fluid percolation also triggered the alteration of the silicate and the formation of secondary chalcopyrite. The PGM (mainly Pd-Pt telluride and Pd-Pt sulfide) which had crystallized from the BSM were not affected. Thus, it allows the formation of PGM-rich alteration zones at the contact between the BSM and the silicate minerals.

The variation in the grade of Pd (or PGE) observed along the J-M Reef of the Stillwater Complex probably reflects the different contribution of each of these processes in various places along the reef.

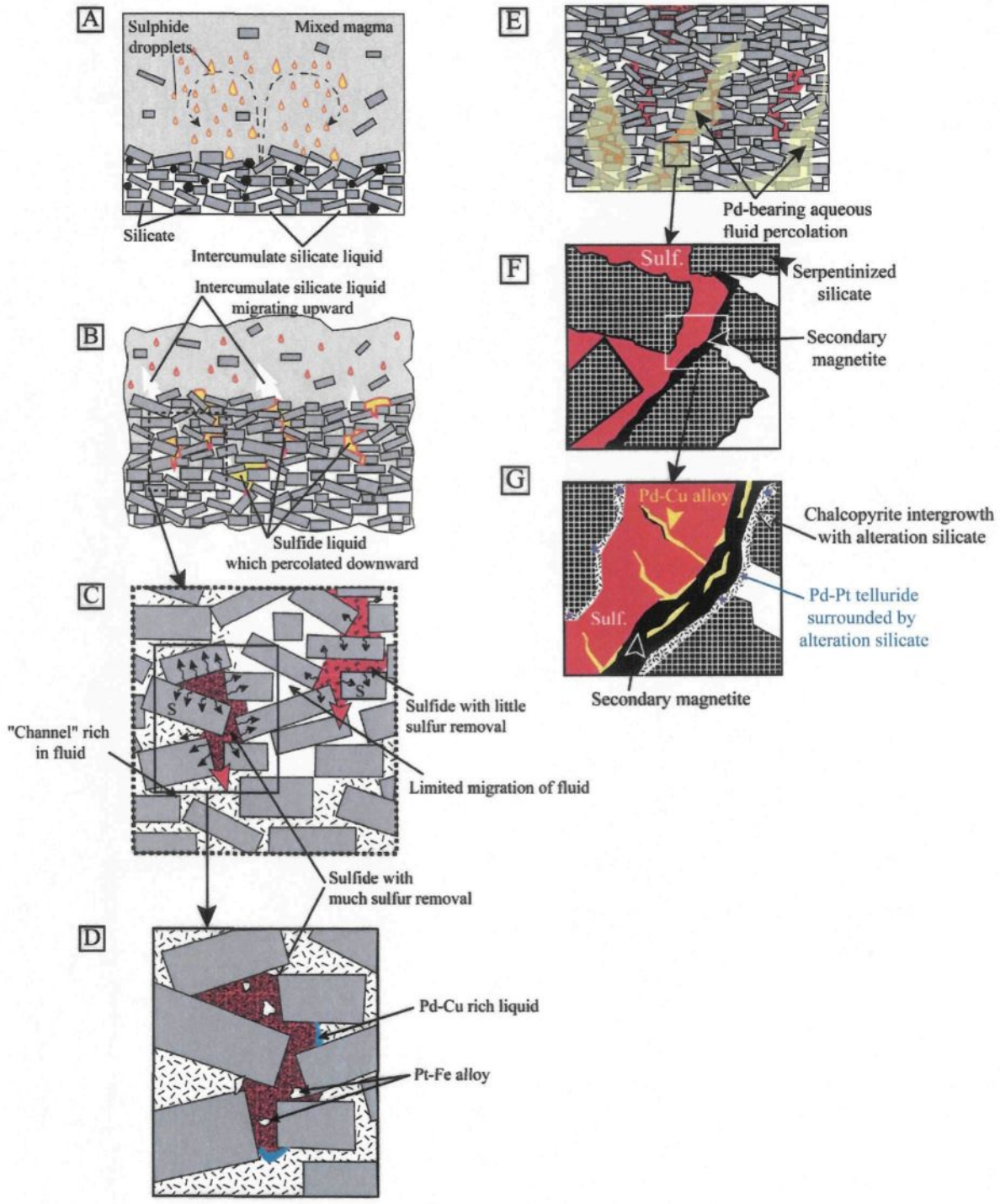

Figure 5.15: Model of formation for the J-M Reef.

5.8. - CONCLUSION

The platinum-group minerals observed in four mineralized (~140 up to 419 ppm of PGE with a Pd/Pt ratio averaging 3) samples of the J-M reef of the Stillwater Complex consist of Pd-Pt sulfides, Pt-Fe alloy, Pd-Pt tellurides and Pd-Cu alloy with minor Pd-Pd alloy, Ru(Ir, Os) sulfides and Au-Pd-Ag alloy.

Most of the PGM found in the sections are closely associated with BMS (either included in or located at the contact between the BMS and the silicate or oxides). This probably reflects the fact that PGE, Ni, Cu, Te, Bi were initially hosted by a sulfide liquid. The textural observations and PGM assemblage indicate that at least two alteration events may have occurred since the formation of an immiscible sulfide liquid.

Firstly, the presence of Pt-Fe alloy hosted by pyrrhotite and crosscut by secondary magnetite stringers indicate that Pt-Fe alloy formed before secondary magnetite crystallization. The formation of Pt-Fe alloy is thought to be the result of the partial desulfurization of the BMS.

Secondly, the presence of Pd-Cu alloy (skaergaardite) and Pd sulfides found associated either with secondary magnetite (included in or located at the contact between the magnetite and base metal sulfide or silicates) or as veinlets crosscutting the base metal sulfide indicates that at Stillwater, the Pd-Cu alloy may have formed coeval to secondary magnetite formation and after the base metal sulfide solidification. Furthermore, the Pd-Cu phase diagram indicates that skaergaardite may have adapted a CsCl-structure at temperature between 250°C to 465°C. Thus, most of the Pd enrichment observed in the J-M Reef may have occurred during a second alteration event, where a fluid enriched in Pd

percolated in the cumulate pile and interacted with the base metal sulfides. The origin of the fluid is not known. However, whole rock data indicate that Pd may have been leached out of the footwall of the J-M Reef. This may have occurred during the greenschist facies metamorphism which has affected the Stillwater Complex.

5.9. - ACKNOWLEDGMENTS

Stillwater Mining Company is thanked for hosting the "9th International Platinum Symposium" field trip and allowing sampling of the J-M Reef cores. Marc Choquette (Laval University) is thanked for his assistance with the microprobe analysis. Michael Zientek (USGS) is thanked for providing us his data on PGM as a comparison. This work was funded by a Discovery Grant from Natural Science and Engineering Research Council of Canada and the Canadian Research Chair in Magmatic Metallogeny.

5.10. - REFERENCES

Baker, H., Okamoto, H., Henry, S. D., Davidson, G. M., Flemming, M. A., Kacprzak, L., and Lampman, H. F., 1992, Alloy phase diagrams: Ohio, U.S.A.

Barkov, A. Y., Fleet, M. E., Martin, R. F., and Halkoaho, T. A. A., 2005, New data on "Bonanza"-type PGE mineralization in the Kirakkajuppura PGE deposit, Penikat layered complex, Finland: Canadian Mineralogist, v. 43, p. 1663-1686.

Barnes, S.-J., and Maier, W. D., 1999. The fractionation of Ni, Cu and the noble metals in silicate and sulfide liquid, *in* Keays, R. R. L., C.M.; Lightfoot, P.C. and Farrow, C.E.G,

ed., Dynamic Processes in Magmatic Ore Deposits and their application in mineral exploration, Vol. 13. Short Course Notes, Geological Association of Canada, p. 69 - 106.

Barnes, S. J., and Naldrett, A. J., 1986, Geochemistry of the J-M Reef of the Stillwater Complex, Minneapolis Adit Area II. Silicate Mineral Chemistry and Petrogenesis: Journal of Petrology, v. 27, p. 791-825.

Boudreau, A., 1999, Fluid fluxing of cumulates: The J-M reef and associated rocks of the Stillwater complex, Montana: Journal of Petrology, v. 40, p. 755-772.

Boudreau, A. E., and McCallum, I. S., 1992a, Concentration of Platinum-Group Elements by Magmatic Fluids in Layered Intrusions: Economic Geology and the Bulletin of the Society of Economic Geologists, v. 87, p. 1830-1848.

Boudreau, A. E., and McCallum, I. S., 1992b, Infiltration Metasomatism in Layered Intrusions - an Example from the Stillwater Complex, Montana: Journal of Volcanology and Geothermal Research, v. 52, p. 171-183.

Bow, C., Wolfgram, D., Turner, A. R., Barnes, S. J., and Evans, J., 1982, Investigations of the Howland Reef of the Stillwater Complex, Minneapolis Adit area: stratigraphy, structure, and mineralization: Economic Geology, v. 77, p. 1481-1492.

Brenan, J. M., and Andrews, D. R. A., 2001, High-temperature stability of laurite and Ru-Ir-Os alloy and their role on PGE fractionation in mafic magmas: Canadian Mineralogist, v. 39, p. 341-360.

Cabri, L. J., and LaFlamme, J. H. G., 1981, Analyses of minerals containing platinum-group elements, Platinum-Group Elements: Mineralogy, Geology, Recovery Special volume 23, Canadian Institute of Mining, Metallurgy and Petroleum, p. 151-173.

Cabri, L. J., and Traill, R. J., 1966, New palladium minerals from Noril'sk, western Siberia: Canadian Mineralogist, v. 11, p. 514-550.

Campbell, I. H., Naldrett, A. J., and Barnes, S. J., 1983, A Model for the Origin of the Platinum-Rich Sulfide Horizons in the Bushveld and Stillwater Complexes: Journal of Petrology, v. 24, p. 133-165.

Craig, J. R., and Kullerud, G., 1969, Phase relations in the Cu-Fe-Ni-S system and their application to magmatic ore deposits.: Economic Geology, v. Monograph 4, p. 344-358.

Czamanske, G. K., and Loferski, P. J., 1996, Cryptic trace-element alteration of anorthosite, Stillwater Complex, Montana: Canadian Mineralogist, v. 34, p. 559-579.

Fleet, M. E., Crocket, J. H., Liu, M., and Stone, W. E., 1999, Laboratory partitioning of platinum-group elements (PGE) and gold with application to magmatic sulfide-PGE deposits: Lithos, v. 47, p. 127-142.

Garuti, G., Zaccarini, F., Moloshag, V., and Alimov, V., 1999, Platinum-group minerals as indicators of sulfur fugacity in ophiolitic upper mantle: an example from chromitites of the Ray-Iz ultramafic complex, Polar Urals, Russia: Canadian Mineralogist, v. 37, p. 1099-1115.

Godel, B., Barnes, S.-J., and Maier, W. D., 2006, 3-D Distribution of Sulphide Minerals in the Merensky Reef (Bushveld Complex, South Africa) and the J-M Reef (Stillwater

Complex, USA) and their Relationship to Microstructures Using X-Ray Computed Tomography: Journal of Petrology, v. 47, p. 1853-1872.

Godel, B. and Barnes, S.J., 2007, Platinum-group elements in sulfide minerals and the whole rocks of the J-M Reef (Stillwater Complex): implication for the formation of the reef: Chemical Geology, doi: 10.1016/j.chemgeo.2007.05.006

Godel, B., Barnes, S.-J., and Maier, W. D., 2007, Platinum-Group Elements in Sulphide Minerals, Platinum-Group Minerals, and the Whole Rock of the Merensky Reef (Bushveld Complex, South Africa): Implication for the Formation of the Reef: Journal of Petrology, 48, 1589-1604.

Hanley, J. J., Mungall, J. E., and Spooner, E. T. C., 2005, Fluid and melt inclusion evidence for platinum-group element transport by high salinity fluids and halide melts below the J-M reef, Stillwater Complex, Montana, U.S.A.: 10th International Platinum Symposium "Platinum-Group Elements - from Genesis to Beneficiation and Environmental Impact", Oulu, Finland, p. 94-97.

Heyse, J. V., 1983, The mineralogy of the Stillwater platinum-palladium ore in the Frog Pond and Minneapolis adits: Richmond, California, Chevron Research Company Report, p. 41.

Hiemstra, S. A., 1979, The role of collectors in the formation of the platinum deposits in the Bushveld Complex: Canadian Mineralogist, v. 17, p. 469-482.

Hoffman, E., and MacLean, W. H., 1976, Phase Relations of Michenerite and Merenskyite in the Pd-Bi-Te System: Economic Geology, v. 71, p. 1461-1468.

Karup-Möller, S., and Makovicky, E., 1999, The phase system Cu-Pd-S at 900 degrees, 725 degrees, 550 degrees, and 400 degrees C: Neues Jahrburch für Mineralogie, p. 551-567.

Kingston, G. A., and El-Dosuky, B. T., 1982, A contribution on the Platinum-Group Mineralogy of the Merensky Reef at the Rustenburg Platinum Mine: Economic Geology, v. 77, p. 1367-1384.

Komppa, U., 1998, Oxide, sulphide and platinum mineralogy of the South Kawishiwi and Partridge River Intrusions of the Duluth Layered Intrusion Complex, Minnesota, U.S.A., University of Oulu, Finland, 104 p.

Li, C., Ripley, E. M., Merino, E., and Maier, W. D., 2004, Replacement of base metal sulfides by actinolite, epidote, calcite, and magnetite in the UG2 and Merensky Reef of the Bushveld Complex, South Africa: Economic Geology, v. 99, p. 173-184.

Maier, W. D., Prichard, H. M., Barnes, S. J., and Fisher, P. C., 1999, Compositional variation of laurite at Union Section in the western Bushveld Complex: South African Journal of Geology, v. 102, p. 286-292.

Makovicky, E., 2002, Ternary and quaternary phase systems with PGE, *in* Cabri, L. J., ed., Geology, Geochemistry, Mineralogy and Mineral benefication of Platinum Group Element, Special Volume 54, Canadian Institute of Mining, Metallurgy and Petroleum, p. 121-175.

Naldrett, A. J., Gasparrini, E. C., Barnes, S. J., Von Gruenewaldt, G., and Sharpe, M. R., 1986, The Upper Critical Zone of the Bushveld Complex and the Origin of Merensky-Type Ores: Economic Geology, v. 81, p. 1105-1117.

Nunes, P. D., and Tilton, G. R., 1971, Uranium-lead ages of minerals from the Stillwater Complex and associated rocks, Montana: Geological Society of America Bulletin, v. 82, p. 2231-2250.

Peregoedova, A., Barnes, S.-J., and Baker, D. R., 2004, The formation of Pt-Ir alloys and Cu-Pd-rich sulfide melts by partial desulfurization of Fe-Ni-Cu sulfides: results of experiments and implications for natural systems: Chemical Geology, v. 208, p. 247-264.

Peregoedova, A., Barnes, S.-J., and Baker, D. R., 2006, An experimental study of mass transfer of platinum-group elements, gold, nickel and copper in sulfur-dominated vapor at magmatic temperatures: Chemical Geology, v. 235, p. 59-75.

Peregoedova, A., and Ohnenstetter, M., 2002, Collectors of Pt, Pd and Rh in a S-poor Fe-Ni-Cu sulfide system at 760 degrees C; experimental data and application to ore deposits: The Canadian Mineralogist, p. 527-561.

Polovina, J. S., Hudson, D. M., and Jones, R. E., 2004, Petrographic and geochemical characteristics of postmagmatic hydrothermal alteration and mineralization in the J-M Reef, Stillwater Complex, Montana: Canadian Mineralogist, v. 42, p. 261-277.

Premo, W. R., Helz, R. T., Zientek, M. L., and Langston, R. B., 1990, U-Pb and Sm-Nd ages for the Stillwater Complex and its associated sills and dikes, Beartooth Mountains, Montana: Identification of a parent magma?: Geology, v. 18, p. 1065-1068.

Prichard, H. M., Barnes, S.-J., Maier, W. D., and Fisher, P. C., 2004, Variations in the nature of the platinum-group minerals in a cross-section through the Merensky Reef at

Impala Platinum: Implications for the mode of formation of the reef: Canadian Mineralogist, v. 42, p. 423-437.

Rudashevsky, N. S., McDonald, A. M., Cabri, L. J., Nielsen, T. F. D., Stanley, C. J., Kretzer, Y. L., and Rudashevsky, V. N., 2004, Skaergaardite, PdCu, a new platinum-group intermetallic mineral from the Skaergaard instrusion, Greenland: Mineralogical Magazine, v. 68, p. 615-632.

Subramanian, P. R., and Laughlin, D. E., 1991, Cu-Pd (copper-palladium): Journal of Phase Equilibria, v. 12, p. 231-243.

Talkington, R. W., and Lipin, B. R., 1986, Platinum-Group Minerals in chromite seams of the Stillwater Complex, Montana: Economic Geology, v. 81, p. 1179-1186.

Todd, S. G., Keith, D. W., Le Roy, L. W., Schissel, D. J., MANN, E. L., and Irvine, T. N., 1982, The J-M Platinum-Palladium Reef of the Stillwater Complex, Montana: I. Stratigraphy and Petrology: Economic Geology, v. 77, p. 1454-180.

Turner, A. R., Wolfgram, D., and Barnes, S. J., 1985, Geology of the Stillwater County sector of the J-M Reef, including the Minneapolis Adit, *in* Czamanske, G. K., and Zientek, M. L., eds., The Stillwater Complex, Montana : geology and guide, Special Publication, no. 92: Butte, Montana, Montana Bureau of Mines and Geology, p. 210-230.

Willmore, C. C., Boudreau, A. E., and Kruger, F. J., 2000, The halogen geochemistry of the Bushveld Complex, Republic of South Africa: Implications for chalcophile element distribution in the lower and critical zones: Journal of Petrology, v. 41, p. 1517-1539.

Zientek, M. L., Cooper, R. W., Corson, S. R., and Geraghty, E. P., 2002, Platinum-Group Element Mineralization in the Stillwater Complex, Montana, *in* Cabri, L. J., ed., Geology, Geochemistry, Mineralogy and Mineral benefication of Platinum Group Element, Special Volume 54, Canadian Institute of Mining, Metallurgy and Petroleum, p. 459 - 481.

Zientek, M. L., Czamanske, G. K., and Irvine, T. N., 1985, Stratigraphy and nomenclature for the Stillwater Complex, *in* Czamanske, G. K., and Zientek, M. L., eds., The Stillwater Complex, Montana : geology and guide, Special Publication, no. 92: Butte, Montana, Montana Bureau of Mines and Geology, p. 21-32.

Zientek, M. L., Foose, M. P., and Mei, L., 1986, Palladium, Platinum, and Rhodium Contents of Rocks near the Lower Margin of the Stillwater Complex, Montana: Economic Geology, v. 81, p. 1169-1178.

Zientek, M. L., and Oscarson, R. L., 1986, Textural association of platinum-group minerals from the J-M Reef, Stillwater complex, Montana: U.S. Geological Survey, v. Circ. 995, p. 75-76.

CHAPITRE 6

SYNTHESE ET CONCLUSIONS: MERENSKY REEF vs J-M REEF SIMILITUDES ET DIFFERENCES

6.1. – INTRODUCTION

Les études microtomographiques, microstructurales, géochimiques et minéralogiques ont permis de mettre en évidence les points communs et les différences entre deux minéralisations enrichies en EGP : le Merensky Reef dans le complexe du Bushveld en Afrique du Sud et le J-M Reef dans le complexe de Stillwater aux Etats-Unis. Ces deux complexes ont des degrés d'altération et de métamorphisme très différent. Le Merensky Reef n'a subit pratiquement aucune altération et/ou métamorphisme après sa solidification. Au contraire, le J-M Reef fréquemment considéré dans la littérature comme « altéré » a subit plusieurs épisodes d'altération et de métamorphisme (Bow et al., 1982 ; Czamanske and Zientek, 1985 ; Czamanske and Loferski, 1996 ; Polovina et al., 2004). Ces épisodes sont résumés en Table 1.3.

Cette étude nous a permis d'évaluer le rôle des liquides sulfurés enrichis en métaux de base et de l'altération sur la collection et la redistribution des EGP. Les résultats montrent que la distribution et l'enrichissement en EGP de ces niveaux peuvent être expliqués par une superposition relativement complexe de processus physiques (compaction) et chimiques (collection par les liquides sulfurés, désulfurisation, altération par fluides). Ces processus ont joué un rôle plus ou moins important dans la formation de chacune des deux zones enrichies en EGP (voir ci-dessous).

6.2. – SYNTHESE DES RÉSULTATS

L'analyse des roches totales montre que le Merensky Reef (Table 3.5) et le J-M Reef (Table 4.4) contiennent des quantités variables d'EGP, de métaux communs et nobles. Les spectres (PGE, Ni, Re, Au et Cu) normalisés au manteau pour les roches silicatées du Merensky Reef (Fig. 3.14) et du J-M Reef (Fig. 4.4) ont des formes différentes. Les chromitites du Merensky Reef montrent un enrichissement particulier en EGP. Cet enrichissement n'est pas corrélable avec l'abondance modale accrue de sulfures et par conséquent d'autres processus doivent être envisagés (voir discussion Chapitre 3). Dans les deux zones minéralisées, le platine et le palladium sont les principaux EGP contenu dans ces roches mais celles du J-M Reef sont plus enrichies en Pd, Pt, Re, Os et Au que les roches du Merensky Reef. Le palladium est plus enrichi dans les roches du J-M Reef (Pd/Pt variant de 1 à 5.2, moyenne 3.3) que dans les roches silicatées du Merensky Reef (Pd/Pt variant de 0.38 à 0.77, moyenne 0.66). Pour les roches silicatées du Merensky Reef et du J-M Reef, la concentration en EGP, Ni et Cu est corrélable avec la quantité de soufre (*i.e.* de sulfures) présente dans les roches. Cette observation indique que les sulfures seraient bien les principales phases contrôlant initialement ces éléments. Les sulfures observés dans le Merensky Reef et le J-M Reef consistent en un assemblage de pyrrhotite, pentlandite et chalcopyrite disséminés dans les roches (0.5 à 8 vol% en fonction de la position stratigraphique, voir Chapitre 2). Les sulfures se retrouvent (en 3-D et en 2-D) sous forme de réseaux verticaux (paléovertical) de quelques millimètres à quelques centimètres de long. Ces sulfures sont, en général, localisés à la périphérie des cristaux de silicates

(orthopyroxène, olivine ou plagioclase). Les processus physiques qui ont engendré cette répartition seront décrits à la section 6.3.

L'analyse *in situ* des sulfures a permis de déterminer que la pentlandite et la pyrrhotite sont les principaux sulfures contenant des EGP en solution solide (Table 3.6 pour le Merensky Reef et Table 4.5 pour le J-M Reef). En générale, la chalcopyrite contient très peu d'EGP et les valeurs sont souvent, pour certains éléments, sous les limites de détection. Les spectres normalisés au manteau de la pentlandites et de la pyrrhotite du Merensky Reef et du J-M Reef ont une forme semblable ce qui laisse supposer que les EGP ont eut un comportement relativement similaire durant la formation de ces sulfures (Fig. 6.1 et 6.2).

Dans les échantillons du Merensky Reef et du J-M Reef, le Pt et Au ne se concentrent pas dans les sulfures (voir Table 3.6 et Appendix 3). Ce comportement explique les anomalies négatives observées sur les spectres de pentlandite et de pyrrhotite (Fig. 6.2 et Fig. 6.3). Le Pt et l'Au se retrouvent essentiellement sous forme de minéraux du groupe du platine (MGP) et d'électrum. Les MGP enrichis en Pt pour le J-M Reef et le Merensky Reef consistent pour l'essentielle en un assemblage de: (i) sulfures de Pt (braggite, cooperite) ; tellures de Pt +/- Pd (moncheite essentiellemt), et (iii) d'alliage de Pt et Fe (isoferroplatinum).

Les autres élements du groupe du platine sont, pour le Merensky Reef et le J-M Reef, essentiellement contenus dans les sulfures enrichis en métaux de base (pentlandite et pyrrhotite). Le reste de ces éléments se retrouvent sous forme de MGP, essentiellement : des tellures de Pd +/- Pt (merenskiite, telluropalladinite, et kotulskite) ; des sulfures de Pd

(vysotskite et braggite essentiellement) ; des sulfures de Ru +/- Ir +/- Os (laurite) ; des alliages de Pd-Cu (skaergardite) pour le J-M Reef.

6.3 – LES PROCESSUS PHYSIQUES

Les études microtomographiques et microstructurales ont permis de mettre en évidence pour chaque zone minéralisée le rôle de la compaction dans la migration des liquides sulfurés dans la pile de cumulats.

La microtomographie au rayon-X est une technique puissante qui nous a permis de déterminer pour chacun des échantillons étudiés la distribution des minéraux en 3-D. L'étude microstructurale a permis de mettre en évidence que ces échantillons ont subit une déformation importante lors de la formation des cumulats. Les indices de déformation de haute température permettent de définir la direction de la compression maximale ($\sigma 1$) qui a engendré cette déformation. Dans chacun des échantillons, la direction de $\sigma 1$ est orientée selon la direction de la paléovertical. Cela indique que cette déformation serait provoquée par la compaction. Durant cette compaction, des dilatances verticales se formeraient au contact entre les cristaux (pyroxènes, olivines et plagioclases majoritairement). Ces dilatances permettraient une migration préférentielle des liquides sulfurés dans des zones de moindres contraintes. L'étude détaillée du Merensky Reef a permis de mettre en évidence le rôle des niveaux de chromite dans la migration et la distribution des sulfures.

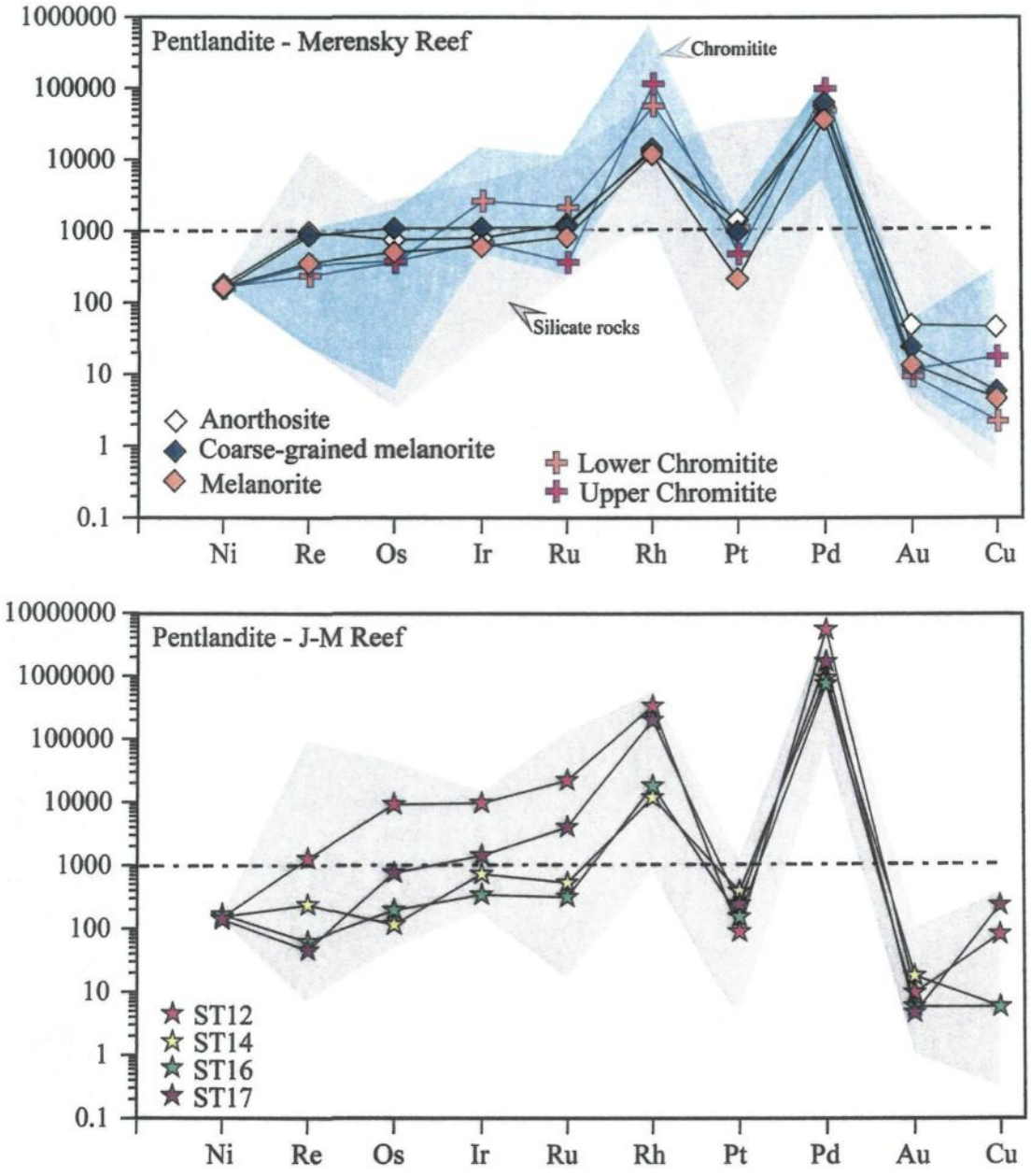

Figure 6.1: Spectres normalisés au manteau des pentlandites du Merensky Reef et du J-M Reef

Les zones grises représentent la gamme de valeurs observées. Chaque courbe représente la moyenne géométrique calculée pour chaque échantillon à partir de l'ensemble des données (Table 3.6 et Appendix 3). Les valeurs de normalisation utilisées sont celles de Barnes et Maier (1999).

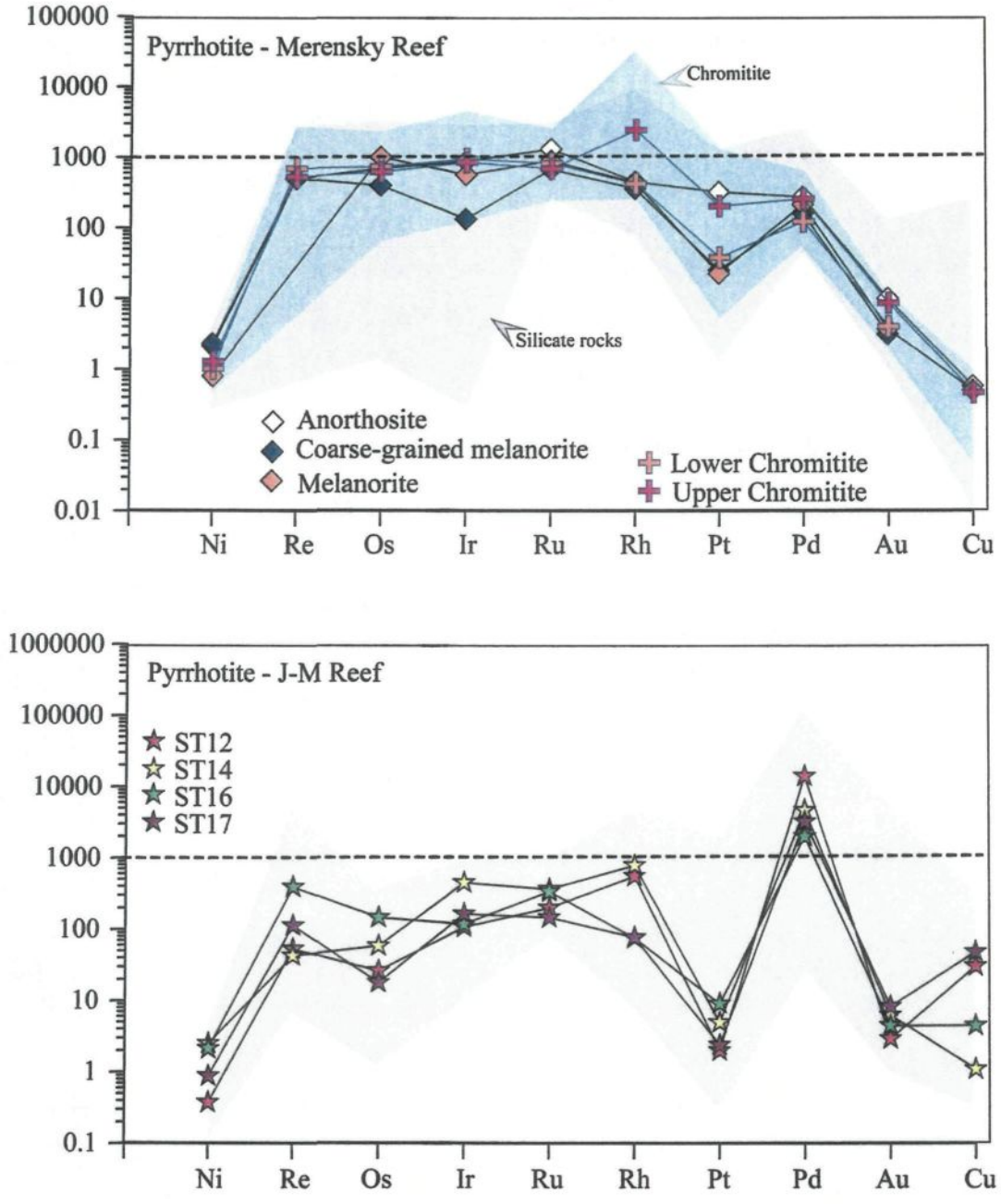

Figure 6.2 : Spectres normalisés au manteau des pyrrhotites du Merensky Reef et du J-M Reef

Les zones grises représentent la gamme de valeurs observées. Chaque courbe représente la moyenne géométrique calculée pour chaque échantillon à partir de l'ensemble des données (Table 3.6 et Appendix 3). Les valeurs de normalisation utilisées sont celles de Barnes et Maier (1999).

L'analyse des angles dihédraux (Chapitre 2) montre que la topologie des liquides sulfurés est différente entre les mélanorites et les niveaux de chromite. Dans les mélanorites, la connectivité des liquides sulfurés est importante (angles dihédraux entre silicates et sulfures < 60°). Par conséquent, la percolation du liquide sulfuré est favorisée. Dans ces roches silicatées (du Merensky Reef et du J-M Reef), la percolation du liquide sulfuré s'arrêterait simplement lorsque la perméabilité des cumulats devient trop faible (lors de la cristallisation des minéraux intercumulus).

Au contraire, dans les niveaux de chromite la connectivité et la percolation du liquide sulfuré sont limitées (angles dihédraux entre chromite et sulfures >> 60°). Les niveaux de chromite agiraient comme des barrières réduisant fortement la migration des liquides sulfurés vers le bas. Dans ce cas, la composition du liquide sulfuré aurait un rôle prépondérant sur la migration. Les liquides riches en Cu possèdent une viscosité plus faible et une meilleure mouillabilité (Ebel and Naldrett, 1996 ; 1997). Par conséquent, ces derniers seraient plus susceptibles de percoler vers de bas et franchir la « barrière » des chromitite. Cela permettrait d'expliquer, pour l'échantillon du Merensky Reef, l'enrichissement particulier en chalcopyrite observé dans les niveaux de chromitite et dans les roches silicatées situées juste en dessous de ces derniers.

De plus, la présence d'instabilités dans les chambres magmatiques (par exemple des séismes de faible magnitude) pourrait également favoriser la connexion des liquides sulfurés et ainsi améliorer leur migration dans la pile de cumulats. Ces instabilités pourraient également provoquer une liquéfaction partielle de la pile de cumulats et par conséquent auraient de grandes incidences sur la migration des fluides présents. Cette

percolation de fluide pourrait permettre une désulfurisation plus ou moins importante des sulfures et aurait une incidence sur la formation de minéraux du groupe du platine (alliage de Pt-Fe notamment).

Les processus physiques joueraient donc un rôle important dans la distribution et la mobilisation des liquides sulfurés. Cependant, ces processus ne permettent pas d'expliquer à eux seuls l'enrichissement en EGP observés dans les zones minéralisées comme le J-M Reef ou le Merensky Reef. Des processus chimiques (primaires et secondaires) doivent être évoqués pour tenter d'expliquer les différences géochimiques et minéralogiques observées dans ces échantillons.

6.4. – LES PROCESSUS GEOCHIMIQUES

6.4.1. – Rôle des liquides sulfurés

Dans le Merensky Reef et le J-M Reef, les liquides sulfurés ont joué un rôle primordial dans la collection et la concentration des EGP et autres métaux.

Les modélisations réalisées à partir des données des magmas parents reconnus comme étant à l'origine du Merensky Reef (Chapitre 3) indiquent que pour les roches silicatés les concentrations en EGP observé dans les roches totales peuvent entièrement être expliquées par l'interaction entre un liquide et un magma silicaté et la collection des EGP par les liquides sulfurés. Les EGP trouvés dans les sulfures *in situ* et sous forme de minéraux du groupe du platine auraient initialement été présents dans les liquides sulfurés.

Ces minéraux enrichis en EGP se seraient formés par désulfurisation partielle (pour Pt-Fe) et par exsolution à partir des sulfures pendant le refroidissement pour les sulfures et tellurures notamment (voir processus ci-dessous). Pour les niveaux de chromite, une cristallisation primaire (*i.e.* avant la saturation en sulfures du magma) de minéraux du groupe du platine est nécessaire pour expliquer les concentrations en EGP observées dans ces niveaux (voir Chapitre 3).

Pour le J-M Reef, les modélisations (Chapitre 4) indiquent que les EGP observés dans les échantillons étaient initialement présents dans un liquide sulfuré qui aurait interagit avec un magma silicaté ayant une composition proche de celle proposée pour le Merensky Reef. Mais contrairement au Merensky Reef, les modélisations pour le J-M Reef impliquent que d'autres processus (désulfurisation poussée, altération et ajout de Pd et Pt possiblement par des fluides) aient eut lieu.

6.4.2 – Rôle de la désulfurisation

L'étude des rapports S/Se pour les échantillons du J-M Reef et du Merensky Reef permet de mettre en évidence le rôle de la désulfurisation dans la formation de ces zones minéralisées (voir Chapitre 4 et 5). Les échantillons du J-M Reef ont subit une désulfurisation plus importante (20 à 50% des sulfures initiale enlevés) que ceux du Merensky Reef (<10 % de sulfures enlevés).

Le Merensky Reef et le J-M Reef contiennent des alliages de Pt-Fe (isoferroplatinum). Des travaux expérimentaux récents (Peregoedova and Ohnenstetter,

2002 ; Peregoedova *et al.*, 2004 ; Peregoedova *et al.*, 2006) et des analyses d'échantillons du J-M Reef à Stillwater Mine (Li and Ripley, 2006) ont montré le rôle de la désulfurisation dans la formation de ces alliages de Pt-Fe. Ces alliages se formeraient par désulfurisation partielle de la MSS (Peregoedova *et al.*, 2006). Lors de la désulfurisation, le Pt-Fe s'exsolverait à partir le la MSS ce qui provoquerait un appauvrissement de la « MSS résiduelle ». Lorsque la température diminue (T < 600°C), de la pyrrhotite et de la pentlandite s'exsolvent à partir de la MSS. Par conséquent, les pyrrhotites et pentlandites qui cristallisent à partir de cette MSS devraient être appauvries en Pt par rapport aux autres éléments qui se concentrent préférentiellement dans la MSS (*i.e.* Ir, Os, Ru et Rh).

L'analyse des spectres normalisés au manteau des pentlandites et pyrrhotites du Merensky Reef et du J-M Reef (Fig. 6.1 et Fig. 6.2) montre que le platine est appauvri par rapport au IPGE dans ces sulfures. Le diagramme S/Se vs Pt/Pt* (Fig. 5.12) pour les pyrrhotite et les pentlandite du Merensky Reef et du J-M Reef ont montré que plus les roches ont subit une désulfurisation, plus l'anomalie en Pt est prononcée. De plus, les échantillons du J-M Reef qui ont subit plus de désulfurisation contiennent une proportion plus importante (~24 %) de Pt-Fe que les échantillons du Merensky Reef (~9 % de Pt-Fe) qui eux ont subit beaucoup moins de désulfurisation. Ces résultats suggérent que la désulfurisation a provoqué la formation d'alliage de Pt-Fe mais que le Pt était initialement présent dans les sulfures.

6.4.3 – Rôle de l'altération et du métamorphisme

Contrairement aux échantillons du Merensky Reef, certains des échantillons du J-M Reef ont subit au moins un autre épisode de migration de fluide (plus tardif). Ce dernier se serait superposé aux processus décrits ci-dessus et aurait également permis un enrichissement et/ou une redistribution de certains EGP, principalement Pd et Pt (voir ci-dessous).

Ces fluides ont provoqué l'altération des silicates primaires (olivine, pyroxènes et plagioclase) localisés au contact avec les sulfures et la formation de magnétite secondaire autour des sulfures (par oxydation vraisemblablement). Dans les zones d'altération, les minéraux secondaires (chlorite, tremolite, actinote, talc, serpentine) sont associés avec de la chalcopyrite secondaire et des minéraux du groupe du platine (essentiellement des tellures de Pd-Pt et des sulfures de Pd-Pt). Il est probable que les minéraux du groupe du platine entourés par ces silicates d'altération étaient initialement localisés au contact entre les sulfures et les silicates primaires. Lors de l'altération des sulfures, le soufre aurait été enlevés et remplacés par des silicates d'altération. Ce soufre aurait ensuite reprécipité *in situ* (*i.e.* associés au silicates d'altération) sous forme de chalcopyrite.

La présence de skaergaardite (alliage de Pd-Cu) associée à de la magnétite secondaire qui recoupe certains grains d'isoferroplatinum (Fig. 5.4) indique que la magnétite et la skaergaardite se seraient formées après la désulfurisation partielle des sulfures ayant engendré la formation de l'isoferroplatinum. Le diagramme de phase Pd-Cu (Fig. 5.13) indique que la skaergaardite aurait cristallisé à des températures variant de ~260 à 465 °C.

L'origine du Pd reste incertaine, cependant les analyses géochimiques ont montrée (Fig. 4.3 et Fig. 4.5) que les roches situées sous la zone minéralisée du J-M Reef sont appauvries en Pd. Par conséquent, il est suggéré que les fluides qui ont provoqué la formation de magnétite et la formation d'alliage de Pd aient lessivé le Pd de la pile de cumulat sous-jacent, et percolés jusqu'au niveau actuel de la zone minéralisée et précipité le Pd. Ce fluide aurait également permis l'enrichissement de la pentlandite (et dans une moindre mesure de la pyrrhotite) observée dans les échantillons. Ces résultats sont en accord avec les résultats basés sur l'étude des inclusions fluides dans des échantillons localisés (<100 m) sous le J-M Reef (Hanley *et al.*, 2005) et avec la présence d'amphibole (ferropargasite) riche en Cl ayant cristallisé à des températures ~350 °C (Polovina *et al.*, 2004).

6.5. – IMPLICATIONS POUR LE MODELE DE FORMATION DES NIVEAUX ENRICHIS EN EGP

L'analyse multi-disciplinaire d'échantillons du Merensky Reef et du J-M Reef permet de proposer un scénario de formation des minéralisations enrichies en EGP. Les modèles propres à chaque zone minéralisée sont décrits en détails dans les chapitres 3, 4 et 5. Afin de pouvoir comparer plus aisément le J-M Reef et le Merensky Reef, seul les minéralisations et les processus associés aux roches silicatées sont pris en compte dans le scénario. Les processus envisagés pour l'enrichissement des niveaux de chromites du Merensky Reef ne sont pas rediscutés (voir Chapitre 3 et 4).

La formation des minéralisations sulfurées enrichies en EGP peut se résumer par les étapes suivantes :

(i) Une nouvelle injection de magma entre dans la chambre magmatique et se mélange (plus ou moins vigoureusement) avec le magma résident. Cela provoque la saturation en soufre du magma « mixte » et la formation de gouttelettes de sulfures immiscibles. Ces gouttelettes interagissent avec le magma silicaté et collectent les EGP, Ni, Cu, Te, Bi qu'il contient. Ces gouttelettes de sulfures enrichies en EGP tombent dans la pile de cumulats en cours de formation.

(ii) Lors de la compaction de la pile de cumulat, des dilatances se formeraient et permettraient une percolation accrue des liquides sulfurés. Cette migration s'arrêterait lorsque la perméabilité n'est plus suffisante.

(iii) Des instabilités dans la chambre magmatique (seismes, par example) pourraient également améliorer cette percolation vers le bas et/ou provoquer la migration de fluides (magmatiques, hydrothermaux, ou vapeurs ?) présents dans la chambre magmatique. Ces fluides pourraient provoquer une désulfurisation des sulfures présents ce qui pourraient entraîner la formation d'alliage de Pt-Fe.

(iv) Lorsque le système se refroidit, les minéraux du groupe du platine tels que les tellures de Pt-Pd, les sulfures de Pd-Pt etc. s'exsolveraient des sulfures enrichis en métaux de base.

(v) Si le complexe subit d'autres épisodes d'altérations et de métamorphisme (exemple du faciès schistes verts pour le J-M Reef). La percolation de fluide (dont la composition reste difficile à contraindre, mais sans doute riche en Cl) peut engendrer la remobilisation du Pd et du Pt et provoquer l'appauvrissement en ces éléments dans certaines zones et leurs enrichissement dans d'autres (zone minéralisée du J-M Reef).

6.6. – INVESTIGATIONS FUTURES

Suite aux études réalisées, plusieurs questions (liste non-exhaustive) peuvent être soulevées :

- Les chromites du Merensky Reef contiennent-elles des EGP (notamment Ru, Ir, Os, et Rh) dans leurs structures?
- Quel est le rôle de la composition des liquides sulfurés sur la migration de ces derniers dans les cumulats composés de pyroxènes et/ou olivine et/ou plagioclase et/ou chromite?
- Les magnétites secondaires du J-M Reef contiennent-elles des EGP dans leurs structures?
- Quelle est l'origine de cette magnétite secondaire ? Sa formation peut-elle être corrélée avec un des épisodes de déformations ou d'altération du complexe de Stillwater?

- Y-a-t-il une relation (sur un grand nombre d'échantillons) entre les rapports S/Se, la proportions de magnétite secondaire et l'enrichissement en EGP de la roche ?

6.6. – REFERENCES

Barnes, S.-J. and Maier, W. D. 1999. The fractionation of Ni, Cu and the noble metals in silicate and sulfide liquid. In: Keays, R. R. L., C.M.; Lightfoot, P.C. and Farrow, C.E.G (eds.) Dynamic Processes in Magmatic Ore Deposits and their application in mineral exploration. Geological Association of Canada, Short Course Notes, **Vol. 13** :69 - 106.

Bow, C., Wolfgram, D., Turner, A. R., Barnes, S. J. & Evans, J. 1982. Investigations of the Howland Reef of the Stillwater Complex, Minneapolis Adit area: stratigraphy, structure, and mineralization. Economic Geology, **77**:1481-1492.

Czamanske, G. K. and Zientek, G. K. 1985. The Stillwater Complex, Montana : geology and guide. Butte, Montana: Montana College of Mineral Science and Technology, Special publication / Montana Bureau of Mines and Geology, no. 92, 396.

Czamanske, G. K. and Loferski, P. J. 1996. Cryptic trace-element alteration of anorthosite, Stillwater Complex, Montana. Canadian Mineralogist, **34**: 559-579.

Ebel, D. S. and Naldrett, A. J. 1996. Fractional crystallisation of sulfide ore liquids at high temperature. Economic Geology, **91**: 607-621.

Ebel, D. S. and Naldrett, A. J. 1997. Crystallization of sulfide liquids and the interpretation of ore composition. Canadian Journal of Earth Sciences, **34**(4): 352-365.

Hanley, J. J., Mungall, J. E. & Spooner, E. T. C. 2005. Fluid and melt inclusion evidence for platinum-group element transport by high salinity fluids and halide melts below the J-M Reef, Stillwater Complex, Montana, U.S.A. 10th International Platinum Symposium "Platinum-Group Elements - from Genesis to Beneficiation and Environmental Impact", Törmänen, T. O. & Alapieti, T. T. (eds.), Oulu, Finland, Geological Survey of Finland, Extended Abstract, 94-97.

Li, C. & Ripley, E. M. 2005. Empirical equations to predict the sulfur content of mafic magmas at sulfide saturation and applications to magmatic sulfide deposits. Mineralium Deposita, **40**: 218-230.

Peregoedova, A. and Ohnenstetter, M. 2002. Collectors of Pt, Pd and Rh in a S-poor Fe-Ni-Cu sulfide system at 760 °C; experimental data and application to ore deposits. Canadian Mineralogist, **42**: 527-561.

APPENDIX 1: IMAGE SUPPLEMENTAIRE DE LA DISTRIBUTION 3-D DES MINERAUX SULFURES DANS LE MERENSKY REEF

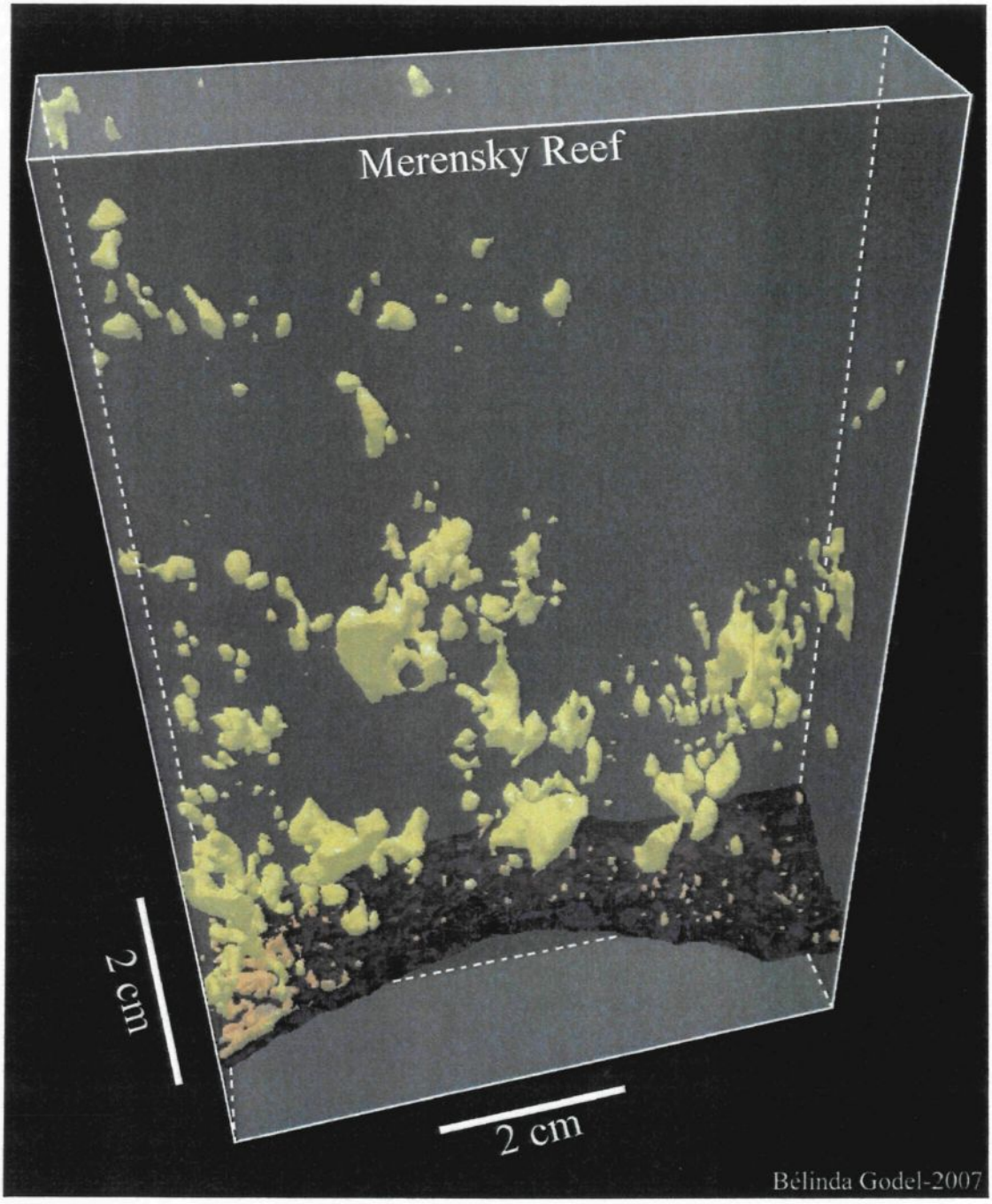

Répresentation 3-D d'une partie du niveau de chromite inférieure (bordeaux) et des sulfures (jaunes). Les sulfures dans le niveau de chromite apparaissent sous formes de gouttellettes.

APPENDIX 2: ANALYSES IN SITU DES SULFURES DU J-M REEF

PENTLANDITE

Section	^{61}Ni wt%	^{65}Cu wt%	^{59}Co wt%	^{185}Re ppm	^{192}Os ppm	^{193}Ir ppm	^{101}Ru ppm	^{103}Rh ppm	^{195}Pt ppm	^{105}Pd ppm	^{197}Au ppm	^{107}Ag ppm	^{111}Cd ppm	^{67}Zn ppm
ST12a	30.91	0.18	1.42	26.260	146.300	50.920	452.31	381.99	0.792	20529	0.014	22.430	2.213	229
ST12a	35.88	1.08	1.78	6.209	155.700	52.030	588.61	385.89	0.530	23729	0.021	23.040	2.821	864
ST12a	29.17	0.42	2.14	0.072	40.970	33.750	119.61	292.89	0.836	23509	0.009	8.742	1.655	30
ST12a	30.49	0.39	2.12	0.095	43.470	51.440	118.61	385.69	0.734	26799	0.008	8.931	1.847	250
ST12b	31.09	0.01	2.13	0.096	24.130	38.470	81.25	469.79	0.756	25869	0.006	9.229	1.765	279
ST12b	28.13	0.16	2.03	0.080	20.430	31.840	66.48	386.29	0.592	21789	0.007	8.410	1.865	798
ST12b	28.22	0.27	1.54	0.074	14.720	26.460	46.47	332.69	0.442	18789	0.005	8.736	1.546	193
ST12b	27.14	0.26	1.79	0.237	16.230	29.180	52.32	359.99	0.565	20959	0.005	9.383	1.518	185
ST12b	26.54	0.19	1.80	0.115	16.420	28.070	54.28	348.29	0.496	19139	0.006	8.294	3.831	4610
ST12b	26.87	0.71	1.52	4.542	18.800	25.090	68.99	300.99	0.863	18829	0.009	11.510	1.810	244
ST12b	26.81	0.33	1.82	3.267	22.390	30.350	79.97	347.89	0.597	22249	0.012	11.550	1.845	133
ST12b	26.63	0.35	1.52	0.014	25.130	16.540	216.51	83.16	0.525	20179	0.054	24.980	27.720	5204
Average ST12	*28.99*	*0.36*	*1.80*	*3.42*	*45.39*	*34.51*	*162.12*	*339.63*	*0.64*	*21864*	*0.01*	*12.94*	*4.20*	*1085*
Geometric mean ST12	*28.88*	*0.25*	*1.78*	*0.35*	*31.14*	*32.78*	*110.22*	*318.69*	*0.63*	*21720*	*0.01*	*11.77*	*2.47*	*381*
ST14a	20.25	0.009	0.40	0.028	0.165	1.655		8.73	1.322	1329	0.008	1.707	0.584	2
ST14a	31.65		0.63	0.009	0.314	2.681	2.84	16.61	1.457	2492	0.005	1.656	0.810	4
ST14b	29.08	0.009	0.63	0.088	0.354	2.672	1.89	4.16	2.930	3478	0.026	3.802	1.628	60
ST14b	36.43	0.002	0.89	0.030	1.633	7.574	25.69	476.19	6.773	8550	0.020	2.625	1.669	20
ST14b	24.90	0.012	0.57	0.353	0.247	1.722		17.02	3.745	4979	0.014	3.413	1.252	13
ST14b	32.41	0.703	0.71	0.024	0.505	1.419	3.13	1.56	6.578	7905	0.012	3.150	1.556	13
ST14b	30.40	0.134	0.94	4.140	0.240	5.130	4.32	0.80	0.509	328	0.034	9.247	1.851	37
ST14b	33.27	0.098	0.93	0.601	0.247	7.957	10.88	1.14	0.480	329	0.111	5.636	2.427	67
ST14b	34.17	0.001	0.68	0.024	0.366	0.970	0.96	70.10	6.010	28279	0.019	5.514	2.237	9
ST14b	33.52	0.005	0.75	0.025	1.137	2.289	3.75	48.23	7.912	12799	0.014	3.607	1.870	32
ST14b	26.62	0.032	0.585	0.011	0.331	1.027	0.09	15.14	5.667	11499	0.019	7.181	1.769	26
Average ST14	*30.25*	*0.10*	*0.70*	*0.48*	*0.50*	*3.19*	*5.95*	*59.97*	*3.94*	*7452*	*0.03*	*4.32*	*1.60*	*26*
Geometric mean ST14	*29.87*	*0.02*	*0.68*	*0.07*	*0.39*	*2.47*	*2.64*	*11.21*	*2.73*	*3693*	*0.02*	*3.78*	*1.49*	*17*

APPENDIX 2

PENTLANDITE

Section	^{61}Ni wt%	^{65}Cu wt%	^{59}Co wt%	^{185}Re ppm	^{192}Os ppm	^{193}Ir ppm	^{101}Ru ppm	^{103}Rh ppm	^{195}Pt ppm	^{105}Pd ppm	^{197}Au ppm	^{107}Ag ppm	^{111}Cd ppm	^{67}Zn ppm
ST16	35.37	0.01	0.54	0.02	1.034	2.104	2.74	33.25	0.039	4261	0.001	0.484	0.764	
ST16	41.03		0.63	0.02	1.011	2.085	2.76	32.75	0.064	4584	0.004	0.531	0.930	
ST16	32.85	0.01	0.50	0.14	0.571	1.390	0.33	19.14	0.035	2944		0.568	0.737	
ST16	37.33	0.001	0.57	0.70	0.753	1.600	0.63	20.06	0.078	3184	0.002	0.626	0.894	5
ST16	28.38		0.49			0.711		9.60	4.992	5290				
ST16	37.68	0.002	0.54	0.005	0.558	0.750	1.00	8.58	5.544	3959	0.008	1.362	1.028	
ST16	24.32	0.002	0.42	0.003	0.206	1.223		5.00	5.919	1921	0.014	3.178	0.824	
ST16	20.84	0.21	0.38	0.002	0.334	2.093		6.79	4.411	1684	0.011	1.945	0.739	18
ST16	35.96	0.01	0.34	0.004	0.626	0.616	1.21	40.00	3.773	2857	0.015	2.225	1.495	131
ST16	33.12	0.32	0.32	0.01	0.620	0.653	1.60	38.28	3.577	2596	0.008	4.598	1.630	348
ST16	37.72	0.18	0.36	0.02	1.120	0.722	3.38	44.54	3.681	2897	0.007	2.780	1.861	382
ST16	29.72		0.29	0.01	1.213	1.297	5.19	6.54	3.612	1824	0.005	1.019	0.802	0.5
ST16	32.79	0.045	0.45	0.08	0.731	1.270	1.71	22.04	2.977	3167	0.008	1.756	1.064	
Average ST16	*32.86*	*0.08*	*0.45*	*0.08*	*0.73*	*1.27*	*2.05*	*22.04*	*2.98*	*3167*	*0.01*	*1.76*	*1.06*	*147*
Geometric mean St16	*32.33*	*0.02*	*0.44*	*0.02*	*0.66*	*1.15*	*1.57*	*17.20*	*1.08*	*2992*	*0.01*	*1.36*	*1.01*	*30*
ST17	31.36	0.81	0.53	0.02	3.257	4.381	18.44	189.69	2.210	6280	0.006	4.895	0.781	28
ST17	27.61	0.75	0.53	0.01	2.931	4.347	17.26	198.39	2.504	9264	0.005	10.670	0.991	231
ST17	25.03	0.64	0.47	0.01	2.406	5.367	26.32	189.59	1.131	5670	0.004	6.035	0.883	96
ST17	25.03	0.65	0.43	0.01	1.876	5.397	19.60	181.09	1.381	6186	0.004	6.736	0.893	122
Average ST17	*27.26*	*0.71*	*0.49*	*0.01*	*2.62*	*4.87*	*20.41*	*189.69*	*1.81*	*6850*	*0.00*	*7.08*	*0.89*	*119*
Geometric mean ST17	*27.14*	*0.71*	*0.49*	*0.01*	*2.56*	*4.85*	*20.13*	*189.59*	*1.71*	*6721*	*0.00*	*6.79*	*0.88*	*94*

APPENDIX 2

PYRRHOTITE

Section	^{61}Ni wt%	^{65}Cu wt%	^{59}Co wt%	^{185}Re ppm	^{192}Os ppm	^{193}Ir ppm	^{101}Ru ppm	^{103}Rh ppm	^{195}Pt ppm	^{105}Pd ppm	^{197}Au ppm	^{107}Ag ppm	^{111}Cd ppm	^{67}Zn ppm
ST12a	0.457	0.050	0.179	0.006	0.313	0.617	1.48	2.06	0.005	371.00		0.988	0.756	26
ST12a	0.048	0.022	0.028	0.004	0.087	0.500	0.93	0.29	0.002	22.28		0.410	0.662	
ST12a	0.021	0.324	0.023	0.092	0.097	0.515	0.95	0.31	0.025	39.34		1.372	0.657	22
ST12a	0.028	0.029	0.023	0.337	0.150	0.535	0.88	0.29	0.040	11.15		0.683	0.633	
ST12b	0.533	0.389	0.192	0.391	0.349	0.492	1.64	4.77	0.030	469.20	0.002	3.955	0.695	137
ST12b	0.031	0.799	0.020	0.002	0.017	0.188	0.57	0.29	0.008	39.03	0.002	2.296	0.505	43
ST12b	0.094	0.024	0.049	0.001	0.043	0.195	0.79	0.46	0.006	91.76	0.001	1.685	0.493	7
ST12b	0.023	0.089	0.011	0.009	0.019	0.290	0.55	0.14	0.022	5.44		0.695	0.451	4
ST12b	0.136	0.067	0.038	0.007	0.192	0.264	2.15	0.70	0.065	174.40	0.018	4.359	1.242	604
Average ST12	*0.05*	*0.13*	*0.03*	*0.065*	*0.086*	*0.355*	*0.97*	*0.35*	*0.024*	*54.77*	*0.007*	*1.64*	*0.66*	*136*
Geometric mean ST12	*0.07*	*0.09*	*0.04*	*0.015*	*0.090*	*0.366*	*1.00*	*0.53*	*0.014*	*56.41*	*0.003*	*1.38*	*0.65*	*35.*
ST14a	0.558		0.080	0.003	0.252	1.682	2.27	0.95	0.016	24.71		0.769	0.456	
ST14a	0.372		0.051	0.001	0.274	1.855	2.46	1.02	0.017	5.12		0.472	0.378	
ST14a	0.967	0.001	0.146	0.039	0.315	2.128	2.95	1.28	0.134	65.65	0.002	1.132	0.506	
ST14a	0.576	0.026	0.113	0.003	0.145	1.307	0.88	0.46	0.046	77.52	0.004	1.131	0.386	
ST14a	0.520	0.001	0.084	0.005	0.093	0.973	1.54	0.20	0.108	85.74	0.003	0.917	0.496	
ST14a	0.467		0.066	0.003	0.178	1.356	1.76	2.05	0.011	7.96		0.290	0.588	
ST14a	0.399	0.001	0.060	0.605	0.490	2.142	2.63	1.84	14.750	4.19	0.018	0.746	0.591	
ST14a	0.429		0.057	0.002	0.327	2.358	3.51	1.73	0.003	0.62		0.401	0.647	
ST14a	0.580	0.013	0.103	0.005	0.130	1.345	0.94	0.86	0.045	49.86	0.002	0.656	0.668	2
ST14a	0.340	0.001	0.058	1.457	0.142	1.130	0.79	0.70	0.029	2.21		0.406	0.619	
ST14a	0.743	0.013	0.129	0.068	0.293	2.311	2.80	0.95	0.134	69.38		0.691	0.656	0.6
ST14a	0.436	0.003	0.070	0.007	0.319	2.440	2.95	0.96	0.002	10.93		0.361	0.621	
ST14b	0.608	0.011	0.095	0.007	0.207	0.680	1.49	0.41	0.145	218.20	0.058	1.422	1.235	68
ST14b	0.642	0.012	0.132	0.006	0.012	0.254	0.84	0.37	0.006	46.20		3.205	0.745	13
ST14b	0.329	0.001	0.043	0.006	0.263	2.155	1.56	0.46	0.007	21.12	0.012	0.790	0.808	8
ST14b	0.260	0.001	0.027	0.009	0.371	3.064	3.21	0.70	0.010	2.04	0.004	0.426	0.766	3
ST14b	0.528	0.003	0.096	0.041	0.338	2.470	2.15	0.38	0.076	105.90	0.006	1.016	1.170	30
Average ST14	*0.52*	*0.01*	*0.08*	*0.13*	*0.24*	*1.74*	*2.04*	*0.90*	*0.91*	*46.90*	*0.01*	*0.87*	*0.66*	*16*
Geometric mean	*0.49*	*0.01*	*0.08*	*0.01*	*0.20*	*1.53*	*1.83*	*0.75*	*0.03*	*18.76*	*0.01*	*0.72*	*0.63*	*3.0*

APPENDIX 2

PYRRHOTITE

Section	^{61}Ni wt%	^{65}Cu wt%	^{59}Co wt%	^{185}Re ppm	^{192}Os ppm	^{193}Ir ppm	^{101}Ru ppm	^{103}Rh ppm	^{195}Pt ppm	^{105}Pd ppm	^{197}Au ppm	^{107}Ag ppm	^{111}Cd ppm	^{67}Zn ppm
ST16	0.375		0.022		0.736	0.426	1.51	0.06				0.254	0.500	
ST16	0.310		0.019	0.097	0.170	0.194	0.72	0.10	0.032	11.45		0.490	0.575	
ST16	0.632	0.006	0.067	0.015	0.679	0.216	3.01	0.07	0.166	58.45		2.297	0.504	
ST16	0.324	0.016	0.018	0.198	0.356	0.586	1.27	0.06	0.106	2.03	0.022	1.028	0.605	
ST16	0.494	0.025	0.045	0.235	1.194	0.768	5.07	0.07	0.115	6.08	0.002	3.883	0.582	
ST16	0.420		0.025	0.050	0.422	0.378	1.36	0.09	0.027	12.64		0.314	0.692	
ST16	0.544		0.037	0.351	0.587	0.450	1.68	0.07	0.068	15.66		0.592	0.679	
ST16	0.342		0.017	0.160	0.420	0.521	1.44	0.06	0.036	1.30	0.002	0.804	0.645	
Average ST16	*0.43*	*0.02*	*0.03*	*0.16*	*0.57*	*0.44*	*2.01*	*0.07*	*0.08*	*15.37*	*0.009*	*1.21*	*0.60*	
Geometric mean	*0.42*	*0.02*	*0.03*	*0.11*	*0.50*	*0.40*	*1.70*	*0.07*	*0.06*	*8.01*	*0.004*	*0.80*	*0.59*	
ST17		0.014	0.002	0.315	0.269	1.611	1.00	0.12	0.016	0.71		0.065	0.471	
ST17		0.027	0.002	0.072	0.233	1.613	1.05	0.13	0.006	8.82		0.103	0.519	
ST17	0.077	0.112	0.024	0.002	0.163	1.300	0.94	0.08		38.48		0.132	0.482	
ST17			0.001	0.498	0.171	0.462	0.52	0.01	0.010	0.05		0.093	0.544	
ST17	0.600	0.282	0.101		0.007	0.051	0.40	0.04	0.023	106.70		0.587	0.632	193
ST17	0.269	0.999	0.044		0.004	0.067	0.48	0.08	0.052	141.90		0.618	0.716	278
ST17	0.335	0.194	0.072	0.005	0.066	0.434	0.80	0.20	0.014	43.66		0.530	0.585	
ST17		0.008	0.003	0.008	0.132	1.286	1.02	0.05		0.11		0.073	0.559	
ST17	0.671	0.767	0.123	0.063	0.077	1.089	0.79	0.12	0.009	182.20		0.984	0.773	2172.
ST17	0.126	0.100	0.028	0.323	0.147	1.095	0.74	0.05	0.012	10.72	0.002	0.403	0.675	376
ST17	0.274	0.644	0.067	0.030	0.035	0.988	0.71	0.09	0.034	67.71		0.389	0.959	1262
ST17	0.043	0.037	0.008	0.019	0.063	1.098	0.88	0.06	0.049	8.64	0.013	1.034	1.040	55
ST17	0.026	0.376	0.004		0.028	0.292	0.60	0.11		20.93	0.022	0.313	0.916	582
ST17	0.217	0.968	0.027	0.003	0.035	0.273	0.77	0.16	0.010	171.50		0.751	1.767	3517
Average ST17	*0.26*	*0.35*	*0.04*	*0.12*	*0.10*	*0.83*	*0.76*	*0.09*	*0.02*	*57.30*	*0.01*	*0.43*	*0.76*	*1054*
Geometric mean	*0.17*	*0.14*	*0.01*	*0.03*	*0.06*	*0.56*	*0.74*	*0.07*	*0.02*	*12.99*	*0.01*	*0.30*	*0.718*	*531*

APPENDIX 2

CHALCOPYRITE

Section	^{61}Ni wt%	^{65}Cu wt%	^{59}Co wt%	^{185}Re ppm	^{192}Os ppm	^{193}Ir ppm	^{101}Ru ppm	^{103}Rh ppm	^{195}Pt ppm	^{105}Pd ppm	^{197}Au ppm	^{107}Ag ppm	^{111}Cd ppm	^{67}Zn ppm
ST12a		20.552	0.001	0.002	0.089	0.243	0.43		0.018	0.55	0.004	1.976	0.821	431
ST12a		26.247	0.001	0.002	0.120	0.414	0.61	0.12	0.010	3.34	0.006	3.689	1.223	226
ST12a	0.028	32.745	0.018	0.009	1.660	0.358	1.08	0.47	0.314	68.90	0.065	2.825	1.856	734
Average ST12	*0.03*	*26.51*	*0.007*	*0.004*	*0.62*	*0.34*	*0.71*	*0.30*	*0.11*	*24.26*	*0.02*	*2.83*	*1.30*	*464*
Geometric mean	*0.03*	*26.04*	*0.003*	*0.003*	*0.26*	*0.33*	*0.66*	*0.24*	*0.04*	*5.02*	*0.01*	*2.74*	*1.23*	*415*
ST14a	0.096	32.870	0.018	0.008	0.017	0.097	0.29	0.05	0.125	14.62	0.018	21.620	4.470	2702
ST14a	0.009	32.860	0.002	0.003	0.006	0.011	0.44	0.13	0.015	1.22	0.026	16.060	1.447	451
ST14b	0.893	32.368	0.164	0.035	0.028	0.051	0.86	0.32	0.286	260.11	0.009	13.940	1.910	686
ST14b	0.111	31.805	0.016	0.010	0.010	0.008	0.95	0.35	0.071	18.97	0.014	29.180	1.706	444
ST14b	0.050	34.738	0.004	0.005	0.008	0.018	0.87	0.42	0.021	34.33	0.030	11.110	1.788	572
ST14b	0.592	32.136	0.103	0.007	0.009	0.010	0.94	0.31	0.015	0.74	0.047	32.030	1.989	652
Average ST14	*0.29*	*32.79*	*0.05*	*0.01*	*0.01*	*0.03*	*0.72*	*0.26*	*0.09*	*54.60*	*0.02*	*20.66*	*2.22*	*917*
Geomean	*0.12*	*32.78*	*0.02*	*0.01*	*0.01*	*0.02*	*0.66*	*0.21*	*0.05*	*11.44*	*0.02*	*19.21*	*2.05*	*719*
ST16	0.001	30.280	0.001	0.004	0.013	0.009	0.08	0.00	0.004	0.17	0.004	1.689	12.130	802
ST17	0.043	29.960	0.004	0.067	0.163	1.285	0.11	n-d	0.010	0.05		1.011	0.659	453
ST17	0.143	28.600	0.020	0.006	0.017	0.010	0.01	n-d	0.139	0.53	0.002	3.668	1.844	1943
ST17	0.213	33.832	0.030	0.004	0.003	0.002	0.01	n-d	0.072	0.62	0.002	3.324	2.390	1998
ST17	0.261	35.805	0.008	0.007	0.004	0.020	0.05	0.24	0.087	0.65	0.004	2.979	2.354	1917
Average ST17	0.16	32.05	0.02	0.02	0.05	0.33	0.05	0.24	0.08	0.46	0.003	2.75	1.81	1577
Geomean	0.13	31.92	0.01	0.01	0.02	0.03	0.03	0.24	0.05	0.32	0.003	2.46	1.62	1355

APPENDIX 2

MSS or ISS : MIXED VALUES

Section	^{61}Ni wt%	^{65}Cu wt%	^{59}Co wt%	^{185}Re ppm	^{192}Os ppm	^{193}Ir ppm	^{101}Ru ppm	^{103}Rh ppm	^{195}Pt ppm	^{105}Pd ppm	^{197}Au ppm	^{107}Ag ppm	^{111}Cd ppm	^{67}Zn ppm
ST12a	5.008	29.641	0.643	0.003	0.001	0.002		0.35	0.000	4348.0	0.016	26.600	5.310	7672
ST12a	2.335	33.803	0.313	0.005	0.006	0.001		0.74	0.026	1926.0	0.050	11.490	5.486	5991
ST12a	1.628	38.740	0.216	0.006	0.009	0.004		0.72	0.018	1354.0	0.156	8.776	2.633	935
ST12a	29.120	8.156	4.743	0.020	2.568	9.282	6.97	240.99	0.507	22310.0	0.012	20.560	3.739	4171
ST12a	4.932	27.622	0.699	8.483	0.616	0.377		4.59	0.255	3973.0	2.918	17.330	213.300	44890
ST12a	6.367	31.375	0.894	0.652	0.016	0.021		0.40	0.034	4601.0	0.012	18.530	20.960	42620
ST12a	2.342	40.535	0.334	0.001	0.003	0.002		0.53	0.028	1839.0	0.015	11.280	16.750	31430
ST12a	32.750	6.610	3.421	0.104	74.610	37.030	298.41	280.59	0.541	20140.0	0.026	22.840	3.676	2890
ST12a	12.327	24.929	1.235	1.422	6.010	9.012	21.58	68.26	0.563	7952.0	0.012	21.330	4.739	7240
ST12a	28.459	3.207	2.941	1.716	29.630	28.460	107.71	222.49	0.298	15880.0	0.006	18.520	1.498	133
ST12a	4.257	11.824	0.484	0.145	1.185	2.382	5.71	19.88	0.633	2072.0	0.009	7.991	6.543	2598
ST12a	17.130	26.520	2.128	3.607	1.483	0.769	4.00	7.00	0.090	9199.0	0.017	34.030	3.668	2702
ST12a	25.321	10.084	3.836	0.073	47.710	38.220	131.91	323.39	1.377	20380.0	0.019	16.540	2.846	2571
ST12a	0.080	11.814	0.005		0.002	0.002		0.23	0.039	13.8	0.029	2.598	3.859	3319
ST12a	0.853	19.921	0.125	0.005	0.074	0.032		0.37	0.037	849.4	0.035	5.894	4.880	3695
ST12a	6.136	39.392	0.892	0.008	0.006	0.005		0.59	0.168	5771.0	0.031	17.670	3.762	3759
ST12a	0.029	7.770	0.013	0.002	0.018	0.075		0.26	0.007	16.2	0.012	2.821	1.533	186
ST12a	0.022	7.038	0.007		0.001	0.086		0.15		2.9	0.004	2.636	0.974	23
ST12a	0.024	8.748	0.007		0.004	0.096		0.16	0.001	8.0	0.013	2.898	3.183	3306
ST12a	0.338	29.335	0.056	0.005	0.003	0.031		0.50	0.095	374.8	0.134	4.443	34.070	68480
ST12a	3.762	41.494	0.511	0.008	0.006	0.010		0.68	0.024	3528.0	0.126	18.990	5.119	5479
ST12a	3.977	31.579	0.579	0.012	0.012	0.008	0.82	1.01	0.037	3270.0	0.158	16.120	12.440	16220
ST12a	2.919	38.984	0.442	1.929	2.152	0.438		0.61	0.089	2686.0	0.051	11.280	2.277	1696
ST12a	2.159	41.045	0.348	0.010	0.007	0.005		0.59	0.014	1833.0	0.068	7.585	1.965	837

APPENDIX 2

MSS or ISS : MIXED VALUES

Section	^{61}Ni wt%	^{65}Cu wt%	^{59}Co wt%	^{185}Re ppm	^{192}Os ppm	^{193}Ir ppm	^{101}Ru ppm	^{103}Rh ppm	^{195}Pt ppm	^{105}Pd ppm	^{197}Au ppm	^{107}Ag ppm	^{111}Cd ppm	^{67}Zn ppm
ST12b	22.455	3.986	3.533	0.059	18.470	27.040	65.80	319.80	0.851	17240.0	0.865	24.800	7.792	12370.0
ST12b	28.086	2.311	4.330	0.104	19.540	28.750	64.63	355.60	0.650	20160.0	0.009	29.320	3.152	2494.0
ST12b	19.962	8.195	3.020	0.048	17.300	25.420	66.70	291.00	0.730	16540.0	0.006	29.030	1.748	658.7
ST12b	23.320	4.058	3.706	0.043	10.040	25.700	44.99	251.00	0.925	18530.0	0.006	28.480	1.719	413.7
ST12b	28.561	2.160	4.433	0.052	11.200	27.440	49.30	276.30	0.689	23520.0	0.005	18.860	1.848	208.3
ST12b	25.220	2.105	3.605	0.008	6.259	10.380	46.74	50.71	0.620	20170.0	0.005	15.800	3.271	3598.0
ST12b	0.478	2.934	0.074	0.161	0.094	0.244	0.56	0.21	0.045	266.7	0.001	2.112	0.529	101.5
ST12b	1.325	7.197	0.232	0.003	0.095	1.780	0.95	14.94	0.273	1158.0	0.003	4.127	0.701	244.9
ST12b	0.107	2.785	0.022	0.004	0.026	0.067	0.70	0.52	0.075	38.6	0.003	2.754	0.953	766.2
ST12b	0.129	3.576	0.008	0.001	0.008	0.043	0.61	0.24	0.010	7.3	0.003	2.652	0.625	197.9
ST12b	14.767	3.097	1.996	8.972	2.428	6.113	1.90	34.26	0.668	12190.0	0.007	13.870	2.855	1746.0
ST12b	2.286	13.521	0.358	0.015	0.236	0.493	1.46	5.30	0.183	1153.0	0.014	5.159	0.886	615.6
ST12b	2.369	3.623	0.499	0.055	0.020	0.114	0.64	0.21	0.017	2470.0	0.001	14.260	1.386	2315.0
ST14a	6.762	0.000	0.470	0.447	0.280	1.834	2.22	0.33	1.863	531.1	0.007	2.249	0.551	1.5
ST14a	3.528	0.027	0.301	0.003	0.124	1.163	0.93	0.48	0.052	320.0	0.007	2.299	0.519	11.7
ST14a	18.079	1.612	1.599	0.040	0.119	1.294	1.69	0.96	0.829	2357.0	0.021	8.309	0.951	13.1
ST14a	12.213	0.226	0.960	0.004	0.109	1.185	1.52	0.62	0.485	1507.0	0.011	4.197	0.896	14.7
ST14a	11.587	0.004	0.893	0.024	0.123	1.291	2.78	1.27	1.019	1547.0	0.008	2.938	0.753	1.0

APPENDIX 2

MSS or ISS : MIXED VALUES

Section	^{61}Ni wt%	^{65}Cu wt%	^{59}Co wt%	^{185}Re ppm	^{192}Os ppm	^{193}Ir ppm	^{101}Ru ppm	^{103}Rh ppm	^{195}Pt ppm	^{105}Pd ppm	^{197}Au ppm	^{107}Ag ppm	^{111}Cd ppm	^{67}Zn ppm
ST14b	4.140	0.098	0.423	0.004	0.191	0.559	1.31	0.16	0.382	2222.0	0.011	18.990	0.809	8.4
ST14b	2.948	0.004	0.231	0.042	0.271	2.765	2.96	0.77	0.296	303.3	0.002	1.694	0.730	7.7
ST14b	1.935	0.047	0.198	0.015	0.022	0.251	1.11	0.41	0.137	61.1	0.030	4.826	1.093	43.6
ST14b	7.841	0.043	0.645	0.005	0.520	0.782	4.09	7.80	0.530	1137.0	0.014	6.839	0.738	
ST14b	2.945	0.004	0.151	0.004	0.018	0.468	0.93	1.05	0.261	236.3	0.002	1.565	0.965	8.9
ST14b	9.564	0.241	0.461	0.049	0.239	1.757	1.77	0.84	0.429	1163.0	0.008	11.190	0.889	8.3
ST14b	65.841	2.440	3.415	0.012	0.189	3.660	6.16	0.64	0.227	251.8	0.039	10.990	1.582	19.5
ST16	0.616	2.273	0.010	0.008	0.653	0.498	1.65	0.08		0.6	0.000	2.420	1.251	66.3
ST16	5.117	18.772	0.169	0.070	0.756	0.491	3.38	3.42	3.422	282.6	0.259	86.490	14.560	1262.0
ST17	0.000	3.015	0.001	0.003	0.124	1.099	0.89	0.13	0.005	3.2		0.265	0.494	29.1
ST17	0.219	2.791	0.009	0.022	0.021	0.311	0.77	0.22	0.040	13.0	0.014	1.287	0.922	13.3
ST17	13.185	13.905	0.415	0.157	0.359	2.644	3.66	26.42	1.934	2682.0	0.013	6.283	3.683	3494.0
ST17	6.219	19.594	0.151	1.184	2.825	1.901	18.95	1.46	0.247	1593.0	0.007	6.290	5.417	4888.0
ST17	8.644	19.562	0.216	0.201	2.441	1.417	14.85	0.99	0.032	1382.0	0.001	5.244	2.710	630.0
ST17	1.824	4.869	0.064	0.001	0.018	0.260	0.89	0.24	0.002	398.0		1.729	1.407	1524.0

APPENDIX 3: CALCULATION OF THE ABLATION RATE OF THE LASER IN BASE-METAL SULFIDES

Sulfide	Depth ablation (μm)	Tf (ms)	Ti (ms)	Tf-Ti (ms)	Ablation rate (μm/s)
Pn	90	70845	45282	25563	3.52
Ccp	90	80816	28015	52801	1.70
Pn+Ccp	90	78846	29521	49325	1.82
Pn+Ccp	90	88294	30928	57366	1.57
Pn+Ccp	90	84489	33459	51030	1.76
Pn+Ccp	90	87244	28219	59025	1.52
Po	90	83440	43830	39610	2.27
Ccp	90	58381	34550	23831	3.78
Ccp	90	56938	33274	23664	3.80
Ccp	90	58260	32491	25769	3.49
Po	90	59300	31250	28050	3.21
Po	90	59431	31500	27931	3.22
Po	90	59300	31346	27954	3.22
Po	90	59562	31668	27894	3.23
Ccp	90	70187	38649	31538	2.85
Ccp	90	65466	29567	35899	2.51
Po	80	49854	29029	20825	3.84
Po	80	55233	32693	22540	3.55
Po	90	55758	30999	24759	3.64
Po	90	51034	29376	21658	4.16
Po	90	52084	30390	21694	4.15
Po	90	48804	27943	20861	4.31
Po	90	55758	28683	27075	3.32
Po	90	60874	28552	32322	2.78
Po	90	55102	30808	24294	3.70
Po	90	54102	30808	23294	3.86
Po	90	54708	28612	26096	3.45
Po	90	52740	28982	23758	3.79
Po	90	52090	29280	22810	3.95
Po	90	53658	30283	23375	3.85
Ccp	90	75306	31416	43890	2.05
Ccp	90	71370	30260	41110	2.19
Pn	90	75998	29208	46790	1.92
Pn	90	81841	29638	52203	1.72
Pn	90	75961	30771	45190	1.99
Pn	90	86064	30425	55639	1.62
Pn	90	86195	29602	56593	1.59
Pn	90	76618	29924	46694	1.93
Pn	90	78979	32071	46908	1.92
Pn	90	73371	30700	42671	2.11
Po	90	68613	29077	39536	2.28

Sulfide	Depth ablation (µm)	Tf (ms)	Ti (ms)	Tf-Ti (ms)	Ablation rate (µm/s)
Po	90	66384	31595	34789	2.59
Po	90	75043	30354	44689	2.01
Po	90	64154	29113	35041	2.57
Po	90	63760	29577	34183	2.63
Po	90	66647	30545	36102	2.49
Po	90	66516	29853	36663	2.45
Po	90	80291	29470	50821	1.77

APPENDIX 4: LASER-ABLATION OF CHROMITE GRAINS OF THE MERENSKY REEF AND J-M REEF

Laser ablation ICP-MS analysis of the chromite grains of the Merensky Reef and the J-M Reef was carried out in order to test whether the chromite grains may contain PGE in their lattices. Time-resolved spectra of the chromite grains (Fig. A4-1) indicate that no PGE occur in chromite grain lattices. The only PGE rich phases observed during the laser ablation are small inclusions. All the inclusions observed on TRA-spectra are summarized in Table A4-1.

The composition of the chromitite grains was evaluated for several elements (Table A4-2) using the time-resolved spectra and the NIST612 standard.

In this case, the composition of the chromite (C^i_{CHR}) for the element *i* was calculated as follows:

$$C^i_{CHR} = ((P^i_{CHR} - BC_{CHR}) / (P^i_{SDT} - BC_{SDT})) * C^i_{SDT}$$

where P^i_{CHR} is the intensity of the peak (in counts per second) for the element *i* in the chromite grains; P^i_{SDT} is the intensity of the peak (in counts per second) for the element *i* in the standard (NIST612); C^i_{SDT} is the concentration of the element *i* in the standard and BC_{CHR} and BC_{SDT} are the background counts for a given element in chromite and standard, respectively.

Our results were compared with electron microprobe data of Li et al. (2005), Mathez and Nicholson (1995), Kruger and Marsh (1985), Tiegler and Eales (1993) and Legg (1969) for the Merensky Reef.

REFERENCES

Cameron, E. M. 1977. Chromite in the central sector of the Eastern Bushveld Complex, South Africa. American Mineralogist, **62**: 1082-1096.

Kruger, F. J. and Marsh, J. S. 1985. The Mineralogy, Petrology, and Origin of the Merensky Cyclic Unit in the Western Bushveld Complex. Economic Geology, **80**: 958-974,

Li, C., Ripley, E. M., Sarkar, A., Shin, D. and Maier, W. D. 2005. Origin of phlogopite-orthopyroxene inclusions in chromites from the Merensky Reef of the Bushveld Complex, South Africa. Contributions to Mineralogy and Petrology, **150**: 119-130.

Nicholson, D. M. and Mathez, E. A. 1991. Petrogenesis of the Merensky Reef in the Rustenburg section of the Bushveld Complex. Contributions to Mineralogy and Petrology, **107**(3): 293-309.

Teigler, B. and Eales, H. V. 1993. Correlation between chromite composition and PGE mineralization in the Critical Zone of the western Bushveld Complex. Mineralium Deposita, **28**(5): 291-302.

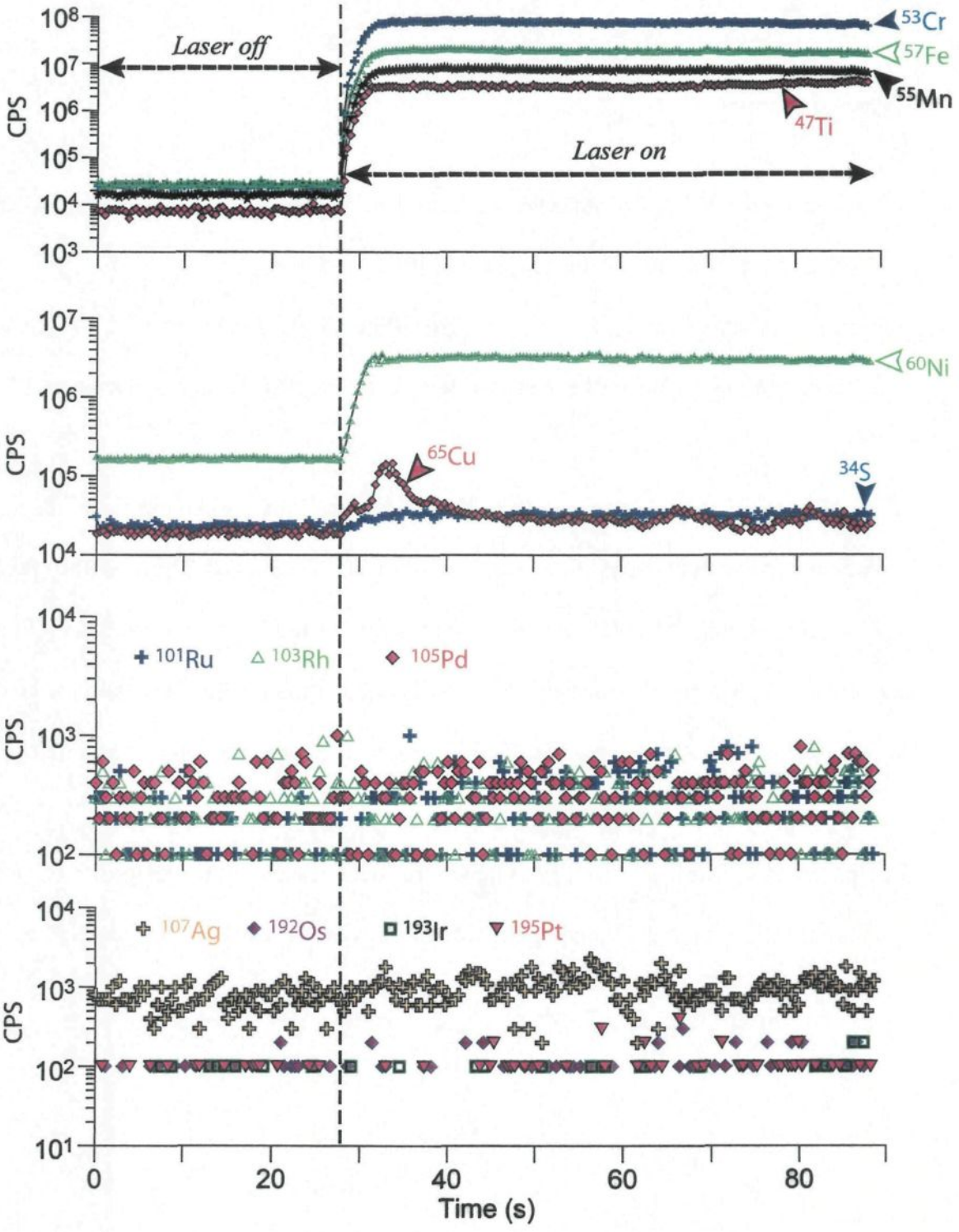

Figure A4-1: Example of time-resolved spectra for chromite grains of the Merensky Reef

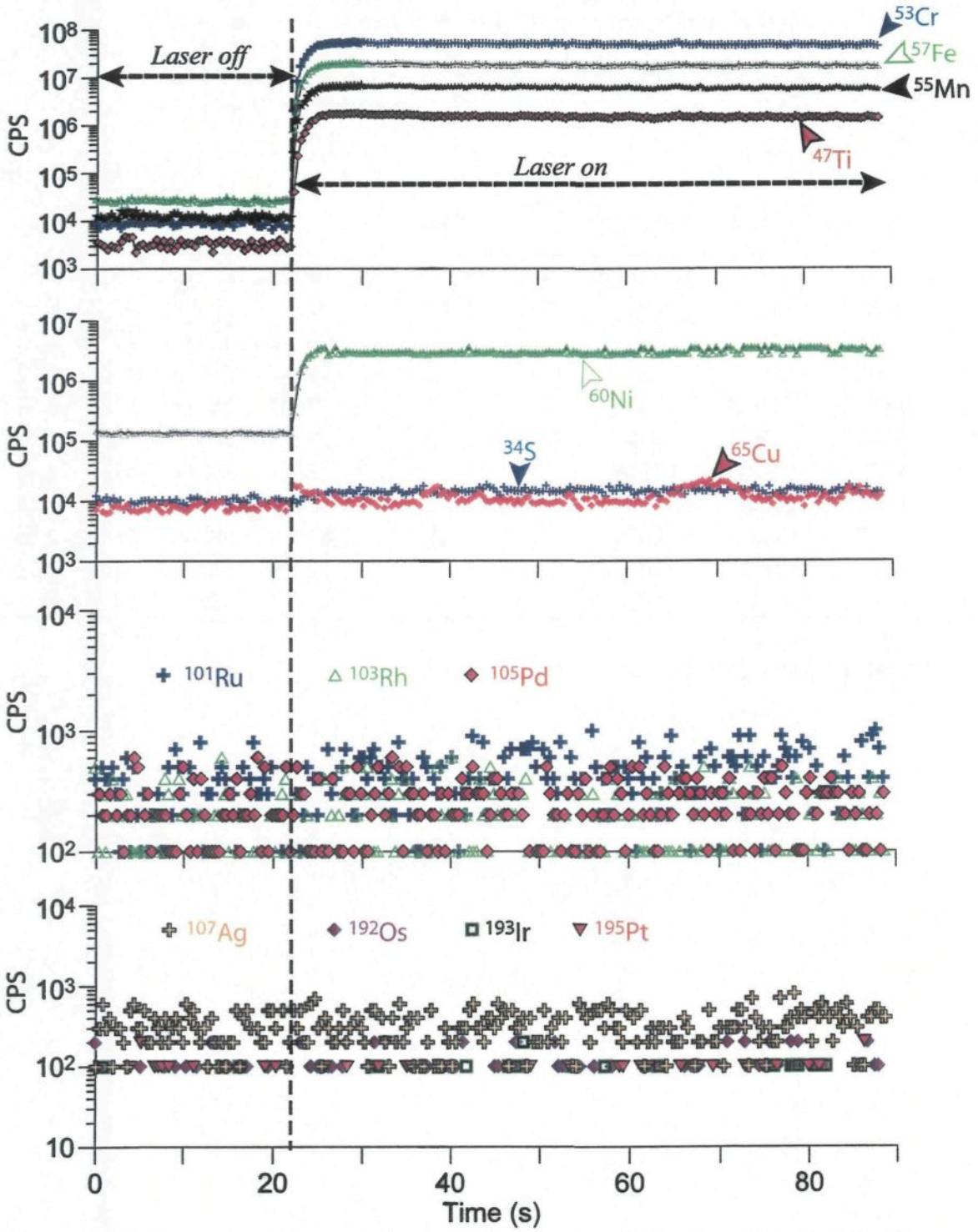

Figure A4-2: Example of time-resolved spectra for chromite grains of the J-M Reef

Table A4-1: *Summary of PGE- and noble metal-rich inclusions observed during laser ablation of the chromite grains of the Merensky Reef.*

Section	Name	Lithology	Major element	Number	Ti (ms)	Tf (ms)	Tf-Ti (ms)	Length* (μm) Max.	Min.
MRE2	CHR2	LC-CGM	Rh	1	42725	43119	394	0.28	0.16
MRE2	CHR3	LC	Ru	1	35553	35991	438	0.31	0.18
MRE2	CHR3	LC	Ag	1	73272	73731	459	0.32	0.19
MRE2	CHR3	LC	Pt	1	66187	66603	416	0.29	0.17
MRE2	CHR7	LC	Rh	1	77667	78542	875	0.61	0.35
MRE2	CHR9	CGM	Pd-Rh	1	33126	33651	525	0.37	0.21
MRE4	CHR1	UC-M	Pt	1	28731	29344	613	0.43	0.25
MRE4	CHR7	UC	Ag	1	73469	73862	393	0.28	0.16
MRE4	CHR8	UC	Ag	1	51428	52084	656	0.46	0.27
MRE4	CHR-T3	UC	Pd-Ag	1	52609	53119	510	0.36	0.21
MRE4	CHR-TB5	UC	Ru	1	47886	48279	393	0.28	0.16

* Estimate using an ablation rate of 0.7 μm/s

***Table A4-2:** Composition of the chromite grains of the Merensky Reef (Bushveld Complex).*

Analysis	n	Height mm	Lithology	Mg wt%	Al wt%	Ti ppm	V ppm	Mn ppm	Co ppm	Ni ppm	Cu ppm	Zn ppm	Sn ppm
MRE-2-CHR01-Average	5	10*	LC-CGM	4.69	13.69	11948	1098	1380	229	859	d.l	683	0.38
MRE-2-CHR01-Stdev				*0.13*	*0.41*	*485*	*36*	*44*	*6*	*28*		*45*	*0.02*
MRE-2-CHR02-Average	5	10.5*	LC-CGM	4.53	13.65	12317	1106	1357	226	929	d.l	664	0.39
MRE-2-CHR02-Stdev				*0.21*	*0.53*	*533*	*53*	*66*	*11*	*44*		*21*	*0.04*
MRE-2-CHR03-Average	4	8.8*	LC	5.03	13.55	12608	1020	1226	198	623	1.23	629	0.56
MRE-2-CHR03-Stdev				*0.33*	*0.97*	*582*	*90*	*110*	*5*	*53*	*3.72*	*45*	*0.03*
MRE-2-CHR04-Average	5	8.6*	LC	4.76	14.57	12403	1120	1305	221	858	d.l	665	0.48
MRE-2-CHR04-Stdev				*0.27*	*0.61*	*173*	*74*	*82*	*14*	*48*		*31*	*0.04*
MRE-2-CHR05-Average	5	6.6*	AN-LC	5.01	17.20	10539	1356	1608	268	862	d.l	835	0.31
MRE-2-CHR05-Stdev				*0.18*	*0.91*	*948*	*42*	*64*	*10*	*29*		*77*	*0.04*
MRE-2-CHR06-Average	5	6.2*	AN-LC	4.12	13.43	13096	1189	1411	225	820	d.l	642	0.30
MRE-2-CHR06-Stdev				*0.17*	*0.62*	*713*	*56*	*67*	*11*	*42*		*37*	*0.02*
MRE-2-CHR07-Average	5	6.5*	LC	4.43	12.14	15668	1021	1109	187	715	3.25	477	0.28
MRE-2-CHR07-Stdev				*0.48*	*1.30*	*1370*	*113*	*120*	*20*	*94*	*3.34*	*55*	*0.01*
MRE-2-CHR08-Average	5	4.8*	LC-CGM	5.24	15.23	12315	1185	1396	235	871	d.l	661	0.36
MRE-2-CHR08-Stdev				*0.18*	*0.40*	*287*	*42*	*46*	*8*	*26*		*33*	*0.04*
MRE-2-CHR09-Average	5	13*	CGM	3.06	8.46	12380	979	1091	187	657	d.l	504	1.40
MRE-2-CHR09-Stdev				*0.56*	*1.55*	*332*	*179*	*197*	*35*	*147*		*120*	*0.31*
MRE-2-CHR10-Average	5	13.2*	CGM	3.34	9.50	12671	1126	1260	214	783	d.l	597	1.70
MRE-2-CHR10-Stdev				*0.16*	*0.34*	*148*	*62*	*68*	*12*	*44*		*26*	*0.09*

Table A4-2 (continued)

Analysis	n	Height mm	Lithology	Mg wt%	Al wt%	Ti ppm	V ppm	Mn ppm	Co ppm	Ni ppm	Cu ppm	Zn ppm	Sn ppm
MRE-2-CHR11-Average	5	28.9*	CGM	2.01	5.79	12843	946	938	174	474	d.l	454	2.08
MRE-2-CHR11-Stdev				*0.03*	*0.10*	*471*	*19*	*11*	*5*	*7*		*38*	*0.06*
MRE-2-CHR12-Average	5	28.7*	CGM	1.90	5.82	13080	971	989	178	538	d.l	517	2.36
MRE-2-CHR12-Stdev				*0.02*	*0.03*	*672*	*3*	*10*	*1*	*19*		*49*	*0.10*
MRE4-CHR01-Average	4	22.4**	UC-M	3.48	8.76	13789	1959	1456	193	1221	1.5	867	1.4
MRE4-CHR01-Stdev				*0.18*	*0.43*	*612*	*93*	*66*	*10*	*62*	*0.9*	*86*	*0.1*
MRE4-CHR02-Average	4	18**	UC-M	3.58	8.94	13329	1952	1462	185	1123	1.0	866	1.7
MRE4-CHR02-Stdev				*0.18*	*0.38*	*411*	*105*	*31*	*11*	*52*	*0.5*	*55*	*0.1*
MRE4-CHR03-Average	4	17.2**	UC-M	3.79	9.27	15048	2034	1473	200	1243	1.8	875	2.1
MRE4-CHR03-Stdev				*0.20*	*0.38*	*856*	*99*	*58*	*10*	*59*	*0.3*	*68*	*0.2*
MRE4-CHR05-Average	4	10.8**	UC-M	3.91	11.52	12800	2152	1794	200	937	d.l	1051	1.5
MRE4-CHR05-Stdev				*0.23*	*0.53*	*1101*	*122*	*92*	*11*	*62*		*64*	*0.1*
MRE4-CHR06-Average	4	12.1**	UC-M	4.00	11.75	14376	2215	1787	223	1225	d.l	1027	1.8
MRE4-CHR06-Stdev				*0.19*	*0.45*	*277*	*116*	*105*	*16*	*183*		*63*	*0.3*
MRE4-CHR07-Average	2	1.3**	UC	3.50	9.43	9360	1236	1261	170	991	d.l	602	1.4
MRE4-CHR07-Stdev				*0.12*	*0.09*	*387*	*34*	*17*	*4*	*20*		*7*	*0.0*
MRE4-CHR08-Average	2	0.9**	UC	3.56	9.56	11346	1279	1263	179	1040	d.l	634	1.6
MRE4-CHR08-Stdev				*0.27*	*0.54*	*875*	*88*	*1*	*11*	*56*		*27*	*0.1*
MRE4-CHR09-Average	3	2.8**	UC	3.84	10.21	12873	1081	1270	182	993	d.l.	687	0.7
MRE4-CHR09-Stdev				*0.13*	*0.18*	*2190*	*36*	*23*	*4*	*1*		*10*	*0.0*
MRE4-CHR10-Average	2	2.4**	UC	3.51	9.29	8812	1141	1248	169	954	d.l	602	0.6
MRE4-CHR10-Stdev				*0.35*	*1.44*	*904*	*100*	*55*	*15*	*92*		*81*	*0.1*

Table A4-2 (continued)

Analysis	n	Height mm	Lithology	Mg wt%	Al wt%	Ti ppm	V ppm	Mn ppm	Co ppm	Ni ppm	Cu ppm	Zn ppm	Sn ppm
MRE4-CHR-T1-Average	4	10.2**	UC	4.48	12.17	16308	2379	1856	263	1521	1.6	1031	1.8
MRE4-CHR-T1-Stdev				*0.27*	*0.65*	*881*	*149*	*109*	*16*	*34*	*0.1*	*82*	*0.1*
MRE4-CHR-T2-Average	3	10**	UC	4.78	13.01	17983	2556	1993	277	1482	1.3	1108	2.1
MRE4-CHR-T2-Stdev				*0.29*	*0.60*	*999*	*176*	*118*	*24*	*57*	*0.1*	*55*	*0.1*
MRE4-CHR-T3-Average	3	9.9**	UC	4.69	12.65	16051	2433	1906	271	1501	1.5	1038	1.8
MRE4-CHR-T3-Stdev				*0.27*	*0.54*	*775*	*154*	*115*	*18*	*96*	*0.4*	*44*	*0.0*
MRE4-CHR-T4-Average	3	9.6**	UC	4.51	12.53	15462	2415	1821	242	1229	d.l	1018	1.5
MRE4-CHR-T4-Stdev				*0.31*	*0.72*	*850*	*198*	*142*	*20*	*95*		*45*	*0.0*
MRE4-CHR-TB1-Average	2	9.6**	UC	4.03	11.30	12120	1586	1400	210	1152	d.l	726	1.3
MRE4-CHR-TB1-Stdev				*1.55*	*4.43*	*5345*	*760*	*470*	*92*	*502*		*249*	*0.7*
MRE4-CHR-TB2-Average	3	7.7**	UC	4.83	13.72	15145	2002	1636	259	1428	d.l	918	1.8
MRE4-CHR-TB2-Stdev				*0.28*	*0.71*	*677*	*118*	*93*	*16*	*82*		*18*	*0.0*
MRE4-CHR-TB3-Average	3	6.5**	UC	3.26	8.87	9835	1136	1135	154	859	d.l	561	1.4
MRE4-CHR-TB3-Stdev				*0.14*	*0.30*	*780*	*48*	*43*	*5*	*24*		*11*	*0.0*
MRE4-CHR-TB4-Average	3	4.9	UC	3.49	9.30	9654	1227	1265	165	849	d.l	621	1.4
MRE4-CHR-TB4-Stdev				*0.18*	*0.38*	*254*	*53*	*24*	*6*	*16*		*10*	*0.0*
MRE4-CHR-TB5-Average	3	3.7	UC	3.19	9.20	7643	1227	1244	160	747	d.l	608	1.3
MRE4-CHR-TB5-Stdev				*0.13*	*0.31*	*203*	*58*	*26*	*6*	*10*		*4*	*0.0*

*Height above the lowest point of the lower chromitite layer

** Height above the lowest point of the upper chromitite layer

n number of "integration box" for the calculation of the chromite composition

Table A4-3: *Composition of the chromite grains of the J-M Reef (Stillwater Complex).*

Analysis	*n*	Mg wt%	Al wt%	Ti ppm	V ppm	Mn ppm	Co ppm	Ni ppm	Cu ppm	Zn ppm	Sn ppm
ST17-CHR1	5	4.66	18.17	4692	1261	1716	307	1122	d.l	1286	d.l
Stdev		*0.29*	*1.18*	*319*	*68*	*90*	*16*	*57*		*39*	
ST17-CHR2	5	4.78	18.94	5022	1326	1722	306	1100	d.l	1243	d.l
Stdev		*0.10*	*0.41*	*89*	*41*	*48*	*10*	*30*		*42*	
ST17-CHR3	5	4.89	18.84	4986	1351	1809	312	1112	d.l	1351	d.l
Stdev		*0.26*	*0.89*	*265*	*74*	*93*	*9*	*36*		*33*	

n number of "integration box"

APPENDIX 5: LASER-ABLATION OF ORTHOPYROXENE GRAINS OF THE MERENSKY REEF

Laser ablation ICP-MS analysis of the orthopyroxene and plagioclase grains of the Merensky Reef was carried out in order to test whether these grains may contain PGE in their lattices.

As observed for the chromite, the time-resolved spectra (Fig. A5-1) indicate that no PGE were found in orthopyroxene and plagioclase lattices. The only PGE rich phases observed during the laser ablation occur as small inclusions. All the inclusions observed are summarized in Table A5-1.

The composition of the orthopyroxene was evaluated using the method described above. The results are summarized in Table A5-2. Results were compared with published values of Arndt *et al.*, 2005 and Wilson *et al.*, 1999.

REFERENCES

Arndt, N., Jenner, G., Ohnenstetter, M., Deloule, E. & Wilson, A. 2005. Trace elements in the Merensky Reef and adjacent norites Bushveld Complex South Africa. Mineralium Deposita, **40**(5): 550-575

Wilson, A. H., Lee, C. A. & Brown, R. T. 1999. Geochemistry of the Merensky reef, Rustenburg Section, Bushveld Complex: controls on the silicate framework and distribution of trace elements. Mineralium Deposita, **34**(7): 657-672.

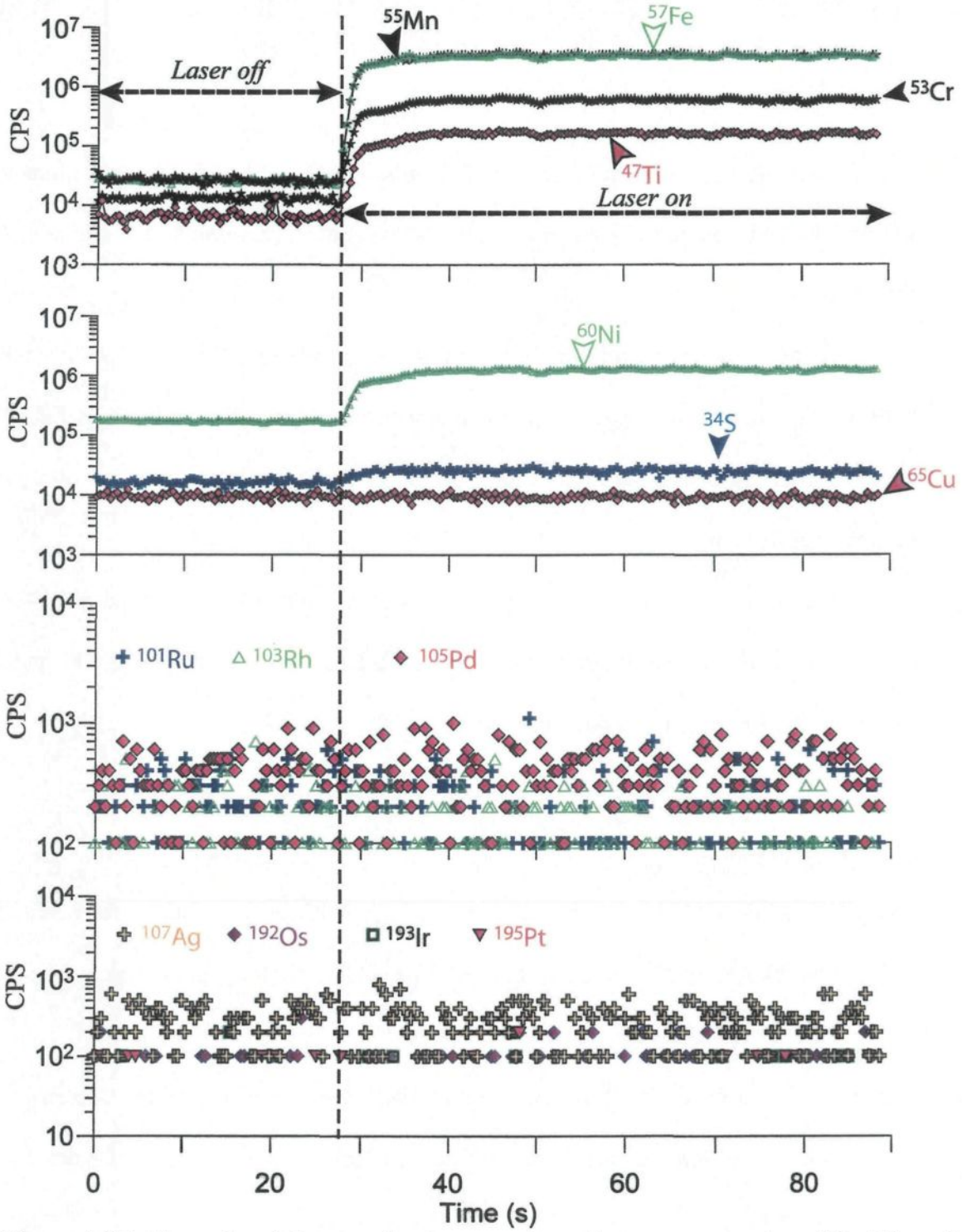

Figure A5-1: Example of time-resolved spectra for orthopyroxene grains of the Merensky Reef.

Table A5-1: *Summary of PGE- and noble metal-rich inclusions observed during laser ablation of the Merensky Reef of the Merensky Reef.*

Section	Name	Lithology	Inclusions	Number	Ti (ms)	Tf (ms)	Tf-Ti (ms)	Length (μm) Max.	Min.
MRE2	OPX4	LC	Pt + Sn	1	24139	24927	788	0.79	0.45
MRE2	OPX5	CGM	Ag	1	41457	41982	525	0.53	0.30
MRE2	OPX6	CGM	Pt (without Te-Bi-As)	1	82784	84752	1968	1.97	1.14
MRE2	OPX7	CGM	Sn-Pt-Cu	1	24927	26501	1574	1.57	0.91
MRE2	OPX8	CGM	Pt	1	27944	28469	525	0.53	0.30
MRE2	OPX9	CGM	Pt-Cu	1	24664	27288	2624	2.62	1.51
MRE4	OPX4	M1	Ru	1	49067	49591	524	0.52	0.30
MRE4	OPX5	M1	Ag	1	75699	76093	394	0.39	0.23

Table A5-2: *Composition of the orthopyroxene and plagioclase grains of the Merensky Reef.*

Region	*n*	Lithology	Al wt%	Ca wt%	Ti ppm	V ppm	Cr ppm	Mn ppm	Co ppm	Ni ppm	Zn ppm
MRE-2_OPX1	2	CGM	2.29	2.29	1029	150	5998	2670	145	1027	45
Stdev			*0.14*	*0.15*	*79*	*11*	*517*	*209*	*9*	*30*	*21*
MRE-2_OPX2	3	CGM	2.47	2.24	1112	154	5736	2579	136	1078	61
Stdev			*0.14*	*0.13*	*77*	*10*	*365*	*183*	*6*	*42*	*8*
MRE-2_OPX3	2	CGM	2.56	2.34	1103	148	5161	2627	146	1055	72
Stdev			*0.03*	*0.16*	*40*	*7*	*280*	*86*	*6*	*15*	*10*
MRE-2_OPX6	3	CGM	1.91	1.96	1173	131	4278	2023	116	1182	64
Stdev			*0.02*	*0.35*	*15*	*10*	*283*	*48*	*1*	*124*	*3*
MRE-2_OPX8	2	CGM	2.04	2.27	983	128	4229	1945	127	912	78
Stdev			*0.00*	*0.00*	*18*	*8*	*270*	*47*	*2*	*25*	*5*
MRE2_OPX9	2	CGM	2.97	4.87	1848	190	4104	1556	88	974	43
Stdev			*0.00*	*0.21*	*14*	*7*	*204*	*75*	*7*	*59*	*2*
MRE-4-OPX1	3	M	1.69	1.80	688	105	3284	1757	85	691	78
Stdev			*0.14*	*0.23*	*57*	*10*	*316*	*188*	*9*	*58*	*10*
MRE-4-OPX2	3	M	1.65	1.14	2390	197	8089	2005	86	757	98
Stdev			*0.34*	*0.13*	*459*	*84*	*5597*	*247*	*14*	*65*	*65*
MRE-4-OPX4	2	M	1.30	1.47	660	81	2353	1358	66	531	39
Stdev			*0.03*	*0.05*	*18*	*1*	*30*	*19*	*0*	*7*	*2*
MRE-4-OPX5	2	M	1.21	0.76	1204	76	1655	1322	66	516	49
Stdev			*0.12*	*0.00*	*14*	*5*	*83*	*27*	*0*	*8*	*2*

CGM: coarse-grained melanorite
M: melanorite

APPENDIX 6: ELECTRON MICROPROBE AND LASER-ABLATION-ICP-MS ANALYSIS OF THE SECONDARY MAGNETITE OF THE J-M REEF

Laser ablation ICP-MS analysis (without collision cell) of the secondary magnetite grains of the J-M Reef was carried out in order to test whether these grains may contain PGE in their lattices.

As observed for the chromite, the time-resolved spectra (Fig. A6-1) indicate that no PGE are found in magnetite. However, several strong anomalies in Pd content (up to 3000 ppm) were observed during the ablation of some magnetite grains. These grains were then analysed using an electron microprobe (at Laval University). The results (Table A6-1) indicate that no-PGE are present in these secondary magnetite grains.

The "anomalous" Pd contents observed in some magnetites are principally due to the ablation of skaergaardite aggregates which were not observed with the optical microscope (used for LA-ICP-MS) but were then detected on the BSE images. In addition, a minor proportion of Pd (few ppm) is due to Cu-argide ($^{65}Cu + {}^{40}Ar \Rightarrow {}^{105}Pd$). This argide also explains the presence of Rh (at few ppm level) in the same magnetite grains (with $^{63}Cu + {}^{40}Ar \Rightarrow {}^{103}Rh$).

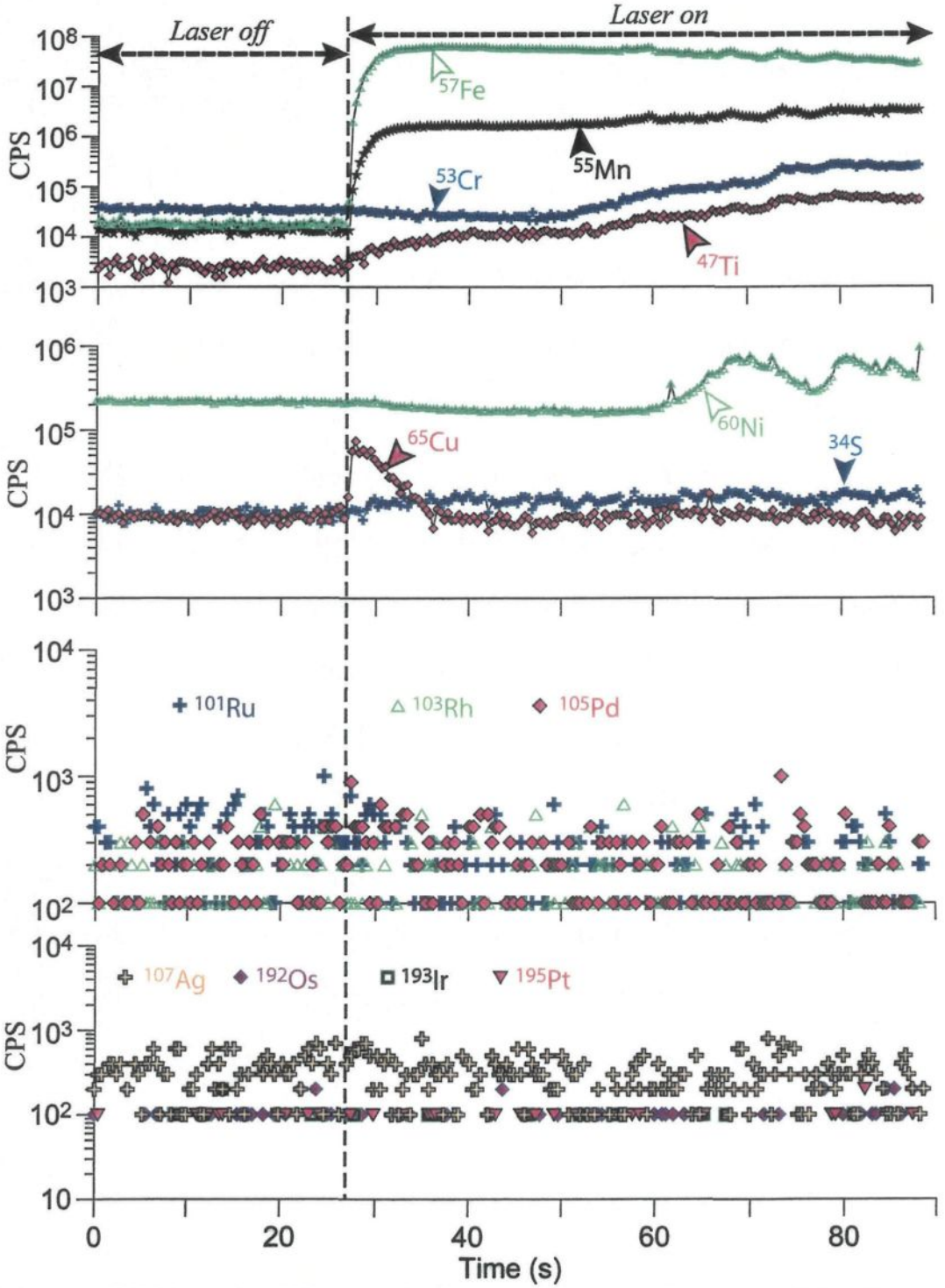

Figure A6-1: Example of time-resolved spectra for magnetite grains of the J-M Reef.

Table A6. 1: *Electron microprobe analysis of the secondary magnetite grains of the J-M Reef, Stillwater Complex.*

Section	SiO_2 wt%	TiO_2 wt%	Al_2O_3 wt%	Cr_2O_3 wt%	Fe_2O_3 wt%	MgO wt%	MnO wt%	FeO wt%	NiO wt%	CuO wt%	PdO wt%	Total wt%
ST17 M1	0.69	DL	DL	DL	68.01	0.62	0.08	29.42	DL	0.05	DL	98.90
ST17 M2	0.59	0.04	DL	DL	67.72	0.05	DL	30.46	DL	DL	DL	98.90
ST17 M3	0.61	0.05	0.10	DL	67.18	0.67	0.05	29.14	DL	0.31	DL	98.12
ST17 M4	0.07	DL	DL	DL	67.03	DL	DL	30.18	DL	DL	DL	97.34
ST17 M5	0.28	DL	DL	DL	67.10	0.08	DL	30.05	DL	0.15	DL	97.67
ST17 M6	DL	DL	DL	DL	67.92	0.04	DL	30.49	DL	DL	DL	98.47
ST17 M7	0.02	DL	1.25	DL	67.56	DL	DL	31.27	DL	DL	0.01	100.11
ST17 M8	0.86	DL	DL	DL	67.15	DL	DL	30.20	DL	DL	DL	98.25
ST17 M9	DL	DL	DL	DL	67.26	DL	DL	30.26	DL	DL	DL	97.56
ST17 M10	DL	DL	DL	DL	67.87	DL	DL	30.53	DL	DL	DL	98.43
ST17 M11	0.25	DL	DL	DL	68.17	0.29	DL	30.12	0.07	0.07	DL	99.02
ST17 M12	0.07	DL	DL	DL	68.18	DL	DL	30.65	DL	DL	DL	98.93
ST17 M13	0.05	DL	0.06	DL	67.61	DL	DL	30.43	0.06	0.04	DL	98.28
ST17 M14	DL	0.06	DL	DL	68.12	DL	DL	30.72	DL	DL	0.02	98.97
ST17 M15	0.22	DL	DL	DL	67.77	0.08	DL	30.36	DL	DL	DL	98.44
ST12 M1	0.04	DL	0.05	DL	67.83	0.12	DL	30.32	0.03	DL	DL	98.45
ST12 M2	0.02	0.03	DL	DL	68.05	DL	DL	30.65	0.04	DL	DL	98.81
ST12 M3	DL	DL	DL	DL	68.33	DL	DL	30.72	DL	DL	DL	99.09
ST12 M4	DL	DL	DL	DL	68.82	0.88	DL	29.36	DL	DL	DL	99.16
ST12 M5	0.04	DL	0.06	DL	67.83	DL	0.07	30.44	DL	DL	DL	98.51
ST12 M6	DL	DL	DL	DL	67.95	DL	DL	30.55	DL	DL	DL	98.54
ST12 M7	DL	DL	DL	DL	67.68	DL	DL	30.42	DL	DL	DL	98.16
ST12 M8	0.10	0.10	DL	DL	67.88	0.06	DL	30.59	0.04	0.06	DL	98.89
ST12 M9	0.16	DL	DL	DL	67.89	0.14	DL	30.30	0.03	DL	0.01	98.56
ST12 M10	DL	DL	DL	DL	67.60	DL	DL	30.44	0.10	0.04	0.01	98.24
ST12 M11	0.60	DL	DL	DL	67.52	0.30	DL	29.87	DL	0.05	DL	98.39
ST12 M12	0.17	0.03	DL	DL	68.13	0.06	0.05	30.56	DL	DL	DL	99.02
ST12 M13	0.22	0.05	DL	DL	69.48	1.17	DL	29.24	DL	DL	0.02	100.21
ST12 M14	0.25	DL	DL	DL	67.77	DL	DL	30.49	DL	DL	0.01	98.55
ST12 M15	0.22	DL	DL	DL	68.43	0.09	DL	30.65	DL	0.04	0.01	99.50